



HAL
open science

Synthesis and Biological Evaluation of Gold Glyconanoparticles: Ligands for Studying Multivalence Effects

Michael Reynolds

► **To cite this version:**

Michael Reynolds. Synthesis and Biological Evaluation of Gold Glyconanoparticles: Ligands for Studying Multivalence Effects. Chemical Sciences. Université Joseph-Fourier - Grenoble I, 2009. English. NNT: . tel-00462627

HAL Id: tel-00462627

<https://theses.hal.science/tel-00462627v1>

Submitted on 12 Mar 2010

HAL is a multi-disciplinary open access archive for the deposit and dissemination of scientific research documents, whether they are published or not. The documents may come from teaching and research institutions in France or abroad, or from public or private research centers.

L'archive ouverte pluridisciplinaire **HAL**, est destinée au dépôt et à la diffusion de documents scientifiques de niveau recherche, publiés ou non, émanant des établissements d'enseignement et de recherche français ou étrangers, des laboratoires publics ou privés.

**UNIVERSITE DE GRENOBLE I – JOSEPH FOURIER
ECOLE DOCTORALE CHIMIE ET SCIENCES DU VIVANT**

THESE

Pour l'obtention du diplôme de

DOCTEUR DE L'UNIVERSITE JOSEPH FOURIER

Discipline : Chimie Physique Moléculaire et Structurale

Présentée publiquement le 14 Décembre 2009

Michael Reynolds

**Synthesis and Biological Evaluation of Gold
Glyconanoparticles :
Ligands for Studying Multivalence Effects**

**Synthèse et Evaluation Biologiques des Glyconanoparticules d'Or :
Ligands pour Etudier l'Effet de Multivalence**

Jury

Eric Defrancq	Président
Johannis Kamerling	Rapporteur
Monica Palcic	Rapporteur
Soledad Penades	Examineur
Serge Perez	Directeur de Thèse

Thèse préparée au CERMAV-CNRS

Acknowledgements

I would first like to thank Professors Hans Kamerling and Monica Palcic for refereeing this thesis manuscript. I would equally like to extend my thanks to Professors Soledad Penadés and Eric Defrancq for also having accepted to take part on the thesis committee. I would also like to thank the GlycoGold network for funding this work, their superb organisation and the quality training opportunities I received.

To Serge, I extend my warmest gratitude; I don't think I could have had a better thesis director. Thank you for accepting me in to your group and allowing me to be in such a friendly and productive environment. I appreciate all of the conversations we had, all of the help and support you have given me throughout my time here professionally, scientifically and personally. Merci beaucoup!

I would also like to thank Anne Imberty for her helpful advice, and Christelle Breton for welcoming me and accepting me into the Molecular Glycobiology research group – it mustn't have been easy accepting a dirty chemist in to a group of super clean biologists – merci!

Thanks to all of the Mesdemoiselles of the group and their lovely accents: Laurence Miguet (I have no idea what she said to me that first morning, but I do remember thinking “please say it again”!), Emilie, Magalie, Sophie, Claire and Annabelle as well as Karoline, Alessandra, Sara and the “new arrivals” Raquel, Soumaira and Anita – thank you all for your kindness and patience, as well as your superb scientific expertise which I was privileged to be a student of. They should also be commended for acting with a high degree of professionalism in the face of my natural, James Bond-like, dashing good looks, charm and Englishness. Thanks must also go to the only other bloke in the group, Bertrand, for all of your help, kindness and letting me drive your car that one time! I don't know if those were tears of laughter or sheer horror that you shed, perhaps one day you'll tell me when you finally learn how to drink a whole pint of beer! To the group technicians, Catherine and Valerie, thank you both for your kindness and the enormous amount of help and patience you had with me. Thanks also to the students that were in the Molecular Glycobiology group either on secondment or “passing through”; Charles, Peter, Michal, Maria and Sami. There are sure to be more who I have forgotten to mention...in any case, you all suffered my incessant whistling without having to resort to physical means to shut me up, for that I congratulate you!

There are of course the cermavians, without whom there would be no CERMAV; Isabelle C, Patrick and Greg, Martine, Martine and Magalie, and the IT technicians Alain, Cyril and Jena-Daniel. Special thanks to Isabelle P, Amandine and Patricia Donnadiou (SIMAP) for looking at my golden balls (microscopy!) and Isabelle J for helping me with my NMRs. I would also like to thank the Glycomaterials group; Jean-Luc, Laurent, Bruno, Marie-France and Christine, for letting me use some of their lab space to do my dirty chemistry experiments – I promise I'll move my stuff out soon!

I would also like to thank Soledad Penadés, her group, and the rest of CICbiomaGUNE (San Sebastian) for the excellent training they gave me and their unlimited kindness during my stay there. In particular Marco, Olga, Paolo, Isa y todos mis profesores de español y compañeros de surfing – muchas gracias! I would also like to thank the other members of the GlycoGold training network, in particular Dr. Bas Leeftang and Prof. Hans Vliegthart, as well as my good friends Anja, Michael, Dodi and the others for their kindness and good humour which is equal to their scientific quality.

Thanks also to Gemma and Juan-Angel of ID22 at the ESRF for our very brief but interesting collaboration which I hope is to be continued...

Throughout my time in CERMAV I had the privilege of crossing paths with almost everybody. So, in no particular order: My adopted family Jimmy, Maria and my “baby brother” Javier, I couldn't have asked for a more welcoming home-from-home, nor could I have imagined such kind and helpful people. My good friends Roberto, Issei and Eduardo, there are no words in any language to express my gratitude for the quantity and quality of good times had during coffee breaks and post-work ethanol-enhanced scientific discussion sessions. There were of course many other participants to such deep discussions from a wide range of scientific and non-scientific backgrounds; Lillie, Ana, Maxou, Ondrej, Yoko (poco ma gioco), Lina, Anna, Hélène, Julie, Caroline, Claire, Ali, Pierre, Sami H, Laurine, Mialy, Camelia, Karim, the Italians, the Japanese and the Colombians...again it is probable that several people may have been missed off this long but distinguished list to whom I apologise profusely.

I would like to thank my family, who has supported me throughout the past few years. I promise one day I will get a “real job” ...but maybe not just yet. I again apologise for becoming (slightly) French, I'll keep working on my Eengleesh! Finally, to Johanna my dear-princesa-reina-sweetheart, thank you for supporting me throughout everything, particularly these last few months...gracias mi chiquita!

...CHEERS EVERYBODY !

List of Abbreviations

α	Cooperativity coefficient
AFM	Atomic force microscopy
AuNP	Gold nanoparticle
β	Affinity enhancement coefficient
b	statistical factor – ratio of permutations in forward reaction to permutations in the reverse reaction
Bc	<i>Burkholderia cenocepacia</i>
BcIA	<i>Burkholderia cenocepacia</i> lectin A
C_{bulk}	Bulk concentration
CD	Cyclodextrin
C_{eff}	Effective concentration
CM5	Carboxymethylated dextran chip for SPR studies
Con A	Concanavalin A lectin
DC	Dendritic cell
DC SIGN	DC specific intracellular adhesion molecule-3-grabbing non-integrin
DFT	Density functional theory
DGL	<i>Dioclea grandiflora</i> lectin
DLS	Dynamic light scattering
DOTA	1,4,7,10-tetraazacyclododecane-1,4,7,10-tetraacetic acid
<i>E. coli</i>	<i>Escherichia coli</i>
EA	Elemental analysis
ECorL	<i>Erythrina corallodendron</i> lectin
EDC	1-ethyl-3-(3-dimethylaminopropyl)carbodiimide
EDTA	ethylenediaminetetraacetic acid
ELISA	Enzyme linked immunosorbent assay
ELLA	Enzyme linked lectin assay
FPLC	Fast protein liquid chromatography
FimA	Fimbrial protein A
FimH	Fimbrial protein H

FT-IR	Fourier transform infra red spectroscopy
G	Gibbs free energy
Gal	D-Galactose
GalNAc	<i>N</i>-acetyl-D-galactosamine
GM1	Glycolipid ganglioside oligosaccharide 1
GNP	Glyconanoparticle
gp120	HIV glycoprotein 120 kDa
H	Enthalpy
HEPES	4-(2-hydroxyethyl)-1-piperazine ethanesulfonic acid
HIA	Haemagglutination inhibition assay
HIV-1	Human immuno virus
HOMO	Highest occupied molecular orbital
HPLC	High performance liquid chromatography
IC₅₀	Concentration of inhibitor required to induce 50 % inhibition
ITC	Isothermal titration (micro)calorimetry
Lac	Lactose
LacNAc	<i>N</i>-acetyl Lactosamine
sLe^x	Sialyl-Lewis X
Man	D-Mannose
MBL	Mannose binding lectin
MIC	Minimum inhibitory concentration
MIP	Mean inner potential
MNP	Magnetic nanoparticle
NeuAc	<i>N</i>-acetylneuraminic acid, Sialic acid
NHS	<i>N</i>-hydroxy succinimide
NP	Nanoparticle
PA	<i>Pseudomonas aeruginosa</i>
PA-IL	<i>Pseudomonas aeruginosa</i> lectin I
PAMAM	Poly(amidoamine)
PBS	Phosphate buffered saline
PEG	Poly(ethylene glycol)
PEI	Poly(ethylene imine)
<i>p</i>MBA	<i>para</i>-mercaptobenzoic acid
PNA	Peanut agglutinin

PPI	Poly(propylene imine)
QD	Quantum dot
RAFT	Regioselectively addressable functionalised templates
RCA 120	Ricinus lectin
RMSD	Root-mean-squared deviation
RU	Response units
siRNA	Small interfering Ribonucleic acid
S	Entropy
SAM	Self-assembled monolayer
SARS	Severe acute respiratory syndrome
SAXS	Small angle X-ray scattering
SPR	Surface plasmon resonance
T	Absolute temperature
TEM	Transmission electron microscopy
TGA	Thermogravimetric analysis
Tris	Tris(hydroxymethyl)aminoethane
VAA	<i>Viscum albumin</i> agglutinin
WGA	Wheat germ agglutinin
XPS	X-ray photoelectron spectroscopy
XRF	X-ray fluorescence

CONTENTS

INTRODUCTION GENERALE (Français)	1
GENERAL INTRODUCTION	3
CHAPTER 1 : Carbohydrates, Lectins and the Cluster Glycoside Effect	5
1.1 Carbohydrates	6
1.1.1 Ring structure	7
1.1.2 Glycosidic linkage	8
1.2 Biological Importance of Carbohydrates	10
1.2.1 Glycoconjugates	11
1.2.2 Interactions with the local environment	12
1.3 Lectins	13
1.3.1 Immunity	13
1.3.2 Bacterial infection	14
1.3.3 Viral infection	15
1.3.4 HIV-1 infection	15
1.3.5 Cancer metastasis	16
1.3.6 Lectin interaction with monosaccharides	16
1.3.7 Lectin interaction with oligosaccharides	17
1.4 Lectin Architectures	17
1.4.1 Con A	17
1.4.2 BclA	19
1.4.3 PA-IL	20
1.5 Multivalence	22
1.5.1 Types of multivalence	24
1.6 Cluster Glycoside Effect	26
1.6.1 Monovalent reaction kinetics	27
1.6.2 Monovalent thermodynamics	28
1.6.2.1 Enthalpy	28

1.6.2.2 Entropy	29
1.6.3 Monovalent to multivalent	30
1.6.3.1 Multivalent kinetics and free energies	30
1.6.3.2 Cooperativity	31
1.6.3.3 Enthalpies of multivalent interactions	33
1.6.3.4 Entropy of multivalent interactions	37
1.6.4 Enthalpic and entropic contributions to multivalent free energies of interaction	40
1.6.5 Effective concentration	41
1.6.5.1 Reaction kinetics and the effective concentration	42
1.6.6 Conclusion	44
1.7 Synthetic Multivalent Scaffolds	45
1.7.1 Small molecule glycoclusters	46
1.7.2 Cyclodextrins and calixarenes	49
1.7.3 Dendrons and dendrimers	52
1.7.4 Functionalised polymers	53
1.7.5 Micelles and capsules	54
1.7.6 <i>Neoglycoproteins</i>	56
1.7.7 Self-assembled monolayers (SAMs)	57
1.7.8 Coupling methods	60
1.8 Conclusion	61
CHAPTER 2 :Glyconanoparticles	63
2.1 Gold	64
2.2 Gold Atom Clusters	64
2.2.1 Vocabulary	64
2.2.2 Synthesis and assembly	65
2.2.2.1 Brust-Schiffrin method	66
2.2.2.2 Citrate reduction	67
2.2.2.3 Other syntheses	67
2.2.3 AuNP Structure	68
2.2.4 Gold-ligand interactions	71
2.2.5 Other ligands	71
2.3 Physical Properties	72

2.3.1 Surface plasmon resonance	73
2.3.2 Fluorescence	73
2.3.3 Magnetism	74
2.3.4 Mean inner potential	75
2.3.5 Ligand presentation	75
2.4 Applications	76
2.4.1 Surface plasmon resonance	76
2.4.2 Catalytic activity	76
2.4.3 Drug delivery vectors	77
2.4.4 Hyperthermia therapies	78
2.5 AuNPs as Multivalent Scaffolds	79
2.5.1 Applications to carbohydrate interactions	80
2.6 Other functionalities	82
2.7 Other NP systems and their applications	83
2.8 Conclusion	84
RESEARCH AIMS	85
CHAPTER 3 : GNP Synthesis and Characterisation	87
3.1 Chemical Synthesis	88
3.2 GNP Characterisation	88
3.2.1 Nuclear magnetic resonance (NMR)	89
3.2.2 UV/vis Spectroscopy	91
3.2.3 Fourier transform infrared spectroscopy (FT-IR)	92
3.2.4 Transmission electron microscopy (TEM)	93
3.2.5 Elemental analysis (EA)	95
3.2.6 TEM combined with EA	96
3.2.7 Phenol-sulfuric acid method	96
3.3 Other Techniques	97
3.3.1 Mass spectrometry	97
3.3.2 Thermogravimetric analysis (TGA)	97
3.3.3 Small angle X-ray scattering (SAXS)	97
3.3.4 Dynamic light scattering (DLS)	98

3.3.5 “Reverse” ITC	98
3.4 Culture and Expression of Recombinant Proteins and Large Scale Lectin Production	99
3.4.1 BclA	99
3.4.2 PA-IL	99
CHAPTER 4 : Biophysical Analysis of Protein-Carbohydrate Interactions	101
4.1 Haemagglutination Inhibition Assay (HIA)	102
4.1.1 Principle	102
4.1.2 Applications to carbohydrate interactions	104
4.2 Surface Plasmon Resonance (SPR)	104
4.2.1 Principle	104
4.2.2 General applications	107
4.2.3 Applications to protein-carbohydrate interactions	108
4.3 Isothermal Titration (micro)Calorimetry	109
4.3.1 Principle	109
4.3.2 General applications	113
4.3.3 Applications to carbohydrate interactions	114
4.4 Other Methods	115
4.4.1 Enzyme-linked lectin assay (ELLA)	115
4.4.2 Dynamic light scattering (DLS)	115
4.4.3 Analytical ultra centrifugation	116
4.4.4 Crystallography	117
4.4.5 Molecular modelling	118
4.4.5.1 Growing chain methods	118
4.4.5.2 Exhaustive search	119
4.4.5.3 Heuristic or Guided search	119
4.4.5.4 Monte Carlo	119
4.4.5.5 Genetic algorithm	120
4.4.5.6 Molecular dynamics	120
4.4.5.7 Force fields	120
4.4.5.8 Modelling lectin-carbohydrate interactions	121
4.4.6 UV aggregation studies	122

4.5 Conclusions	122
CHAPTER 5 : Synthesis and Biological Evaluation of GNPs	125
5.1 Article 1	127
5.2 Chemical Synthesis	162
5.3 Further Synthesis	166
5.4 Biophysical Analysis	170
5.4.1 Haemagglutination inhibition assay	170
5.4.2 Isothermal titration (micro)calorimetry	171
5.4.3 Inter-ligand distance calculations	171
5.5 Cluster Glycoside Effect at GNPs	177
GENERAL CONCLUSIONS	182
CONCLUSIONS GENERALE (Français)	186
CHAPTER 6 : Experimental – Biochemistry and Interactions Studies	189
6.1 Lectin Expression and Purification	190
6.2 Haemagglutination Inhibition Assay	190
6.3 Surface Plasmon Resonance	191
6.4 Microcalorimetry	192
6.5 Transmission Electron Microscopy	193
6.6 Monosaccharide analysis	193
CHAPTER 7 : Experimental – Chemical Synthesis	195
7.1 General Protocol for GNP Synthesis	220
BIBLIOGRAPHY	225
ANNEX I : Further GNP Characterisation	234

ANNEX II : Further GNP Applications I	236
1 Self-organisation of GNPs	236
2 Self-organisation of Lectin-Carbohydrate Complexes	239
3 Self-organisation of Lectin-GNP complexes	239
ANNEX III : Further GNP Applications II	241
Article 2 (3 pages)	243
ANNEX IV : Molecular Modelling of Carbohydrates	247
1 3D Biologically Active Oligosaccharide (3D BAO) Database	247
2 NanoGoldBuilder	248
3 Hydration Studies of Carbohydrates	249
Article 3 (p447-460)	251
ANNEX BIBLIOGRAPHY	266
ABSTRACT	267

INTRODUCTION GENERALE

Les interactions entre les protéines et les glucides sont impliquées dans plusieurs processus biologiques normaux ou bien pathologiques, tels que la communication et l'adhésion cellulaires, la fertilisation, l'entrée de pathogènes dans les cellules ou encore de carcinomes métastatiques.

Le premier chapitre de cette thèse porte sur la nature des glucides au niveau moléculaire, et plus particulièrement sur leurs structures, leurs propriétés et leurs importances biologiques. Ensuite après une description des protéines, les lectines, qui se lient spécifiquement avec les glucides, ils sont également présentés les mécanismes et les paramètres thermodynamiques et cinétiques des interactions de ces lectines, avec une description de plusieurs plateformes multivalentes qui existent actuellement (naturelles, synthétiques et semi-synthétiques), suivie d'une évaluation de l'effet de multivalence, ou « effet cluster glycosidique » (cluster glycoside effect).

Le deuxième chapitre est consacré à la synthèse des nanoparticules d'or, à leurs propriétés physicochimiques, leur structure et à leur utilisation comme plateforme multivalente. La dernière partie de ce chapitre décrit d'autres nanoparticules métalliques qui se sont aussi révélées être utiles en tant que plateformes multivalentes. Leurs propriétés physiques sont également citées.

Le troisième chapitre traite de la synthèse et de la caractérisation des glyco-nanoparticules (GNPs) avec une présentation des techniques utilisées dans ce travail, ainsi que d'autres techniques actuellement disponibles. Le quatrième chapitre introduit les méthodes biophysiques classiques et modernes utilisées pour la caractérisation des interactions protéines-glucides avec une description des techniques générales mais aussi des techniques plus spécifiques aux GNPs.

Le cinquième chapitre présente les résultats obtenus suite à la synthèse des GNPs ainsi que ceux obtenus lors des études d'interactions lectines-GNPs. Ces résultats ont été interprétés par rapport aux architectures des GNPs et des lectines d'une part, et par rapport aux théories relatives à l'effet de multivalence d'autre part. Ces travaux sont présentés sous forme d'un article scientifique incluant des résultats complémentaires et des discussions approfondies. Les deux derniers chapitres décrivent les méthodes expérimentales que nous avons utilisées lors des études biophysiques, ainsi que les synthèses chimiques et les caractérisations des molécules organiques et des GNPs.

Les annexes contiennent des informations et des résultats complémentaires sur les caractérisations des GNPs obtenus avec l'utilisation d'une source de rayons X synchrotrons (ESRF, Grenoble). Les propriétés d'auto-organisation des GNPs et leurs applications potentielles dans les domaines des nanoélectroniques et de la nano-chimie sont aussi présentées. De plus, l'utilisation des GNPs pour le développement des méthodes permettant d'étudier le « potentiel intérieur moyen » (mean inner-potential) en utilisant la microscopie électronique à transmission (TEM) est décrite sous forme d'article.

La dernière partie porte sur la description d'une base de données des glucides, ainsi que d'une étude structurale en milieu aqueux. Les comportements des molécules d'eau et des molécules glucides ont été étudiés par des méthodes bioinformatiques et les résultats sont présentés sous forme d'article scientifique.

GENERAL INTRODUCTION

Protein-carbohydrate interactions are implied in many important biological processes, both normal and pathological. These interactions include cell-cell communication and adhesion, fertilisation, pathogen invasion and the migration and invasion of metastatic carcinoma.

The first chapter of this thesis discusses the nature of carbohydrate molecules, with particular reference to structure, properties and their importance in biology. Secondly, carbohydrate-specific proteins (lectins) are discussed. Finally the mechanisms, thermodynamic and kinetic parameters, and theories which govern these interactions are discussed followed by a description of various natural, synthetic and semi-synthetic multivalent scaffolds which currently exist, and an evaluation of how they interpret the cluster-glycoside effect. The second chapter discusses Gold nanoparticles, their synthesis, structure and some of their physicochemical properties. Their use as multivalent scaffolds is also described with particular emphasis on carbohydrate interactions. Finally, the reader is introduced to other nanoparticle systems which also present interesting potentials as multivalent scaffolds and their physical properties.

The third chapter describes the synthesis and characterisation of GNPs. Techniques used in this study, as well as other techniques currently available, are also discussed. The fourth chapter introduces biophysical methods of characterising carbohydrate-lectin interactions. Well established techniques as well as modern analysis apparatus are discussed regarding carbohydrate-protein interactions in general and techniques specific to GNP-lectin interactions. Again, techniques used in this study, as well as other techniques available are described.

The fifth chapter lists the results obtained from GNP synthesis and GNP-lectin interaction studies. The results are then interpreted with reference to GNP and lectin architecture as well as the current theories towards the cluster-glycoside effect. Results are presented in an article format, as well as additional results and further discussion included afterwards.

The annexes include discuss further GNP characterisation using synchrotron radiation, self-organisation properties of GNPs and potential implications in nanoelectronics and nanochemistry. The application of GNPs towards the development of experimental methods for investigating the mean-inner potential of AuNPs is also discussed. Finally, carbohydrate structure and their documentation is discussed as is carbohydrate structure in aqueous solution, molecular behaviour and solute behaviour are described using computational methods.

CHAPTER 1 :
Carbohydrates, Lectins and the Cluster
Glycoside Effect

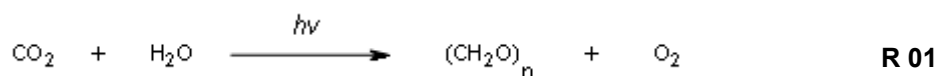
CHAPTER 1 :

Carbohydrates, Lectins and the Cluster Glycoside Effect

1.1 Carbohydrates

Carbohydrates comprise one of the most abundant classes of biomolecules and along with peptides and lipids make up the molecules essential for life. They are typically found in biological systems as monosaccharides, oligosaccharides or polysaccharides. Due to their versatile nature, carbohydrates have several biological roles corresponding to their physical properties. They are used as energy storage and transport, in the form of starch or glycogen in plant and animal systems respectively, as well as structural and architectural elements in plant systems and crustaceans as cellulose and chitin. Carbohydrates are also implied in other roles as discussed later, such as recognition, viral and bacterial invasion as well as signal transmission and communication.

Carbohydrates, from the German word “Kohlenhydraten” meaning “carbon hydrates”, are synthesised by plants during photosynthesis. CO₂ is “fixed” during the Calvin cycle where CO₂ is reduced with water to give carbohydrates and oxygen, with the general formula C_n(H₂O)_n.



Carbohydrates are polyhydroxy alkanes which comprise a large variety of monosaccharide units with backbones of varying length. These monosaccharides contain carbonyl groups, either aldo- or keto- groups, as well as primary and secondary alcohols. Linear structures are characterised by the sequence of stereogenic centres, each of which has an influence on how the monosaccharide occupies 3D space. Also, each monosaccharide has its own enantiomer relative to the most distant stereogenic centre from the carbonyl group. The prefixes D and L are given to determine between the two (Fig. 1).

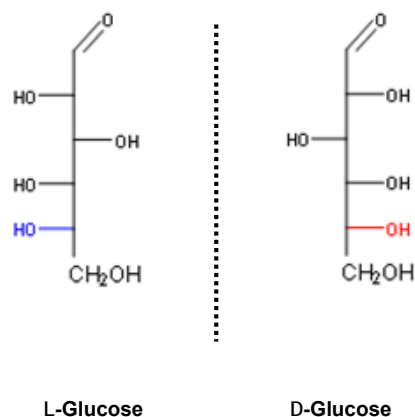


Figure 1 : Fischer projections of L-Glucose (left) and D-Glucose (right). The stereogenic centre at C5 is used as the reference atom to distinguish the two.

1.1.1 Ring structure

Due to the presence of a carbonyl group and a multitude of alcohol functionalities, the linear structures can undergo intramolecular addition to form cyclic hemiacetal or hemiketals. The new stereogenic centre formed upon hemiacetal ring closure is denoted the anomeric centre. Five or six membered rings being the most common cyclic structures formed; giving the furanoses and pyranoses respectively (Fig. 2). The 3D structure of the cyclic monosaccharide is subject to the influence of the starting enantiomer, therefore D and L monosaccharides are significantly different in both linear and cyclic structures. Furthermore, functionalisation of the anomeric hydroxyl group (the hydroxyl group of the hemiacetal) will block the ring opening/closing mechanisms thus the monosaccharide is locked in its cyclic conformation.

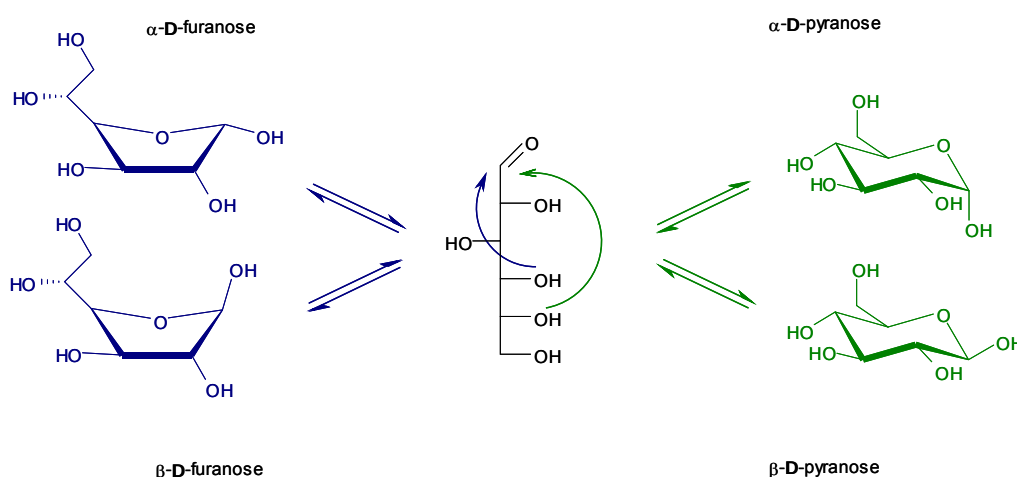


Figure 2 : Monosaccharide equilibrium between linear and cyclic (furanose and pyranose) forms.

In the case of pyranoses, several ring conformations are possible. Typically, a chair conformation is adopted, with C2, C3, C5 and O5 all in the same plane. The pyranose ring can thus adopt two conformations depending on where C4 and C1 are situated. If C4 is above the plane and C1 below, this gives the 4C_1 conformation. If C4 is below the plane and C1 above the plane, this gives the 1C_4 conformation. Depending on the substitution of the ring, one conformation will be preferred over the other. Substitutions will prefer to adopt equatorial positions however a trade off between minimising 1,3-diaxial steric hindrance and maximising anomeric orbital overlaps (O_{lp} lone pair to σ^*_{C1-O1}) is made. Ring puckering and ring distortion are also possible depending on internal angle and torsion strain, which can lead to boat or skew conformations.¹ As ring puckering and ring flipping induce large conformational changes (as all axial positions become equatorial and vice versa) this occurs only very rarely, particularly if considering sterically large substitutions, such as oligosaccharides, on the ring (Fig 3, below).



Figure 3 : Ring conformations of D-Glucose. 4C_1 is preferred over 1C_4 due to minimisation of 1-3 diaxial steric hindrance. This preference is increased upon increasing Van der Waals volumes of substituent R.

1.1.2 Glycosidic linkage

Condensation of a monosaccharide with an alcohol or any other heteroatom will lead to the construction of glycoconjugates. Reaction with another monosaccharide will lead to disaccharide molecules. Further reaction to tri-, tetra-, oligo- and polysaccharides is also possible via subsequent glycosidic linkage formations. It is via this condensation reaction that biological systems build the required carbohydrate molecule and conjugate it to proteins, peptides or lipids. This results in the glycoproteins, glycopeptides and glycolipids

respectively. Upon conjugation, typically the monosaccharide is linked via the anomeric position. This allows further stereochemical variation as this can produce two stereoisomers at the anomeric centre, referred to as *anomers*, denoted α - or β - with regards to the stereochemistry at the most distant stereogenic centre.

Although the monosaccharide units themselves are fairly rigid structures as mentioned above, oligo- and polysaccharides are known to be flexible. This is due to the considerable freedom of rotation about the glycosidic linkages connecting the monosaccharide units. This flexibility leads to oligosaccharide molecules having conformational heterogeneity and often several conformations are accessible at ambient temperatures. The rotations of these linkages are typically described by the torsion angles involved, Φ and Ψ where $\Phi = \text{O5-C1-Ox-Cx}$, and $\Psi = \text{C1-Ox-Cx-C(x+1)}$, for disaccharides as shown below. A third torsion angle is used to describe the rotational freedom at the primary hydroxide in the C6 position, denoted as ω and corresponds to O5-C5-C6-O6 (Fig 4, below).

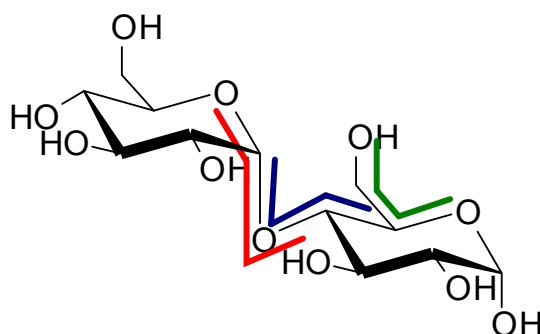


Figure 4 : Structure of Glc- α -(1-4)-Glc denoting the torsion angles Φ (red), Ψ (blue) and ω (green).

The torsion angle around C5-C6 can also be described by the additional torsion angle C4-C5-C6-O6. Combining this torsion angle with ω , the relationship between the ring atoms and the hydroxyl can be described by *trans* / *gauche* denominations. The torsion angles are said to be in *gauche* (*g*), conformation when they are $\pm 60^\circ$ and *trans* (*t*), when they are 180° . The sign of the torsion angles is defined in agreement with the IUPAC Commission of Biochemical Nomenclature.² This allows the description of the three principal rotamers of the primary hydroxyl group as *gg*, *gt* and *tg* (figure 5).

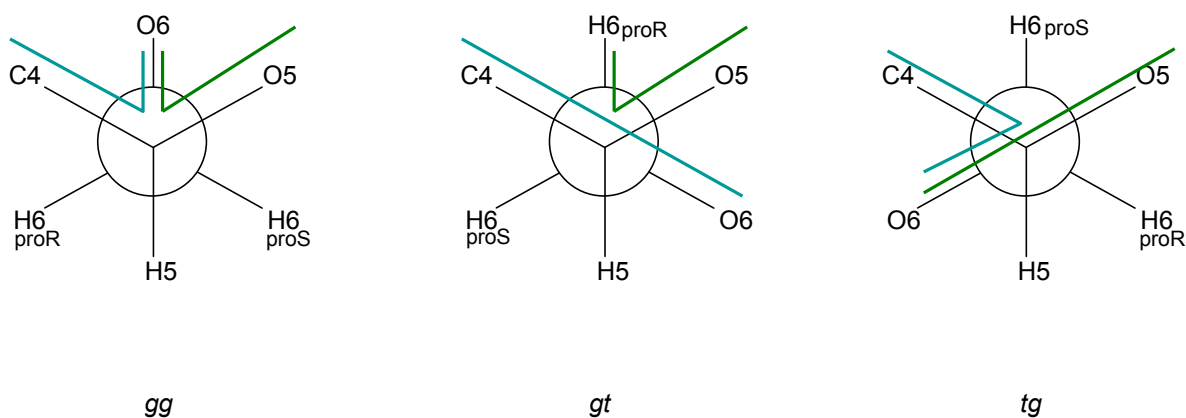


Figure 5 : Descriptions of the torsion angles around C5-C6 *gg* (left), *gt* (centre) and *tg* (right).

Modifying any of the alcohol groups of the monosaccharide by oxidation, reduction or substitution can give carboxylic acid, deoxy- and amino- functionalities as well as phosphates and sulfates etc. Replacement of the endocyclic oxygen of the cyclic structures may also lead to the unnatural *pseudo*-sugar derivatives such as carba-, aza- or phospho- sugars and inositols.^{3,4}

The variation of monosaccharide structure with respect to backbone length, the number of stereogenic centres, and disposition of carbonyl groups, hemiacetals and hemiketals as well as further chemical modification allows for the construction of a multitude of monosaccharide building blocks. This means that, upon further glycosylation to any one of several available functional groups, an enormous variety and combination of functionalities and structural arrangements are possible including cyclic (cyclodextrins), branched polymers and oligomers – unique to polysaccharides and oligosaccharides. This leads to the chemical, physical and structural properties of the final carbohydrate which in turn will influence how the molecule occupies 3D space and how it interacts with solvent molecules, ultimately leading to its biological activity. The vast amount of potential information that can be stored within the macromolecular carbohydrate structure is phenomenal and unrivalled in the biological world in terms of diversity and almost unlimited structural variations.

1.2 Biological Importance of Carbohydrates

As mentioned earlier, carbohydrates are exploited by plants for their physical properties in cellulose for example. However, on a cellular level, carbohydrates exhibit a multitude of

functions. Often, they are covalently linked to other non-carbohydrate biomolecules giving the glycoconjugates. These molecules play important roles in cell communication; however, the relationship between their structure and their specific role is not yet fully understood.

1.2.1 Glycoconjugates

Glycoconjugates can be found in large quantities and many varieties at the exterior of all cell surfaces. This is known as the glycocalyx, and it is through this constantly changing and evolving surface that cells express their current status in terms of cell type, development stage and pathological status.^{4, 5} Glycoconjugate presentation is particularly important for bacterial cells for invasion and occupation of host environments (respiratory or digestive tracts for example) and epithelial and blood cells for host self-self and non-self identification discrimination. The glycocalyx is involved in other biological processes such as cell recognition and discrimination and cell-cell adhesion. However, despite specific glycoconjugates having specific functions, the glycocalyx is a very dense and complex medium which can be greater than 50 nm thick.⁶ Therefore, when considering carbohydrate interactions at the cell surface, it is simply not enough to consider only one glycoconjugate. One is obliged to consider the effects of the local environment – disposition of adjacent glycoconjugates and indeed, solvent molecules as well as other biomolecules and ions.

Glycosylation of proteins is thought to be one of the most common post-translation modifications used by nature, along with phosphorylation. Carbohydrate presentation is important for providing a quality control mechanism for protein folding, the carbohydrate residue adopting a particular presentation. If the folding is incorrect, this is exaggerated by incorrect carbohydrate presentation and hence, the protein is recognised as a malfunction and degraded.⁷^(and references therein) After post translational modification, the oligosaccharide may also play important roles in the function of the conjugated protein, as a significant portion of the molecular weight and the occupied volume of the glycoprotein consists of the oligosaccharide. Molecular dynamics of a glycoprotein showed indeed that the oligosaccharide fragment occupied a large volume equalling that of its protein conjugate.⁵ The glycosylation pattern would determine protein size, solubility and may encode information such as destination or transport cargo.

1.2.2 Interactions with the local environment

Saccharide molecules, with a cyclic carbon skeleton and pendant hydroxyl groups, have an inert capability of interacting with local solvent molecules forming a hydrogen bond network. In rare cases they are also capable of interacting via electrostatic interactions as well as metal ion coordination via hydroxyl groups. Interaction with aromatic groups is also possible due to electrostatic attractions between aromatic π electron clouds and the δ^+ charged axial hydrogens of the aliphatic carbon ring.⁸ Van der Waals interactions are typically small, yet can be important collectively. Saccharides are known to be polyamphiphilic surfaces due to the presence of hydroxyl groups which can act as hydrogen bond donors and acceptors. The electronegativity of the hydroxyl groups substituted on the ring distorts the electron density, drawing it away from the ring. This means that there is a slight negative charge surrounding the hydroxyls which in turn induces a slight positive charge on the carbon skeleton and aliphatic hydrogens leading to the perturbation of the surrounding shells of water.⁹

Water molecules are particularly important in biological interactions, this is due to their small size, degrees of translational and rotational freedom and ability to act as both hydrogen bond acceptor and donor via the electron density deprived hydrogen atoms and oxygen lone pairs. Water has been described by Lemieux as a molecular mortar, and serves as holding and stabilising binding partners in a particular conformation before, during and after an interaction.⁹

This perturbation and solvent interaction induced by the electronics of saccharides is relevant both on an intra- and intermolecular level. With oligosaccharides as small as trimers, one can observe the presence of “bridging” water molecules which are indeed structural and hold the oligosaccharide in a particular conformation.¹⁰⁻¹² This has also been seen intermolecularly with the Le^x dimer crystal solved by Perez *et al.*¹³

Therefore, as one considers how several molecules in close proximity exert particular structural changes on each other as well as the global change in the structured water, one can imagine that the polyamphiphilic surfaces implied by the specific organisation of hydrophilic / hydrophobic groups of one monosaccharide unit may indeed induce a large structural change in the global presentation of the glycoconjugates to their respective binding partners. This of course is another attribute to the myriad of structural variations of glycoconjugates at the

monosaccharide level and their ability to store and present vast quantities of glycoded information.

1.3 Lectins

Where DNA molecules with a base set of 4 provide the coding for our genetic make up, carbohydrates, with a myriad of base molecules are capable of communicating a code with a language many orders of magnitude more complicated. This carbohydrate language has been termed the *glycocode*, a specific 3D arrangement of carbohydrate molecules which is read and translated by carbohydrate binding proteins known as *lectins*. Lectins are protein structures which can read the glycocode without modifying them or invoking an immune response.¹⁴ In general, they are oligomeric proteins which contain several sub-units, at least one of which will contain a carbohydrate binding site. They can be of different sizes, specificities and exhibit dependencies on other complimentary elements in order to facilitate carbohydrate recognition (the presence of metal ions for example)¹⁴⁻¹⁶ as well as different 3D structural organisations of their sub-units (tetrahedral, planar etc). Lectins were first thought to be unique to plant cells; however lectins associated with bacterial, viral and higher organisms are now well documented. As they do not perform any biochemical process in their own right, it is thought that lectins are used by cells as a form of exploring the local environment, reading the glycocode and communicating to the host cell and are thus implied in the initial steps of several normal and pathological biological processes. These processes include cell aggregation and agglutination, immunity (gp120 of DC-SIGN), bacterial and viral infection.

1.3.1 Immunity

The role of lectins in innate immunity is well documented and includes examples such as the collectins and lectins found on dendritic cell (DC) surfaces. The collectins are a family of lectins involved in the agglutination and clearance of bacterial and viral organisms. The surfactant protein D (SP-D) and mannose binding lectins (MBLs) were used by Sorensen *et al.* for the detection and screening of the severe acute respiratory syndrome (SARS) coronavirus.¹⁷ They have also been shown to protect against opportunistic fungal pathogens.¹⁸ The dendritic cells act as pathogen scavengers in the body, foreign microorganisms which infiltrate the organism are captured and internalised by the DCs via the lectin DC-specific intracellular adhesion molecule-3-grabbing non-integrin (DC-SIGN).¹⁹ Once internalised,

they are transported to the lymphatic system and presented in antigenic form. This allows the T-cells present in the lymphatic tissue to organise an adaptive response in order to destroy the invading microorganisms. These mammalian lectins presented at the DC surface bind to specific carbohydrate epitopes presented by pathogens.⁶ These epitopes, or rather specific molecular patterns, are recognised as non-self and thus set off the immune system.

1.3.2 Bacterial infection

Many bacterial infections involve the secretion or release of toxins into the local environment. The cholera-causing bacteria, *Vibrio cholerae* is an example of such an organism. The bacteria release a multimeric lectin-based toxin which exhibits an AB₅-type structure.²⁰ The lectin domains (B) form a planar pentameric structure with all carbohydrate binding sites on one face. The toxin domain (A) is situated above the lectin sub-units. The role of the lectin domains is to explore the epithelial cell surfaces in the gut and bind to the cell surface glycolipid ganglioside GM1. Upon association with the cell surface, the toxin sub-unit invades the cell and activates adenylate cyclase stimulating mucosal cells in the small intestine, inducing diarrhoea in the host.²¹

Other pathogenic bacteria such as *Pseudomonas aeruginosa* and *Berkholderia cenocepacia* also use oligosaccharide-mediated recognition to adhere to host tissues. As part of their invasion strategy, they utilise several mechanisms in order to adhere to the host epithelial surface. They are known to have carbohydrate-binding proteins located on the flagellum, as well as the pili. They also use soluble lectins which are located in the extracellular matrix or conjugated to the bacterial cell surface. Two soluble lectins have been identified in *P. aeruginosa*; the PA-IL and PA-IIL lectins which are similar in structure but exhibit specificities for galactosides and fucosides respectively.²² Soluble lectins identified in *B. cenocepacia* include BclA and BclB which have specificities for mannosides and fucosides respectively.^{23, 24} Both *P. aeruginosa* and *B. cenocepacia* affect the lungs and respiratory tract and pose a mortal threat to immuno compromised patients such as cystic fibrosis sufferers. The lectins are known to be implied in the initial interactions of the pathogens with the host surface, initiating adhesion and aiding in biofilm formation which in turn leads to antibiotic resistance. Indeed, carbohydrate based vaccines have been developed for various bacterial infections.^{25, 26}

1.3.3 Viral infection

The Influenza A virus is one of the most infectious human diseases and is responsible for recurrent annual epidemics. The H1N1 (Spanish flu) pandemic of 1918-1920 caused 20-50 million deaths worldwide, and the current H1N1 pandemic (Swine flu) has caused over 526 000 cases of infections with at least 6700 confirmed mortalities to date.²⁷ The virus is characterised according to two proteins found on its surface; haemagglutinin (H) and neuraminidase (N). The structure of these proteins differs from strain to strain to which the sub-types are numbered hence H1N1 referring to haemagglutinin type 1 and neuraminidase type 1. Influenza viruses are capable of infecting cells and crossing species barriers by modifying their specificities for host cell receptors. Host cells present glycoproteins terminating in sialic acid residues, which are common targets for many human bacterial and viral pathogens.^{28, 29} It is these residues which are exploited by influenza and other pathogens for recognition, attachment/invasion and host specificity processes. The role of the haemagglutinin protein being to bind these sialic acid residues. Once the lectin-carbohydrate interaction takes place, the viral membrane fuses with the host-cell membrane and thus invades the cell.³⁰(and references therein) In particular, the human influenza virus presents haemagglutinins which bind preferentially to NeuAc- α 2,6-galactose residues, as opposed to NeuAc- α 2,3-Gal for example in ducks and chickens. However, one concern presented by Dunham *et al.* with reference to the H5N1 (Bird flu) strain is that ducks and chickens present both the 2,3- and 2,6- sialic acid residues and are thought to allow infection by both human and avian viruses providing a route to genetic re-assortment and species crossover.²⁹ Carbohydrate based vaccines have also been developed for viral infections such as Relenza® (aka Zanamivir) for the influenza virus.³¹

1.3.4 HIV-1 infection

As mentioned above, it is thought that oligosaccharide epitopes conjugated to the viral coat interact with lectins at host cell surfaces and are recognised as non-self organisms. The HIV-1 virus takes advantage of this process in order to gain access to lymphatic organs and infect T-cells. The virus presents glycoprotein 120 (gp120), a high mannose structure, at high density and concentration at the viral coating. This in turn interacts with the DC-SIGN lectin present on the dendritic cell surface and the viral cell is internalised and transported.⁶

1.3.6 Cancer metastasis

A family of lectins known as the galectins, in particular galectin-1 is associated with malignant cancerous cells. The lectin is known to induce apoptosis in activated T-cells and so is directly involved in the auto-defence mechanisms adopted by cancerous cells to evade the host immune system. Galectin-1 expression is up-regulated or over-expressed in many cancer types such as prostate, breast and lung cancers. In breast cancer, it has also been implied in adhesion mechanisms and identified as a metastasis associated protein thus the lectin would aid in the invasion of other tissues via interactions with epithelial cell surfaces.³²(and references therein)

1.3.6 Lectin interaction with monosaccharides

Lectins often exhibit high specificity towards their binding partner, even at the monosaccharide level. Due to the number of stereocentres in a monosaccharide, subtle changes in its structure will induce large changes in its physico-chemical properties. Inversion of the stereochemistry will give rise to its epimer, and a different monomer structure. The C2 epimer of glucose is mannose, and due to this stereochemical inversion, mannose has a hydroxyl in the axial position. The same can be applied to the C4 epimer of glucose, which gives galactose. A change in monomeric structure will ultimately change the nature of the saccharide, in particular the electrostatic and potential hydrogen bonding surfaces. Ultimately dictating how the monosaccharide will interact with a binding partner. The electrostatic surfaces of methyl β -D-glucopyranoside and methyl β -D-galactopyranoside can be seen in figure 6.

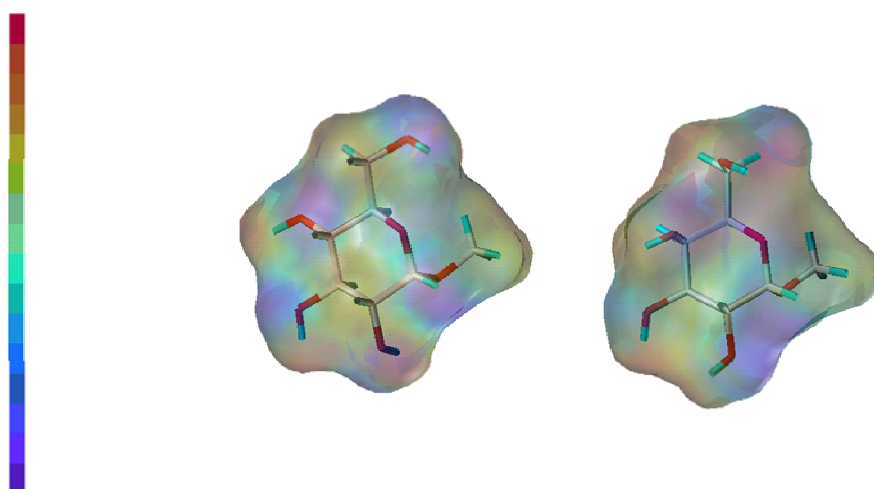


Figure 6 : Electrostatic potential surfaces of β -D-Glucose and β -D-Galactose. Blue surfaces indicate regions of electronegativity and red indicates electropositivity. Subtle changes in monomeric structure can lead to large differences in physico-chemical properties.

1.3.7 Lectin interaction with oligosaccharides

As mentioned earlier, oligosaccharides as macromolecules are considerably flexible, allowing multiple conformations to be accessible and adopted at any one time. Due to this structural heterogeneity, one oligosaccharide can present itself in several different conformations altering their topography and influence on the 3D space around them. Typically, lectins will recognise only one conformation, that which is most complimentary to the binding site, which may not necessarily be the lowest energy conformation.³³ As a result, one oligosaccharide can present itself as several topographically different molecules, allowing several different lectins to bind with them. Effectively, an oligosaccharide can transmit several messages which can be decoded by different lectins – each with their own interpretation of the glycode.

1.4 Lectin Architectures

As we have seen, lectins are found all through nature and are involved in many biological and biochemical processes. Their specificity, and thus their function, is related to their structure and architectural features defined by the amino acid sequences of their genetic make-up. This, like all proteins, directs the folding of the 2D linear peptide to the 3D structures giving rise to its specificity. The dimerisation or oligomerisation of several 3D structures gives the quaternary lectin structure leading to the multivalent nature of the protein and defining their overall function. The multimeric structure comprises of at least one carbohydrate recognition subunit linked to at least one other domain which may bind to other saccharides, other biomolecules, or conjugated to a protein subunit which may bind the lectin to a particular position of the cell (cell membrane, flagella, pili etc).

1.4.1 Con A

Concanavalin A (Con A) is a leguminous lectin from the jack-bean *Canavalia ensiformis* and is probably one of the most studied and characterised lectins. It adopts several isoforms depending on the environmental conditions. At a pH < 6, it exists as a homodimer whereas above pH 7 it exists as a homotetramer (or rather a dimer of dimers) with inter-binding site distances of ~70 Å as seen in figure 7.³⁴ Between pH 6 – 7, the lectin is in equilibrium between dimer and tetramer. The monomeric weight is 25.5 kDa, and each monomer contains one carbohydrate recognition domain and two metal binding sites. Con A is a C-type lectin,³⁵ requiring the presence of Ca²⁺ ions for activity and thus one Ca²⁺ ion occupies one of the

metal binding sites. The second metal binding site is reserved for a transition metal such as Mn, Co, Ni or Cd, all in the oxidation state II.³⁶ Due to the steric requirements imposed by several amino acids which form the topology of the binding pocket, Con A is specific for α -pyranose forms of mannosides and glucosides (which includes GlcNAc), which are C2 epimers of each other, with binding occurring between hydroxyl groups of the 3, 4 and 6 positions of the pyranose ring.^{37, 38} More specifically, cooperative hydrogen bonding occurs between the aforementioned hydroxyl groups and the binding pocket as well as hydrophobic stacking and Van der Waals interactions. Hydrogen bond networks are also formed which are mediated by water molecules. Indeed, five structural water molecules are displaced upon monosaccharide binding.³⁷(and references therein) Affinity for the mannoside is approximately 6 times greater than for the glucoside, (K_a of $1.2 \times 10^4 \text{ M}^{-1}$ and $2 \times 10^3 \text{ M}^{-1}$ for Me- α -D-Mannose and Me- α -D-Glucose respectively) and 12 times greater than GlcNAc ($1 \times 10^3 \text{ M}^{-1}$).^{39 40}

*Distance between anomeric carbon atoms of the Me-mannosides in the binding pockets taken as the inter-binding site distance.

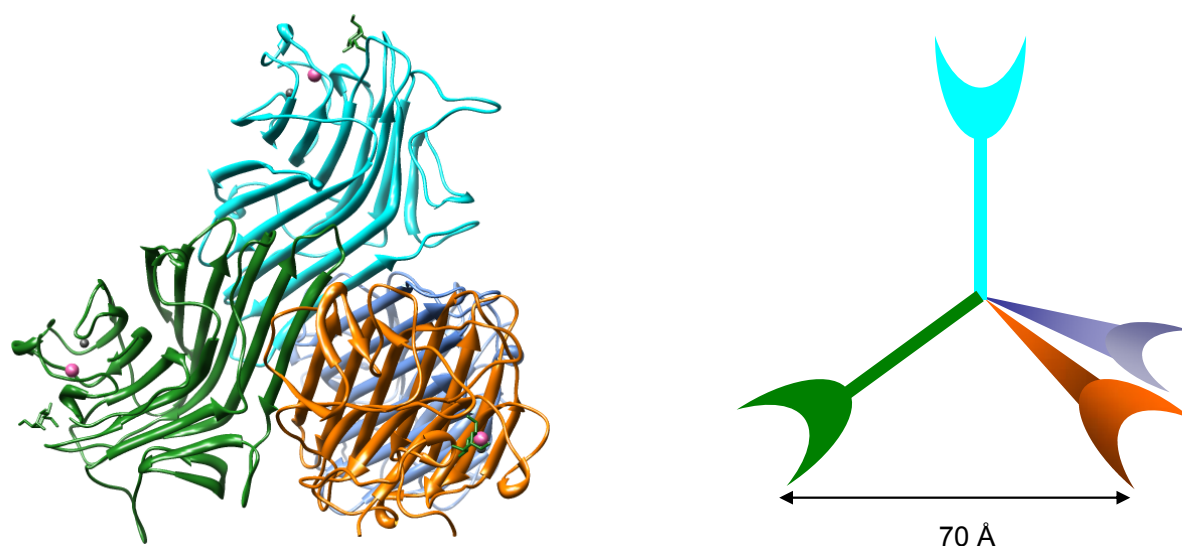


Figure 7 : Crystal structure of Con A complexed with Me- α -D-Man (left) and its tetrameric architecture (right).³⁴

Con A is known to have an extended binding site with an increased affinity for high-mannose oligosaccharides.⁴⁰ The binding modes of a number of ligands ranging from monosaccharides to oligo- and polysaccharides and de-oxy analogues have contributed to the wealth of knowledge collected on Con A, relating its particular structural features to its function. This lectin has become the model system for investigating protein-carbohydrate interactions. Also, due to its multimeric nature, it is also used as a model for studying the phenomenon of multivalence, and has been tested with a number of multivalent scaffolds ranging from small glycoclusters to polymers and dendrimers.

1.4.2 BclA

A lectin from *Burkholderia cenocepacia*, known as *Burkholderia cenocepacia* lectin A (BclA) is a recently-characterised soluble bacterial lectin implied in bacterial invasion and biofilm formation, particularly in patients suffering from cystic fibrosis.²³ This lectin is significantly smaller than Con A, forming homodimers in physiological conditions, with each monomer exhibiting a molecular mass of 13.8 kDa and an inter-binding site distance of ~40 Å (figure 8). Like Con A, BclA is a C-type lectin and each monomer contains one carbohydrate recognition domain which includes two Ca²⁺ ions directly involved in ligand binding. It is specific for mannose and is strictly limited to D-mannose and D-mannose-containing oligosaccharides. This specificity is related to a particular axial/equatorial arrangement of hydroxyls in the 2, 3 and 4 positions for direct coordination to the two Ca²⁺ ions and the topology of the carbohydrate binding site. The hydroxyls of positions 2, 3, 4 and 6 are also involved in hydrogen bonds to amino acids of the binding sites. Hydrophobic and aromatic interactions are also evident. For Me- α -D-Man, BclA exhibits an association constant ~25 times stronger than that of Con A (K_a of $\sim 3 \times 10^5 \text{ M}^{-1}$).

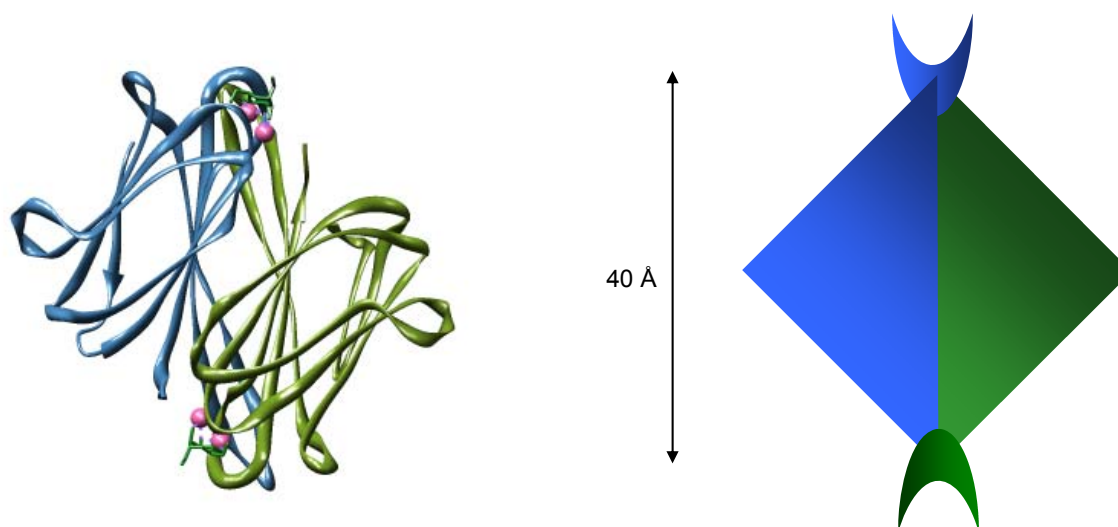


Figure 8 : Crystal structure of BclA complexed with Me- α -D-Man (left) and its dimeric architecture (right).²³

With respect to studying the binding of monosaccharides to BclA, this lectin is quite unique. Firstly, the association constant is relatively large, particularly for monosaccharide binding. Secondly, by isothermal micro-calorimetry (ITC), all previously studied lectins exhibit non-cooperative binding to their monosaccharide binding partners i.e. a 1 : 1 binding model is fitted to the ITC data and all of the binding sites are thought to interact independently of one another. However, in the case of BclA, it was found that the binding of one mannoside to one binding site facilitates the binding of the second mannoside to the second binding site; although with a lower affinity but higher enthalpy. Therefore a cooperative binding model was fitted to data obtained from BclA, giving information on both binding events.²³

BclA is relatively unknown in comparison to Con A, however several studies involving oligosaccharides have been carried out.²⁴ Interaction studies involving polymer-based micelles have also been conducted, taking advantage of the multivalent nature of both the lectin and the micellular scaffold.^{41, 42}

1.4.3 PA-IL

One of several lectins from *Pseudomonas aeruginosa*, LecA (PA-IL), like BclA is a soluble C-type bacterial lectin implied in bacterial invasion, surface adhesion, biofilm formation and antibiotic resistance. Again, this lectin, in combination with other *P. aeruginosa* lectins, is known to play an important role in pulmonary infections of patients suffering from cystic fibrosis.²² The lectin has a monomeric molecular weight of ~12.8 kDa, which associate to form tetramers under physiological conditions, with an elongated square-planar architecture

as shown in figure 9.^{16, 43} The inter-binding site distances were measured as 29, 78 and 82 Å in the x, y and diagonal axes respectively. Like BclA, PA-IL has a strict specificity however in this case for D-galactose and D-galactose-containing oligosaccharides. PA-IL is also known to bind GalNAc, although with a lower affinity, and adenosine.^{44, 45} Each monomer contains one carbohydrate binding domain and one Ca²⁺ ion. In the crystal structure of PA-IL co-crystallised with galactose, the formation of hydrogen bonds between hydroxyls in the 2, 3 and 4 positions can be seen whilst the hydroxyls of the 3 and 4 positions are also involved in complexing the Ca²⁺ ion. Hydrophobic interactions and bridging structural water molecules are also observed.¹⁶ For D-galactose, PA-IL exhibits a K_a of $3.4 \times 10^4 \text{ M}^{-1}$ as calculated by equilibrium dialysis.⁴⁶

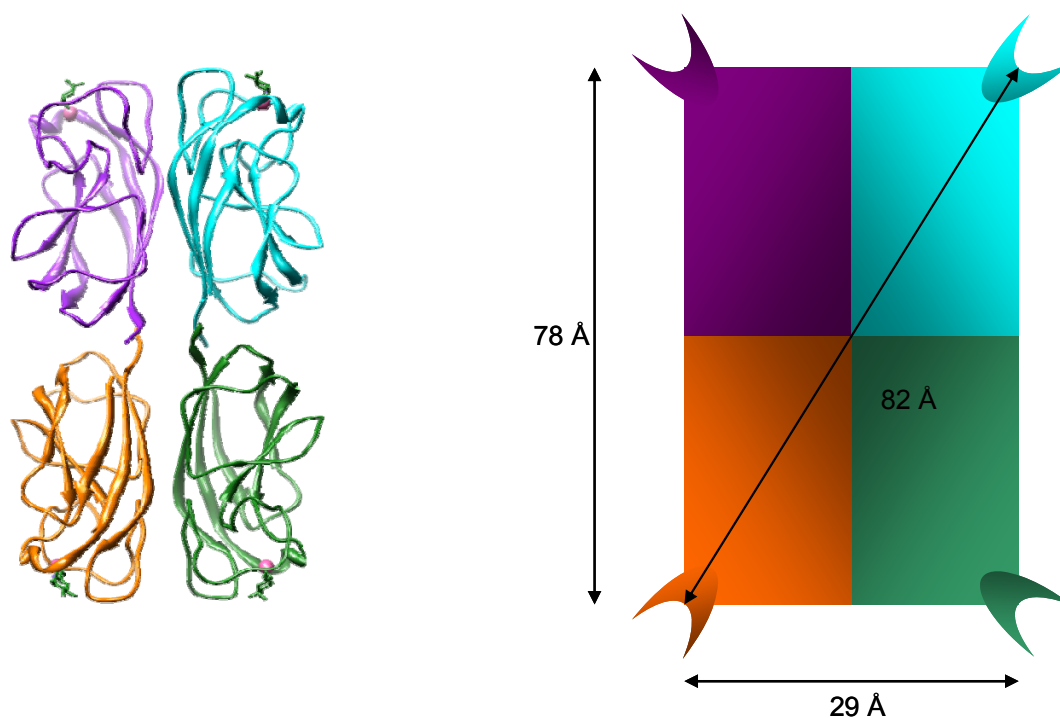


Figure 9 : Crystal structure of PA-IL complexed with Me-β-D-Gal (left) and its square planar architecture (right).¹⁶

When binding galactose and its monosaccharide derivatives, stereochemistry at the anomeric position is not so important. However, when binding disaccharides or higher oligosaccharides, only those with a terminal α- stereoisomer are allowed. Crystallography and molecular dynamics studies have shown that the penultimate galactose in the oligosaccharide makes a number of specific hydrogen bond and hydrophobic contacts with the lectin surface.⁴³ Due to its implied role in bacterial infection, PA-IL has become the target of several galactose-based

inhibitors. These include *neo*-galactosides which incorporate hydrophobic groups to form complimentary non-covalent bonds with the extended binding pocket as well as multivalent structures from dimers and other small architectures to polymeric and dendritic structures.^{43, 47, 48}

1.5 Multivalence

The valence of a material, an atom or molecule, macromolecule, protein or indeed a cell is defined as the number of separate, identical connections that can be made between that material and its binding partner(s). In general, this can be defined as a material presenting n binding sites which bind to n ligands, where $n > 1$. This of course would include the case where a material presenting n binding sites interacts with a second material presenting n ligands, thus forming n interactions, where both the binding sites and ligands are presented multivalently (figure 10).

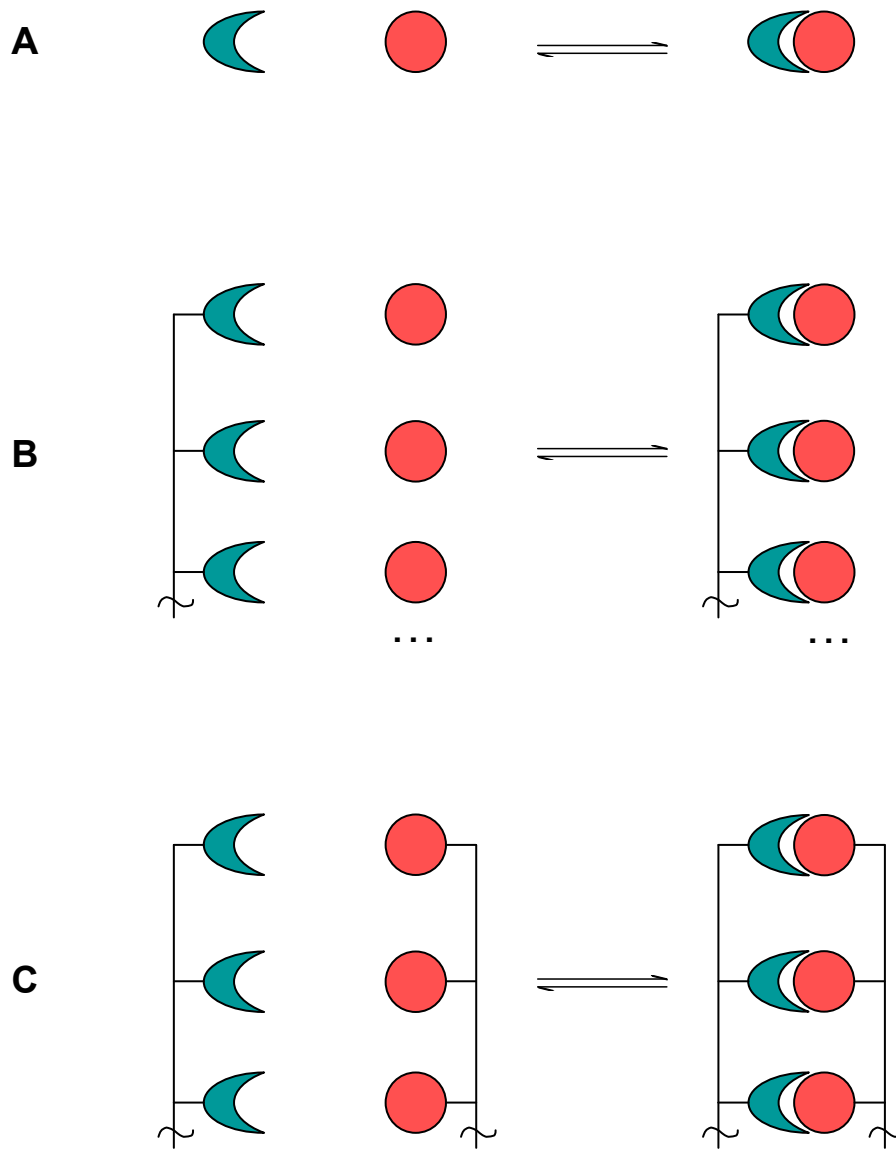


Figure 10 : Monovalent receptor binding with a monovalent ligand (A). Receptors presented multivalently binding with several monovalent ligands (B). Receptors presented multivalently binding with ligands presented multivalently (C).

These multivalent interactions occur frequently in biological systems, in many different situations as well as the synthetic world. The pairing of deoxyribonucleic acids may be considered as multivalent. As one DNA monomer pairs with its complementary partner, hydrogen bonds form between the two molecules. As a molecular pair, these hydrogen bonds are easily broken, resulting in the starting monomers. When a single strand of DNA binds to its complementary strand, all of the bases align with their binding partners to form the double helix, and thus a multitude of hydrogen bonds are formed. The intermolecular hydrogen bonding between the two strands becomes significantly more stable, so stable that enzymes, high energy radiation or chemical modification are required to break the DNA double strand.

Multivalence therefore, incorporates another dimension to binding interactions, as the physical, chemical and biological surfaces may indeed change upon the occurrence of multiple binding events. Indeed, at the biological level, many molecules which form non-covalent bonds exhibit only weak binding affinities for their ligands (compared to say biotin-streptavidin $K_d = 1 \times 10^{-15}$ M, $K_a = 10^{15}$ M⁻¹). If several binding domains are presented multivalently, the overall binding affinity of its ligands increase. This would result in a change in the physical properties of the non-covalent bonds formed, making the global interaction much more important.

1.5.1 Types of multivalency

Multivalence can range from one molecule to self-assembled monolayers and 3D platforms. Biological systems use various types of multivalency depending on the local environment and function. Several examples of lectins which exhibit diverse architectures related to their function have already been discussed. Con A and PA-IL for example are both tetrameric proteins with tetrahedral and planar structures respectively, with all carbohydrate binding sites facing different directions. PA-IL is a soluble lectin whose role may be to explore local environments (in solution or on surfaces) therefore its structure may reflect this purpose. The cholera toxin has an AB₅ architecture, with all lectin domains facing the same direction. This is indicative of its function – exploring 2D surfaces in order to find a suitable invasion site at the host cell membrane.⁴⁹ These lectins exhibit “architectural multivalence”, consisting of one macromolecular structure which presents several, equivalent carbohydrate recognition domains. Other lectins, such as the adhesins, are membrane bound and consist of a lectin structure which presents only one carbohydrate recognition domain, attached to fimbriae or flagella tethered to the cell surface.^{14,50} Several fimbrial structures clustered together at the cell surface would also give a multivalent presentation of the lectins at the extra cellular surface. The galectins, which are membrane bound and specific for β -galactosides, as well as other C-type lectins exhibit many different macrostructural formations giving rise to several different forms of multivalent presentation. Galectins-1 and 2 form homodimers in solution, whereas Galectin-3 exhibits a carbohydrate recognition (lectin) domain tethered to a non-lectin domain which form oligomeric structures in solution and on surfaces. Other galectins (-4, 8) form tandem repeat units, where the two carbohydrate recognition sub-units are attached via a (relatively) flexible linking molecule.^{14,51} The collectins are a group of mannose binding lectins (C-type III lectins) that associate together forming oligomers. Three subunits combine to form a trimer, the trimers are bound together via a collagen-like α -helix which is tethered

to the cell membrane. Trimer structures associate to form larger oligomers as bouquets of trimers (where all binding domains are presented adjacent to one another) or cruciform (cross-like) structures where 4 bouquet trimer sets present their recognition domains in four different directions.^{14, 51, 52} Biological systems take advantage of several modes of multivalence in many normal and pathological processes depending on their position and function (Fig. 11). Often, these systems will present a wide variety of different “tools” in order to increase the likelihood of successful interactions or invasion pathways.

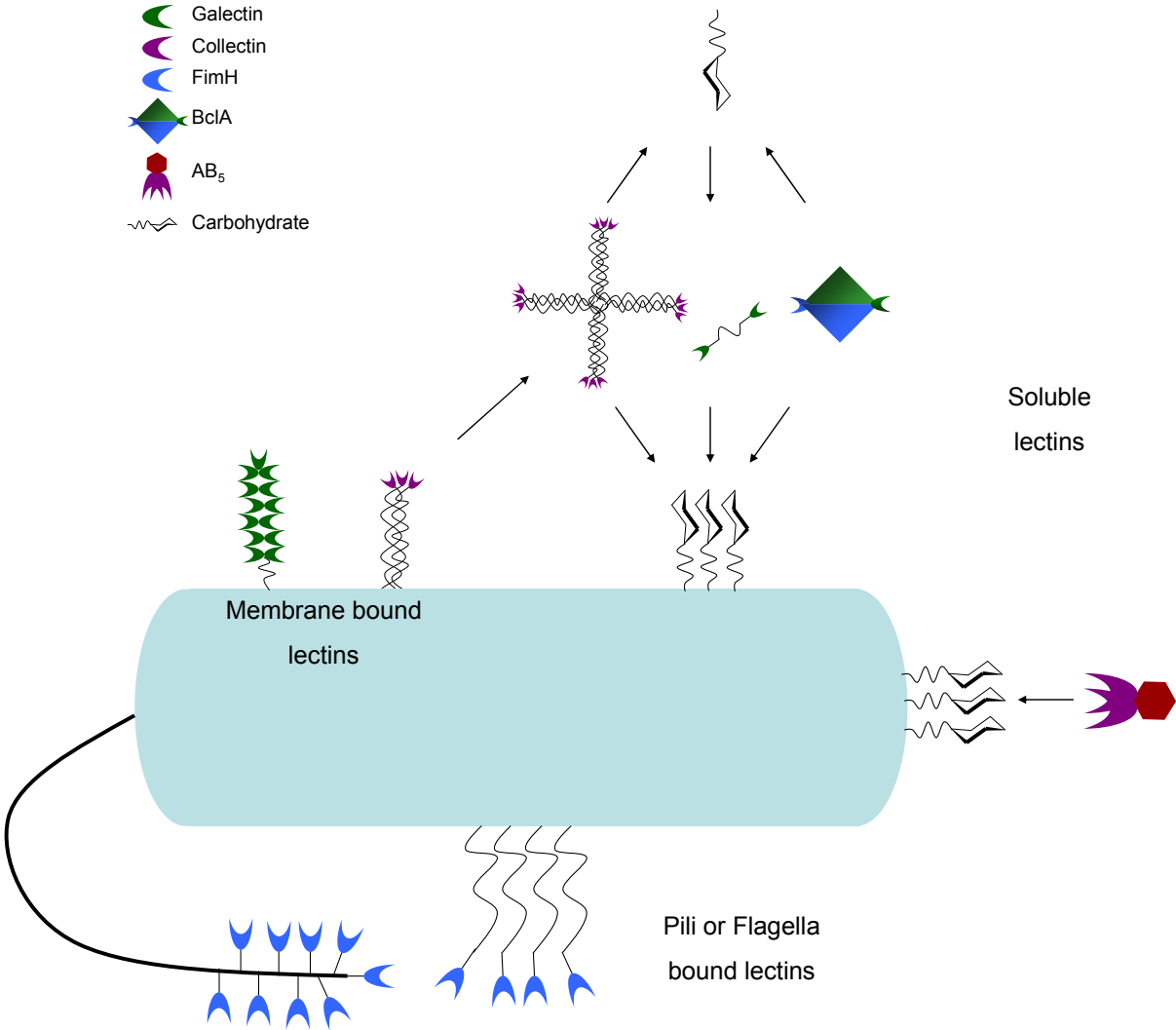


Figure 11 : Different modes of multivalence observed in biological systems (not to scale).

1.6 Cluster Glycoside Effect

Increasing the clustering of receptors allows for several identical interactions to take place. This increase in local valency will therefore increase the overall interaction strength. This is often seen in biological systems in order to increase the interaction strength of typically weak binding partners and has been suggested as being evolutionary in nature, being easier to multiply the number of binding sites to increase binding strengths than evolving more complex binding partners.⁵³ However, an effect which is seen throughout biology where multivalence occurs is that the global interaction appears stronger than the sum of the individual monovalent interactions. This phenomenon is often seen between lectins and their carbohydrate binding partners, and is known as the “cluster glycoside effect”.⁵⁴ Typically, the cluster glycoside effect is common to most lectins. However, this effect is noted even more so when the multivalent lectins bind with carbohydrates that are also presented multivalently. It is thought that a complementarity is observed between the binding sites of the lectin and the carbohydrate molecules which augments binding strength.

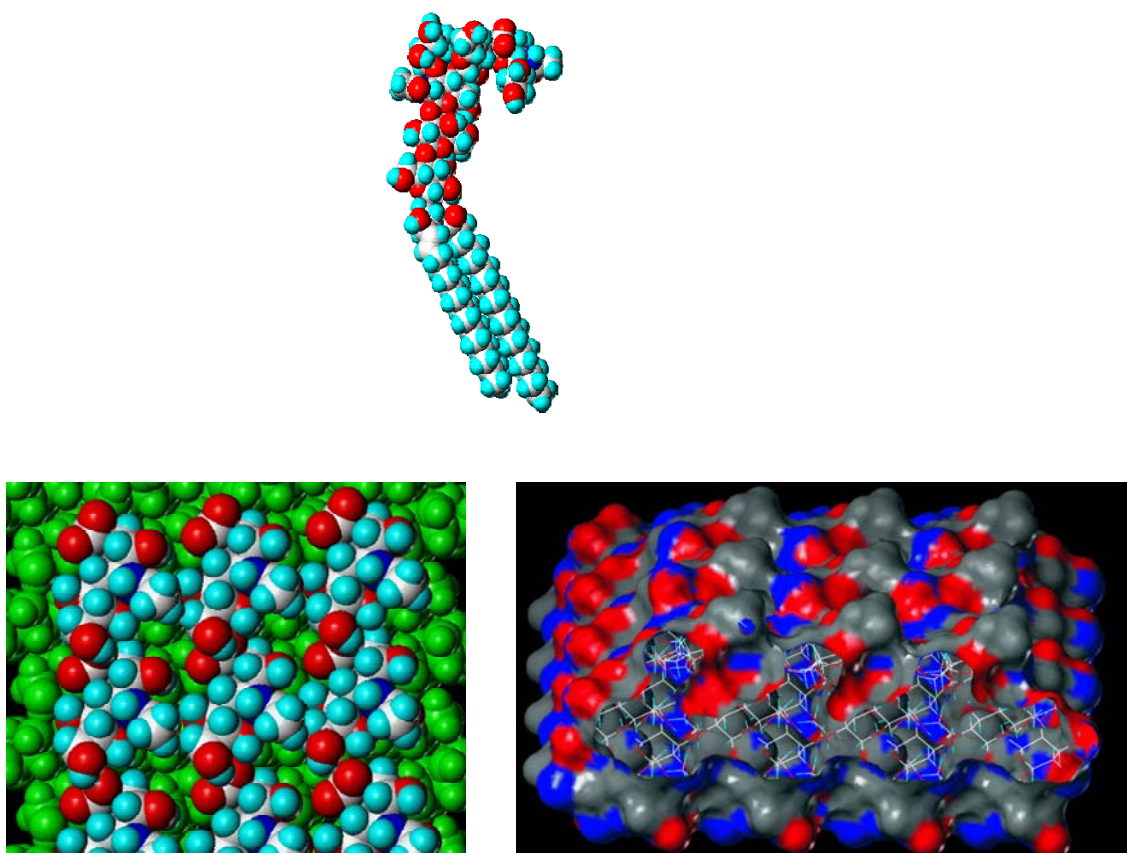
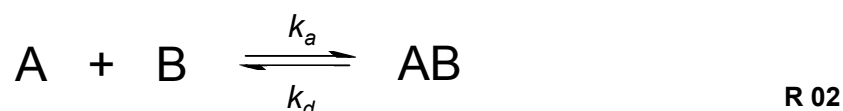


Figure 12 : Above: SialylLe^x Below: Several SialylLe^x molecules conjugated to a 2D surface, view from above, coloured by atom type (left) and hydrogen bond potential (right).⁵⁵

In figure 12, above, one can see a single sialyl Lewis x molecule (above, centre). Several of these molecules have then been fixed to a 2D surface, as they would be presented at the cell surface.⁵⁵ The diagrams on the bottom show the birds-eye view of these molecules, as seen by an extra-cellular object such as a lectin. The diagram on the bottom right shows the molecules coloured by hydrogen-bonding potential. Clearly, the interactions experienced by the lectin at the outside of the cell is not only a multiplication of several monovalent interactions, rather it experiences the effects of several closely-knit molecules on the surface. One analogy is the presentation of a single tree, when in fact one should consider the whole forest canopy. In the following discussion, the principles and the kinetic and thermodynamic explanations of the cluster glycoside effect will be explained with reference to lectin-carbohydrate interactions.

1.6.1 Monovalent reaction kinetics

First, we shall consider these interactions at the monovalent level. If we take the example of figure 10(A), the monovalent association of a ligand to its receptor. We will assume that the reaction follows the typical reaction kinetics and thermodynamics where:



A is one binding partner, B is the second binding partner, AB is the bound complex and k represents the reaction constant for the forward (association) and reverse (dissociation) reactions. From the van't Hoff equation, one can link the effects of association constant (a kinetic parameter) to the Gibbs free energy (G , a thermodynamic parameter).

$$\Delta G^{mono} = -RT \ln K_a^{mono} = \Delta H^{mono} - T\Delta S^{mono} \quad \text{E 01}$$

The Gibbs free energy is in turn associated with the enthalpy (H) and entropy (S) of the interaction. Thus one can see the dependence kinetics and thermodynamics have over each other, and the dependence on temperature.

1.6.2 Monovalent Thermodynamics

1.6.2.1 Enthalpy

The change in enthalpy, ΔH , is the difference between the final and initial enthalpic states of all components in the reaction, and can be separated into several components:

$$\Delta H^{mono} = \Delta H_{AB} + \Delta H_{conf} + \Delta H_{sol} \quad \text{E 02}$$

ΔH_{AB} represents the enthalpy change upon bond formation between the two reactants. In the case of lectin-carbohydrate interactions these non-covalent bonds may be hydrogen bonds between the hydroxyl groups of the carbohydrate and the amino acids of the binding pocket, as well as coordination bonds to metal ions or indeed aromatic stacking and stabilisation of hydrophobic surfaces on either binding partner. Van der Waals and dipole-dipole interactions may also be included in this term.

ΔH_{conf} represents the enthalpy change upon a particular conformational change of either binding partner. For example the rotation of hydroxyl groups in order to maximise hydrogen bond formation, the rotation of glycosidic bonds or the twisting or displacement of any large amino acid groups to better accommodate the ligand such as the histidine residue around the binding pocket of BclA,²³ or the “tyrosine gate” in FimH.⁵⁶

ΔH_{sol} is the solvent contribution to the enthalpy of the interaction. More specifically, this would represent the making and breaking of hydrogen bonds between the solvent molecules and the binding pocket, the carbohydrate ligands and bulk solvent upon the displacement of ordered water molecules during lectin-carbohydrate binding (figure 13).

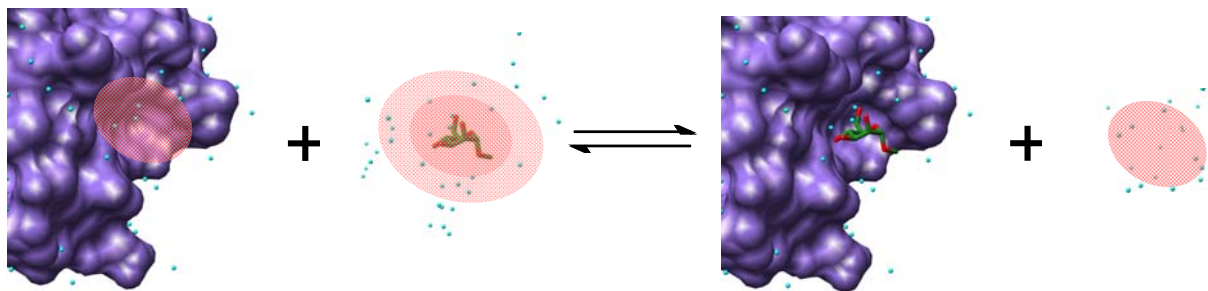


Figure 13 : Enthalpy changes during lectin-saccharide interactions. The red shaded regions represent regions of ordered water, where hydrogen bonds with solvent molecules would occur. Upon interaction, these hydrogen bonds are broken and replaced by non-covalent

bonds between the lectin and the saccharide. These regions of ordered water are thus expelled to the bulk solvent where they form hydrogen bonds between themselves and the bulk solvent.

1.6.2.2 Entropy

The change in entropy, ΔS , is the difference between the final and initial entropic states of all components in the reaction and represents the change in disorder of the system during association of the reactants. Like enthalpy, entropy can be separated into several components:

$$\Delta S^{mono} = \Delta S_{rot} + \Delta S_{trans} + \Delta S_{conf} + \Delta S_{sol} \quad \text{E 03}$$

The translational entropy, ΔS_{trans} , of a molecule arises from its freedom to translate independently through space in any of the x, y and z axes. It also refers to the translation of individual atoms or groups of atoms within the molecule, giving rise to bending and stretching of covalent bonds within the molecule however these will not be considered here.

ΔS_{rot} refers to the entropy of rotational which arises from the free rotation about the principal axes by the molecule. ΔS_{rot} is also related to the rotational freedom of individual atoms and groups of atoms. The protein structure will not change greatly upon interaction with its ligand. However, particular groups in or around the binding pocket may find themselves restricted rotationally upon ligand binding where before they were not. The saccharide however will experience conformational restrictions imposed by the sterics of the binding pocket, ΔS_{conf} .

In particular, the rotational and translational freedom of the saccharide molecule will be dramatically reduced upon entering the binding site. In free solution, the saccharide is free to rotate and translate in all (x, y and z) dimensions. As the saccharide becomes bound, translation will be restricted as the lectin-saccharide complex becomes one entity. Rotation about the axes will be severely restricted due to the multiple non-covalent bonds formed between the reactants. Hydroxyl groups will be “fixed” by hydrogen bonding and coordination to metal ions. Glycosidic torsions will also be restricted due to the steric requirements of the binding site which would lock the saccharide in a particular conformation.

Finally, ordered solvent molecules in the binding pocket and those surrounding the saccharide molecules will be displaced to the bulk solvent upon interaction, contributing to an increase in the disorder of the system, ΔS_{sol} (figure 14).

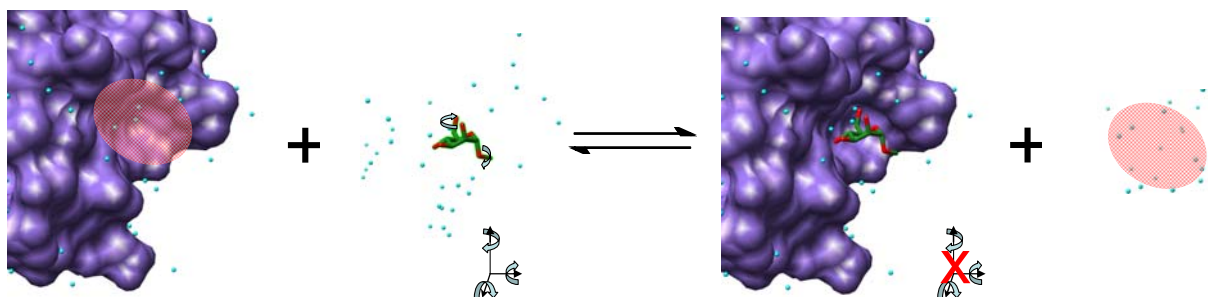


Figure 14 : Saccharide freedom of translation and rotation about x, y and z axes as well as conformational freedom about the glycosidic bond and hydroxyl groups. This freedom of movement is restricted in the protein binding pocket. The red regions represent regions of ordered water expelled to the disordered bulk.

1.6.3 Monovalent to multivalent

Described above are the various contributions to the enthalpy and entropy of a monovalent lectin-saccharide interaction. These in turn influence the Gibbs free energy of this monovalent event which itself influences the kinetics of the interaction. The association constant representing the affinity of the lectin for its monovalent ligand. However, on a multivalent scale, one must also consider additional contributions to the enthalpy and entropy in addition to the monovalent contributions discussed above, and their influence on the kinetics of the interaction.

1.6.3.1 Multivalent kinetics and free energies

In figure 10(A) we showed the monovalent association of two binding partners. As the valency increases, the free energy released upon multiple independent interactions increases also. With a given number of n independent interactions, the quantity of free energy released can be denoted as $\Delta G^{mul,n}$. The average free energy released can be described as the total free energy released for all interactions divided by the total number, n , of interactions.

$$\Delta G_{avg}^{mul,n} = \frac{\Delta G^{mul,n}}{n} \quad \text{E 04}$$

Similar statements can be made with respect to the association constant, K_a , using the van't Hoff equation where:

$$\Delta G_{avg}^{mul,n} = -RT \ln K_{a,avg}^{mul,n} \quad \text{E 05}$$

$$\frac{\Delta G^{mul,n}}{n} = -RT \ln K_{a,avg}^{mul,n} \quad \text{E 06}$$

$$\Delta G^{mul,n} = -RT \ln (K_{a,avg}^{mul,n})^n \quad \text{E 07}$$

$$K_a^{mul,n} = (K_{a,avg}^{mul,n})^n \quad \text{E 08}$$

Assuming of course that the interactions were independent of one another, one can see that in fact:

$$\Delta G_{avg}^{mul} = \Delta G^{mono} \quad \text{E 09}$$

and

$$K_{a,avg}^{mul} = K_a^{mono} . \quad \text{E 10}$$

However, multivalent lectin-carbohydrate interactions often exhibit an association constant much greater than that seen for their monovalent counterparts. Therefore, there are several factors that cannot be explained by the increase in valency. As these factors result in increased kinetic activity of the interaction, they must play a significant role in the thermodynamics of the system on a molecular level.

1.6.3.2 Cooperativity

The average free energy released upon the interaction of a lectin binding site presented multivalently and their ligands (which may or may not be presented multivalently) may be equal to its monovalent analogue. However, the average free energy released may also be greater than, or less than the monovalent analogue. This difference is defined as the “cooperativity”, the degree of which is defined as α .

$$\Delta G_{avg}^{mul,n} = \alpha \Delta G^{mono} \quad \text{E 11}$$

If α is equal to one, no cooperativity is observed in the multivalent interaction in comparison to its monovalent analogue. Positive and negative cooperativity is observed if α is greater

than or less than 1 respectively. Cooperativity will thus have a direct effect on the kinetics of the interaction:

$$K_a^{mul,n} = (K_{a,avg}^{mul,n})^{\alpha n} \quad \text{E 12}$$

Positive cooperativity occurs when the interaction of one ligand to one binding site increases the affinity of the other binding sites, facilitating the following binding events. The most well known example of this in biological systems is the association of oxygen to tetrameric haemoglobin.⁵⁷ The free energy released upon the binding of the second oxygen molecule is significantly higher than that of the first. Negative cooperativity would occur when the binding of the first ligand to the first binding site impedes the binding of the second ligand to the following site.

However, as the cooperativity factor has an exponential influence on the association constants, an interaction which has an enhanced multivalent affinity with respect to the monomer ($K_{avg}^{mul,n} > K_a^{mono}$) may exhibit negative cooperativity but a significant enhancement of affinity all the same. I.e. tight binding would not necessarily require positive cooperativity, only sufficient affinity enhancement ($\alpha > 1/n$). This has been labelled the affinity enhancement factor, β , by Whitesides *et al.* where the enhancement factor is a ratio of the global affinity constant to the monomeric association constant :⁵⁷

$$\beta = \frac{K_a^{mul,n}}{K_a^{mono}} \quad \text{E 13}$$

In terms of free energies, this becomes:

$$\Delta G^{mul,n} = -RT \ln K_a^{mul,n} \quad \text{E 14}$$

$$\Delta G^{mul,n} = -RT \ln(\beta K_a^{mono}) \quad \text{E 15}$$

$$\Delta G^{mul,n} = \Delta G^{mono} - RT \ln \beta \quad \text{E 16}$$

When investigating the interaction between a multivalent receptor and several monovalent ligands, cooperativity and enhanced affinity typically emerge from structural changes in the

receptor which are induced by the first binding event. From the perspective of the ligands, no change occurs – each individual ligand acts independently to the others, and does so without memory. However, when considering the binding of a multivalent ligand to a multivalent receptor, the binding of one ligand would direct or hinder the following binding events, depending on the nature of their multivalent presentation, which in turn would influence the thermodynamics and kinetics of the following interactions. In order to study the reason for this affinity enhancement, one must look closer at the enhanced free energies and their enthalpic and entropic contributions to explain what results in this enhanced affinity, cooperative or not, from presenting ligands multivalently.

1.6.3.3 Enthalpies of multivalent interactions

The multimeric free energy, $\Delta G^{mul,n}$, consists of its enthalpic and entropic components where:

$$\Delta G^{mul,n} = \Delta H^{mul,n} - T\Delta S^{mul,n} \quad \text{E 17}$$

ΔH^{mul} representing the total enthalpy change for the multimeric interaction which will be related to the enthalpy change of the monomeric interaction.

$$\Delta H^{mul,n} = \alpha n \Delta H^{mono} \quad \text{E 18}$$

α , being as before, the cooperativity coefficient and n , the number of individual binding events. If $\alpha > 1$, the overall enthalpy observed will be greater than the sum of the individual enthalpies. The multivalent interaction is enthalpically enhanced. If $\alpha < 1$, the overall enthalpy observed will be less than the sum of the individual enthalpies, resulting in an enthalpically diminished multivalent interaction.

If we take the example of a dimeric lectin interacting with two monovalent ligands, figure 15(A). The two monovalent ligands interact with the two binding sites in the same fashion. Therefore, the enthalpy involved in the dimeric interaction is double the amount of the monovalent interaction. In the case of a divalent ligand interacting with the divalent receptor, several situations can occur depending on the nature of the linkage between the ligands. Firstly, the linking molecule can be of ideal length to present the two ligands in a fashion complimentary to the receptor binding sites (case B). This means that no effort is required by

the linker to modify the presentation of its ligands, its enthalpic contribution is negligible and the second intramolecular interaction occurs as in case A. In case C, the linking molecule is shorter than the ideal length. The first interaction occurs as before, as this first interaction is independent of the linker molecule. However for the second, intramolecular interaction, to occur the receptor has to alter the position and orientation or conformation of the binding sites. This invokes an energy penalty reducing the observed enthalpy for this second interaction. Likewise for situation D where the linker is too long and rigid. The second interaction has to pay a conformational enthalpy penalty in order for the linker molecules to present the ligands in the correct fashion. In this case, the flexibility of the linker will play an important role. A rigid linker would have to pay a large conformational enthalpy penalty, whereas a flexible linker would pay only a small penalty. Generally, the more conformationally rigid a multivalent entity is, the more likely small spatial mismatches between ligands and receptors will result in enthalpically diminished interactions.⁵⁷

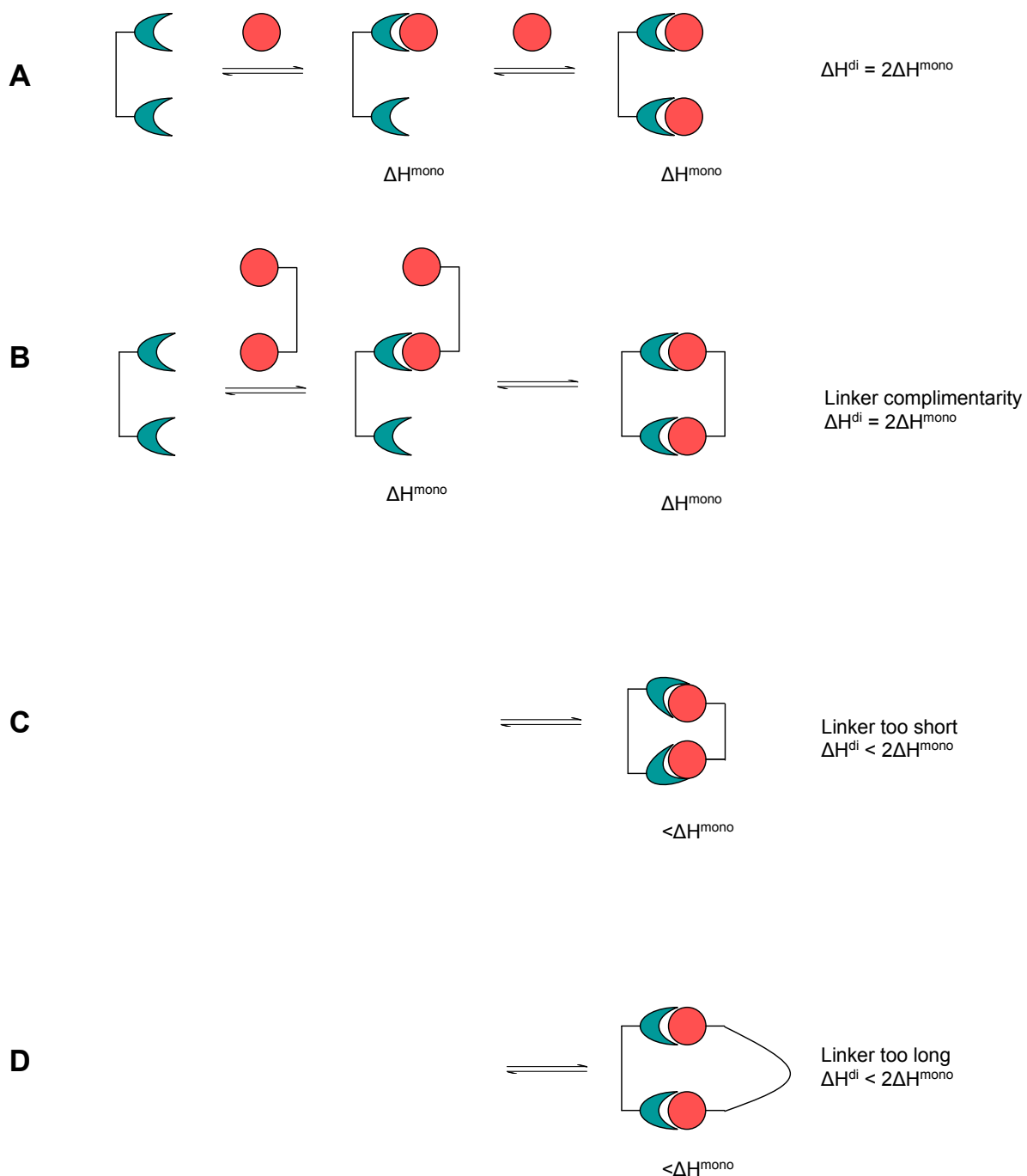


Figure 15 : Bivalent interactions occurring under ideal (A) and non-ideal (B-D) circumstances.

In case C, where the linker molecule is too short, it is unlikely that the receptor will alter its conformation in order to accept the second ligand in an intramolecular interaction. Probably, the receptor will accept only one ligand presented, the second binding site being free to interact with a second bivalent ligand intermolecularly, thus removing the enthalpic penalty (figure 16(A)). In case D, where a long, rigid linker is used, it may be more beneficial for the bivalent linker to bind itself to two separate receptor molecules (figure 16(B)). The above situations where intermolecular association is more favourable than intramolecular

association may lead to the formation of aggregates via ligand-receptor cross-linking. These aggregates may grow in size and become insoluble in the media, resulting in irreversible precipitation.

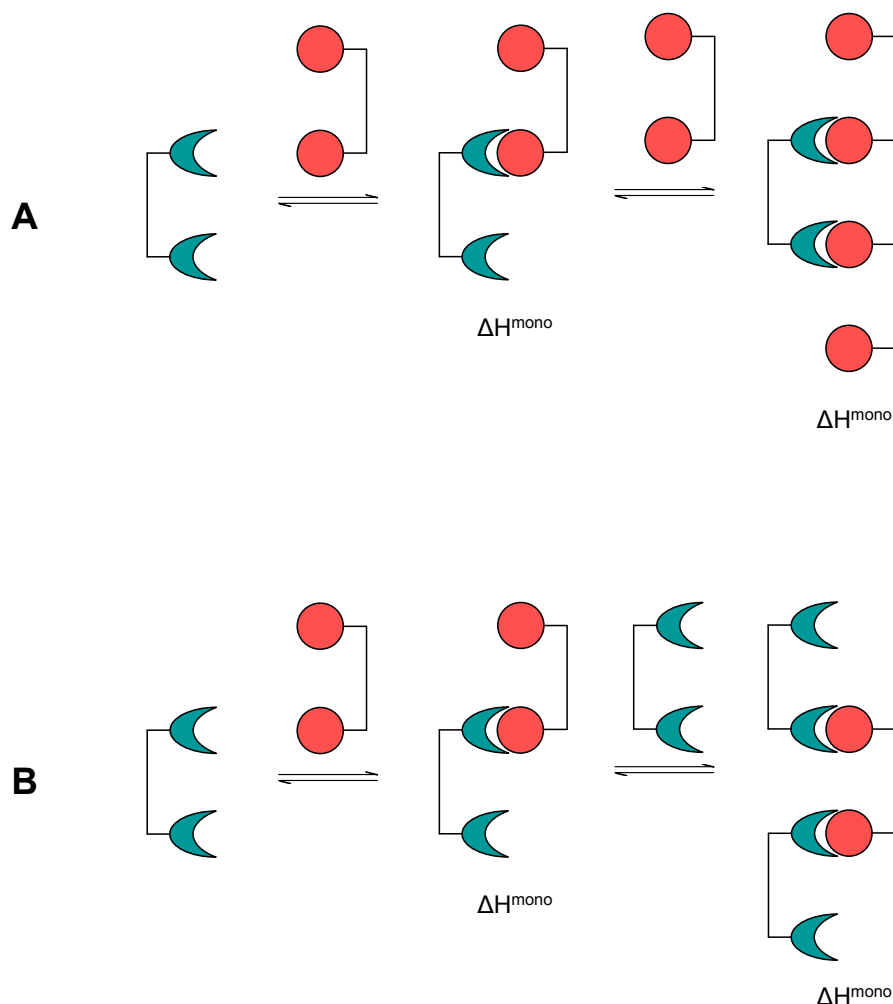


Figure 16 : The alternative intermolecular interactions for bivalent ligands of non-ideal presentation.

One can summarise the multivalent enthalpy change as contributions from the monovalent enthalpy change and the conformational enthalpy dictated by the linker molecule used in the multivalent ligand architecture as follows:

$$\Delta H^{mul} = n\Delta H^{mono} + (n - 1)\Delta H_{link,conf}^{mono} + \Delta H_{link,sol} \quad \text{E 19}$$

The $\Delta H_{link,conf}^{mono}$ term representing the conformation enthalpy penalty induced by the size and rigidity of the linker molecule. The $(n - 1)$ comes from the fact that the first binding event

would not have to pay this conformational enthalpy penalty, only the subsequent binding events. This statement of course assumes that the following binding events would experience identical conformational constraints. $\Delta H_{link,sol}$ refers to the influence of the linker molecule on the surrounding solvent molecules. Depending on the proximity of the linker molecule to the binding domains of the receptors, it may displace ordered water molecules to the disordered bulk, meaning that hydrogen bonds between the receptor and the ordered solvent molecules will be broken upon displacement, and hydrogen bonds to the bulk solvent will be formed. Also, ligands which are presented multivalently may interact with each other, independent of the linker molecules, via hydrogen bond networks. The breaking of this network would also contribute to the overall enthalpy of the interaction.

1.6.3.4 Entropies of multivalent interactions

When moving from a monovalent to a multivalent system, the entropies involved change dramatically. Particularly when considering intramolecular associations. As with the case for enthalpy, the multivalent entropy change (ΔS^{mul}) will be related to the entropy change experienced by each ligand with respect to translational and rotation degrees of freedom of the ligand as it is immobilised in the binding pocket, as well as the release of ordered water molecules (ΔS^{mono}). In the multivalent system, one must also include the effect of linker molecule conformation ($\Delta S_{link,conf}$) and associated solvent effects ($\Delta S_{link,sol}$). Thus, the multivalent entropy contribution can be described as:

$$\Delta S^{mul} = n\Delta S^{mono} + \Delta S_{link,conf} + \Delta S_{link,sol} \quad \mathbf{E\ 20}$$

In the monovalent system, the entropy change was related to the rotational and translational degrees of freedom of the ligand and receptors before and after intermolecular association as well as the entropy related to conformation and solvent effects. By considering case A presented in figure 16, the interaction of a bivalent receptor with two monovalent ligands, the change in entropy (ΔS^{mono}) will be the same for both interactions as, again, the two ligands will be interacting independently of each other and without memory. In terms of molecularity, this would be disfavoured entropically as it would involve the conversion of three entities into one, causing the loss of a total of 12 degrees of translational and rotational freedom (3 translational and 3 rotational for each ligand). This loss of independent translational and rotational freedom has also been referred to as the Gibbs connections energy.⁵⁸ In case B,

where the bivalent ligand is ideally presented, the interaction of a bivalent ligand would again be entropically disfavoured (however less so than the monovalent situation) as this would involve the conversion of only two entities to one, causing the loss of only 6 degrees of rotational and translational freedom i.e. the entropic cost of the perfect bivalent ligand will be half of that of two monovalent ligands. It is for this reason that ΔS^{mono} has to be corrected to $\Delta S^{mono'}$ for multivalent ligands:

$$\Delta S^{mono'} = \frac{l}{n}(\Delta S_{rot} + \Delta S_{trans}) + \Delta S_{conf} + \Delta S_{sol} \quad \text{E 21}$$

Where l is the total number of multivalent ligands associated to the multivalent receptor and n remains as before, the total number of individual receptor-ligand interactions. This means the first ligand-receptor interaction would pay the entropic penalty, whereas the second intramolecular interaction would not, meaning that this interaction occurs with a greater free energy change and hence greater affinity. Therefore this second, intramolecular interaction would be entropically enhanced.

The $\Delta S_{link,conf}$ term in the above statement comes from the inclusion of the linker molecule and its associated degrees of freedom. Assuming that the linker molecule is again perfectly shaped, rigid and conformationally locked (allows for no free rotation about its bonds) the entropy change for intramolecular association ($\Delta S_{link,conf}$) will effectively be zero (figure 17, B). This however is very unlikely, as all linker molecules would assume some form of flexibility (meaning $\Delta S_{link,conf} < 0$, unfavourable), figure 17, C. A linker molecule which is suitable and rigid would require only small entropic constraints ($\Delta S_{link,conf} < \Delta S^{mono}$) and would therefore be in the interests of both molecules to form the second intramolecular interaction, still being entropically enhanced. If, however, the linker molecule is unsuitably shaped or too flexible, this conformational entropy penalty would be very large. If this conformational entropy penalty is larger than the entropic penalty of the monomeric interaction $\Delta S_{link,conf} > \Delta S^{mono}$ (figure 17, C), it would become more economical to form a second intermolecular interaction, than to continue with intramolecular association, as the intramolecular interaction would no longer be entropically enhanced.

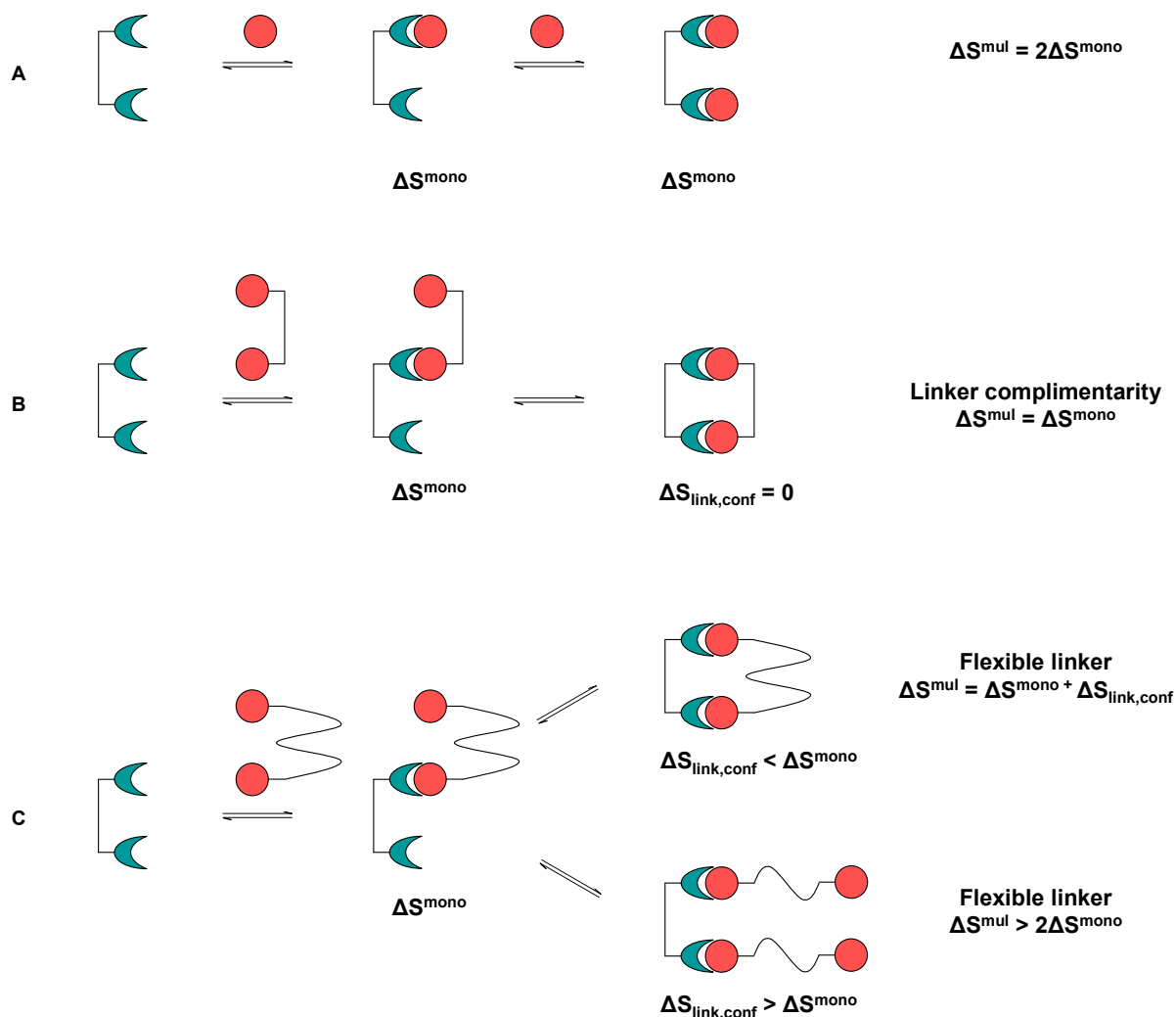


Figure 17 : Change in entropy for multivalent interactions. A: When the linker molecules is perfect for intramolecular association. B: Linker molecule is too flexible, intermolecular interactions may be favoured.

In the case where the entropic penalty of linker conformation equals that of the monomeric interaction, an equilibrium between intra- and intermolecular interactions would occur, as seen in figure 17(C).

$\Delta S_{\text{link,sol}}$ comes from the effect of the linker molecule on the local solvated environment. Assuming that the linker molecule does not affect the ligand-receptor interactions, $\Delta S_{\text{link,sol}}$ will be zero. However, this may not always be the case. The linker molecule may disrupt the organisation of water molecules around the ligand before or during interaction. Therefore, the organised water around the ligand which would be displaced by the receptor binding site upon multivalent interaction may be different to the monovalent interaction due to the influence of the linker molecule. Likewise, organised water molecules around the linker molecule, which

would not be present in the monovalent ligand, may find themselves displaced by the receptor binding site. Also, if the linker molecule interacts in some way (hydrophobic interactions or aromatic stacking for example) the linker may displace ordered water molecules associated with the protein surface which may not have otherwise been disturbed. Finally, the ligand in the monovalent form may organise water around itself in a particular fashion. Upon multivalent presentation, independent of the linker molecule, ligand molecules may associate together by forming close-knit networks of hydrogen bonds and ordered water molecules. Carbohydrate molecules are particularly effective at organising intermolecular hydrogen bond networks (figure 18).

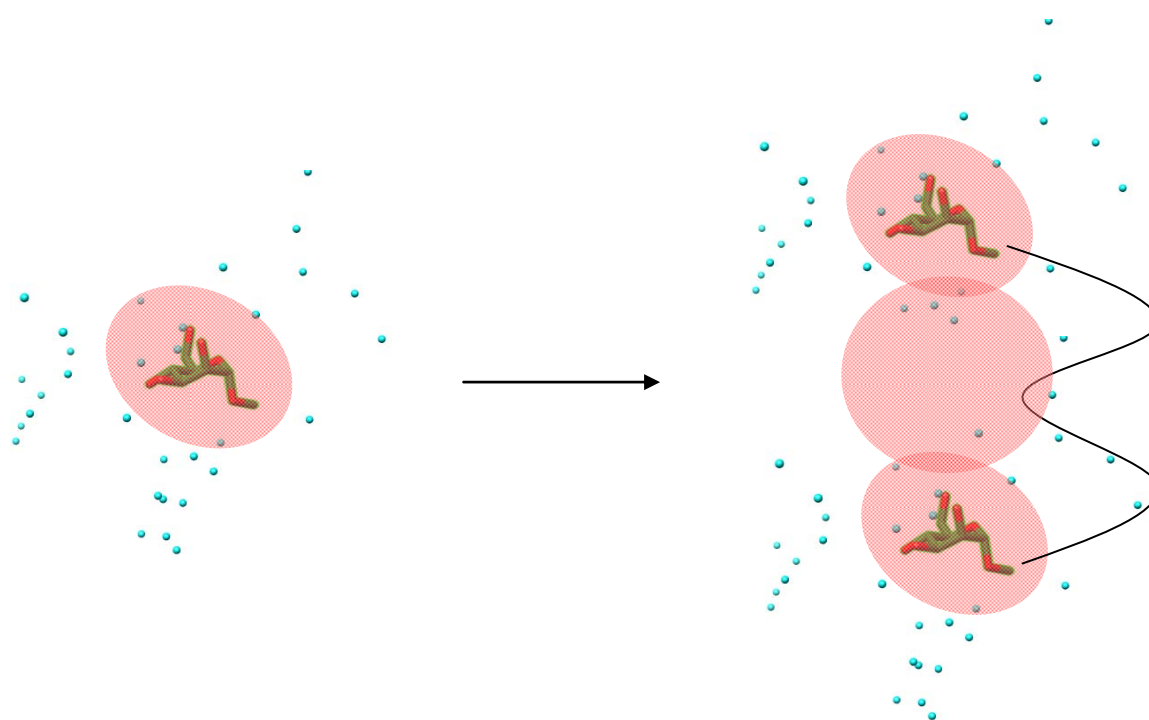


Figure 18 : Representation of inter-ligand hydrogen bond networks formed upon multivalent ligand presentation. Regions of ordered water molecules shaded in red.

1.6.4 Enthalpic and entropic contributions to multivalent free energies of interaction

Above we have discussed the enthalpic and entropic contributions to the Gibbs free energies for both monovalent and multivalent binding. Both the enthalpic and entropic contributions can influence whether an interaction will proceed intramolecularly and multivalently or intermolecularly. From the monovalent to multivalent situations, many factors must be considered as the global interaction becomes more complex. Clearly, the nature of the linker plays a crucial role in influencing ligand-receptor interactions at the multivalent level. In order to influence multivalent binding over aggregation, linker molecules need to be designed

correctly with respect to the target receptor. Presentation of ligand molecules with the correct spacings, conformationally rigid architectures in order to minimise the conformational restraints to be imposed on the ligands as well as incorporating flexibility to maximise the fitting of the ligand-receptor pairs are all important factors in multivalent binding from a thermodynamic point of view.

1.6.5 Effective concentration

The above description of the multivalent effect is based solely on the thermodynamics of the system, which in turn define the Gibbs free energy and its resultant effect on the association constant. Essentially, the multivalence effect (and thus the cluster glycoside effect) was analysed in terms of entropy and is a concept brought by Whitesides *et al.*⁵⁷ An alternative binding model can be used to describe multivalence, in terms of *effective concentrations* (C_{eff}) which was proposed by Kramer *et al.* and applied to carbohydrate-protein interactions by Lees *et al.*^{59, 60} The example by Huskens *et al.* describes the interaction of a β -cyclodextrin receptor dimer with a bis-adamantyl ligand. The bivalent interaction should be treated as a two stage system with an initial intermolecular interaction, followed by a second intramolecular interaction.⁶¹ This first interaction obliges the second ligand of the dimer to be in close proximity to the second available binding site. Therefore, this second binding site experiences a localised high concentration of neighbouring free ligands. If this local concentration density is greater than the ligand concentration in the bulk solution, intramolecular (multivalent) binding will be favoured.⁶² Thus the term effective concentration (C_{eff}) represents this local concentration density experienced by both the ligand and receptor. The theory of effective concentration thus gives a concentration dependent association constant for the second binding event. At low concentrations of ligand, the effective concentration experienced by a multivalent receptor due to a multivalent ligand would be much greater than the concentration of free ligands in the bulk solution ($C_{eff} \gg C_{bulk}$) and thus a multimeric intramolecular interaction is more likely to occur. However, at higher ligand concentrations, ($C_{eff} < C_{bulk}$), the concentration of ligand experienced by the receptor will not be influenced by the ligand molecule already bound and therefore a second intermolecular interaction is more likely to occur (figure 19). Naturally, when $C_{eff} = C_{bulk}$, the system will be in equilibrium between the intra- and intermolecular interactions.

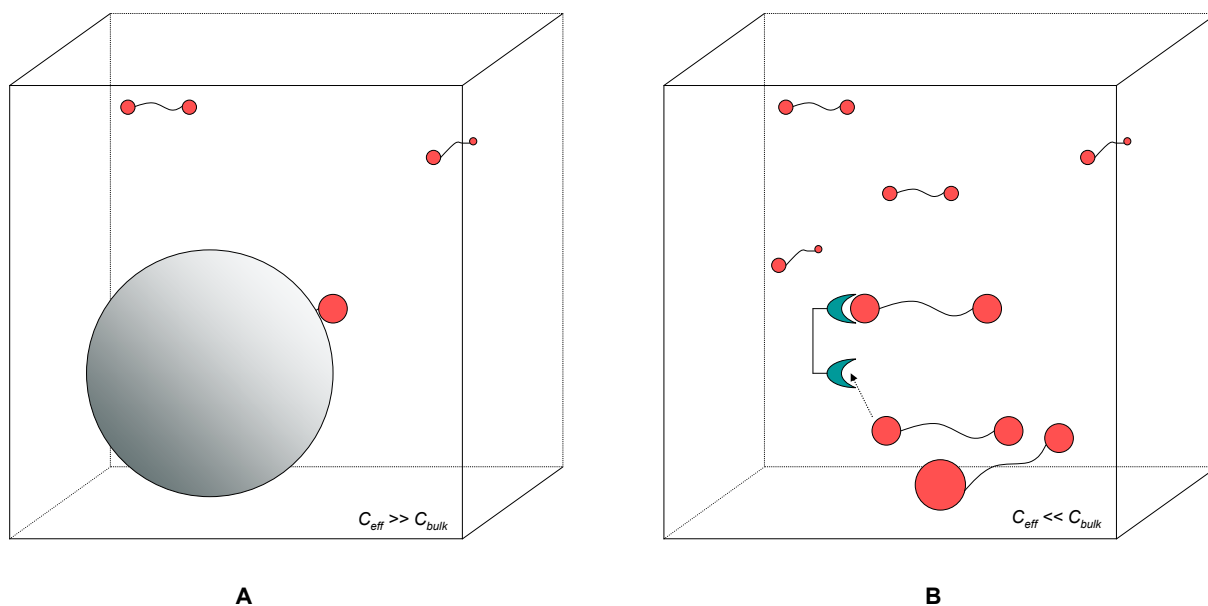


Figure 19 : Concentration dependence of multivalent interactions. Intramolecular association more likely as $C_{eff} \gg C_{bulk}$ (A). The shaded sphere represents the “probing volume” that the ligand can use to search for other binding sites. Intermolecular association more likely as $C_{eff} \ll C_{bulk}$ (B).

C_{eff} is dependent on the ligand-receptor distance, which is also dependent on the length of the linker molecule. C_{eff} will also be influenced by linker molecule flexibility. The length of course determines the radius of the sphere occupied by both potential interacting partners. Longer molecular lengths lead to smaller C_{eff} values, decreasing cubically with the increase in length. Therefore it is important that the linker molecule is long enough and flexible enough to allow the intramolecular interaction, but not too long so that C_{eff} approaches C_{bulk} . The flexibility of the linker molecule would also influence the nature of the theoretical sphere occupied by the second ligand after the first binding event has occurred. A flexible ligand would theoretically be allowed to occupy any position within this sphere (excluding regions occupied by the receptor or the other parts of the ligand). A less flexible linker molecule would reduce the sphere in size or dimensionality depending on the nature of this rigidity. In this reduced system, the C_{eff} would be increased, increasing the probability of the intramolecular interaction occurring. Too rigid however, and the intramolecular interaction may be inhibited thermodynamically (enthalpy or entropy penalties) or logistically (the second ligand is simply blocked from entering the second binding site).

1.6.5.1 Reaction kinetics and the effective concentration

For a divalent receptor interacting with a divalent ligand in the example given by Huskens *et al.*⁶¹ the first binding event would occur more readily by a factor of four in comparison to its

monomeric counterpart, due solely to statistical considerations. These statistic considerations are the ratio of possible permutations of the forward reaction, leading to the mono-linked product, and the permutations of the reverse reaction, dissociation back to the reactants (figure 20).⁶⁰

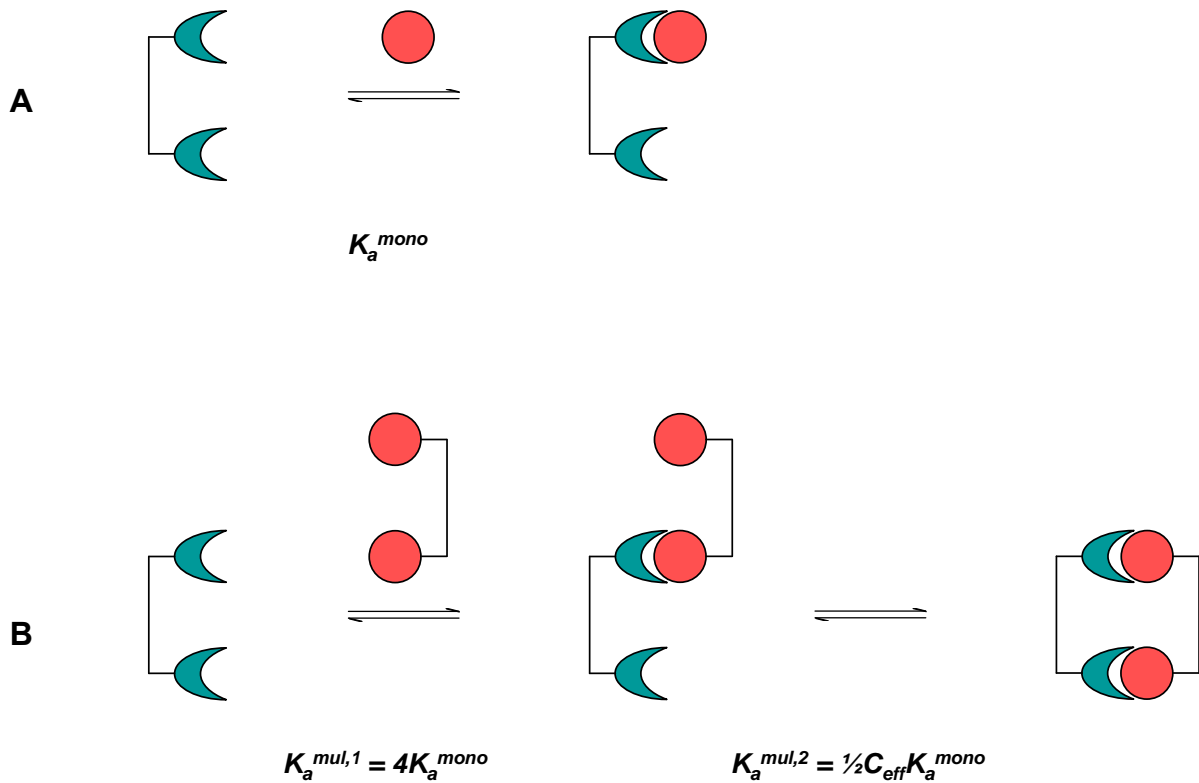


Figure 20 : Kinetics of a divalent interaction by considering the effective concentration.

The overall binding constant for the divalent interaction being dependent on C_{eff} then becomes:

$$K_a^{mul} = 2C_{eff}(K_a^{mono})^2 \quad \text{E 22}$$

Where the general formula for multivalent interactions becomes:⁶³

$$K_a^{mul} = b(C_{eff})^{n-1}(K_a^{mono})^n \quad \text{E 23}$$

Where b is a statistical factor, representing the ratio of permutations leading to products divided by permutations in the reverse reaction.

A theoretical estimate of C_{eff} (mM) is cited as:

$$C_{eff} = \frac{1}{N_{AV}} \left(\frac{3}{2\pi\bar{r}_0^2} \right)^{\frac{3}{2}} \quad \text{E 24}$$

Where N_{AV} is Avogadro's number and \bar{r}_0 is the root mean squared distance between the free ligand and the free receptor of the mono-linked entity (Å). \bar{r}_0 was calculated by Huskens *et al.* statistically for this particular example.⁶¹ The above equations are given for the example of multivalent binding in solution however this model can equally be applied to multivalent binding to SAMs as well as other systems, with some modification (the effective concentration will only vary linearly with \bar{r}_0 in 2D as opposed to \bar{r}_0^3 in solution).

1.6.6 Conclusion

Two models for studying multivalent interactions have been presented. Whitesides *et al.* showed how the kinetics of multivalent interactions to be dependent on the thermodynamics of the interactions and in particular minimising entropic contributions (penalties) to the Gibbs free energy. The influence of the linker molecule used to present the ligands or receptors in a multivalent fashion is shown to be crucial. Linker rigidity (and flexibility) and the mode of presenting their binding epitope are vitally important for controlling or maximising enthalpy changes and minimising entropic penalties to the Gibbs free energy, which in turn maximises binding affinity at the individual and global binding events. The second model, proposed by Kramer *et al.* and applied by Lees *et al.* and Huskens *et al.* investigates the influence of the first binding event on the following binding events. In this case, the kinetics of multivalent interactions are very much dependent on the statistics of the system and concentrations of interacting bodies. Due to this, there are no extrapolations or conclusions relating to the thermodynamics of the systems studied. Again, in this model, the nature of the linker molecule used is crucial for invoking multivalent interactions.

Several assumptions have been made in both models. Firstly, the multivalent receptors do not exhibit cooperativity and that the multiple interactions are independent, equal (of the same motif) and monotopic. Secondly, we have assumed that the multivalence of the receptor is

architectural, like the lectins discussed in the previous section, with the receptors being presented as several subunits each with a ligand binding site.

Cooperativity occurs frequently in biological systems and often involves structural changes in the receptor itself in order to alter the binding of subsequent ligands. This must also be taken in to account when designing a multivalent receptor so that the first interaction occurs in a manner which allows the second ligand to adopt the most appropriate position to interact with the new, “modified” receptor. Architectural multivalence refers to the organisation (clustering) of receptor sub-units which contain the binding domain. This is not always the case, as in biology several different “types” of multivalence exist. In the case of lectins, many do present themselves as multivalent architectures, dimers, trimers or higher symmetric, organised clusters of recognition domains. However others present themselves monovalently but in high density with several other receptors in close proximity (FimH). In this case the entropic and effective concentration arguments presented above change dramatically.

1.7 Synthetic Multivalent Scaffolds

For the study of multivalent interactions, in particular lectin-carbohydrate interactions, many groups have synthesised a range of multivalent scaffolds based on various sub-structures as platforms for presenting carbohydrate ligands, from monosaccharides to larger oligomers. Natural, synthetic and semi-synthetic scaffolds used range from small-molecule clusters, to dendrimers, polymers and micelles, as well as 2D surfaces for applications to inhibit or elicit a biological response.⁶⁴ Scaffolds can vary in size, valency, what form they adopt in solution and their physical properties. Different scaffolds allow different topologies which leads to a particular presentation of the saccharide epitopes. Different scaffolds with the same valence, may exhibit different levels of activity towards the same lectin receptor. Likewise, the same multivalent structure may exhibit different affinity trends towards one lectin than to another, as shown by Brewer *et al.* for interactions of Con A and *Dioclea grandiflora* lectin (DGL).⁶⁵ The scaffold, acting as the linker molecule between ligand epitopes, plays an important role in ligand activity and its mechanism of action. The architecture of the scaffold may also be tailored to influence the macromolecular assembly upon ligand-receptor association. The scaffold used may also be tuned to a particular type of multivalence or to a particular location - binding to a multimeric lectin such as Con A may require a different multivalent ligand to

that binding to several fimbriae-tethered lectins such as FimH. Likewise, a membrane bound lectin would prefer a multivalent scaffold different to that of a soluble lectin – a 2D SAM as opposed to a 3D structure for example. Therefore, by manipulating the multivalent scaffold, one can be selective to the target receptor, as well as incorporate other functionalities (e.g. fluorescence). The valence of the multivalent structure is also important. Often, increasing the valency of the structure will increase the affinity of the lectin, to a point where increasing the valency no longer has any, or only very little, effect on the K_a of the lectin.⁶⁶ Also, the valence of the structure may influence the formation of the macromolecular products. Turnbull *et al.* showed that increasing the valency altered the kinetics and aggregation mechanisms resulting in intermolecular cross-linked aggregates as opposed to intramolecular interactions.⁶⁷ It may also be the case that, where a particular structure was an effective inhibitor in monomeric form, yet when grafted to a multivalent scaffold the inhibitor may lose some potency. This is because one must consider inter-ligand interactions which would not occur at the monovalent level, but may affect dramatically ligand presentation on a multivalent scaffold.⁶⁸

1.7.1 Small molecule glycoclusters

A great number and variety of ligands have been reported with the specific purpose of investigating multivalent interactions. A large proportion of these include small clusters (dimers, trimers, tetramers etc) fixed on to small multivalent scaffolds of varying size and flexibilities. Often, these small synthetic molecules can incorporate multiple functionalities.

Brewer *et al.* tested several small divalent glycoclusters when investigating interactions with Con A and DGL. Several of these clusters were developed around aromatic (alkyne or benzylic) scaffolds, giving very short, rigid structures. Also presented are dimers connected by alkyl chains of varying length or aromatic rings bound via thiourea bridges, again of varying length.⁶⁵ Further work by Brewer *et al.* investigated di-, tri- and tetravalent trimannoside structures with a longer, more flexible thiourea bridge to an aromatic core.³⁹ All multivalent structures showed some improvement in K_a with enhancements ranging from ~2 to 10 fold for the monosaccharide structures and up to 1000 fold for the trimannosides in the case of Con A. Larger improvements were observed for DGL. Summaries can be found in table 1 for the most efficient of each cluster type. Isothermal titration microcalorimetry (ITC) was used to determine the K_a of each cluster. Toone *et al.* also investigated the cluster glycoside effect observed in Con A. Several multivalent clusters were developed around an aromatic core allowing the synthesis of di, tri, tetra- and hexa-mannosides, the most potent of

which being the dimer structure, shown in table 1. It must be noted that the results from Toone *et al.* are presented with respect to mannose equivalents, whereas results from Brewer *et al.* are presented with respect to the whole cluster.

Other small glycoclusters used for lectin-carbohydrate interactions were developed by Roy *et al.* for the lectin PA-IIL.⁶⁹ These scaffolds include aromatic centres or ethylene glycol chains coupled to Le^a moieties via triazole rings by the commonly used “click” chemistry. Several dimers and trimers were synthesised, the most potent of which are listed in table 1.

Other glycoclusters include mannose functionalised Pentaerythritol and bis-pentaerythritol scaffolds developed by Roy *et al.* for the inhibition of Con A activity on Mesenchymal stromal cells and the inhibition of the FimH lectin.^{70, 71} As well as aromatic molecules, other scaffolds can be found in the literature. Lindhorst *et al.* used carbohydrates as the scaffold base, with mannose functionalised linkers coupled to the pendant hydroxyl groups (figure 21).⁷²⁻⁷⁴ These “octopus” clusters were used to study multivalence in and inhibiting Con A and FimH. Lindhorst’s group also added further functionalities to several of these clusters.⁷⁵

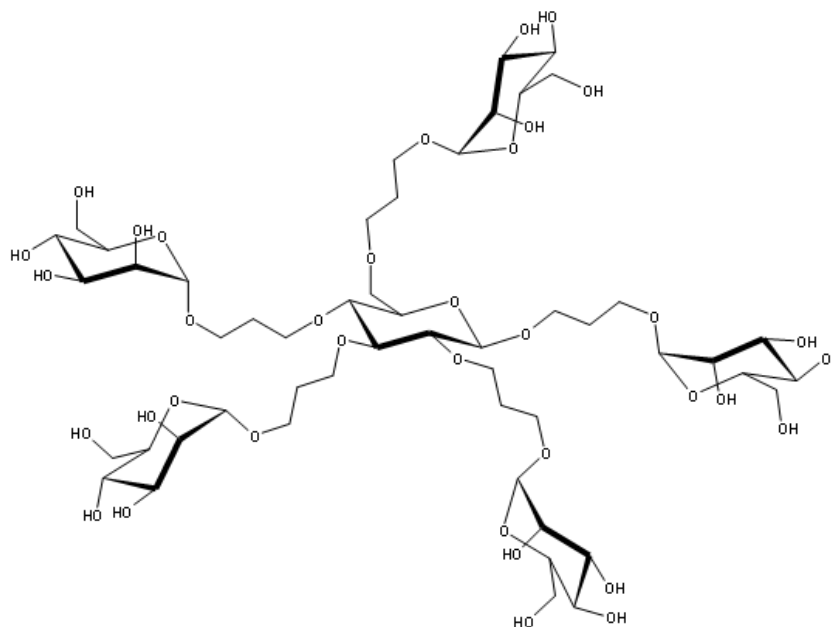


Figure 21 : Example of one of several Mannose functionalised “octopus” glycoclusters developed by Lindhorst *et al.* for the inhibition of FimH.⁷³

In relation to the application of the cluster glycoside effect, small molecules have proven to be very efficient. The di-, tri-, tetra- and hexavalent scaffolds designed by Brewer *et al.* and Toone *et al.* all show increased affinities towards their target ligand. However, in considering the thermodynamic and kinetic applications of the cluster glycoside effect with respect to the interactions studied, the inter-binding site distance of the lectin is significantly larger than the inter-ligand distance. This would lead to the situation described in figure 15(C), where it is more likely that the lectin will choose to pay the entropic penalty and interact with two separate ligands (intermolecular association) than pay the enthalpy penalty of internal structural change for intramolecular association. This of course means that the ligands designed exhibit an effective valency of one (when considering one multivalent ligand interacting with one lectin). However, Brewer *et al.* observed that n values calculated from calorimetry data were inversely proportional to the functional valency of the multivalent ligand. This demonstrates that all carbohydrate epitopes were still available and interacting with a lectin binding site. This leads to the conclusion, which they also show with microscopy data, that cross-linking occurs, where a network of lectin-ligand complexes are formed driven by intermolecular association. They also show that multivalent scaffolds with flexible linker molecules exhibit greater changes in enthalpy but larger entropy penalties as predicted in the theory section – flexible linkers allow optimum ligand-binding site interaction yet a larger entropy penalty has to be paid resulting from constricted movement of flexible groups. This still leads however to an enthalpically enhanced affinity. This was also observed by Toone *et al.* with the aggregation of tetrameric Con A. Enthalpically enhanced affinities which are partly compensated by unfavourable entropic penalties. However, in both cases, enthalpic enhancement may not be the only cause of increased affinity. Due to their small sizes, these multivalent molecules exhibit a high local concentration of ligands. Therefore, upon lectin-ligand association, there may be a greater chance of a successful binding event with one of several ligands presented on the scaffold. This of course is related to the effective ligand concentration and its statistical contribution, the multivalent scaffold providing a “high density” binding partner with more possible binding permutations. However, as experiments were not carried out with monomeric analogues, it is impossible to compare observed affinity enhancements with those calculated from differences in free energy changes.

The small molecules designed by Roy *et al.* also exhibited interesting binding kinetics to PA-III. As expected, the monomer equivalents exhibited normal monomeric kinetics to multimeric receptors. The dimers, based on both aromatic and poly ethylene glycol scaffolds

showed that one saccharide epitope binds to one binding site. The observed enthalpy was shown to be double that of the monomer as both saccharide epitopes are available for binding. However, the entropy contribution to the system's thermodynamics is not proportional to the valency of the scaffold. In fact, a large entropy penalty is incurred which significantly reduces their binding affinities. Even though the aromatic and linear dimer structures are long enough to theoretically induce multiple binding events on the same lectin molecule, this was shown not to occur. One explanation for this is related to the orientation of the ligands, which in linear form point in opposite directions. Therefore, a large conformational change may be required to present the ligands in the correct manner to induce multivalent binding. The trimer exhibited a stoichiometry of 1, indicating that one trimer binds to only one binding site. Thermodynamically, trimer binding is more or less equivalent to monomer binding with reduced enthalpic enhancement and favourable entropic contributions due to its rigid nature.

Lindhorst *et al.* although not dealing with a multimeric lectin, showed the increased inhibitory power of their ligands via ELISA tests. Even though no quantitative thermodynamic or kinetic data can be extracted, it is clear from the data that ligand presentations varied with the carbohydrate scaffold base. This in turn altered the binding/inhibiting properties of the ligands towards the bacterial lectins.

1.7.2 Cyclodextrins and calixarenes

Cyclodextrins are cyclic oligosaccharide molecules of units of α -(1-4)-linked glucose. They exist in three conformations: α -, β - and γ -cyclodextrin which contain 6, 7 and 8 glucose units respectively (figure 22). The structures present a hydrophobic cavity and a hydrophilic exterior and it is for this reason they are very popular in supramolecular chemistry and host-guest interactions; their biocompatibility and the potential use of the cavity acting as a host for a wide range of guest molecules.⁷⁶ Huskens *et al.* used cyclodextrins and guest molecules as a model system for multivalence interactions.^{62, 77} The hydroxyl groups on the two faces of the cyclodextrin can be modified in order to present molecules multivalently. Several cyclodextrins have been functionalised with saccharides giving rise to various glycoclusters for use as drug delivery vehicles,^{78, 79} as well as high affinity ligands for lectins.⁸⁰ Nishimura *et al.* modified β -cyclodextrins with galactose and lactose to study their enhanced binding with the wheat germ agglutinin (WGA) and *Erythrina corallodendron* lectin (ECoRL lectins) showing an enhancement factor of 40 (per epitope) for GalNAc functionalised CDs with

WGA and factors of 2 and 4 for Galactose/GalNAc and LacNAc – CDs respectively with ECorL. Lactose functionalised α -cyclodextrins have also been used for the inhibition of peanut agglutinin (PNA).⁸¹

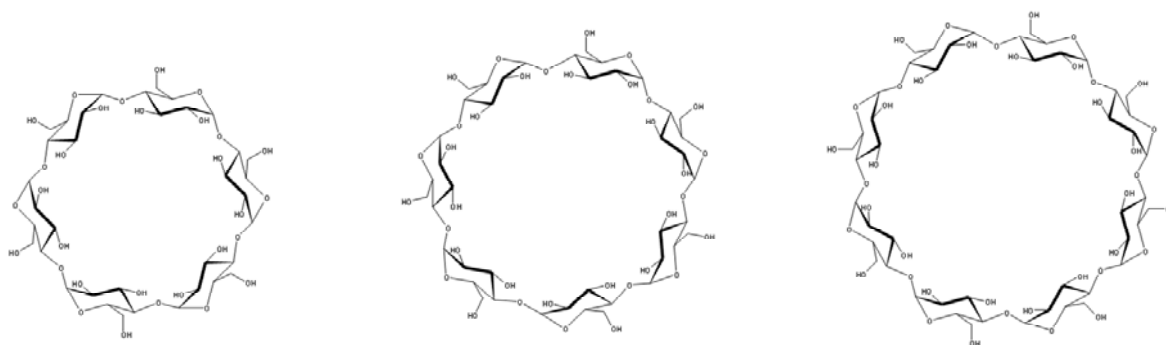


Figure 22 : Structures of α -, β -, and γ -cyclodextrins (left, centre and right respectively).

Calix[n]arenes are similar to cyclodextrins in that they are cyclic ring structures with a hydrophobic cavity capable of hosting a small hydrophobic guest molecule. They are composed of cyclic phenol-formaldehyde oligomers (figure 23), the number of rings in the structure denoted by the [n]. As with the cyclodextrins, n can be varied in order to tune the size of the hydrophobic cavity. The phenol functionality and aromatic nuclei can be converted to most functional groups to attach ligating units. Their conformation can also be altered (conical or tetrahedral), allowing tunability in the presentation mode of functional groups added to the scaffold.^{63,82}(and references therein) There are several examples of the addition of carbohydrate molecules to form glycoclusters.^{82, 83} Aoyama *et al.* functionalised calix[4]arenes with galactose and glucosides to study their specificities with peanut agglutinin (PNA) and Con A respectively, with a view to using the calixarenes as site-specific drug delivery vectors.⁸⁴ Ungaro *et al.* have synthesised several calixarenes ranging from $n = 4$ to $n = 8$.⁸⁵ These calixarenes were functionalised with two to eight galactose or lactose moieties via thiourea bridges. A range of conformers was possible due to the flexibility of the large aromatic scaffold. Inhibition tests were carried out using *Viscum album* agglutinin (VAA), a galactose binding AB type plant toxin from *Viscum album*, and galectins -1, -3 and -4. Inhibitory enhancements of factors of 8, 1.5, 1 (no affinity enhancement) and 0.7 (diminished affinity) were observed. Affinity investigations with cholera toxin were also carried out by fluorescence spectroscopy and SPR, showing an affinity enhancement factor of 5 and 18 respectively per sugar epitope emphasising that different analysis methods may give different results.⁸⁶ Recent studies using galactose functionalised calixarenes tethered to a microarray

for studying the binding of RCA 120 and PA-IL lectins showed an affinity enhancement of 23 per sugar epitope for RCA 120 (no affinities recorded for PA-IL), as measured by fluorescence spectroscopy.⁸⁷ The results support the idea that different glycoclusters are required for different multivalent receptors.

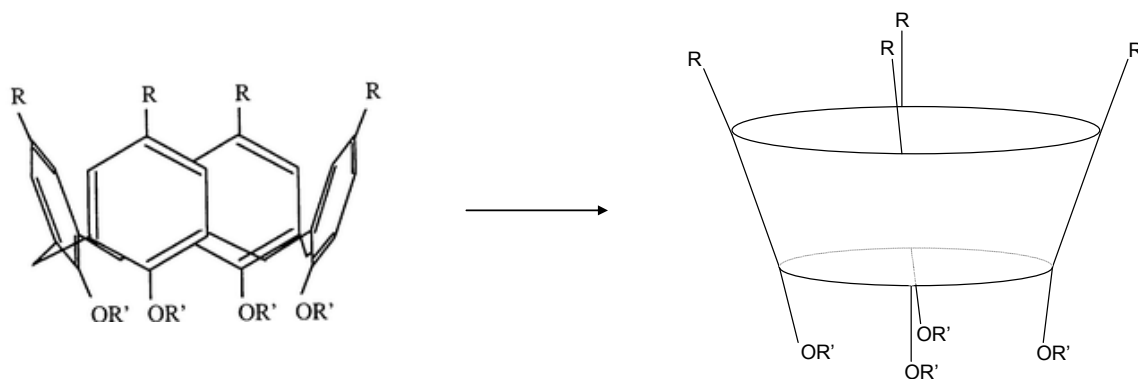


Figure 23 : Structure of calix[4]arenes.

Labbe *et al.* investigated multivalence and clustering using mannose regioselectively addressable functionalised templates (RAFT) polymers – cyclodecapeptide templates with up to four possible ligand attachment sites.^{88, 89} A second, regioselectively distinct site, can be used for adding other functionalities (biomarkers, functional groups for surface attachment etc).

For the interactions of ligands attached multivalently to cyclodextrin and calixarenes there are, as yet, no studies published providing fully quantitative information with regards to the thermodynamics of binding to multivalent lectins. This makes the thermodynamic interpretation of their multivalent properties difficult. Several studies have used ELISA and ELLA type assays to study their inhibition powers. Fort *et al.* showed that polymers functionalised with oligosaccharide functionalised cyclodextrins exhibited stronger inhibition powers per oligosaccharide compared to the monomer unit however no significant synergic effects were noted suggesting that there is no, or only very little, thermodynamic enhancement towards affinity augmentation. Again, this augmentation may be due to an increase in effective ligand densities. The studies of Ungaro *et al.* were also conducted using inhibition effects. They showed that the inhibition power of calixarenes varied between several lectins. This demonstrates that the calixarenes exhibit a relatively rigid platform which can be used for structure selective lectin targeting. This rigid nature would contribute to the increase in entropic enhancement to interaction affinity.

1.7.3 Dendrons and dendrimers

Often, the small glycoclusters, such as those mentioned above, can be functionalised in such a way that they allow multimerisation of the cluster groups themselves. This leads to higher order structures known as dendrons and dendrimers. Dendrimers have a regular branching pattern with predictable physical properties and display multiple copies of functional groups in a spherical arrangement.⁶⁶ Dendrons are branched structures with typically non-spherical arrangements; segments of whole dendrimers. Both dendrimers and dendrons have the capability of producing nanometer scale formations of very high valency (up to 400). The number and nature of the tethered functional groups can be controlled by the number of “generations” allowed, as can various physical properties such as solubility and reactivity.⁹⁰ The use of different sub-units would also allow for multiple functionalities. Several commercially available dendrimer frameworks include poly(amidoamine) (PAMAM), poly(propylene imine) (PPI, figure 24) and poly(ethylene imine) (PEI).^{66, 91} Several dendrimers with the PAMAM framework were developed by Cloninger *et al.* and tested for their ability to bind with Con A, Pea lectins and cyanovirin, stating an affinity enhancement of 350 and 0.38 (reduced activity) for Con A and pea lectins respectively.^{90, 92, 93} Bifunctional dendrimers were also developed to alter mannose presentation and valency.⁹⁴

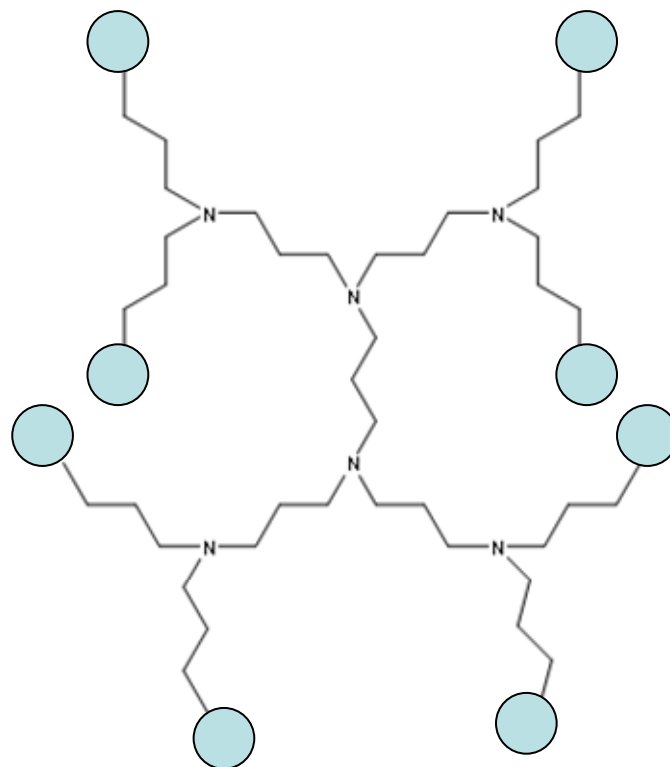


Figure 24 : Third generation poly(propylene imine) dendritic backbone.

Roy *et al.* built several dendron and dendrimer structures in order to inhibit *P. aeruginosa* lectins to great effect. The dendrimers developed included spherical and linear structures with a poly(lysine) and phosphodiester frameworks.^{95, 96} Dual functionality (galactose and fucose) was incorporated in order to bind both PA-IL and PA-IIL. Other dendrimers were developed to inhibit the FimH lectin and as mimics of T-antigen markers from breast cancer, bearing a β -D-Gal-(1-3)- α -D-GalNAc moiety.⁹⁷⁻⁹⁹

Trehalose-centred PAMAM dendrimers were developed by Lindhorst *et al.* following on from the octopus glycosides.⁷² The pendant hydroxyl groups of the trehalose dimer were functionalised with the PAMAM framework, to which mannosides were attached via thiourea bridges. Several carbohydrate based dendrons were developed for FimH inhibition.^{100, 101} There are many other examples of the use of carbohydrate functionalised dendrimers and dendrons in the literature using different core structures for studying different interactions.^{91,}
102

There is little data available for quantitative measurements of thermodynamic contributions to the multivalence effect offered by dendrimers. ITC experiments by Cloninger *et al.* showed that interactions with monomeric Con A demonstrated that all epitopes were available for binding. Increasing dendrimer valency lead to increased enthalpy contributions per epitope, but also increased entropy penalties thus only marginally increasing the free energy of the interactions and interaction affinities. Interactions with dimeric Con A showed similar traits with respect to enthalpy and entropy, yet the affinity increases were much more exaggerated, suggesting that effective concentrations of both ligands and binding sites is important, however, in some cases more than half of the carbohydrate epitopes were unavailable for binding. Typically, the larger generation dendrimers have larger binding constants, which could be a reflection of the larger inter-ligand distance and flexibility allowing for optimised interactions.

1.7.4 Functionalised polymers

Polymers are linear structures which present functional groups as branches from the main chain. Polymers, like dendrimers, are constructed by the polymerisation of building units of natural or synthetic origin, and can be of controlled size and valency. Due to their potential large size, they can exhibit very high valency. Their nature and physical properties can be

controlled by the use of different building blocks and side-chain functionalities resulting in highly tuneable platforms. A wide range of building block molecules can be used to synthesise the polymer. Poly(phenylacetylene) was used by Kakuchi *et al.* for the construction of glucose and galactose polymers for interaction studies with Con A and PNA lectins.¹⁰³ The polymers also gave chiral helical structures, the chirality imparted by the saccharide, which showed enhanced affinity towards the lectins. Block copolymers had also been developed by Li *et al.* for the glucose sensitive aggregation of Con A.⁸⁵ Kiessling *et al.* synthesised galactose functionalised polymers based on ROMP in order to investigate bacterial signalling in *E. coli*.¹⁰⁴ Usui *et al.* developed *N*-linked glycopolypeptides to inhibit influenza infections.¹⁰⁵ More recently, Garber *et al.* have used naturally occurring branched polysaccharides, normally used as food additives, for their anti-infection properties towards *P. aeruginosa*, *C. violaceum* and *R. solanacearum*.⁴⁷ Natural polymers such as polypeptides can also be used as multivalent scaffolds.¹⁰⁶

As for several cases above, there is little quantitative data available for interpreting the thermodynamic and kinetic contributions of the cluster glycoside effect with polymer scaffolds. Brewer *et al.* have conducted a thorough analysis of lectin binding to carbohydrate functionalised polymers. They show that a “bind and slide”, or “bind and hop” model explains the large augmentations in lectin affinity.¹⁰⁷ This model was designed to describe how enzymes bind to DNA, initially binding to a low affinity site then sliding along the DNA chain until a high affinity site is reached. In lectin-carbohydrate systems, the first lectin molecule binds with high affinity to the first available epitope. Dissociation - re-association occurs rapidly so that the overall kinetics show highly favourable binding. Upon saturation of the carbohydrate epitopes, subsequent binding events occur with increasingly negative cooperativity. This resembles the effective concentration model for multivalent binding, with statistical effects strongly influencing the first and subsequent binding events - a reduction in further binding permutations upon saturation of the ligands presented on the polymer chain. The effective concentration model may not be able to fully explain this large augmentation in activity however, as steric effects may arise under high saturation conditions, reducing the affinity further.

1.7.5 Micelles and capsules

Molecules which consist of hydrophobic and hydrophilic building blocks allow for the construction of amphiphilic structures. When placed in polar solvents, the hydrophobic

components collapse on themselves in order to be shielded from the aqueous environment. Simultaneously, the hydrophilic components expose themselves to the external environment, forming stable particles. This is one of the bases of the formation of capsules and micelles. Capsules are typically made of diblock polymers, whereas micelles consist of molecules which exhibit hydrophilic and hydrophobic components. If the hydrophilic components are functionalised with saccharides, these molecules will be presented on the micelle surface, in a multivalent arrangement. Micelles and capsules typically have a size range of nm - μm . Auzely-Velty *et al.* have produced several capsules as models for smart drug carriers, functionalised with mannosides, and tested with the BclA lectin.^{41, 42} Amphiphilic capsules based on polysaccharides (hyaluronic acid) and other biopolymers were also developed.^{108, 109} These hyaluronic acid capsules were developed by the layer by layer (LbL) adsorption of oppositely charged polymers around a sacrificial nanoparticle core. Iwasaki *et al.* also developed capsules to specifically target and tag non-natural carbohydrate molecules presented on carcinoma cells.¹¹⁰ Micelles of mannose functionalised glycolipids have also been synthesised as multivalent ligands for Con A.^{111, 112} These nano- and micro- structures present interesting candidates for intelligent drug delivery vectors as various biologically important molecules (drugs, fluorophores etc) can be trapped inside this hollow core to be released when and where necessary.

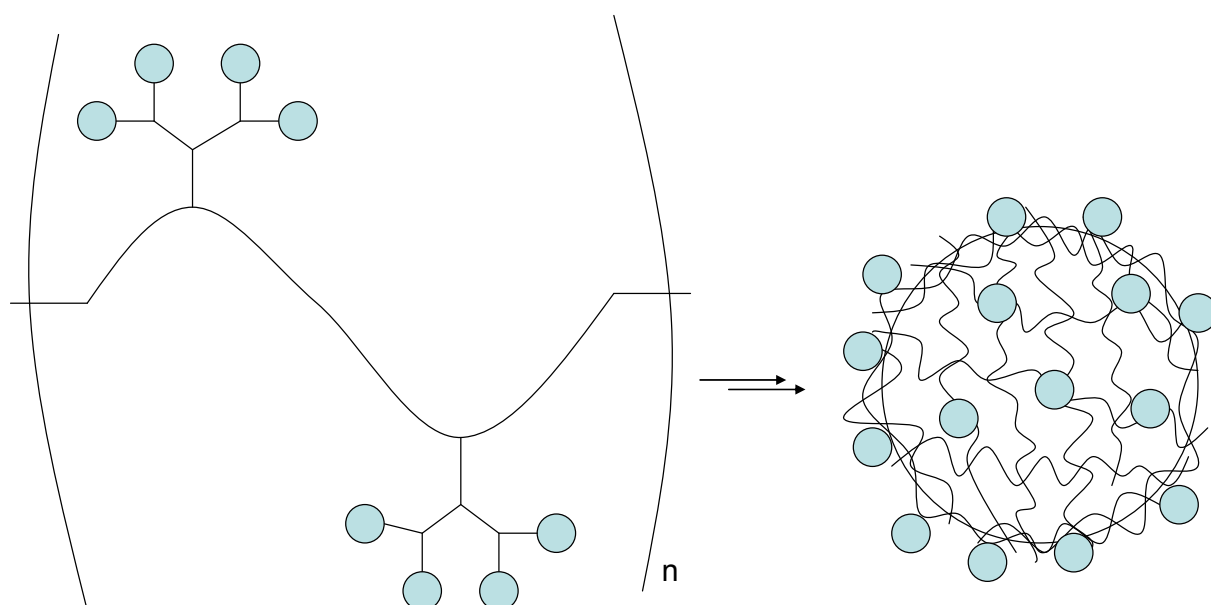


Figure 25 : Schematic representation of functionalised polymer structures aggregating to form capsules.

ITC studies conducted by Auzely-Velty *et al.* on polyethylene oxide – poly caprolactone micelles revealed that most of the saccharide epitopes were available for binding with the BclA lectin. However, the enthalpy change of the interaction is slightly smaller, as is the entropy contribution, leading to an association constant one order of magnitude lower than that of Me- α -D-Mannose. This demonstrating a negative cluster glycoside effect, with no cooperativity or affinity enhancement - only diminished affinity.

1.7.6 Neoglycoproteins

Proteins and peptides are often glycosylated in nature, with glycosylation representing up to 70 % of post translational modifications.⁷ Amino acids presenting O (serine or threonine) and N (asparagine) atoms on the peptide side chain provide potential glycosylation sites. Up to 90 % of these naturally occurring glycosylation sites are occupied.⁵ To produce this synthetically however, solid state peptide methodologies have to be employed, requiring protection / deprotection of both saccharides and amino acids, and is limited to only 50 amino acids.⁷ However, a variety of methods are available for introducing non-natural glycosylation sites. Typically, chemically modified saccharide molecules are coupled to modified amino acids in the peptide chain. Such examples include the use of thiohexoses which give thioether-linked (S-linked) glycoproteins upon coupling to sulfamidate-modified serine residues and Michael addition to unsaturated amino acids. Several site-specific methods have also been used such as disulfide bridge formation between thiohexoses (or functionalised thiohexoses: selenyl sulfides, methanethiosulfonates) and cystein residues.¹¹³

Apart from only a few examples of their use as multivalent platforms for carbohydrate presentation, “glycodendriproteins” have so far not been widely used, despite their advantages as biocompatible, site-specific and targeting capabilities. Inhibition studies with galactose specific FimA and mannose specific Con A were reported, however only a small (1.5 fold) increase in affinity enhancement was noted for Con A.²⁶ Yet a 20 nM inhibition of FimA was recorded, 10⁶ enhancement compared to that of lactose.¹¹⁴

The disadvantage of the use of neoglycoproteins is that they are often produced in heterogeneous mixtures, although the protein is coded for by DNA, the addition of carbohydrates is not controlled genetically. The carbohydrate functionalities are thus subject to various conditions such as enzymatic degradation etc. which leads to the production of several different glycan structures, termed “glycoforms”.^{5,7}

As for functionalised polymers above, there is no information available describing the thermodynamic parameters of the cluster glycoside effect observed in *neoglycoproteins*. However, one can imagine that, even with modification of the amino acid sequence at particular positions, it would be very difficult to control the display and presentation of the carbohydrate ligands. It may also be difficult to control the valency and presentation density of these ligands, as increased conjugation of carbohydrate molecules may denature the protein, effectively giving an (oligo)saccharide functionalised polypeptide.

1.7.7 Self-assembled monolayers (SAMs)

Carbohydrate functionalised (Glyco-)SAMs provide a 2D model of the glycocalyx. They allow control over ligand density and orientation in addition to being supported by analytical techniques such as microarrays, surface plasmon resonance (SPR), quartz crystal microbalances and atomic force microscopy (AFM). Several surfaces can be used to which saccharide molecules are mobilised. Typically, target molecules consist of a thio- or thioacetate functionalised linker molecule to allow the formation of a stable S-Au bond upon SAM formation, for which there are many examples.¹¹⁵⁻¹¹⁷ The linker molecule will terminate in the sugar epitope. Dilution of these carbohydrate functionalised alkane thiols with non-functionalised alkane thiols allows density control on the 2D matrix. The ligands form highly organised, densely packed, oriented monolayers. Although density control is possible, distribution is not, meaning that the inter-carbohydrate distance may not be regular throughout the SAM. With SPR applications, gold surfaces and SAMs were popularised, as were various surface immobilisation methods. Dextran can typically be found coated onto the gold sensor chips to which a wide variety of functional groups can be coupled (amines, thiols, carbonyls and streptavidin-biotin coupling as well as hydrophobic and bilayer attachment). There are numerous examples of the use of monolayers for the multivalent presentation of carbohydrate ligands and their interactions with lectins. In microarray technology, several hundreds of amine functionalised glycans have been immobilised to functionalised glass slides. Plastics and modified cellulose have also been used to immobilise carbohydrate molecules.¹¹⁸ Glycan arrays are often, if not always, used to determine the preferences of lectins for particular mono- or oligosaccharide structures and motifs.

Due to the limited dimensionality of SAMs, there are currently no experimental methods for evaluating the thermodynamic contribution to the multivalence effect – only affinity

measurements by SPR or similar experiments. Also, the current technology for immobilising molecules to 2D surfaces does not yet allow for a great deal of control. For example, one can control well the *quantity* of material immobilised to form the SAM, however, the *distribution* of ligands on the surface would be at random, assuming experimental design has no effect on ligand deposition (flow direction, flow speed, surface size etc).

Multivalent Platform	Carbohydrate Motif	Target Lectin	K_b	Relative Affinity Score	n	Measured by	Reference
Me- α -D-Man	Me- α -D-Man	ConA	1,20E+04	1 ^a	1	ITC	65
Alkyne Linker	α -D-Man	ConA	2,50E+04	2,1 ^a	0,52	ITC	65
Alkyl Linker	α -D-Man	ConA	5,30E+04	4,4 ^a	0,54	ITC	65
Aromatic-thiourea	α -D-Man	ConA	4,50E+04	5,7 ^a	0,6	ITC	65
Aromatic-thiourea	3,6-di-O-(α -D-Man)- α -D-Man	ConA	6,50E+07	1170 ^{*a}	0,26	ITC	39
Aromatic	α -D-Man	ConA		2,4	1	ITC	119
6th Generation PAMAM dendrimer	α -D-Man	ConA		350		Haemagglutination	90
6th Generation PAMAM dendrimer	α -D-Man	ConA		5350		Haemagglutination	94
Me- α -D-Man	Me- α -D-Man	DGL	4,60E+03	1	1	ITC	65
Alkyne Linker	α -D-Man	DGL	2,20E+04	4,8	0,68	ITC	65
Alkyl Linker	α -D-Man	DGL	1,06E+05	23	0,56	ITC	65
Aromatic-thiourea	α -D-Man	DGL	4,50E+04	9,8	0,52	ITC	65
Aromatic-thiourea ^a	3,6-di-O-(α -D-Man)- α -D-Man	DGL	6,50E+07	14,000	0,25	ITC	39
Lewis a	Lewis a	PA-III	4,70E+06	1	1,08	ITC	69
bis-Triazole functionalised tetraethylene glycol	Lewis a	PA-III	1,10E+07	2,3	0,66	ITC	69
tris-triazole functionalised aromatic ring	Lewis a	PA-III	9,68E+06	2,1	1,11	ITC	69
GlcNAc	GlcNAc	WGA			1	Haemagglutination	80
Cyclodextrin	GlcNAc	WGA			280	Haemagglutination	80
Gal	Gal	ECoRL			1	Haemagglutination	80
Gal-CD	Gal	ECoRL			14 ^b	Haemagglutination	80
Lactose	Lactose	ECoRL			1	Haemagglutination	80
Cyclodextrin	Lactose	ECoRL			14 ^b	Haemagglutination	80
LacNAC	LacNAC	ECoRL			1	Haemagglutination	80
Cyclodextrin	LacNAC	ECoRL			28 ^b	Haemagglutination	80
Lactose	Lactose	PNA			1	ELLA	81
Penta-cyclodextrin functionalised polymers	Lactose	PNA			4	ELLA	81

^anot per mannose, per molecule

^bReactivity per heptamer, not per galactose/lactose

Table 1 : Summary of various multivalent scaffolds found in the literature.

1.7.8 Coupling methods

In order to produce a library of multivalent scaffolds with different, or even multiple functionalities, it is convenient to use a versatile linker molecule. The linker molecule should be able to attach itself to the scaffold and present a suitable functional group at its terminus which can be functionalised downstream to a range of natural or modified carbohydrate ligands. This synthetic methodology would of course decrease the amount of synthetic work so that multivalent ligands do not require “starting from scratch” in order to insert a different, or more complex saccharide component. Listed below are several coupling methodologies. Coupling methodologies are particularly advantageous if it can be carried out in atmospheric conditions, in a range of solvents without the use of forcing conditions with easy separation of products and, of course, high yields. Particularly popular couplings include the “click” coupling resulting in the triazole, and the thiourea bridge.

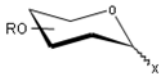
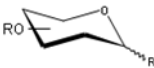
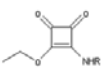
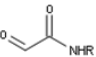
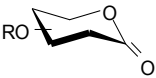
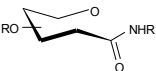
Sugar Functionality	Linker Functionality	Coupling Product	Reference
	$Y-R$		
Glycosyl Donor	Acceptor (HO-R, H ₂ N-R)	O-, N- linked glycoside	
Amine	Carboxylic Acid	Amide	
Amine	<i>Iso</i> -thiocyanate	Thiourea	65
Amine		Squaric diester	73
X-OH ₂		Oxime	
$X \equiv N^+ - O^-$	Alkyne	Isoxazole	
Carboxylic Acid	Amine	Amide	
Alkyne	Azide	Triazole	
Thiol	Thiol	Disulfide bridge	112
Thiol	Alkene	Thioether	112
Selenyl sulfides	Thiol	Disulfide bridge	
	Amine		

Table 2 : Various coupling methods employed to multivalent scaffolds.

1.8 Conclusion

An enormous range of multivalent architectures are available, with an equally wide variety of coupling methodologies. Therefore, the toolbox for studying multivalence and the cluster-glycoside effect is very diverse. As well as providing control over valence; positioning, spacing and presentation of the saccharide moieties can also be controlled. The introduction of multiple functionalities for multiple targets is also possible. By taking advantage of particular properties of a scaffold, one can design molecular, macromolecular and supermolecular tools with a wide range of potential applications. Of course, the multivalent scaffold and functionalities used must reflect the properties of the multivalent receptor to be studied.

CHAPTER 2 :

Gold Glyconanoparticles (GNPs)

CHAPTER 2 :

Gold Glyconanoparticles (GNPs)

2.1 Gold

Gold, chemical symbol Au, has the atomic number 79 and is found in group 11 (IB) of the periodic table, below copper and silver. It has an electron configuration of $[\text{Xe}] 4f^{14} 5d^{10} 6s^1$ and it is thought that relativistic effects on the 6s electron are responsible for the differences between Au and the other elements of the group. The relativistic effect enhances the binding of the 6s electron to the nucleus, so the orbital condenses on the nucleus. To compensate for this increased attraction, the 5d orbitals are destabilised and so expand in size. Several oxidation states are possible, ranging from -I to III and V with I and III dominating. Gold is widely distributed in nature as metals or as ores accompanied by other transition metals. In metallic form, it is soft and the most ductile of the elements. Chemically inert and not subject to oxidation or attack by sulphur, as well as its lustrous colour, have led to its popularity and use as a precious metal in jewellery, sculpture and ornamentation. In medieval times, gold was also often used as a remedy for several illnesses including heart and venereal problems, dysentery, epilepsy, tumours as well as a diagnosis for syphilis.¹²⁰ Metallic gold readily reacts with halogens, or halogen containing solutions such as aqua regia to give chloroauric acid as yellow crystals $[\text{H}_3\text{O}]^+[\text{AuCl}_4]^- \cdot 3\text{H}_2\text{O}$. $[\text{AuCl}_4]^-$ is a strong oxidising agent, used in oxidation of Rh in aqueous solution. It is itself reduced by various reducing agents and gives highly coloured solutions of colloidal gold.¹²¹ Due to its “soft” nature, gold atoms prefer to bind to soft ligands such as thiolates.

2.2 GOLD ATOM CLUSTERS

2.2.1 Vocabulary

Clusters, nanoparticles and colloids are the three most commonly used terms given to nanometer sized gold structures. The difference between them is not clear however it seems to be the case that small structures (tens of atoms) are referred to as clusters, larger structures (up to tens of nanometers in size and spherical) are nanoparticles whereas colloids refers to larger structures which may or may not be spherical in shape. Monolayer protected clusters (MPCs)

is another term referring to particles coated in a protective layer, typically consisting of thiol-functionalised organic molecules.

Gold cluster formation results from the reduction of Au^I or Au^{III} halides by various reducing agents. Depending on the strength of the reducing agent, various nanoparticle types and sizes can be synthesised.

Reduction by NaBH₄, Au_n clusters are formed, where n = 4, 5, 6, 8 and 13. The structure of gold clusters is relatively unknown with most small clusters having an icosahedral based structure such as that of [Au₁₃Cl₂(PMe₂Ph)₁₀] (figure 26).

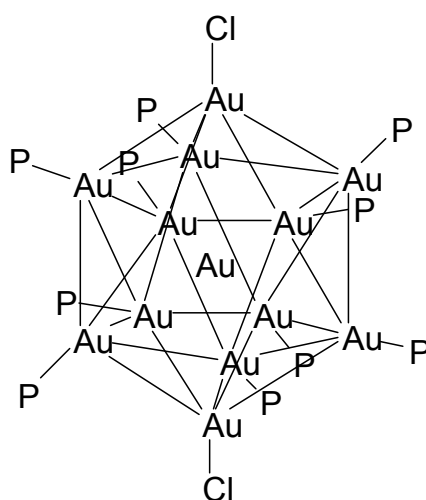


Figure 26 : Icosahedral structure of [Au₁₃Cl₂(PMe₂Ph)₁₀].

The structures of Au₁₁ and Au₉ are fragments of this icosahedral structure, always with a central Au atom, followed by some distortion of the Au-Au bonds. Larger structures have been reported by the use of other reducing agents. Schmidt *et al.* successfully used B₂H₆ in the reduction of (Ph₃PAuCl) resulting in the formation of Au₅₅(PPh₃)₁₂Cl₆. These were the first gold nanoparticles to exhibit “quantum dot” properties.^{120, 121 (and references therein)}

2.2.2 Synthesis and assembly

Several methods exist for the synthesis of gold nanoparticles. Faraday reduced gold salts using Phosphorous dissolved in CS₂ giving colloidal gold at room temperature.¹²² Modern techniques have revealed that this protocol leads to particles of between 40 – 80 nm. Over the last half century, several methods have been implemented to produce Au clusters.

2.2.2.1 Brust-Schiffrin method

In recent decades, the Brust-Schiffrin method has become one of the most popular methods of AuNP fabrication, allowing the facile synthesis of thermal and air stable nanoparticles with reduced dispersity and controlled size.¹²³ This method involves the phase transfer of $[\text{AuCl}_4]^-$ by a phase transfer catalyst, tetraoctylammonium bromide. The organic layer is then separated and reduced by sodium borohydride in the presence of an alkanethiol (dodecanethiol). Upon reduction of the organic phase, the gold atoms agglomerate and form clusters which begin to grow. The clusters are immediately protected by the thiol ligands, due to the soft natures of both Au and S, which prevent further growth and stabilises the nanoparticles in the organic solution. These nanoparticles can be repeatedly isolated and re-dissolved in common organic solvents and are not subject to irreversible aggregation; allowing easy handling and further functionalisation. Due to their remarkable stabilisation, AuNPs stabilised in this way can be treated as any other organic molecule, including the use of standard analytical techniques, adopting the characteristics of their protective ligand. The size of the nanoparticles was found to be dependent on the reaction conditions, in particular the ratio of thiol : gold salt, exhibiting a core size distribution typically between 1 – 3 nm. Higher molar ratios of thiol : gold, fast addition of reductant and cooled solutions gave a higher abundance of smaller, more monodisperse nanoparticles. The structures were observed to be cuboctahedral and icosahedral in shape by TEM. A variation on the Brust-Schiffrin method developed by Murray *et al.* allowed the synthesis of water-soluble, stable nanoparticles. Aqueous solubility is attributed to the polar nature of the protective ligand used – trimethyl(mercaptoundecyl) ammonium.¹²⁴ Aggregation of the nanoparticles was observed by thermogravimetric analysis and TEM. However, this aggregation was between the terminal ammonium groups with no metallic core fusion. The use of amphiphilic ligands, combining the stability of aliphatic chains with hydrophilic groups allows for the direct synthesis of water stable AuNPs without the need for phase transfer catalysts. One example of such a ligand is the monohydroxy (1-mercaptoundec-11-yl) tetraethylene glycol developed by Brust *et al.*¹²⁵ This ligand allows for good chemisorption to the NP surface whilst providing solubility in aqueous environments without aggregation.

The Brust-Schiffrin synthesis is known to tolerate a wide range of conditions including ligand type (non-polar / polar, aromatics). Large bulky ligands have also been used and are known to produce smaller Au core sizes. Mixtures of Au with one or several of the following produces

core alloys; Ag, Cu, Pt and Pd.¹²⁶(and references therein) The nanoparticles are known to be stable for long periods of time (years) under ambient conditions without showing any ageing effects. However, aromatic ligands such as mercaptophenol and short chain alkanethiols (C2-C4) have shown reduced stability.¹²⁷

The exact mechanism of the reaction has not yet been fully elaborated. However, speculative examination of experiments under various conditions (thiol : Au ratio, temperature, large bulky ligands) indicates the formation of an intermediate polymer structure which then collapses to the cluster (see below).^{126, 128, 129} Studies by Luna *et al.* isolated these polymeric structures, which also exhibited self-organisation properties, from the reaction supernatant.¹³⁰



2.2.2.2 Citrate reduction

An alternative synthetic method of producing stable gold nanoparticles is the reduction of gold (III) salts by citrate. Nanoparticles produced via this method are typically larger (~20 nm) than those of the Brust-Schiffrin method described above. First developed in 1951 by Turkevitch *et al.* but is still in use today.^{131, 132} As this reaction is typically carried out in aqueous solutions using an environmentally friendly reductant, this method is popular among “green” chemists.

2.2.2.3 Other syntheses

Other synthesis methods include the condensation of molecular ion beams of aggregated metals, reduction by radiation (γ -rays from ⁶⁰Co).¹²² Reduction of gas phase Au atoms by electron doped MgO surfaces has also been shown to be possible.¹³³ Indeed, there exists a wide range of exotic reductants.

A number of synthetic “aids” have also been applied to the Brust-Schiffrin method in order to allow greater control over particular variables. Wai *et al.* used temperature to control the size of AuNPs between 2.1 and 6.6 nm.¹²⁸ Suzuki *et al.* used thiol functionalised oligonucleotides to control the quantity and spacing of ligands to the Au surface.¹³⁴ Satherley *et al.* have used supercritical ethane to purify and separate clusters of varying size ranges.¹³⁵ Tuning of the separation was done by varying the pressure of ethane, the separation being a function of solute concentration, density and solvation as well as enthalpies of solvation and solute

volatility. Larger NPs would accommodate more interactions with solvent molecules thus increasing their solvation.

2.2.3 AuNP structure

The number of gold atoms in these structures results from the close packing of spherical atoms. The smallest perfect cluster (perfect in terms of symmetry, above) containing 13 atoms consists of one atom surrounded by a layer of 12 atoms. The equation for predicting Au nanoparticle growth being:

$$\text{no. atoms in layer} = 10n^2 + 2 \quad \text{E 25}$$

Where n is the layer number. Therefore, the second layer would consist of 42 atoms, leading to a 55 atom cluster (once the 12 atoms of the first layer, and the central Au atom are included). The third layer would consist of 92 atoms, giving a total number of 147 Au atoms in the cluster etc. These numbers are said to be the “magic numbers” of colloidal structures, predicted theoretically to have the most favourable binding energies for these clusters as well as geometric and electron shell closing.

Monolayer protected nanoparticles are known to form non-perfect clusters with varying geometries. However, very little knowledge of the core structure is known particularly with reference to the nature of the Au-S bond. Characterisation was limited to microscopic and diffraction methods as well as theoretical studies, all of which revealed octahedral packing of the Au atoms. For the Au-S bond, Brust *et al.* had already reported that the Au-S bond is not equivalent to the same gold-sulfide bond as shown by X-ray photoelectron spectroscopy (XPS).¹²³ However, the exact nature of the Au-S bond, the fate of the sulfhydryl proton and the conformation of the organic ligands remained a mystery. Difficulties in fully characterising the NP core result from structural heterogeneity as synthesised, as well as ligand mobility. In return to this requirement for further elucidation of the AuNP structure, several computational methods were developed.¹³⁶(and references therein) However, challenges were met with regards to AuNP parameterisation and force-field development, particularly without the aid of crystal structure data. Following this, Kornberg *et al.* have successfully synthesised *p*-mercaptobenzoic acid (*p*-MBA) functionalised AuNPs in sufficient homogeneity as to produce uniform crystals. They were capable of solving the crystal structure to 1.1 Å resolution (figure 27).¹³⁷ The structure revealed an Au core consisting of 102 atoms,

surrounded by a monolayer of 44 *p*-MBA molecules. They reported that the core structure exhibited C_5 symmetry in the *Z*-axis, with the 13 equatorial atoms occupying one of two possible conformations, giving rise to core chirality. Each Au atom has 12 nearest neighbours, with the exception of the Au atoms at the extremities which may have up to 10 less nearest neighbours. Each Au atom at the surface binds to one sulphur atom, with at least one Au atom binding 2 sulphurs. The sulphur atoms bind in a bridge formation to two Au atoms. The thiol monolayer is stabilised not only by Au-S bonds, but also from contributions of the phenyl ring through stacking or back donation of electron density via S lone pairs. They also state that the *p*-MBA ligands are linked to each other via these interactions, an organisation which extends from pole to pole over the NP surface – exemplifying the “self assembly” around the Au core which also contributes to its chirality.

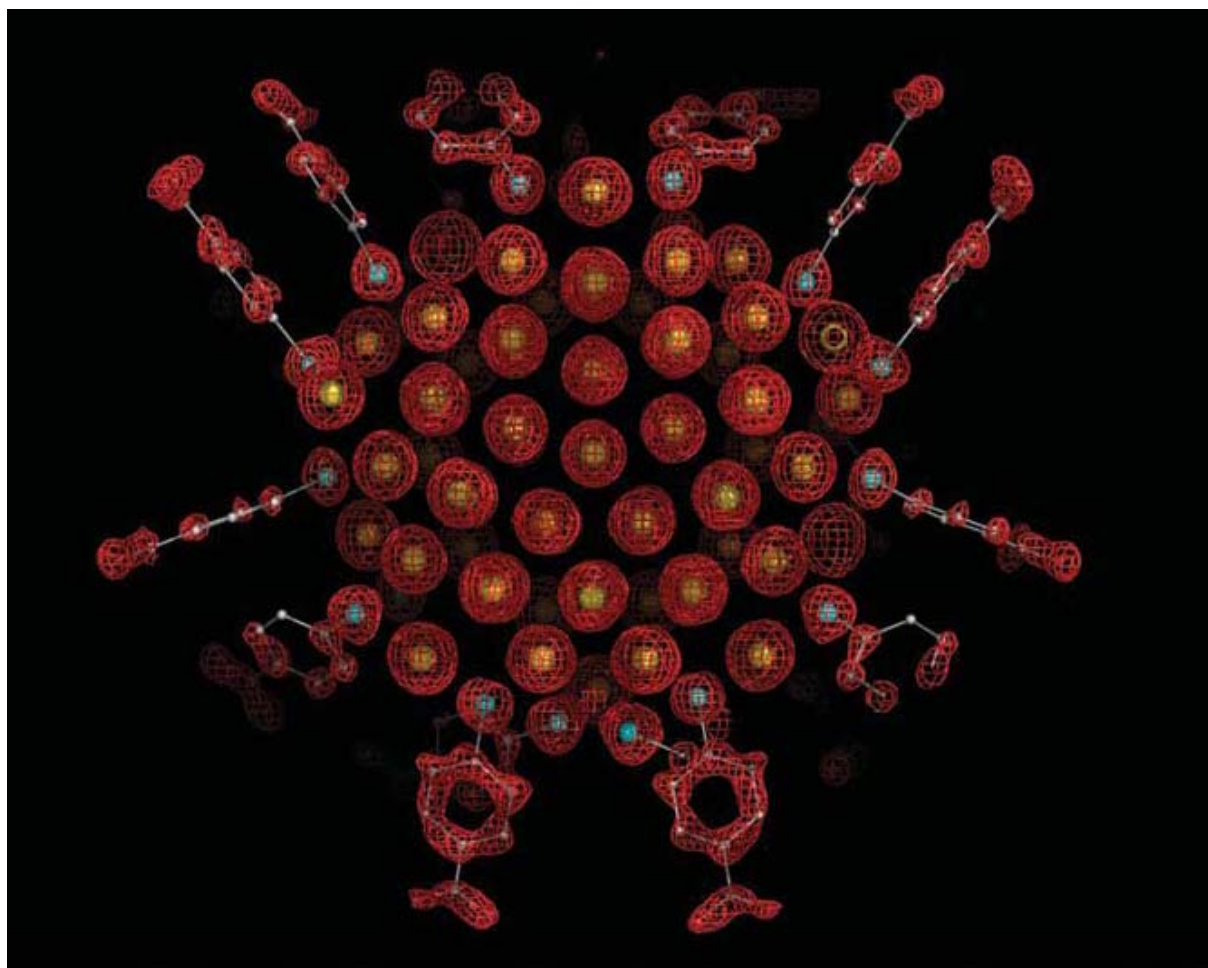


Figure 27 : Crystal structure of $Au_{102}(p\text{-MBA})_{44}$ protected AuNPs by Kornberg *et al.*¹³⁷

A second crystal structure of a thiol-protected AuNP was published by Jin *et al.* shortly after the work by Kornberg *et al.*¹³⁸ This was the crystal structure of an Au_{25} cluster protected by

18 phenyl ethanethiol ligands. The structure of the core Au atoms indicates growth originating from the “magic” Au₁₃ icosahedral core, where the termini of each x, y and z axes of the Au₁₃ shell incorporates an additional pair of Au atoms (figure 28).

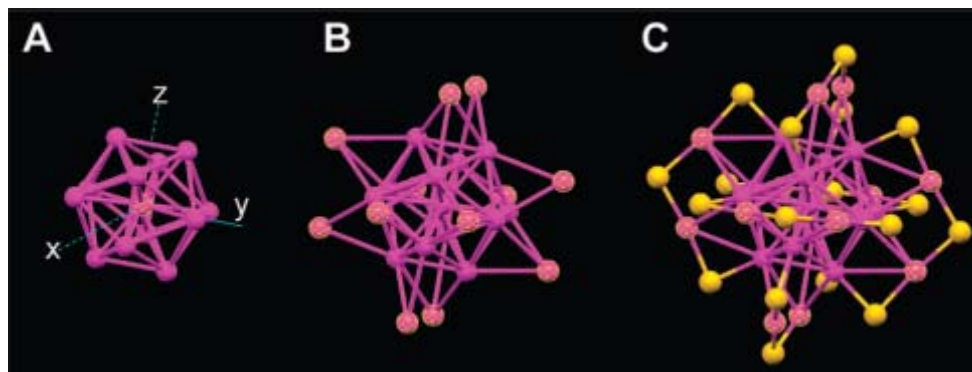


Figure 28 : Icosahedral Au₁₃ core structure (A) Au₁₃ core structure with 12 extra Au atoms on the outer surface (B) and Crystal structure of Au₂₅(phenyl ethanethiol)₁₈ (sulphur atoms shown only, C)¹³⁸

The binding of the thiolates to the Au atoms is again bridging, remaining consistent with Kornberg’s structure, with all Au atoms being bridged by one or two thiolate ligands. However, it is thought the ligands have an influence on the structure of the Au core atoms, in particular to the outer incomplete shell. In this case the core is symmetric, there is no observed chirality as for Kornberg. However, this structure was found to be associated with one tetraoctyl ammonium ion, suggesting that the NP is in fact in a cationic state [Au₂₅(phenyl ethanethiol)₁₈]⁺ which, from time dependent density functional theory (TD-DFT) calculations, explains the optical properties observed experimentally. These theoretical studies also revealed a potential influence of ligand nature on the optical properties. Indeed, Kumar *et al.* have shown a dependence of cluster size on thiolate ligand length.¹³⁹

Further DFT studies carried out by Wang *et al.* have showed the core conformational transition states between Au₁₆⁻ and Au₂₀⁻ clusters, where transition from cage-like to pyramidal structures, the former being more reactive towards O₂ and the latter towards Ar.¹⁴⁰ The growth of the cluster was also shown to be dependent on the growth pathway and overall charge, resulting in several coexisting isomers (figure 29).

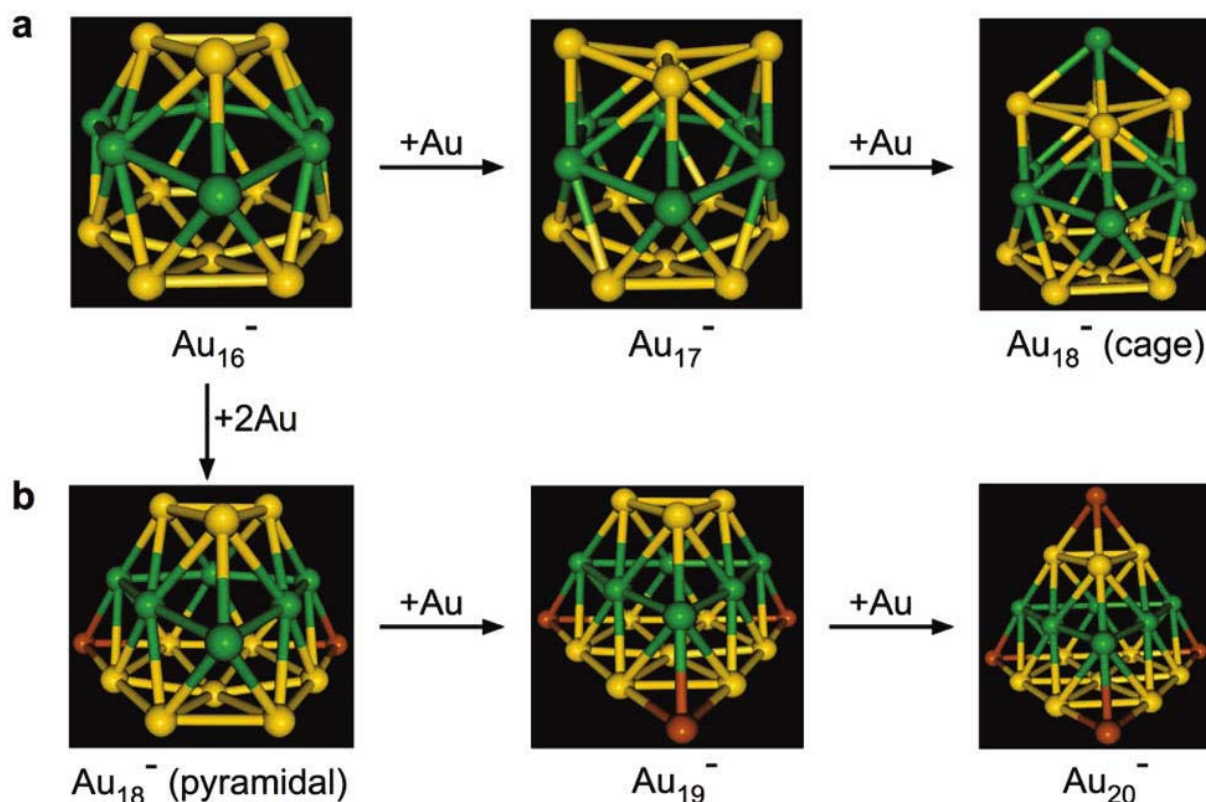


Figure 29 : Transition of core structure from cage Au_{16}^- to pyramidal Au_{20}^- and the isomers that exist between, depending on the growth pathway (a) or (b).

2.2.4 Gold-ligand interactions

Upon reduction of the gold salt, it is assumed that the thiol binds to the gold as a thiolate, consequently losing the hydrogen atom as a proton. In many cases this is indeed the case.¹⁴¹ Ligand exchange at low density surface coverages gives a favourable energetic pathway where hydrogen is lost. However, the thiol has also been shown to remain intact under certain conditions (ligand exchange at high density surface coverage) where hydrogen gas formation is not energetically favourable.¹⁴² What exactly happens to the intact thiol at the AuNP surface is unclear, whether the hydrogen remains with the sulphur, or whether it is adsorbed by the NP surface. This of course could also be a reflection of the different reactivities of the Au atoms on the NP surface.

2.2.5 Other ligands

Thus far only thiolate ligands have been discussed. These ligands are a clear favourite in forming the necessary Au-S bond for stabilising the NP, and the soft nature of both Au and S support the stabilisation of both ligand and NP. However, AuNPs are certainly not limited to thiolate ligands. Indeed, disulfides can be used, which is reduced to thiolate *in situ* upon the addition of NaBH_4 . Above, in the first Au cluster to be identified, phosphine ligands and

halides were observed. Porta *et al.* have shown that amine-functionalised ligands can also be used to stabilise gold clusters, reporting that the Au-N interaction is mildly ionic in nature, and that the amine is in fact protonated, interacting with counter ions on the NP surface.¹⁴³ Amino acids, including lysine, have also been used, which prove promising for biological applications. Phosphine oxides and carboxylic acids have also been used to stabilise Au clusters. Citrate, from citrate reduced AuNPs can also be displaced by acetone and Iodine in fluoruous media.¹²⁰ Typically, these structures are larger than the thiolate protected clusters.

Ligand exchange is also known to take place. Particularly the replacement of weakly bound ligands by more appropriate ones.¹²⁶ The substitution of thiolates by dithiols, 1,2-dithanes or dithiocarbamates is common, where the bidentate binding to the AuNP surface is enthalpically and entropically favoured.

2.3 Physical Properties

The physical properties of NPs are remarkably different from those of bulk material or molecular compounds and present a range of interesting properties which include unexpected size-related electronic, magnetic and optical effects (quantum size effect). As well as an increased surface area : volume ratio upon size reduction, statistical mechanical effects will also be contributing to the quantum size effect. The quantum size effect arises from the fact that the wavelength of the metallic electrons ($6s^1$) is of the same order of size as the nanoparticles themselves ($\lambda \sim 1$ nm). This isolates the electrons in zero-order quantum boxes, where they are subject to quantum-mechanical rules.¹²⁰ Also, in nanoparticles there is a band gap between the valence band and the conduction band, like semiconductors. This band gap is dependent on the cluster size and is observed if the cluster is small enough (less than 20 nm). Single-electron transitions occur in the nanoparticle, promoting a valence band electron to the conduction band if the electrostatic energy (E_{el}) is larger than thermal energy (E_T).

$$E_{el} = \frac{e^2}{2C} \quad \text{E 26}$$

$$E_T = k_B T \quad \text{E 27}$$

Where e is the charge of an electron and C is the capacitance of the nanoparticle, which decreases with decreasing cluster size. Electron promotion results in the charging of the

nanoparticles. In thiolate protected nanoparticles, this metal-like capacitance charging leads to redox-like charging. Indeed, between 10 and 15 redox peaks have been measured for AuNPs of varying sizes.¹²⁰(and references therein)

2.3.1 Surface plasmon resonance

The conduction electrons show an oscillation frequency of plasma resonance, giving rise to the surface plasmon resonance (SPR) band, where inbound light particles couple to these plasma-state electrons, exciting them and producing an evanescent wave field which is emitted to the local environment (chapter 4, section 2).^{120, 127} The main characteristics of the SPR band in gold nanoparticles are cited as: position around 520 nm, sharp decrease in intensity and widening bandwidth with decrease in core size due to quantum effects, and stepwise spectral structures due to discrete unoccupied energy levels in the conduction band for small core sizes. The SPR band is dependent on the refractive index of the local medium, which is in turn dependent on the ligands on the surface of the nanoparticle. A shift in the SPR band can be seen between nanoparticles functionalised with different ligands.

However, AuNPs with core diameters lower than 2 nm show no SPR band due to quantum size effects. As the core size decreases, the valence band of metallic electrons becomes more discrete. As the core size is reduced further (below 2 nm) the AuNP loses its bulk electronic properties and no longer supports plasmon excitations - the valence electron band becomes more molecular-band like.¹³⁸

2.3.2 Fluorescence

As well as exhibiting their own fluorescent behaviour, AuNPs also contribute to the activity of fluorophores which are functionalised to their surface or in free solution. In particular, they exhibit quenching capabilities to a wide range of fluorophores.¹⁴⁴ Murray *et al.* have suggested three mechanisms by which luminescent quenching or enhancement at AuNPs may occur:

1. Structure dependent “static” quenching of thiolated fluorophores bound to the AuNP surface. Static quenching occurs when the fluorophore-AuNP ground state is non-fluorescent. Hybridisation of the fluorophore to the monolayer or aggregation effects may induce quenching whereas the suppression of non-radiative decay pathways may induce luminescence enhancement.

2. The irreversible immobilisation of fluorophores to the AuNP surface (via electrostatic interactions between an anionic functionalised AuNP and a cationic fluorophore for example) may induce static luminescence quenching whilst also reducing dynamic (collision) quenching with other bodies in solution.
3. Quenching of fluorophores in free solution upon non-specific collisions with AuNPs. The AuNP deactivates the fluorophore in its excited state, allowing for a non-radiative decay pathway.

2.3.3 Magnetism

Typically, bulk Au is diamagnetic as all 5d electrons are paired. Therefore upon exposure to an external magnetic field, diamagnetic materials will create a magnetic field in opposition, creating a repulsive effect.

AuNPs however have often been observed to exhibit different magnetic properties. Density functional calculations on unprotected “naked” AuNPs have led to predictions suggesting that dimensionally reduced systems (surface layers, nanowires and nanoclusters) may lead to ferromagnetic ordering typically found with Fe, Co and Ni.¹⁴⁵ Calculations by Luo *et al.* claim that the highest occupied molecular orbital (HOMO) of the gold nanoparticles, occupied by 6s electrons, is highly degenerate and partially filled. The electrons in this partially filled molecular orbital align their spins to give a “superatom” with an outer shell of high spin – leading to ferromagnetic behaviour. Studies by Jin *et al.* also support the superatom theory with their studies of thiol protected Au₂₅ and naked Au₁₃ clusters.¹⁴⁶ They show that paramagnetism is reversible and dependent on surface charge for the Au₂₅ cluster whereas DFT calculations of the Au₁₃ cluster imply an anisotropic unpaired electron spin distributed throughout the structure.

Experimental studies by Fernandez *et al.* suggest a different theory.¹⁴⁷ They found that amine-capped AuNPs exhibited diamagnetism, whereas thiol-capped AuNPs exhibited ferromagnetism. Therefore, the interactions of thiol ligands with the Au atoms of the surface alter the electronic structure of the NPs in a way that the amine ligands and bulk Au do not. Relativistic effects lead to *s-p-d* hybridisation upon interaction with the thiol ligands allowing charge transfer from Au atoms bound to the organic ligands. This induces a localised,

anisotropic magnetic moment giving the appearance of permanent magnetism. Small amounts of Fe impurities in the NP core were thought to contribute significantly to the observed ferromagnetism. However this was later found to be the contrary, with the presence of Fe in the core reducing spontaneous magnetisation and local anisotropy thus blocking the NP-ligand bond induced magnetic moments.¹⁴⁸

2.3.4 Mean inner potential

The crystal lattice potential is the amount of energy released upon the condensation of particles to form a uniform crystal lattice. This crystal potential can be separated in to several contributions. The mean inner potential (MIP) is the volume-averaged electrostatic contribution to the crystal lattice potential – the amount of energy required to break the electrostatic interactions between elements of the crystal lattice.¹⁴⁹ The MIP is sensitive to the electronic state of the outer valence electrons of AuNPs which, upon size reduction, changes rapidly with respect to properties of bulk Au. The mean inner potential of Au increases dramatically from ~25 eV in the bulk state to greater than 40 eV with particles less than 2 nm in diameter, indicating charge transfer interactions between Au and surrounding species.¹⁵⁰ Although the effects of NP size on the MIP are not yet fully understood, it is suspected that this electronic behaviour could be the basis for the catalytic activity and magnetism observed in AuNPs.^{147, 150}

2.3.5 Ligand presentation

As AuNPs are 3D structures with many points on their surface, they present a spherical scaffold to which suitably functionalised ligands can be attached. In particular, multiple copies of the same ligand can be added to the same cluster, giving rise to multivalent presentation. Also, the addition of several different ligands will give “hybrid nanoparticles”, where several different ligands can be associated to the same AuNP. By controlling the relative molar ratios of the different ligands, as well as their coupling to the AuNP core and the core size itself, the degree of hybridisation can be controlled, allowing the controlled modification of presentation density, or “footprint” of a particular ligand.¹⁵¹ Mirkin *et al.* showed that for oligonucleotide functionalised AuNPs with core diameters lower than 60 nm, the presentation density of the ligands was significantly higher than that of a 2D SAM due to a higher surface area : volume ratio. A core size of 60 nm and above exhibited ligand presentation densities approaching those of 2D SAMs.¹⁵¹ Thus, above 60 nm, the ligands would behave as if attached to a 2D surface and the advantages of a 3D scaffold are lost. They

also show the mathematical relationship between core size and area occupied by ligands at the AuNP surface – the presentation density being proportional to the inverse square of the core radius. At the same time, Keating *et al.* showed that as the curvature of AuNP and nanorods increased, the packing of ligands at the NP surface was significantly higher, confirming the inverse proportionality of the core size to presentation density described by Mirkin *et al.*¹⁵² Both papers discuss the importance of considering AuNP core size which may affect ligand activity. In particular, changes in ligand activity with respect to ligand-receptor and inter-ligand interactions with their presentation at the AuNP surface. One can easily imagine that the effective concentrations of ligands would change with presentation density and hence curvature and core size.

2.4 Applications

Applications related to the physical properties are as varied and imaginative as the properties themselves. However, other properties related to the functionalisation of AuNPs are also prevalent in the literature. One advantage of using AuNP systems is of course the multiple functionalisation properties which allow several applications to be used on the same particle.

2.4.1 Surface plasmon resonance

Several examples in the literature take advantage of the SPR band in AuNP systems and in particular, the dependence of the SPR band on the local environment, the solution state of the NPs and the coupling of surface plasmons of AuNPs in close proximity (aggregates). The application of this towards the optical detection of particular molecules in solution are numerous, taking advantage of the SPR band shift upon aggregation induced coupling.^{131, 153} Size / concentration relationships have also been outlined for AuNP systems using SPR.¹⁵⁴

2.4.2 Catalytic activity

Although Au is well known for being chemically inert and resistant to oxidation, Au prepared as nanoparticles, often supported on solid phase-oxides (TiO₂, Fe₂O₃, CeO₂ or activated carbon) become active and selective catalysts for a range of reactions. These include low temperature CO oxidation,¹⁵⁵ styrene oxidation,¹⁵⁶ hydrogenation of alkenes, alkynes, imines and carbonyls,¹⁵⁷ as well as the selective hydrogenation of C=O groups of α,β -unsaturated carbonyls and the hydrogenation of nitro-groups.¹⁵⁸

It was thought that this catalytic activity originated from quantum size effects of the gold clusters as this has been shown to affect AuNP catalytic activity.¹²⁰ However, it has been shown by Freund *et al.* that catalytic activity in some cases arises from the presence of highly uncoordinated Au atoms at the AuNP surface being available to adsorb various substrates.¹⁵⁹ It is also thought that the AuNPs act as co-catalysts by converting the stoichiometric sites of the oxide support to catalytic sites by facilitating their reactivation.¹⁶⁰ When in close proximity to other metal ions, it is thought that the Au clusters invoke electronic effects in these ions, increasing activity.¹⁵⁶

AuNPs have also shown electrochemical properties, with between 10 - 15 oxidation states observed, depending on cluster size.¹²⁰ The redox properties of AuNPs have been applied to the electro-oxidation of CO and MeOH. Deposited onto glassy carbon electrodes and cross-linking lead to a 3D network arrangement of the AuNPs.¹²⁰(and references therein) Cyclic voltammetry showed the oxidation of both CO and MeOH with a very high activity, but only after catalytic activation; Au oxide formation.

2.4.3 Drug delivery vectors

AuNPs also provide a convenient drug delivery vector. The AuNP core, being essentially inert and non-toxic, provides an interesting scaffold to which drug molecules can be immobilised. The ability to form mixed monolayers provides direct access to particular biological systems. For example, tailoring the size and monolayer coating to realise tumour specificity and cell membrane penetration, whilst also carrying chemotherapeutic drugs, would increase site selectivity thus reducing the side-effects of chemotherapy. Tagging with a fluorescent marker would also indicate the time and location of ligand release – the fluorophore being quenched when immobilised to the AuNP core, becoming active upon exchange and release. Ligand exchange at the AuNP surface can also be used to a biomedical advantage. Naturally occurring thiol-functionalised molecules such as glutathione, dihydrolipoic acid and cysteine have been shown to be ideal ligands which could contribute to surface exchange interactions at the AuNP core. Rotello *et al.* showed that ligand exchange by these biologically relevant thiols depends on AuNP surface charge (surface charge, not AuNP core charge) to which *pseudo*-first order kinetics was observed.¹⁶¹ This allows the stability of the ligand-AuNP bonds to be tuned, providing control over the release rate of attached ligands. As the surface exchange depends on the concentrations of these thiol containing

molecules, delivery can be limited to when the AuNPs arrive at the target location. Intracellular glutathione concentrations (1-10 mM) is several orders of magnitude higher than extracellular levels (2 μ M), providing a mechanism for selective intracellular release of AuNP monolayers.¹⁶²

Also, the possibility of adding many copies of the same molecule to one nanoparticle cluster allows for high density drug delivery and much higher drug payloads than other multivalent systems. Albericio *et al.* have synthesised AuNP systems functionalised with the anti-tumour drug Kahalalide F for this purpose.¹⁶³ Kotov *et al.* functionalised AuNPs with the anti-leukaemia and anti-inflammatory drug 6-mercaptopurine. Use of this drug was previously limited due to the short biological half-life and severe side effects. However, by functionalising a AuNP, this molecule has been shown to be more stable with an enhanced activity due to improved intracellular transport and release allowing for the use of lower concentrations.¹⁶⁴ Zubarev *et al.* have developed AuNPs functionalised with the chemotherapeutic drug paclitaxel as an alternative method of better quantifying drug dosage.¹⁶⁵ Rotello *et al.* have also produced AuNPs functionalised with amino acids for gene therapy delivery agents.^{166, 167}

Indeed, many such examples of AuNPs functionalised with drug molecules can be found in the literature. AuNPs provide a versatile platform for optimising both passive and active targeting drug delivery.¹⁶⁸ Other biomedical applications of AuNPs include radical scavengers by functionalisation with antioxidant molecules,¹⁶⁹ imaging and labelling in both passive and active targeting capacities.¹⁷⁰⁻¹⁷⁴

2.4.4 Hyperthermia therapies

As well as their use as smart vectors for drug delivery, AuNPs have also been incorporated in to micelle and liposome based micro- or nano-capsule delivery vehicles. One problem in using polymeric or liposomal capsules is the controlled release of drug molecules encapsulated in their cavities. A solution, used by several groups, is to encapsulate AuNPs or hollow Au nanoshells, as well as the drug molecule, in the same capsule. Upon UV or near-IR radiation, the NPs absorb the radiation and convert this to heat energy. Instantaneous heating of the local environment cause the formation of micro bubbles in solution, disrupting and destroying the polymeric carrier and releasing the encapsulated contents.^{175, 176} The advantage of using UV and near-IR sources is that they can be applied to bodily surfaces (UV) and

within the body non-invasively. This type of treatment is known as localised hyperthermia and has been applied to the non-invasive treatment of tumours and shows particular promise for the treatment of surgically inaccessible primary tumours as well as secondary sites.^{177, 178}

2.5 AuNPs as Multivalent Scaffolds

As mentioned above, the AuNP provides a scaffold to which multiple copies of the same molecule can be added. This of course gives rise to the multivalent presentation of the ligand. Compared to other multivalent scaffolds discussed in the previous chapter (dendrimers, polymers, calixarenes, proteins etc), AuNPs provide a very unique and attractive scaffold to which carbohydrate ligands can be conjugated and their interactions with various lectins studied. The inherent physical properties of the AuNPs described highlight the advantages of using inorganic Au clusters from the organic structures as none of these exhibit SPR phenomena, magnetism, mean inner potentials or direct applications to catalysis (several can exhibit fluorescence and interesting electrochemistry however).

Another advantage of using AuNPs is that they provide a very versatile scaffold for multifunctionalities in high density and high valency. To do this however, the ligand must be functionalised with a suitable tethering group (thiol, disulfide). Once synthesised, this can be grafted onto the AuNP surface in the one-pot Brust-Schiffrin synthesis. It is also significantly easier to manipulate and modify the properties of AuNPs to better suit their integration with biological systems, or indeed change their binding modes, to suit different multivalent receptors. Size control, modifying their surface layer depending on the desired solubility, as well as using hybrid surface layers would allow for a range of presentation densities of the active ligands. All of which, in organic frameworks would require several synthetic schemes, often requiring many protection / deprotection steps to exercise the same degree of control and multifunctionality. This idea of tunability is important when considering interactions with biological systems. *In vivo*, the ligand would have to be selective for the target receptor. Ligand selectivity on an AuNP can be controlled by presentation and presentation density and may be crucially important for targeting purposes. Also, biological systems often have several tools available in order to carry out a particular biochemical process (*P. aeruginosa* for example with PA-IIL and PA-IIIL lectins for bacterial invasion). In order to interfere and block this process completely, a multifunctional inhibitor would be particularly useful. This would

be difficult to do with organic scaffolds, again requiring difficult syntheses and protection / deprotection steps. With AuNPs, this multifunctionality can be incorporated relatively easily.

2.5.1 Applications to carbohydrate interactions

There are many examples in the literature of carbohydrate functionalised AuNPs – Glyconanoparticles (GNPs) for investigating carbohydrate interactions. GNPs are similar in size to many common biomacromolecules and provide an ideal scaffold for presenting carbohydrate molecules in a globular polyvalent configuration, much like the glycocalyx. Also, the physical properties of the AuNPs described above may be applied to the detection and evaluation of their interactions.^{179, 180}

Penades *et al.* have developed several GNP systems as a 3D model of the glycocalyx for studying carbohydrate-protein interactions.^{181, 182} Kataoka *et al.* also demonstrated an interesting 2-step synthesis of GNPs.¹⁸³ Initially, AuNPs are formed by the *in situ* reduction of HAuCl₄ in the presence of acetal functionalised ligands. The acetal was then removed to reveal an aldehyde group which was then functionalised with lactose. Aggregation studies with the galactose specific RCA 120 lectin were subsequently carried out. Wu *et al.* synthesised mannose functionalised GNPs for the labelling of FimH on type I pili, as well as demonstrating an increase in lectin affinity for the GNP scaffolded mannosides.¹⁸⁴ The same group studied the interaction of their mannose GNPs with Con A by SPR showing a 100 fold increase in inhibitory potential with regards to Me- α -D-Mannose.¹⁸⁵ Kamerling *et al.* also developed glucose and mannose functionalised GNPs for studying the interaction of Con A by SPR, UV/vis aggregation and TEM, showing an increased affinity of Con A for the GNP scaffolded mannosides.¹⁸⁶ Lin *et al.* also used SPR competition studies to investigate the interaction between shiga-like toxin and globotriose functionalised GNPs.¹⁸⁷ Relative inhibitory potencies up to 200 000 fold higher were observed for these GNPs with reference to the monomer ligand.

Hybrid lactose / triethylene glycol GNPs of varying lactose presentation density were also produced by Penades *et al.* in order to demonstrate the importance of ligand densities in lectin-GNP interactions.¹⁸⁸ Two galactose specific proteins were investigated; the lectin *Viscum albumin* agglutinin (lectin) and the enzyme *E. coli* β -galactosidase in competition and hydrolysis experiments respectively. It was found that increasing binding affinity was observed with increasing presentation density, up to 30 % lactose presentation. GNPs with a

10 % presentation density exhibited lower lectin affinities and were more susceptible to enzymatic hydrolysis.

Several qualitative investigations involving carbohydrate functionalised GNPs and various lectin partners have also been carried out. Many of which observe the lectin-induced aggregation of GNPs by TEM and UV/vis or the change in the SPR wavelength. Russell *et al.* also developed lactose functionalised GNPs as a colorimetric bioassay for cholera toxin. Presence of the toxin induces aggregation of the GNPs resulting in a strong colour change (red to deep purple) due to the combination of local surface plasmon resonances of the aggregated particles.¹⁸⁹

Cameron *et al.* introduced RAFT-polymers of galactosides on to GNPs, making a form of multivalent polymer thread extension from an AuNP scaffold. Specificities for PNA were recorded by the reversible aggregation between the GNPs and PNA-functionalised agarose beads.¹⁹⁰

Several GNPs have also been developed for investigating carbohydrate-carbohydrate interactions. Penades *et al.* synthesised Le^x functionalised GNPs as a model for the Le^x / Ca²⁺ mediated aggregation and its importance in self-recognition.¹⁹¹ This was later proven kinetically and thermodynamically by SPR and isothermal titration microcalorimetry, showing the specificity of the interaction between Le^x residues and the requirement of Ca²⁺ ions.^{192, 193} Kamerling *et al.* synthesised GNPs functionalised with β -D-GlcNAc(1-3)Fucosides for studying the self-recognition and adhesion of the marine sponge *Microciona prolifera*.¹⁹⁴ Their TEM studies also revealed the requirement of Ca²⁺ ions in solution to mediate this self-self aggregation.¹⁹⁵ This was again confirmed by Russell *et al.* when they showed the reversible aggregation (using cycles of Ca²⁺ and EDTA) of lactose functionalised GNPs as seen by UV/vis aggregation and TEM.¹⁹⁶

As a biomedical application, Penades *et al.* developed oligo-mannose functionalised GNPs as mimics of the structural motif of the high mannose *N*-linked undecasaccharide Man₉(GlcNAc)₂ found on gp120, a coating glycoprotein of HIV.¹⁹⁷ This glycoprotein is used by the virus as both camouflage from the host immune system and an initiator to the invasion of DC-SIGN cells. The GNP mimics are to act as anti-adhesive agents to prevent infection. A library of GNPs was synthesised varying both the structural motif (mono- to

heptamannosides) as well as their presentation density (10, 50 and 100 %) using an inactive glucoside. GNP efficacy was measured using transfection experiments. Raji cells transfected with DC-SIGN were used, which are capable of capturing and transmitting HIV. The GNPs were shown to be non-toxic inhibitors to HIV – DC-SIGN binding with varying effectiveness. Results again showed the importance of presentation density towards inhibition activity, with too low or too high densities having lower activities. Densities of 50 % showed to be optimum. GNPs functionalised with the tetrasaccharide motif showed the greatest inhibitory potential per mannose residue. Subsequent kinetic studies using SPR revealed more than a 20 000 fold increase in affinity of DC-SIGN per mannoside presented on the GNP surface.¹⁹⁸ By SPR however, a dimannose functionalised GNP with a presentation density of 50 % was found to be the most active in terms of DC-SIGN inhibition potency.

Lin *et al.* have also demonstrated potential applications in protein purification and enrichment.¹⁹⁹ Galactose functionalised GNPs were used to induce the aggregation of PA-IL in PBS solution. The aggregates were separated by centrifugation and subject to MALDI-TOF analysis showing the purity of the isolated lectin. They claim that functionalised GNPs could isolate and improve purity levels of proteins in femtomolar concentrations. Suda *et al.* used a similar method to isolate lectins from banana pulp.²⁰⁰ The lectins were recovered by the addition of inhibitory sugars, reversing the aggregation. However, one disadvantage of this application is that it depends on the protein being multimeric and they induce GNP aggregation.

2.6 Other functionalities

Astruc *et al.* have designed gold nanoparticle systems functionalised with ferrocene groups.²⁰¹ The ferrocene groups exhibited redox potentials, which upon multivalently attaching these groups to AuNPs, was enhanced. These NP systems were reported to be excellent sensors for the presence of a range of oxo-anions, also exhibiting a degree of selectivity, as well as applications for electrode modification. Other functionalities with respect to biomolecules include AuNPs functionalised with DNA and oligonucleotides,^{151, 152, 202} amino acids,²⁰³ polypeptides,²⁰⁴ and proteins.^{205, 206}

2.7 Other NP systems and their applications

As well as gold being used for the metallic core, it is also necessary to mention other metallic nanoparticles which have potential for their multivalent applications. “Quantum dots” (QDs) is a general term given to nanocrystals of semiconducting materials which exhibit physical properties which differ from their bulk solid. One of the most interesting applications of quantum dots is their use as luminescent labels for biological systems as they emit light at a variety of precise wavelengths depending on the compound used and their size; they typically have long fluorescent lifetimes and can be conjugated to a variety of biologically important molecules using a thiolated ligand. QDs can be made of a range of different materials and combinations. Some examples include CdS, CdSe and ZnS.¹⁸⁰

Gao and Qi have used CdSe quantum dots as siRNA delivery vectors for gene therapy specifically for their fluorescence properties in order to track the delivery of the payload.²⁰⁷ Their QDs were combined with Amphiphols – linear polymers with alternating hydrophobic and hydrophilic side chains in order to improve cell binding and internalisation. There are also several examples in the literature of mixed-core QDs, where one semiconductor material is used to form the spherical core, which is then capped by a second semiconducting material. Prasad *et al.* used such QDs made of InP (core) and ZnS (shell) particles coated in mercaptosuccinic acid to allow solubility in aqueous solutions.²⁰⁸ The QDs were then further conjugated with pancreatic cancer specific monoclonal antibodies for the specific targeting and bioimaging of pancreatic cancer cells.

Magnetic nanoparticles (MNPs) also offer interesting properties for biomedical applications. As above with AuNPs, they can be used in the hyperthermia treatment of malignant cells, specifically targeted by biologically important molecules conjugated to the MNP surface. They also present interesting candidates for improving image quality in magnetic resonance imaging (MRI).¹⁸⁰(and references therein)

The most common MNPs are made of Iron oxides which typically have a core size ranging from 5-20 nm. Iron oxide MNPs are commercially available but can be fabricated by the co-precipitation of ferric and ferrous salt solutions (by ammonium hydroxide for example). Soluble in organic solvents (toluene), stabilisation using biocompatible molecules such as

biopolymers allows for solubility in aqueous environments. Narrain *et al.* produced such MNPs functionalised with lactobionic and gluconic acids, which showed biocompatibility comparable to commercial MNPs.²⁰⁹

An alternative synthesis is the coating of Fe colloids with Au. This was demonstrated by Penades *et al.* by the reduction of FeCl_3 followed by reduction of HAuCl_4 and stabilisation by thiol ligands.^{210, 211} Glucose, maltose and lactose functionalised MNPs were synthesised and tested for their bioavailability, with all being stable under physiological conditions and only the maltose MNPs showing toxicity. However, upon cell internalisation the MNPs were degraded. Degradation was found to be dependent on sugar functionality indicating the potential to control cell-nanomaterial interactions.

A second alternative to synthesising MNPs is the functionalisation of AuNPs with groups which capture magnetic metals – or rather the immobilisation of magnetic molecules to the AuNP surface. This approach was also adopted by Penades *et al.* Hybrid GNPs of carbohydrates and thiolate functionalised DOTA were synthesised allowing for the chelation of Gd^{III} , giving novel paramagnetic probes for MRI imaging.²¹² Glucose, galactose and lactose – DOTA hybrid GNPs were prepared and incubated with GdCl_3 . It was found that the magnetic relaxation times were greatly dependent on the nature of the sugar functionality, due to the ability of (oligo)saccharides to order and structure local solvent molecules, which in turn affects the magnetic properties of the Gd-DOTA ligands.

2.8 Conclusion

GNPs are an advantageous alternative as multivalent scaffolds. Their simple and flexible preparation allows greater control over the degrees of multivalency and multifunctionality. The natures of the linkers can also be modified for each ligand as a function of the desired presentation. In comparison to other multivalent scaffolds described earlier, GNPs offer a more tuneable tool for investigating multivalence in biological systems. The inherent optical and electronic properties offered by metal nanoclusters allow for quantifying these interactions as well as providing pathways for a variety of biomedical, biotechnological and materials science applications.

RESEARCH AIMS

Multivalence has been shown to play an important role in many normal and pathological biological processes. Many natural, synthetic and semi-synthetic scaffolds have already been designed to improve the fundamental understanding of this phenomenon, as well as controlling and manipulating these interactions with the aim of developing multivalent diagnostics and therapeutics. The aim of this work is firstly to synthesise and characterise a range of GNPs exhibiting different densities of mannose and galactose active ligands. Secondly, using previously established methods, multimeric recombinant lectins are to be expressed and purified, namely the recently elaborated mannose specific lectin, BclA from *Burkholderia cenocepacia*, the more established PA-IL lectin from *Pseudomonas aeruginosa* and the widely used, commercially available lectin Con A. Finally, qualitative and quantitative biophysical methods will be used to investigate whether GNPs induce a multivalence / cluster glycoside effect in GNP-lectin interactions, at what point multivalence is observed, and for what reasons this may be so, comparing to recent theories on the thermodynamic and effective concentrations / statistical effects relating to the kinetics of the multivalent effect. In particular, haemagglutination inhibition assays will be used as a qualitative interaction characterisation method; this is due to its simplicity and ability to rapidly give reliable results and its frequency of use in the literature thus, providing a method which can be universally compared to previous results. Surface plasmon resonance will also be discussed as a method of investigating the kinetics of the interactions when the lectins are immobilised to a 2D surface. This method has been used less frequently for characterising multivalent interactions; however it provides more information than the previously mentioned HIA. Finally, isothermal characterisation will be used and adapted for characterising the specific interactions between functionalised GNPs and their lectin receptors. ITC has been used in several studies for evaluating the kinetic and thermodynamic parameters of interactions. In particular, ITC has so far not been used for evaluating specific NP-ligand interactions.

CHAPTER 3 :

GNP Synthesis and Characterisation

CHAPTER 3 :

GNP Synthesis and Characterisation

3.1 Chemical Synthesis

Several *neo*-glycoconjugates were synthesised for grafting on to AuNP surfaces. All molecules synthesised feature thiol functionalities attached to linker or spacer molecules which connect the thiol group to the saccharide unit (the terms linker and spacer are interchangeable). There are several types of linker used in this study. The first is the [*N*-(23-thio-3,6,9,12-tetraoxa-tricosane)-*N'*-(2-aminoethyl)] thiourea, which is conjugated to the saccharides mannose and galactose. This linker has been designated the “mixed” linker as it combines the properties of the tetraethylene glycol functionality with the undecane alkyl chain. The mixed linker is only used for the active ligands. The second linker, used only for the inactive glucose ligand, consists of a mercaptopentyl chain conjugated directly to the anomeric position of the glucose. The third linker molecule used is a [*N*-(17-thio-3,6,9,12-tetraoxa-heptadecane)-*N'*-(2-aminoethyl)] thiourea designated the “mixed-short” or “mixed(s)” linker, which is analogous to the mixed linker, with the exception that it exhibits a pentyl chain as opposed to an undecyl chain. The synthesis of these molecules have been described in previous work and the following article (chapter 5), as has the synthesis and purification of the GNPs.^{197, 198, 182, 213}

3.2 GNP Characterisation

In order to characterise the GNPs fabricated, several techniques can be employed. However, due to the multifaceted nature of functionalised nanoparticles, a combination of several techniques is often required to quantify the chemo- physico- and biological properties. Also, due to the heterogeneous nature of the GNPs, it is difficult to characterise individual particles. Therefore, one must characterise a sample population of the GNPs produced. This can then be used to observe the distribution of various characteristics in the GNP population. Once the data has been analysed, one can deduce information based on the whole of the population, giving the characteristics of the *average* GNP(s) found in the sample.

3.2.1 Nuclear magnetic resonance (NMR)

NMR is very useful for GNP synthesis, particularly for the synthesis of hybrid GNPs. When preparing the pre-reaction solution of the thiol functionalised neoglycoconjugates, the solution is prepared in deuterated solvents (D_2O or MeOD at 323 K) which is then analysed by NMR. In the case of the mannose functionalised GNPs, 1H NMR can be used as integration of the anomeric protons allows one to confirm or correct the molecular ratios of the pre-reaction solution which in turn allows the correct presentation density on the GNPs produced (Fig 30, A). For the galactose GNPs, quantitative ^{13}C NMR can be used as integration of the anomeric carbon peaks can be used to confirm the ratios present (Fig. 31, A).

As the GNPs themselves are soluble in water, one can analyse them by NMR in deuterated solvents (D_2O). From NMR we can clearly see all of the peaks from the organic ligands. Most importantly, one can identify the anomeric protons of the glucose- and mannosides used. Although integration of the peaks is not possible, broadening of the peaks indicates a heterogeneous environment for the ligands, consistent with the non-homogeneous nature of the GNPs, resembling spectra of polymers. Also, one can note the disappearance of the methylene protons adjacent to the thiol groups (2.57 ppm, 2H) due to their proximity to the gold core (Fig. 30 and 31, C).

Finally, the supernatant of the GNP reaction contains un-reacted molecules as well as salts, aggregates and polymers. Filtration and purification of these products via a Sephadex column allows the complete recovery of the un-reacted material, without the presence of the salts. NMR analysis of ratios of the un-reacted material allows one to see what is *not* functionalised on the GNP surface. Therefore by comparing the NMRs of pre-reaction solutions with the post-reaction supernatant, one can estimate what *is* functionalised on the GNP surface (Fig. 30 and 31, B). As above, quantitative ^{13}C NMR can be used as integration of the anomeric carbon peaks can be used to confirm the ratios present in galactose GNPs (Fig. 31, C).

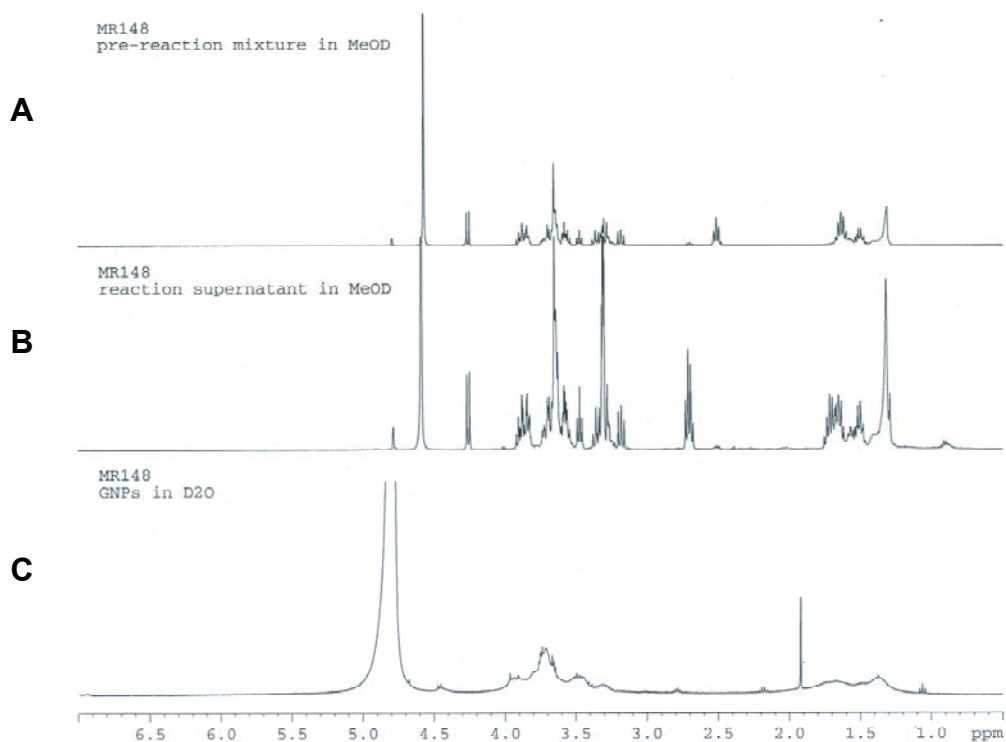


Figure 30 : ^1H NMR of pre-reaction solution (A), post-reaction supernatant, after filtration by Sephadex column (B), and GNP (C) for GNP-3.

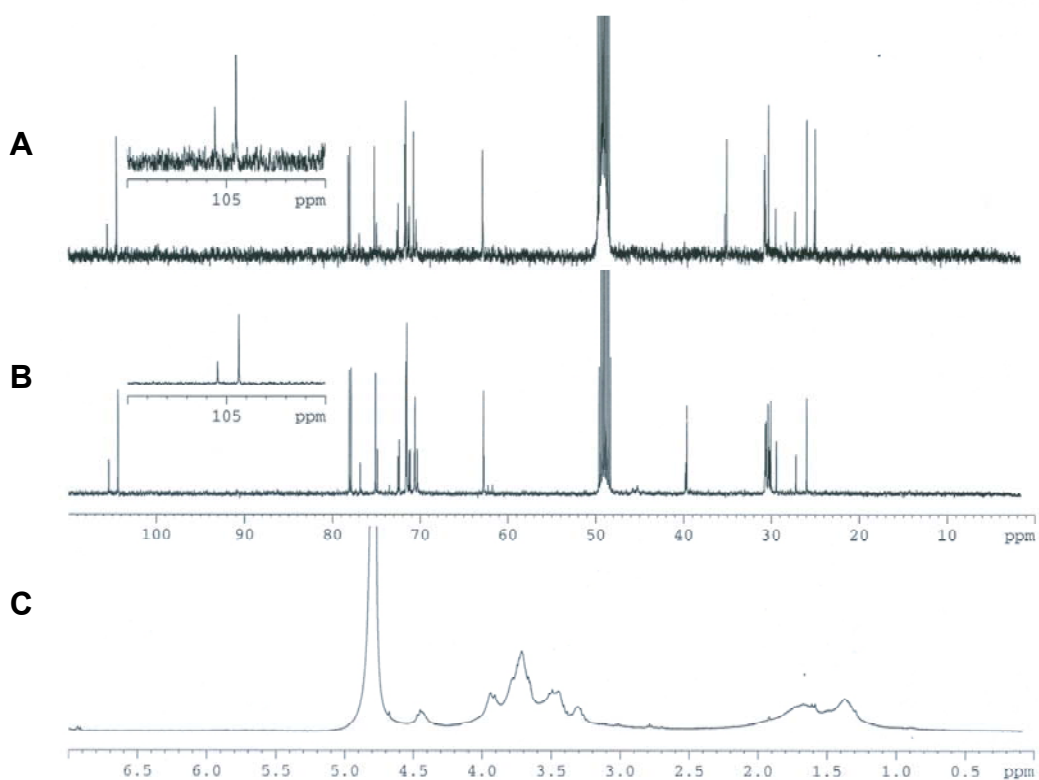


Figure 31 : Quantitative ^{13}C NMR of pre-reaction solution (A) and post-reaction supernatant, after filtration by Sephadex column (B), and ^1H NMR of GNP (C) for GNP-7.

3.2.2 UV/Vis Spectroscopy

Gold nanoparticles in aqueous solutions are typically coloured. The colour depending on the nanoparticle size and solution state (free solution or aggregation). The solutions are red in colour due to the surface plasmon band at 520 nm. As described in later chapters, the surface plasmon band is due to the absorption of light energy which couples to the surface electrons of the metallic material (chapter 4, section 2). The light energy which is not reflected is absorbed by these electrons and dissipates as an evanescent wave field in the local environment. In the case of gold nanoparticles, this plasmon band is due to light of a particular wavelength coupling to the free gaseous electrons in the 6s conduction band.^{120, 127} A study by Khlobystov *et al.* have shown that the SPR band can be used to calculate the core size of gold nanoparticles in solution of a known concentration.¹⁵⁴ Or likewise, the concentration of a nanoparticle solution of known core size can be measured. It is also known that gold nanoparticles with core diameters lower than 2 nm show less intense, broad SPR bands shifted to lower wavelengths due to quantum size effects (figure 32).

Also, as the SPR band is dependent on the refractive index of the local medium, which in turn depends on the ligands on the surface of the nanoparticle, a shift in the SPR band can be seen between nanoparticles functionalised with different ligands. Therefore, as a characterisation method, UV/Vis spectroscopy can provide information on average particle size, shape, ligand properties and concentration as well as purity and oxidation state.

As mentioned above, the SPR band is also dependent on the solution state of the nanoparticles, whether they may be in free solution or aggregates. Generally, a shift of the SPR band from red to violate is seen, due to the coupling of the surface plasmons upon aggregation, which can be reversible. This effect has been used in several applications of functionalised gold nanoparticles as biosensors, discussed in later chapters.

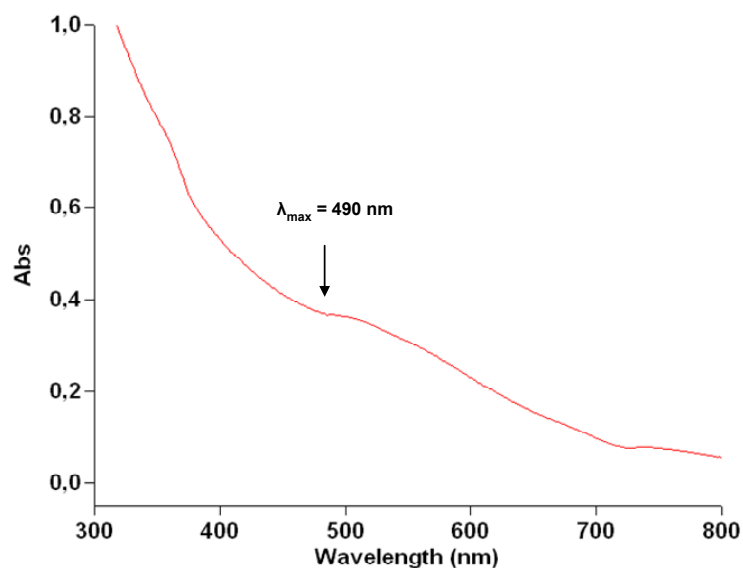


Figure 32 : UV/vis spectrum of GNP-1. The broad SPR band can be seen centred at $\lambda = 490$ nm.

3.2.3 Fourier transform infrared spectroscopy (FT-IR)

GNPs, as amorphous solids, are ground with KBr and pressed in to pellets. Characterisation by Fourier transform infrared (FT-IR) spectroscopy shows the presence of the organic material in the GNP sample. Again, confirming the functionalisation of the GNPs. Figure 33 shows a typical IR spectrum of GNPs.

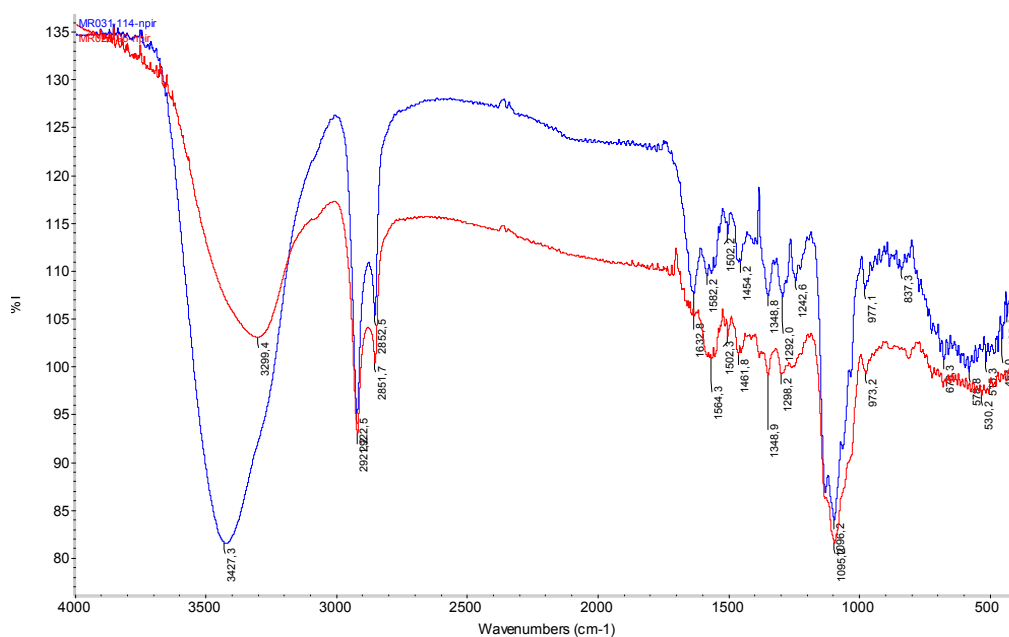


Figure 33 : FT-IR spectrum of GNP-4 (red) and GNP-5 (blue).

3.2.4 Transmission electron microscopy (TEM)

Transmission electron microscopy was used in order to directly measure the GNP core diameter. The procedure used is as described in the experimental section. Briefly, solutions of 0.1 mg mL^{-1} were made and 5 - 10 μL drops were spotted on carbon grids and allowed to dry, with or without the use of filter paper to remove excess water. The images were analysed semi-automatically, in one dimension only (y axis), using the Scandium 5.0 software.²¹⁴ Literature describes semiautomatic methods as the most reliable as fully manual methods are heavily time consuming, yet fully automated methods may measure artefacts mistaken for relevant objects or indeed, exclude certain NPs as mistakenly irrelevant.²¹⁵ The results for all GNPs synthesised are listed in table 3.

Sample	GNP-1	GNP-2	GNP-3	GNP-4	GNP-5	GNP-6	GNP-7	GNP-8	GNP-9	GNP-10	GNP-11	GNP-12	GNP-13
No. Particles	430	1117	1103	1366	500	2982	1869	526	349	408	443	536	511
Min. Diameter / nm	0.56	0.57	0.74	0.56	0.56	0.37	0.46	0.63	0.69	0.60	0.65	0.65	0.74
Max. Diameter / nm	2.49	2.81	3.31	3.49	2.82	4.88	2.52	2.46	2.59	2.08	2.59	3.10	2.45
Mean Diameter / nm	1.34	1.49	1.66	1.61	1.43	1.43	1.27	1.39	1.36	1.24	1.44	1.47	1.43
Standard Deviation / nm	0.33	0.35	0.42	0.42	0.40	0.49	0.32	0.33	0.33	0.26	0.35	0.39	0.26

Table 3 : Summary of TEM results for all GNPs synthesised.

The data were then treated statistically, following the equations given below, and organised into classes of 0.12 nm in value. The average size of the GNPs varies between 1.24 nm and 1.66 nm. All GNPs exhibited a monomodal size distribution, with **GNP-6** being the most poly-disperse and **GNP-7** being the least poly-disperse. From measuring the GNP core size, and previous works,^{182, 216} one can calculate the average number of gold atoms per nanoparticle. This in turns gives the number of gold atoms found at the GNP surface and hence an estimation of the number of gold atoms which can accept ligand molecules.

$$\text{number of measures} = n \quad \text{E 28}$$

$$\text{number of classes} = \sqrt{n} \quad \text{E 29}$$

$$\text{class range} = \frac{\text{max} - \text{min}}{\sqrt{n}} \quad \text{E 30}$$

A typical high resolution electron microscope photograph can be seen below in figure 33, along with the corresponding histogram of size distributions.

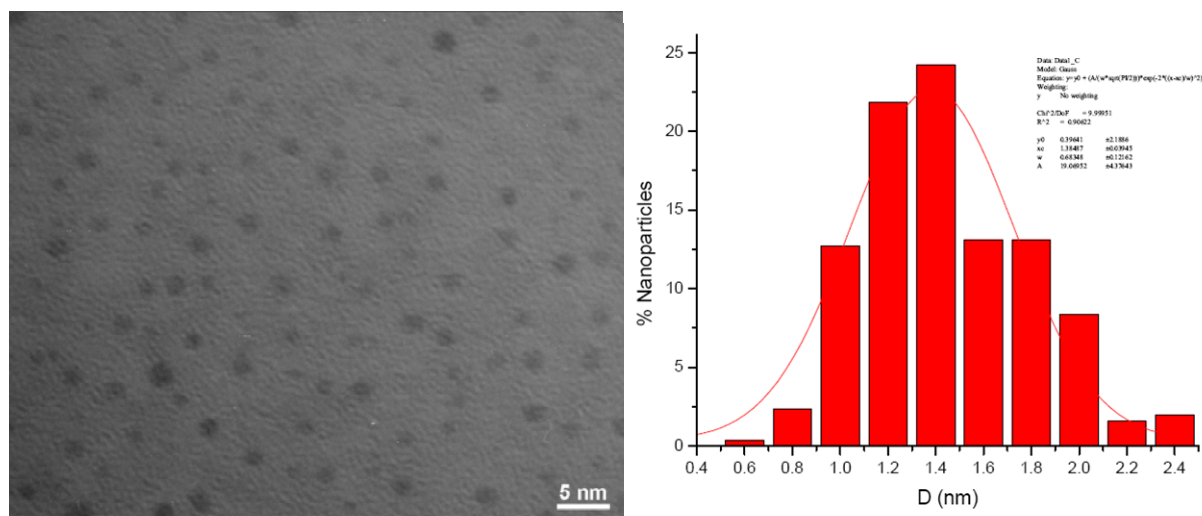


Figure 33 : Electron micrograph of GNP-1 (left) and the corresponding size distribution histogram (right).

3.2.5 Elemental analysis (EA)

Several milligrams of each GNP were sent for elemental analysis in order to study the quantity of organic molecules in the sample, namely the quantity of Carbon, Nitrogen and Hydrogen was measured. In the case of hybrid GNPs, the active ligand contains nitrogen, whereas the inactive ligand does not. Therefore, using EA, the ratio of active : inactive

ligands can be calculated. This could then be used to estimate the composition of the average GNP of each sample as described below.

3.2.6 TEM combined with EA

From the TEM GNP core measurements we were able to estimate the number of gold atoms present in the sample. This could then be used to calculate the quantity of organic molecules attached to the surface. In the case of **GNP-1**, **GNP-5** and **GNP-10**, ligand molecules are “added” to a “theoretical” *average* GNP core, and the elemental analysis results calculated. By trial and error, more ligands are added to this theoretical model until the elemental analysis results calculated match those given experimentally. For the case of the hybrid GNPs, ligands are added to the theoretical model corresponding to the ratios given by NMR or EA until the experimental value for carbon, hydrogen and nitrogen are satisfied. Refinement of the theoretical model is then carried out until all experimental values for the elements measured are satisfied. This gives the structure of the average nanoparticle in the sample.

3.2.7 Phenol – sulfuric acid method

For biophysical investigations using large, non-discrete, multivalent scaffolds such as GNPs, it is imperative to know the saccharide concentration to a high degree of accuracy, particularly for ITC. To this end, the phenol-sulfuric acid method was employed, based on experiments developed by Dubois *et al.* which was in turn adopted by Brewer *et al.*²¹⁷ In this study, solutions of known GNP concentration in buffer are mixed with aqueous phenol. The addition of concentrated sulfuric acid hydrolyses the various glycosidic bonds, converting the saccharides into phenol adducts, giving rise to an absorbance at 490 nm. The intensity of this absorption reflects the saccharide concentration, therefore, with appropriate calibration curves; the saccharide concentration of a GNP solution can be measured.

For the calibration curves, a series of solutions of known concentrations of different ratios of Me- β -D-Glc with Me- α -D-Man or Me- β -D-Gal in buffer were prepared. A concentration range of 31.25 $\mu\text{g mL}^{-1}$ to 1 mg mL^{-1} of mannose or galactose was used and the Glc : Man / Gal ratio reflecting that calculated for the GNPs as measured by NMR or EA. Absorbance at 490 nm for all solutions were made, along with a blank solution containing only buffer, providing the calibration curve relating absorbance to concentration. This curve was then used to

calculate the concentration of mannose and galactose residues in solutions of all GNP presentation densities deduced from TEM/EA.

3.3 Other Techniques

The techniques listed above were employed to characterise the GNPs used in this study before subsequent biophysical investigations with lectins. However, there are other complimentary or alternative techniques which can be employed which have not been used here, several of which are discussed below.

3.3.1 Mass spectrometry (MS)

Mass spectrometry has been used to analyse nanoparticle clusters. Murray *et al.* used temperature-programmed desorption MS to study the composition and fragmentation (and combination) of the mercapto-alkanes at the gold surface, as well as MALDI-MS in combination with TEM and theoretical calculations to study the structure (size and shape) of the gold core.¹²⁶ Wu *et al.* have more recently used MS in combination with NMR and optical spectroscopic techniques. Laser desorption MS (LDI-MS) was used to investigate fragmentation and hence reveal core structure details.²¹⁸ Time of flight – secondary ion MS (TOF-SIMS) studies, both on 2D SAMS and nanoparticles have also shown evidence of the desorption of a gold atom with the sulfide ligand, leading to the conclusion that alkyl sulfides adsorb non-destructively to gold surfaces.^{219, 220}

3.3.2 Thermo gravimetric analysis (TGA)

Thermo gravimetric analysis can be used as a complimentary technique to elemental analysis in order to determine the quantity of organic material in the sample.²¹⁶

3.3.3 Small angle x-ray scattering (SAXS)

Small angle X-ray scattering can also be used to measure the nanoparticle core size and can be used as a complimentary technique to TEM, or indeed as an alternative if TEM is not possible. However, the maximum radii measured by SAXS are significantly larger than measurements made by TEM.²¹⁶ SAXS has also been used to study the dispersion and aggregation properties of gold nanoparticles in the presence of proteins.²²¹

3.3.4 Dynamic light scattering (DLS)

When light passes through a solution, it hits small molecules dissolved in that solution and is scattered in all directions. If the light source is monochromatic and coherent, one observes a time dependent fluctuation in the scattered light related to the Brownian movement of the solute. Following constructive or destructive interference of the scattered light, one can extract information on the velocity of the molecules. Brownian movement of the solute is dependent on its size, where large molecules invoke slow movements and small molecules move faster. The Brownian movement observed is thus dependent on the coefficient of diffusion, which is in turn related to the hydrodynamic radius of the solute. A curve of the relative intensity of diffused light with regards to particle hydrodynamic radius is plotted to which a theoretical model is fitted. From this model, the size and distribution of sizes can be measured, as can a solution containing several populations of different size.

Therefore, by measuring how the light is scattered, one can gain information relating to the volume of a particular solute. For nanoparticle characterisation, this can be used to measure the hydrodynamic radius occupied by the particles in solution. This may be larger than the actual size as the hydrodynamic radius encompasses the largest diameter (for any non-spherical objects) as well as any ordered water molecules which may be bound to the particle surface via non-covalent interactions.

DLS was used to characterise the GNPs produced however, the resolution of the apparatus was not sufficient to probe the hydrodynamic radii of particles below 2 nm in core diameter. In effect, a distribution curve was given, yet the theoretical model was unable to fit correctly and thus grossly overestimated the GNP size.

3.3.5 “Reverse” ITC

As described by Brewer *et al.*²²² and explained in the following chapter, injections of a known concentration of lectin into a solution of GNPs can be made. Providing that all available binding sites on the GNP are occupied, and the experiment reaches saturation, one can calculate the functional valence of the GNP, by studying the stoichiometry (n value) of the experiment. This method however depends strongly on the quality of the protein (i.e. 100 % activity and purity) and the software used, with a consistent and faithful model that can fit the data.

3.4 Culture and Expression of Recombinant Proteins and Large Scale Production of Lectins

3.4.1 BclA

Burkholderia cenocepacia lectin A (BclA) was produced in a recombinant manner following the procedure by Imberty *et al.*²³ *Escherichia coli* BL21 (DE3) cells containing the pRSETbcla plasmid were cultured in LB broth medium at 37 °C in the presence of ampicillin. When the culture reached an optical density (OD₆₀₀) of 0.5 - 0.7, isopropyl β-D-thiogalactoside (IPTG) was added to a final concentration of 0.5 mM. Cells were harvested after 3 h of incubation at 30 °C, washed and re-suspended in equilibrating buffer (20 mM Tris/HCl, 100 mM NaCl and 100 μM CaCl₂, pH 7.5). The cells were broken using a cell disruption system (Constant Cell Disruption System, UK). After centrifugation for 30 mins at 50 000 g, 8 °C and filtration, the supernatant was purified by affinity chromatography on a D-mannose-agarose column (Sigma Aldrich). BclA was allowed to bind to the immobilised mannose in equilibrating buffer. After washing with buffer (20 mM Tris/HCl, 100 mM NaCl and 100 μM CaCl₂, pH 7.5 and 1 mM EDTA), the purified protein was extensively dialysed against 5 mM CaCl₂ for 2 days and against water for a further 2 days before freeze drying. The purified protein (15 mg per litre of culture), as a fluffy white solid, was stored at -20 °C.

3.4.2 PA-IL

Pseudomonas aeruginosa lectin (PA-IL) was also produced in a recombinant fashion following the procedure by Imberty *et al.*⁴³ *Escherichia coli* BL21 (DE3) cells containing the pET25-pa11 plasmid were cultured in LB broth medium at 37 °C. When the culture reached a *D*₆₀₀ of between 0.5 - 0.7, IPTG was added to a final concentration of 1 mM. Cells were harvested after 3 h incubation at 30 °C. Cells were washed and re-suspended in equilibrating buffer (20 mM Trsi/HCl, pH 7.5). The cells were broken using a cell disruption system (Constant Cell Disruption System, UK). After centrifugation for 45 mins at 50 000 g, 8 °C, the supernatant was filtered and purified by affinity chromatography on a Sepharose 4B column (GE Healthcare). PA-IL was allowed to bind to the immobile phase in equilibrating buffer. After washing with buffer (20 mM Tris/HCl, 1 M NaCl, pH 7.5), the purified protein was extensively dialysed against 5 mM CaCl₂ for 2 days and against water for a further 2 days before freeze drying. The purified protein (10 mg per litre of culture), as a fluffy white solid, was stored at -20 °C.

The methods outlined above for the culture and purification of the lectins used in this study were developed in CERMAV-CNRS, France, and allow the production of large quantities of highly stable lectin, in high purity, for carrying out the biophysical analyses discussed in later chapters.

CHAPTER 4 :
Biophysical Analysis of Protein-
Carbohydrate Interactions

CHAPTER 4 :

Biophysical Analysis of Protein-Carbohydrate Interactions

4.1 Haemagglutination Inhibition Assay (HIA)

4.1.1 Principle

This test is based on the observation that red blood cells, typically from mammals or birds, will sediment resulting in a two phase system of blood serum and blood cells which collect together at the bottom of a well plate. As the blood cells are covered in a high density and a large variety of glycoproteins and glycolipids, most lectins will bind to these cells. Due to their multimeric nature, the lectins will bind and form a network with the cells thus inducing agglutination. This gives a gelatinous, single-phased suspension in the sample well visible to the naked eye. Historically, this test was used to detect lectins, or prove that the protein under study was indeed a lectin due to this agglutination property.

For the test to be successful, one must use the correct concentration of lectin. In order to do this, erythrocytes are added to a serial dilution of lectin solutions. The minimum lectin concentration required to induce agglutination is noted and the haemagglutination unit (or equivalence point, the concentration required for further experiments) is taken as 4 fold this minimum concentration. Typically, lectin concentrations in the $\mu\text{g mL}^{-1}$ range are sufficient.

As the lectin solution is incubated with carbohydrate molecules prior to the addition of the red blood cells, the lectin binding sites become occupied, thus the lectin is unavailable to induce agglutination of the red blood cells. Used in sufficient quantities, the carbohydrate can prevent this lectin-induced agglutination of the red blood cells, indicated by the reappearance of sedimented red blood cells. If the carbohydrate used is a particularly efficient inhibitor, only very weak carbohydrate concentrations would be required to prevent this lectin-induced haemagglutination. Thus, one can extract the minimum inhibitory concentration (MIC) required to induce haemagglutination, with an error of ± 1 well, the equivalent error of a factor of 2, assuming a serial dilution was used (figure 34). In order to eliminate any

erroneous results, control tests are required. These involve positive controls, where no lectin is present and thus the erythrocytes are able to sediment freely, ensuring that the quality of the erythrocytes is of standard and that the carbohydrate ligands do not interfere via other processes. Negative controls are also required, where carbohydrate ligands are not used, allowing the lectins to induce the aggregation of the erythrocytes, proving again the quality of the erythrocytes and lectin whilst also proving that any inhibition of the interaction is due solely to carbohydrate-lectin interactions.

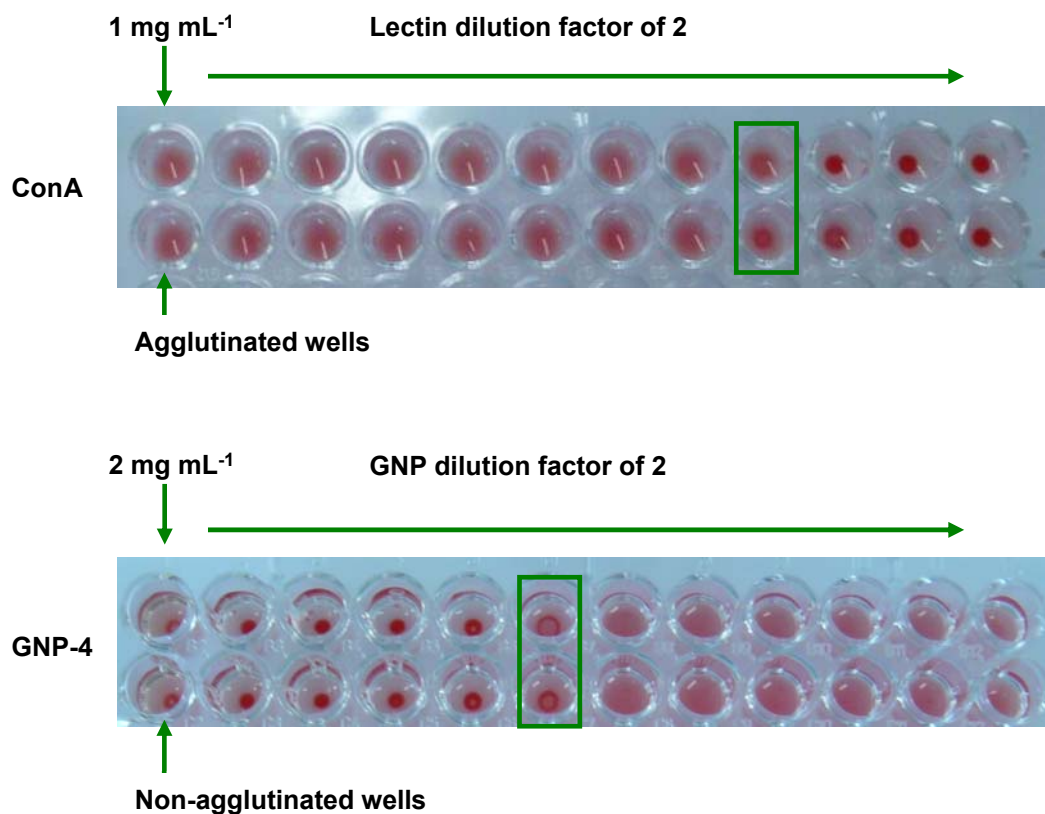


Figure 34 : Haemagglutination unit for Con A (above) with the equivalence point highlighted in green. Inhibition experiment involving GNP-4 (below) with the inhibition concentration limit highlighted in green.

The advantage of this test is that it is sensitive, robust and will work for most lectin systems. It is efficient with regards to time, preparation, and materials required; and often gives good results. The assay allows one to screen and order a large number of candidates using relatively little material, yet this is only in a comparative capacity. Also, one must not consider the MIC values obtained from HIA as one would consider association / dissociation constants as some molecules may inhibit haemagglutination effectively, however this may not necessarily be a reflection of the affinity of the lectin for this particular ligand. One must therefore be careful not to over-interpret the results given by this type of evaluation. Also, as mentioned

previously, this test may not work for all lectins, either because they do not agglutinate the erythrocytes (due to their monovalency with respect to sugar binding),¹⁴ or because they are required in large concentrations in order to inhibit haemagglutination. In this study for example, we were not able to conduct this test with the BclA lectin as this would require concentration of 2 mg mL⁻¹. Thus, the quantity of BclA required to conduct a full series of tests was not feasible.

4.1.2 Applications to carbohydrate interactions

There are several examples where HIA tests have been used to evaluate the inhibitory power of various carbohydrate ligands. Such ligands varying in nature from monosaccharides to larger oligomers, neoglycoconjugates as well as small multivalent systems (dimers etc) to larger multivalent scaffolds.^{80, 90, 92, 94} Here we demonstrate the use of the HIA test for GNP systems. One difficulty observed was the discoloration of the test solutions by strong concentrations of the coloured GNP solutions. In particular, **GNP-1**, which is the most soluble of the GNPs. However, at lower concentrations, the test can be read correctly. Also, as described later, at high concentrations the GNPs appear to exhibit a level of toxicity. This can be seen by the yellow discoloration of the test solutions resulting from haemolysis. This is thought to originate from the presence of ethylene glycol groups of the spacer molecules, which may interfere with the erythrocyte cell membrane inducing haemolysis. However, at lower concentrations, this cytotoxicity is not seen.

4.2 Surface Plasmon Resonance (SPR)

4.2.1 Principle

When monochromatic, plane polarised light approaches a transparent medium it is either reflected or refracted depending on the angle of incidence, θ_i . As θ_i approaches the critical angle (θ_c), more light is reflected back. At θ_c and beyond, total internal reflection of the incident light occurs, and thus no light is refracted. If the opposite surface of the transparent medium is coated in a thin metallic layer (Au or Ag), instead of being internally reflected, some of the light energy may resonate and couple with the electrons cloud (plasma) which propagates at the metal surface. The energy of the light which is coupled to this surface electron cloud may create an evanescent wave field which travels several hundreds of nanometres into the adjacent dielectric medium. The amplitude of the wave field dissipates

exponentially with the distance from the metal surface. Thus, light energy is adsorbed by the surface, and less light is reflected. At a certain angle above θ_c , the surface plasmon resonance angle, θ_{spr} , the coupling of light energy to the plasma is at its most efficient, reducing the intensity of reflected light (I_r). The minimum amount of light reflected occurring at θ_{spr} (Figure 35).

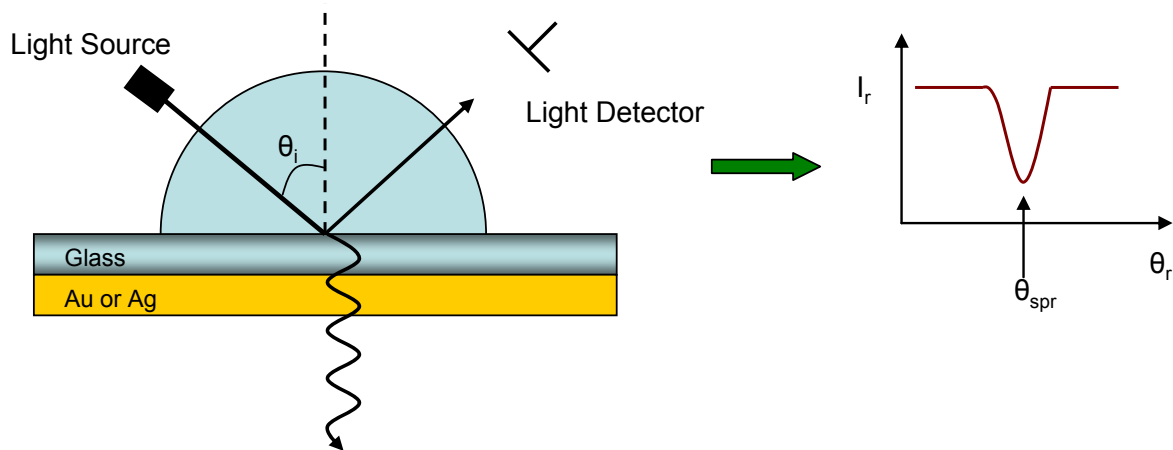


Figure 35 : Schematic diagram of the principals of SPR.

The evanescent wave field is dependent on the refractive nature of the metal boundary. Therefore, any change occurring near to this interface which alters the refractive index will change the resonant energy of this wave field, thus shifting $\theta_{spr,1}$ to $\theta_{spr,2}$. As the monochromatic light shining at the surface does not change in θ_i , a change the intensity of the reflected light is observed. Thus, any change in these environments may be measured quantitatively with respect to the intensity of reflected light.

Although the effect of surface plasmon resonance was discovered over 100 years ago, applications as biosensors evolved in the 1980s and 1990s. For this application, the gold layer forms the internal surface of a flow cell to which one binding partner is immobilised. The corresponding ligand is then injected into the flow cell in buffer solution. As the ligand binds to the immobilised partner, a shift in the refractive index occurs. This in turn shifts θ_{spr} leading to a measureable change in reflected light intensity. As more ligand binds to the surface, the change in θ_{spr} increases in magnitude giving rise to the association curve recorded in the sensorgram by the detector (figure 36, 1_a and 2). As the amount of ligands associating with the surface equilibrates with the amount of ligands dissociating, or the immobilised binding sites are saturated, equilibrium is reached. During the post-injection phase, only buffer passes through the flow cell and the ligands dissociate from the surface leading to $\theta_{spr,2}$ returning to

$\theta_{\text{spr},1}$ and the recording of the dissociation curve (figure 36, 1_d). These variations are recorded as resonance units (RU), whereby 1000 RU corresponds to a $\Delta\theta_{\text{spr}}$ of 0.1 °, the equivalent of 1 ng mm⁻² of ligand attached to the sensor surface. The sensorgram is then subjected to mathematical treatment using analysis software in order to calculate association and dissociation rates and, if possible, equilibrium rate constants.

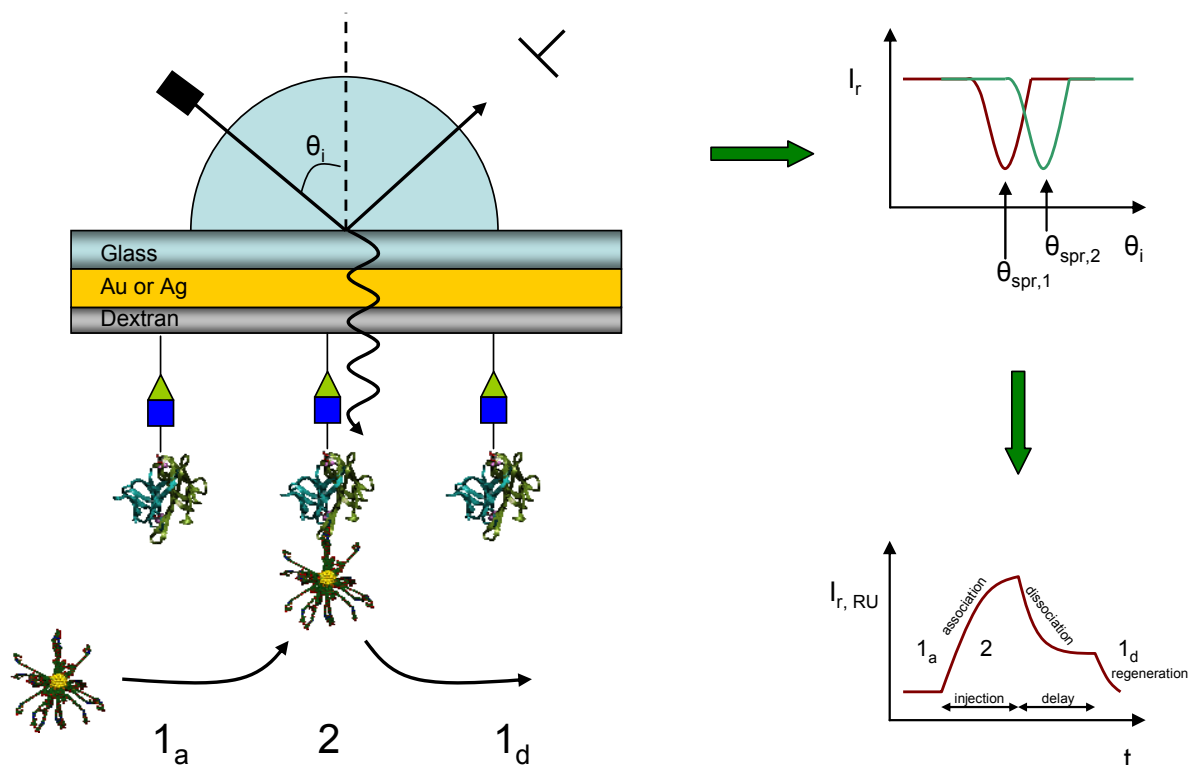


Figure 36 : Association / Dissociation events in SPR and the subsequent responses recorded.

SPR studies provide important insights into protein-carbohydrate interactions, in particular the kinetics of such interactions, using very little material, but have limitations in providing thermodynamic data which make interpretations on the molecular level difficult. Also, one of the interacting partners has effectively been immobilised to a two dimensional surface which may restrict the presentation of this partner, potentially forcing it to adopt a non-natural conformation. For example, if the interaction being studied involves two binding partners which are normally found in free solution in nature, by immobilising one of the partners to the surface, it is greatly restricted in terms of degrees of freedom of movement may be immobilised in a fashion which blocks a binding site or forces the binding partner to present itself in a non-natural form either on an intra- or inter-molecular level. Arguably, the experimental design and conditions can be altered in order to compensate for this.

4.2.2 General applications

With over 1000 references in 2007 reporting data obtained from SPR studies, applications of this technology can be found in many fields of research including protein interactions, antibody interactions, peptides, carbohydrate interactions, lipid interactions as well as self-assembled monolayers, polymers and films.²²³(and references therein) In order to correspond to the terminology used within the SPR community, we use the term “ligand” to refer to the binding partner immobilised to the flow channel surface. The term “analyte” refers to the binding partner in the mobile phase.

SPR apparatus can be applied in several different ways. Firstly, SPR manufacturers offer several chip-types, where the gold surface is not functionalised, or functionalised with other materials which can be activated to accept different functional group types. Chip surfaces available for the Biacore T100 model used in these studies include the plain gold surface, used for surface interaction studies and custom surface design (with functionalisation *in situ* or *ex situ* of the apparatus) of thiol-functionalised ligands. Hydrophobic surface-functionalised chips for lipid monolayer capture. And finally, a range of surfaces functionalised with a dextran matrix. The dextran can be carboxylated to various degrees giving different activities to the surface. The carboxylated dextran surface can be activated to covalently attach many small organic molecules, proteins or nucleic acids via several functional groups including amine coupling, aldehyde coupling, thiol coupling and disulfide bridging. Streptavidin functionalised dextran can also be used for capturing biotinylated molecules. During this study, the CM5 dextran functionalised chip was used, in combination with amine capture of the lectins.

The SPR apparatus has essentially two different modes for interaction studies. The first is more applicable to our studies, where the protein is immobilised to the surface, and analyte solutions are passed through the flow channel. Binding of the analyte to the immobilised protein would provide the required change in refractive index, inducing a positive SPR response. In order to study the multivalent effect of the lectins, only very few lectin molecules were captured on the surface. This is because at larger surface concentrations, one risks a clustering of captured molecules. Therefore, one cannot be sure if the multivalence seen is due to the inherent intramolecular, or intermolecular multivalence due to the clustering of lectins at the surface. Thus low concentrations, in theory, would allow isolated analyte-lectin interactions. Also, low surface concentrations reduce the risk of mass transport, where an

analyte dissociates from the surface, but then re-binds further down the flow channel leading to a larger than expected response. However, using such low concentrations (300 – 600 RUs immobilised) may risk that the response registered by the apparatus is below the limits of detection. This is dependent on the quantity immobilised, the interaction strength, and the M_w of the analyte. For example, immobilising a protein of 60 kDa to the surface, interaction with a small molecule of < 1 kDa would not greatly affect the local refractive index and thus only a small response is registered. However, as the lectins being used are between ~30 – 100 kDa, and the GNPs themselves are relatively similar, an ideal response value was recorded in most cases. The sensorgrams recorded can then be treated mathematically using any SPR software to give the k_{on} and k_{off} rates and, if possible, equilibrium kinetics.

The second mode of operation relevant to protein-carbohydrate studies is the competition experiment. This involves the immobilisation of carbohydrate molecules to the dextran surface, typically capturing the relevant biotinylated-monosaccharide onto streptavidin functionalised dextran. As the lectin is passed over the flow channel, binding to the surface occurs and a response is recorded. Lectin solutions are incubated in the presence of different concentrations of inhibitor, and these solutions are passed over the monosaccharide functionalised surface. Inhibition of the lectin binding to the surface can be seen by the lowered response signal. Therefore, IC_{50} values can be obtained for each inhibitor studied and compared. Therefore, this method is more qualitative than quantitative; however it is more useful for low molecular weight inhibitors.

4.2.3 Applications to carbohydrate-protein interactions

As mentioned above, there are many examples of SPR studies involving carbohydrate interactions. These include self-assembled monolayers, functionalised on the chip surface, whilst passing solutions of lectin.^{89, 224} Mobilisation of lectins to the chip surface in order to screen several carbohydrate ligands.^{23, 111, 225} The latter reference, by Kamerling *et al.* also combines SPR with HPLC in order to identify carbohydrates, from a complex mixture, which bind to Con A and the LTA lectin from *Lotus tetragonolobus purpureus*.

SPR techniques have also been used in the investigation of GNPs, both in carbohydrate-carbohydrate interactions and carbohydrate-lectin interactions.^{185, 226}

In our studies, the proteins Con A, BclA and PA-IL were immobilised to the sensor chip surface via the amine coupling kit supplied by Biacore (Uppsala, Sweden). Solutions of different concentrations of **GNP-1** to **GNP-10** were passed through the flow cell and the responses recorded. The sensorgrams were then fitted using the Langmuir model (1 : 1 binding model). Competition experiments were also attempted, where monosaccharides were immobilised via biotin-streptavidin coupling. Solutions of lectin incubated in the presence or absence of GNPs were passed over the sensor surface. However, the sensorgrams recorded were of too poor quality in order to give reliable data.

4.3 Isothermal Titration microCalorimetry (ITC)

4.3.1 Principle

Calorimetry has long been used for studying the evolution of heat during chemical or physical changes and was an important tool in the beginnings of physical chemistry and thermodynamics. With the evolution of modern technology, the application of calorimetry in interaction studies has also evolved. Modern instruments can detect small changes in heat (microcalories) and are thus suitable for studying biochemical processes. Isothermal titration calorimetry (ITC) is a label free technique used for the direct detection of biological interactions by measuring the evolution of heat during the interaction – contributing to a fundamental knowledge of the molecular basis of interactions. From this, an accurate determination of the binding constants (k_a), reaction stoichiometry (n) and change in enthalpy (ΔH) can be made whilst permitting the calculation of changes in entropy (ΔS) and Gibbs free energy (ΔG). Typically, microcalorimetry is used for studying protein-ligand interactions, enzyme activity and for small molecule drug discovery as well as the screening of biotherapeutics and vaccines. Many applications of which can be found in the literature.²²⁷

The apparatus itself consists of two cells; one sample cell, and a reference cell both connected to a power feedback system (Figure 37). The two cells are wrapped in an adiabatic jacket which is kept at a temperature 1 °C lower than the sample and reference cells. A syringe can be inserted into the sample cell. The injection apparatus and power feedback systems are automated and computer controlled. During the experiment, power is applied to the two cells to maintain a constant temperature and the syringe injects a solution of one of the interacting partners (solution *A*) into the sample cell which contains the complimentary partner (solution

B). As the molecules interact, the release or intake of heat energy occurs in the sample cell. The power feedback system then applies more or less power (depending on the interaction) to the sample cell in order that the temperature returns to the same value of the reference cell. If the interaction is exothermic, the power feedback system will apply *less* power to the sample cell and vice versa for an endothermic interaction.

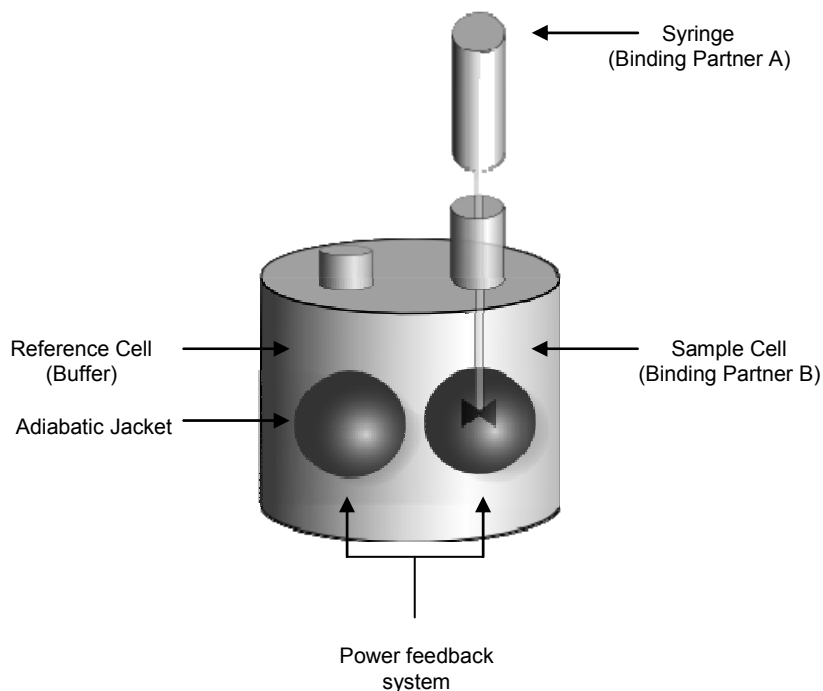


Figure 37 : ITC apparatus.

The raw data recorded by the apparatus is the difference in energy applied to the two cells with respect to time. Typically, a series of 20 to 50 injections occurs during the experiment. After each injection, there will be an evolution of heat compensated by the power feedback system. As shown in the thermogram below in figure 38, a plot of power applied against time will give a series of peaks corresponding to each injection. At the beginning of the experiment, the molecules in solution *B* are all free to interact, therefore, as *A* is injected into the sample cell, all *A* molecules interact with the binding sites of *B* hence a large amount of heat is evolved (figure 38, 1). As the experiment proceeds, more molecules of *A* are injected, and more binding sites of *B* become occupied, thus, less heat is evolved during each subsequent injection (figure 38, 2). Approaching the end of the experiment, the binding sites of *B* are completely saturated; hence further injection of *A* does not induce any further interactions and only heats of dilution are recorded (figure 38, 3).

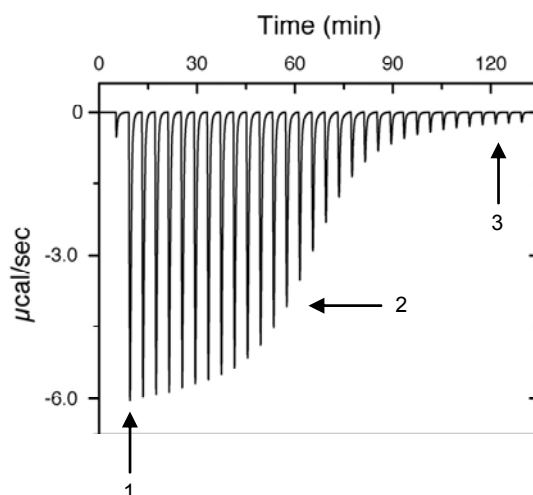


Figure 38 : ITC thermogram showing the difference in power provided to the sample and reference cells with respect to time. At 1, all molecules of *B* are free to interact. At 2, after several injections of *A*, the binding sites of *B* become progressively saturated. Eventually, all binding sites of *B* are saturated, only the dilution of *A* is recorded, 3.

Integration of this data with respect to time gives the evolution of enthalpy with respect to the molar ratio of *A* / *B*, known as the interaction isotherm. The integrations of the raw data are shown as black squares. Following mathematical treatment using ITC software, a theoretical model is fitted to the data, shown as the red curve (figure 39). It is this plot that is used to extract information on the binding constant (gradient of the curve), binding enthalpy (range of the y-axis) and stoichiometry of the interaction (molar ratio at the point of inflection).

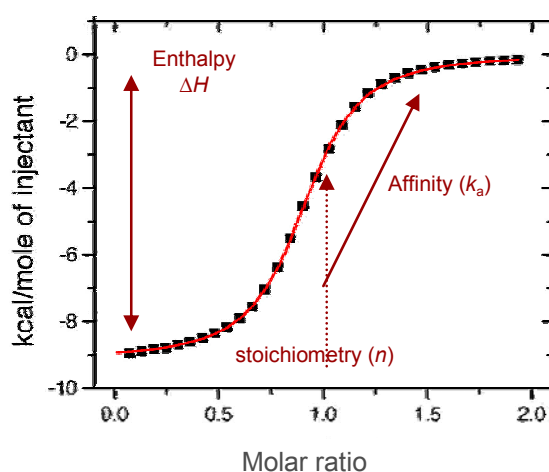


Figure 39 : Interaction isotherm showing the integrated values of the raw data.

The dilution of *A* and *B* can be evaluated from the last few injections of the experiment. If the dilution enthalpy of *A* or *B* is found to be significant in its contribution the interaction enthalpy, “blank” experiments will need to be performed (by injection of *A* into buffer or

injection of buffer into B). These data can then be subtracted from the interaction isotherm during mathematical treatment. The form of the interaction isotherm may depend on several factors; the nature of the interaction, the nature of A and B , their concentrations, the number and volume of injections as well as the spacing between each injection. Therefore, the experiment must be correctly designed in order that the characteristics of the interaction are within the detection limits of the apparatus, solution B is saturated by the end of the experiment and that the inflection point is clearly visible.

Several theoretical models can be fitted to the data; single site model, sequential binding (independent, multiple binding events) and two-site cooperative binding as well as competitive and dissociation binding models. The model used of course reflects the natures of A and B .

Mathematically, the amount of heat released (ΔQ) depends on the stoichiometry (n), the concentration of the complex formed ($[AB]$), the molar enthalpy of the interaction (ΔH°) and the volume of the cell (V_0).

$$\Delta Q = n\Delta[AB]\Delta H^\circ V_0 \quad \mathbf{E\ 31}$$

Mathematical treatment of this with respect to ligand concentration describes the evolution of enthalpy as a function of ligand concentration. One important feature of the resulting equation is the unitless Wiseman parameter, c .²²⁸ Where:

$$c = n[B_0]k_a \quad \mathbf{E\ 32}$$

The Wiseman parameter dictates the form of the sigmoidal interaction isotherm. Large c values lead to very sharp curves. Too high, and the determination of k_a becomes difficult, as the gradient of the sigmoid at the point of inflection approaches infinity. Low c values lead to shallower curves. Indeed, one must adjust the experimental conditions to arrive preferably at c values between 10 and 1000 to give a clear sigmoid curve. Above this limit, one may find that it is necessary to work with lower concentrations in order to reduce c , or contemplate using a competition / displacement titration with a reference ligand of known lower affinity.²²⁹ Below this “experiment window”, one can also employ a competition / displacement titration with a

reference ligand of known higher affinity. Or, one could use high concentrations of the binding partner in the syringe. However, one must alter the experimental set-up in order to work in “low c ” conditions, providing one 1) uses a significant portion of the binding isotherm, 2) knows the binding stoichiometry, 3) concentrations are accurately known and 4) the signal-to-noise recorded by the apparatus is sufficiently large.²³⁰

Overall, the applications of ITC are wide and varied, and a great deal of information can be extracted from one experiment. However, quite a significant amount of material is required for one experiment (e.g. several milligrams of protein). Also, as for SPR, if the binding partners are forced in to non-natural situations, such as increased freedom of movement or a non-natural intra- or inter-molecular presentation, then this experiment may not be the most suitable.

4.3.2 General applications

Typically, solution A , in the syringe, is a solution of the ligand under study whilst solution B , in the sample cell, is the macromolecule or protein. Injection of the ligand solution until the macromolecule is saturated provides the relevant thermodynamic parameters. There are many examples of this method applied to protein-ligand interactions in the literature. It is also possible to carry out “reverse” ITC experiments. Reverse experiments involve the injection of *macromolecules* into a solution of *ligands*. This permits the determination of the thermodynamic binding parameters to each of the individual epitopes of [multivalent] analogues and was first used by Brewer *et al.*²²² This method also permits the measurement of the *functional valency* of a particular scaffold, which may differ from the *structural valency*, assuming one knows the concentration of the macromolecule with a high degree of confidence.

With over 600 references involving this technique in 2007 alone, ITC has been used to study a wide range of biological / biochemical interactions as well as the study of macromolecule formations and synthetic host-guest interactions. Examples of ITC studies investigating all types of bio-molecules can be found; protein-protein and protein-small molecule (inhibitor, drug candidates, nucleotides etc) interactions, as well as protein-lipid, protein-polymer and protein-metal interactions.^{227, 231}(and references therein) Enzyme activity and enzyme kinetics can also be investigated. Several examples of cyclodextrin-guest interactions, the investigation of micellar systems and polymer-surfactant and polyelectrolyte interactions also exist.²³²(and

references therein) In the same review by Bouchemal, examples of ITC usage for the quantification of nanoparticle systems can also be found.

4.3.3 Applications to carbohydrate interactions

There are numerous examples of the use of ITC for protein-carbohydrate interactions. Brewer *et al.* and Toone *et al.* have conducted extensive experiments using Con A to explore the binding parameters of this lectin. In particular they investigated the affinity of various mannoside monosaccharides, de-oxy analogues as well as small aromatic multivalent scaffolds.^{38-40, 65, 119, 233, 234} With regards to “large” multivalent scaffolds such as nanoparticles, micelles or dendrimers, there are few examples of the employment of ITC in order to study the multivalent character of these ligands.⁹² One problem is the solubility of these scaffolds. In the traditional ITC setup the syringe contains the ligand in high concentration, which is injected into solutions of the macromolecule. These scaffolds are soluble in the buffer solutions used, however they are rarely soluble in high concentrations.⁹⁰ Therefore only weak concentrations can be used. Con A is typically used as the macromolecule, which exhibits a significant, but not particularly large affinity for the mannosides presented on the scaffolds. Therefore, a combination of low concentrations used, coupled with the low affinity exhibited by Con A, often the ITC raw data is too weak to be processed. The use of high concentrations of the lectin and the ligand often lead to irreversible aggregation which in turn does not allow for the use of ITC in a fully quantitative context.⁹⁰ However, by using reverse ITC, in combination with lectins with stronger affinities such as BclA or PA-IL, ITC can be used quantitatively as seen in few examples in the literature.^{41, 42} Penades *et al.* have also used ITC to study carbohydrate-carbohydrate interactions. In particular, the Le^x-Le^x interaction implied in various biochemical processes such as cell-cell communication and aggregation.¹⁹³ Calorimetry has also been used in materials chemistry to study the addition of ligands (amino acids) to gold nanoparticle surfaces.²⁰³

4.4 Other Methods

Although only the methods mentioned above have been used in this work, several other techniques exist which should not go without mention.

4.4.1 Enzyme-linked lectin assay (ELLA)

The ELLA is a variation of the well known enzyme-linked immunosorbent assay (ELISA) whereby microtiter plate wells are coated in a high molecular weight polysaccharide such as yeast mannan, which acts as an immobilised ligand. The lectin-enzyme conjugate is then added and left to incubate, after which the micro plate is rinsed, and a revelation solution is added (*O*-phenylenediamine, OPD). The colour development seen in the micro plate is proportional to the concentration of immobilised lectin. The incubation of lectin with the ligand to be studied (inhibitor), in a dilution series, prevents binding of the lectin to the immobile surface. Therefore, inhibition of lectin immobilisation (or rather lack of) can be seen by the intensity of the developed colour. Thus, IC_{50} values can be obtained for each ligand studied. This technique is similar in principal to the competition experiments using SPR and like the HIA test uses very little material. However, the lectin needs to be labelled with an enzyme conjugate, and the results obtained are semi-quantitative. It was not used in this study as it would not give any new or different information as the HIA and would certainly not give any more details of the interactions on a molecular level.

4.4.2 Dynamic light scattering (DLS)

As mentioned in earlier chapters with respect to nanoparticle characterisation, DLS is capable of measuring the hydrodynamic radii of various solutes in a given solution in relation to its size-dependent coefficient of diffusion. If one considers a protein molecule in free solution, upon interaction with a small monovalent ligand, the hydrodynamic radius will not change greatly. However, interaction with a large monovalent ligand would increase the hydrodynamic radius seen in the scattered light, relating to the volume of the protein and the ligand. If a polyvalent ligand is used, aggregation may occur, and thus the change in hydrodynamic radius could indicate the size of the aggregate clusters and the number of each species involved in this aggregation. By measuring the change in aggregation over time, a comparison can be made between the aggregation abilities of several ligands. As for HIA, this may not reflect the dissociation constant for a particular interaction, but may provide other

useful information. As mentioned previously, this technique was not used in this study either for characterising the GNPs or for investigating the aggregation properties of the GNPs with multivalent lectin systems.

4.4.3 Analytical ultra centrifugation

Analytical ultra centrifugation is an older technique in comparison to DLS, developed first in the 1920s and has long been used for the study of macromolecules.²³⁵ It remains an attractive method due to theoretical simplicity and basis on first principals.²³⁶ With the development of new apparatus and computational models, more detailed information can be extracted from experimental data.²³⁷

Two methods can be used with this apparatus; the first is sedimentation velocity (SV), where a high centrifugal force is applied and the analysis of the time dependent sedimentation process monitored. The second method is sedimentation equilibrium (SE), which uses low centrifugal forces that allows an equilibrium to form between diffusion and sedimentation thus giving a time independent gradient. Both SV and SE approaches can be used for studying proteins.

The first method is dependent on the gravitational force, the buoyancy and the hydrodynamic friction of the sample. Thus, this method is used to measure the mass and size of a macromolecule whilst also giving information on its shape. Typically, macromolecules within the range of 0.1 – 1000 kDa and 1 – 5000 nm can be studied.^{236, 238} SV can also give information on the heterogeneity of a sample. This method can also be applied to interacting species; the interaction of a protein with another species (dimer formation or ligand interaction) will change the diffusion boundary and sedimentation profile. Therefore, association, aggregation and agglomeration of molecules of the same or different species can be investigated.⁶⁷ Also, reaction kinetics can also be measured, using the change in sedimentation profile with respect to time representing the change in reactant concentration.

The second method, SE, balances the transport of sample down the cell, with the diffusion of sample back up to the cell as a function of the concentration gradient. This experiment is insensitive to the shape of the molecules and is used to evaluate the molar mass. Equilibrium constants can be measured due to the changing concentration gradients.

4.4.4 Crystallography

X-ray crystallography is probably one of the most powerful tools available for studying interactions at the molecular level. In particular, the co-crystallisation of a protein with its receptor can provide details at the molecular level on interaction mechanism, specificity as well as complimentary effects of solvation and secondary or complimentary interactions. The first step is crystallogenesis of the protein with its receptor. Typically, a solution of the protein is mixed with a solution of the receptor, and a small drop is placed on a silicon disc. This disc then covers a micro well containing the precipitant reservoir. The precipitant is typically a mixture of high salt concentration mixed with other molecules such as polyethylene glycols or other additives and detergents. With time, liquid from the protein-receptor drop on the silica plate evaporates and diffuses into the precipitant reservoir. Eventually, the protein-receptor drop becomes more and more concentrated, and the molecules in this solution begin to form precipitates in a fashion allowing the formation of ordered solids – crystals. This phase is often dependent on numerous physico-chemical parameters such as salt concentration, temperature, pH etc and is known as the hanging drop method.²³⁹

Once crystals of sufficient size have been formed, they are extracted and stored cryogenically, using a cryo-protectant. As the crystals formed are highly ordered macrostructures, they permit the ordered diffraction of phased, monochromatic radiation, in this case x-rays, depending on electron density at an atomic level. It is due to this ordered structure that interference of the x-rays occurs, providing regions of high and low intensity relating to constructive or destructive interference. The diffraction pattern is collected and recorded using sophisticated equipment (cameras etc). Finally, once the crystal electron density has been mapped the structure can be built using computational methods and specific software. If the structure of a similar protein exists, molecular replacement may be used to help build the structure, again using computational methods. Otherwise, the structure will have to be phased using heavy atoms, such as mercury, during crystallogenesis. The structure is then refined and validated, with the coordinates of all atoms and substructures recorded.

X-ray crystallography remains the most powerful technique to study protein-ligand interactions and has been vastly applied to the study of lectins and their carbohydrate receptors. This method also provides important structural details which can be used in conjunction with NMR studies or applied to molecular modelling/dynamics as either a

starting structural template, or validation of previous studies. These structural details may also be used in designing new, more potent ligands, by taking advantage of subsidiary or secondary interactions. The major disadvantage of this method is that crystallogenesi s can often be very difficult as it depends on many physico-chemical parameters. One must therefore screen a wide range of conditions, but also must use high quality protein and receptor samples, with a strong emphasis on sample homogeneity. In the case of small molecule receptors and inhibitors and the advent of computer controlled crystallogenesi s this may well be possible, however, in the case of GNPs, there is still a significant degree of heterogeneity relating to core size, number of ligands on the surface and ligand distribution which currently impede co-crystallogenesi s and is the reason why it was not employed in this study (although attempts were made).

4.4.5 Molecular modelling

Determining the structure of complex carbohydrates and understanding their associations and interactions at the molecular level is one of the main challenges in glycoscience. Therefore, in conjunction with crystallographic and NMR studies, the elucidation of 3D structures and dynamics of oligosaccharides is a necessary step in understanding their interactions in detail. Also, as carbohydrates are a very particular group of biomacromolecules, previous studies involving other biomacromolecules are unable to fully describe their structure related interactions. To this end, several molecular modelling methods have been developed specifically for carbohydrates, with focus on their structural behaviour and interaction with their local environment. With the advancement in computer technology and more complex algorithms available, the simulation of carbohydrates in “natural” environments (solvated, in concentrated solution or binding with a receptor) is possible with a certain degree of accuracy.

The first challenge to overcome is predicting the structure of the carbohydrates themselves. Crystal structures are particularly useful for giving search starting points however these may not always be available. Also, the structure of a carbohydrate in a binding site may be very different to that of a free molecule in solution. Therefore, computational tools may be required, and for this there are several methods for conducting a structural search.

4.4.5.1 Growing chain method

The first is the growing chain method, where a simple base structure is modelled (a disaccharide for example), after which an additional sub-unit is added, its energy calculated,

and fixed in its lowest energy position. This is a very fast method as the algorithm used is not complex. However, in some rare cases this may not be the most appropriate, especially if there are intramolecular interactions which influence molecular structure.

4.4.5.2 Exhaustive search

An alternative search strategy would be to conduct an “exhaustive search”, which gives a complete energy description of the oligosaccharide and its conformational space. This algorithm is naturally very complex as it is obliged to consider all degrees of freedom of every monosaccharide sub-unit (Φ , Ψ and ω glycosidic linkages), the complexity increasing in several orders of magnitude as the oligosaccharide increases in size. Therefore it is often necessary to reduce these degrees of freedom, by limiting their freedom to discrete increments of rotation, as opposed to allowing full 360° rotation about the glycosidic linkages.

4.4.5.3 Heuristic or Guided search

A guided search algorithm provides an efficient method of exploring the conformation energy hyperspace of complex carbohydrate molecules. This algorithm searches only along the low energy valleys of the hyperspace, cutting out the less important regions studied in an exhaustive search, thus being more time efficient. Although not guaranteed to find all of the low energy minima, it is relatively successful. The CICADA algorithm is an example of a guided search, and has been used to predict the structures of several oligosaccharides.²⁴⁰

4.4.5.4 Monte Carlo

The Monte Carlo method is very well known and applied to many computational situations from the fundamental to the complex. It is an efficient and robust method for exploring the conformational hyperspace. Essentially, the algorithm starts at a random conformation of known energy. The conformation is then altered randomly and its energy evaluated. If the energy of the new structure is lower than that of the old, it becomes the start point for the next round. If the next structure does not meet this energy criterion it may still be accepted if this state is statistically accessible at the given temperature (Boltzmann distribution and statistical factors). Random changes and criteria can be controlled which alter the efficiency of the algorithm. Several searches can be run in parallel so that local as well as global minima may be found.

4.4.5.5 Genetic algorithm

Genetic algorithms are inspired by nature, where a population of configurations is considered. Each conformer is given a fitness score relative to its energy. Those with the best score are kept into the next round as the “parents”. Genetic factors such as inheritance, mutation and cross-over of various attributes (as well as “wild cards”) allow the formation of the “offspring”, the whole population is re-evaluated and the cycle repeats. This method is one of the more complex, however it allows for rapid determination of low energy conformers without having to explore the entirety of the conformational hyperspace.

4.4.5.6 Molecular dynamics

Molecular dynamics is an excellent tool for mapping the low energy conformations of large molecules. Information on population distributions over different conformations, movement trajectory and translations between conformations can be recorded. Evaluations in solvated environments are also possible, with the solvent molecules being included implicitly. This allows the study of both molecule and solvent behaviour. However, this method is very cost intensive. Also, the method will explore in great detail a particular low energy conformation, yet may fail to overcome large energy barriers, becoming trapped in a local minima and failing to study others which would normally be accessible. Running several short dynamics simulations in parallel or a simulation at high temperature may overcome this problem. High temperature simulations should be approached with caution as this may also allow transitions which would normally be forbidden at ambient temperature.

4.4.5.7 Force fields

Predicting molecular structures using molecular modelling requires the application of parameters – attributes assigned to individual atoms, molecules or parts of molecules to describe their behaviour in a particular environment (charge, charge distribution, bond length for example). These descriptions can be calculated from first principals, known as *ab initio* calculations. These calculations are very complex and time consuming, even small molecule evaluations require a lot of computer time. However, these parameters can be simplified by the use of force fields. The parameters for force fields come from a combination of experimental results as well as simplified quantum mechanics calculations. This method is termed a *semiempirical* approach. The vast amount of experimental data available from crystal structures of lectin-carbohydrate binding events was an essential contribution to the development of their molecular modelling and force field parameterisation. Force fields

designed for carbohydrates typically would include monosaccharide rigidity as well as anomeric effects and Van der Waals interactions. Examples of such force fields are MM3, AMBER (glycam) and CHARMM.^{241, 242}(and references therein)

4.4.5.8 Modelling lectin-carbohydrate interactions

As mentioned above, crystallographic studies of protein-carbohydrate interactions are the primary source of structural information. However, crystallography provides only a snapshot of the whole interaction. With the aid of molecular modelling, all processes of the interaction can be evaluated from initial binding, to the molecular contacts made, types of contacts (Van der Waals, aromatic, electrostatic or hydrogen bonding) and calculations of the thermodynamic parameters as well as a comprehensive structure, function and activity relationship. Modelling can also be used to rationalise molecular specificity as well as the study of glycomimetics and screening of large amounts of potentially therapeutic analogues to give pharmaceutical lead compounds. Modelling has the advantage that all experiments are conducted *in silico* which allows greater productivity than *in vitro* experiments.

Several approaches to studying lectin-carbohydrate interactions by molecular modelling are possible.²⁴³ Molecular docking is one of the least expensive methods for predicting lectin-carbohydrate interactions. The method locates the binding site and finds the correct placement for the ligand. The “best fit”, having the lowest energy conformation, is then energy minimised and taken for further evaluation. Solvent molecules are typically ignored or included only implicitly. The loss of degrees of freedom is also often ignored. Docking is typically used as a starting point for further calculation if only little information is known about the binding partners. Molecular dynamics can also be used to evaluate the binding of interacting partners. As above, it allows the study of ligand flexibility in the binding site in order that the most stable binding conformation is found, as well as other low energy alternatives. Likewise, the binding site can be isolated and included in the simulation so its ligand accommodation and behaviour upon occupation can be evaluated. Solvent molecules can also be included explicitly to allow the evaluation of the solvation behaviour of both the ligand and binding sites. One can also study the behaviour and importance of solvent molecules throughout the interaction. As above, dynamics simulations require large amounts of computer power, therefore only short simulations are ran.

Although there are several examples of AuNP modelling, this is still only at a basic stage. Correct parameterisation of the Au core as well as the behaviour of ligands immobilised to the GNP surface are yet to be implemented in a coherent GNP-force field. Nevertheless, participating groups of the GlycoGold network have been working towards this aim, with the intention of modelling and evaluating multivalent GNP-lectin interactions.

4.4.6 UV aggregation studies

Specific to GNP-lectin interactions, this technique is none-the-less valid for investigating protein-carbohydrate interactions. In principle, this method takes advantage of the fact that GNPs have a surface plasmon resonance of their own, which is size-dependent. Typically, in solution GNPs have an SPR band at 520 nm. Upon aggregation, this SPR band may undergo a shift to a higher wavelength (620 nm).^{183, 186} This is due to the coupling of surface plasmons of GNPs in close proximity with one another.¹²⁰(and references therein) Therefore, using UV/Vis spectroscopy, kinetic measurements of the disappearance of the SPR band at 520 nm, or the appearance of the SPR band corresponding to aggregation at 620 nm can be carried out. Again, as for HIA and DLS, this may not reflect the dissociation constant; however several applications take advantage of this effect.^{131, 153, 189, 244}

UV/Vis aggregation studies were attempted with this study, however, as the nanoparticles are particularly small, their SPR signal is not visible and thus no workable results were obtained.

4.5 Conclusions

Biophysical analysis is used in order to find the relationships between the structure and function of a ligand. The evaluation of protein-carbohydrate interactions can be carried out using several methods available. However, an understanding of each method is crucial for the optimal development of experimental procedures, the analysis and critics of the results given as well as the material advantages and disadvantages and limits of each technique. We have seen in this chapter that some techniques are heterogeneous in nature (SPR, ELLA) where one binding partner is immobilised to a surface, and others which are homogeneous (ITC, DLS, UV/vis spectroscopy) where both binding partners are in free solution. We have also seen that some techniques are qualitative or comparative and others quantitative and that each technique often has different functioning modes. It is therefore the responsibility of the

investigator to choose the most appropriate experiments to carry out with respect to the natures of the interacting partners, the level of information needed to give the required interpretations as well as any material constraints. One must also bear in mind that results obtained from one technique may not be compared to the results of another, as the fundamental differences in the experiments may (and most likely will) influence the overall outcome.

CHAPTER 5 :
Synthesis and Biological Evaluation of
GNPs

CHAPTER 5 :

Synthesis and Biological Evaluation of GNPs

5.1 Article 1

**Gold Glyconanoparticles : Influence of ligand presentation density on
multivalent in protein – carbohydrate interactions**

Article in preparation

Gold Glyconanoparticles : Influence of ligand presentation density on multivalent protein-carbohydrate interactions

*** Corresponding author**

Dr. Serge Perez, European Synchrotron Radiation Facility, F-38043, Grenoble Cedex 9, France ; Email : serge.perez@esrf.fr

Running title: Multivalent GNP-lectin interactions, influence of ligand presentation density.

Key words: gold glyconanoparticles, protein-carbohydrate interactions, multivalence, surface plasmon resonance, isothermal titration (micro) calorimetry.

Abstract

Carbohydrate functionalised gold nanoclusters, (Glyconanoparticles, GNPs) show promising potential as multivalent tools for studies in fundamental glycobiology research as well as applications in diagnostics and clinical applications. Here the influence of ligand density on the recognition by protein receptors (lectins) was evaluated by examining the interaction of mannose and galactose functionalised GNPs with three lectin systems; commercially available Con A, the recently characterised mannose specific lectin BclA from *Berkholderia cenocepacia*, and the galactose specific lectin PA-IL from *Pseudomonas aeruginosa*. Results show that the correct selection of ligand density at the GNP surface is required to induce optimal multivalent binding strengths and affinities depending on the lectin studied.

Introduction

Carbohydrates at the cell surface (glycolipids and glycoproteins) play key roles in the recognition mechanisms of various biological cells and their external environment. Specific, reversible interactions between these carbohydrates and protein receptors (lectins) are of great importance in many normal and pathological biological and biochemical processes ranging from fertilization and inter-cellular communication to bacterial invasion and tumour metastasis.¹ These lectin-carbohydrate interactions typically exhibit high specificity and weak affinities toward their carbohydrate ligand. In nature, this low affinity is compensated by the architecture of the lectin itself, containing typically two or more carbohydrate binding sites, and by the host presenting the oligosaccharide ligands multivalently or as clusters on the cell surface.² The resulting interaction thus being a combination of several binding events, yet the overall binding is significantly greater than the combination of the individual binding events. I.e. the “whole” of the interaction is greater than the sum of its parts. This effect is known as the multivalence or cluster-glycoside effect, and is well documented for lectin-carbohydrate interactions.^{3,4}

Several theoretical models have prevailed in recent years to explain the observations involving the multivalence effect. The most prominent by Whitesides *et al.* which gave a comprehensive review of multivalent interactions and the thermodynamic implications towards multivalently enhanced interaction affinities.² A second alternative theory, first suggested by Kramer *et al.*⁵ and applied to protein-carbohydrate interactions by Lees *et al.*⁶ implies that the binding partners experience a high local *effective concentration* of each other, increasing the probability of intramolecular interactions taking place. Several complimentary studies and reviews have supported this theory and its inner-workings.⁷⁻⁹

Due to their function, lectins are important targets for many analytical, diagnostic and therapeutic applications. Thus, in order to study and potentially interfere, control or block these interactions, many multivalent “scaffolds” have been developed. Synthetic oligosaccharides, themselves functionalised with suitable “spacer” molecules, have been conjugated to a number of multivalent scaffolds from carrier proteins,¹⁰ dendrimers,¹¹⁻¹⁴ micelles¹⁵ and polymers^{16, 17} to nanoparticles and quantum dots.^{18-20 (and ref therein)} Several examples of gold nanoparticles functionalised with biologically active oligosaccharides (Glyco-Nanoparticles, GNPs) can also be found in the literature,^{21, 22} as well as a myriad of

other examples of nanoparticles coated with other biologically important molecules exhibiting a multivalent effect.^{20, 23-26}

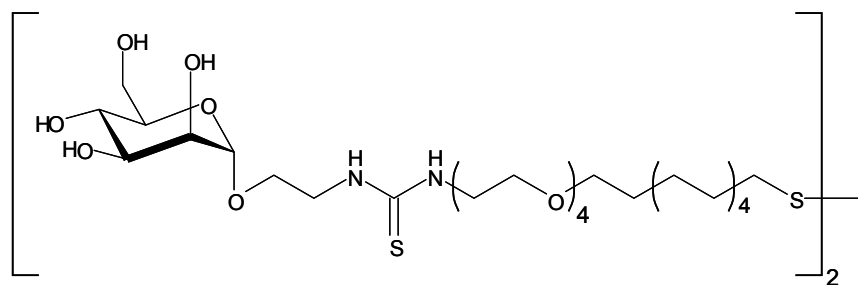
Functionalising nanoparticles with oligosaccharides has several advantages over other multivalent scaffolds: Their synthesis and functionalisation is a simple, one step process which allows the tuning of various physical properties (stability, water solubility, cytotoxic activity, particle core composition etc). They also have sizes similar to those of other common biomolecules, which can also be influenced by tuning particular experimental conditions. Nanoparticles are also globular in shape, making them ideal for providing a glycocalyx-like surface for presenting oligosaccharide molecules. Also, by altering the quantities and ratios of the molecules to be conjugated to the GNP surface, the presentation density of a particular ligand can be controlled whilst at the same time several molecules of interest can be attached to the same nanoparticle, giving rise to multifunctionality. For this reason in particular, GNPs are very attractive, as to perform this on other multivalent scaffolds would require complicated syntheses and protection / deprotection procedures for each desired functionality. Finally, nanoparticles of this size exhibit several interesting physical properties due to quantum size effects, which could also be exploited in numerous applications.^{27, 28}

In order to quantify the interactions between the functionalised GNPs and their lectin partners, modern biophysical techniques such as surface plasmon resonance (SPR) and isothermal titration (micro)calorimetry (ITC) have emerged in recent decades as suitable techniques to investigate protein-carbohydrate interactions.^{29, 30} Although there are several examples of analysing protein-GNP interactions using SPR, there are few examples of using ITC in a fully quantitative context.^{31, 32} This is due to several factors: Firstly, the lectin studied is habitually Concanavalin A (Con A), which has a relatively weak association constant ($\sim K_a \approx 1 \times 10^4 M^{-1}$ for Me- α -D-Mannoside by ITC)³³ which in turn requires high concentrations of both lectin and oligosaccharide ligand. These high concentrations often, in the cases of multivalent ligands, lead to irreversible aggregation and precipitation and thus failed experiments.³⁴

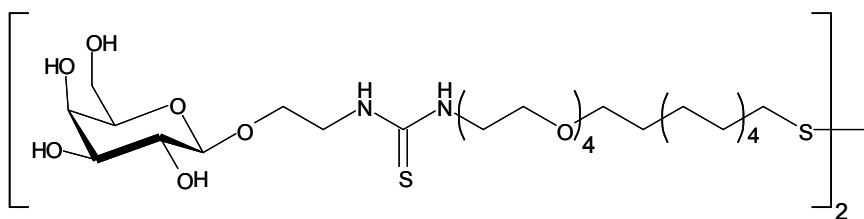
Recently, our laboratory has characterised several bacterial lectins which exhibit high affinities for monosaccharide ligands. Two of these in particular are the BclA lectin from *Burkholderia cenocepacia complex* and the PA-IL lectin from *Pseudomonas aeruginosa*.^{35, 36} These lectins exhibit association constants in the range of $10^5 M^{-1}$ and $10^4 M^{-1}$ for

mannosides and galactosides respectively, showing no significant specificity for any other monosaccharide. We were also able to synthesise several mannoside, galactoside and glucoside ligands functionalised with thiol-capped spacer molecules. This in turn allowed the fabrication of several GNPs in order to study the effect of GNP surface presentation density on the affinity of the lectins for the GNPs. Using a protocol outline by Penades *et al.* we were able to produce stable, water soluble GNPs exhibiting mannoside presentations of 13, 25, 46 and 100% and galactoside presentations of 17, 33, 80, 90 and 100%.^{37, 38} The glucoside was used as the inactive ligand. Combining the relatively high affinity of the lectins used, and the solubility of the GNPs fabricated, we were able to conduct quantitative biophysical characterisation of these multivalent interactions using ITC. For BclA, PA-IL and Con A, we were also able to use SPR as a second, quantitative characterisation method. Haemagglutination inhibition assays with PA-IL and Con A were also carried out. We have shown that, by changing only the presentation density on the GNP surface, the affinity of the lectin can be augmented.

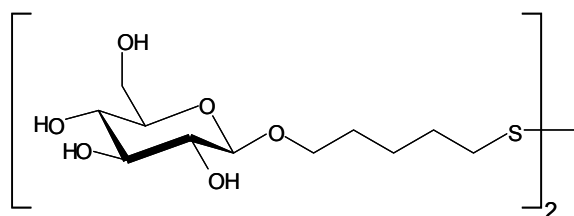
Results



1



2



3

Figure 1 : Ligands 1-3, synthesised for protecting Au clusters.

Synthesis of neoglycoconjugates 1-3: Thiol-derivatised neoglycoconjugates of mannose (**1**) and glucose (**3**) are as previously reported.³⁸ The galactose neoglycoconjugate (**2**) was prepared as for **1**. The neoglycoconjugates were conjugated to the GNP surface via the thiourea-bridged linker as in previous studies. This linker imparts good chemisorption to the GNP surface as well as ligand flexibility and aqueous solubility.

Preparation of gold Glyconanoparticles: The *gluco-*, *manno-* and *galacto-*protected glyconanoparticles (**GNP-1**, **GNP-5** and **GNP-10**) proved to be stable and soluble in aqueous environments exhibiting GNPs with high presentation densities for investigating lectin-carbohydrate interactions. GNPs (**GNP-2** to **GNP-4**) have been prepared as hybrids of neoglycoconjugates **1** and **3** in order to study the influence of (active) ligand presentation density on the molecular recognition of mannosides by the BclA and Con A lectins. Likewise, **GNP-6** to **GNP-9** were fabricated to study the influence of ligand presentation density on the molecular recognition of galactosides by PA-IL.

All GNPs were prepared and characterised using procedures previously developed.^{37, 39} A methanolic solution of the corresponding neoglycoconjugates was added to an aqueous solution of tetrachloroauric acid (HAuCl₄). Reduction of the resulting mixture with NaBH₄ gave a dark brown mixture which was shaken for 2 hours. The solvent was removed and the aggregates re-suspended in water. Exhaustive dialysis against water, followed by centrifugation and lyophilisation gave the GNPs as amorphous brown solids. They were characterised by ¹H NMR, FT-infrared spectroscopy, UV-vis spectroscopy, transmission electron microscopy (TEM) and elemental analysis. The GNPs prepared are water soluble, stable and can be treated as water-soluble macromolecules.

The resulting GNPs show an exceptionally small average core size (1-2 nm) as seen by TEM, with a uniform dispersion. ¹H NMR spectra of the GNPs featured broader peaks with regard to the neoglycoconjugates in free solution. Elemental analysis confirms for all GNPs that the desired coverage density was obtained ($\pm 5\%$) for Mannose GNPs. Less presentation density control was observed for the Galactose GNPs. From GNP core size and elemental analysis, an average molecular formula was estimated according to previous work.⁴⁰

All GNPs are soluble in water and stable for long periods. However, some GNPs were insoluble, or not soluble in sufficient quantity, in buffer solutions such as **GNP-5**, **GNP-8**,

and **GNP-9**. Thus, ITC experiments involving these GNPs proved difficult. A summary of the GNPs produced can be found in the table 1 below.

GNP	Active Neoglycoconjugate	Average Core Diameter (nm)	Average number of Au atoms	Average molecular formula	Number of active ligands	Desired Presentation density (%)	Actual Presentation Density	Average M_w
GNP-1	-	1,34	100	$(C_{11}H_{21}O_6S)_{41}Au_{100}$	-	-	-	31 222
GNP-2	1	1,49	125	$(C_{28}H_{56}N_2O_{10}S_2)_{11}(C_{11}H_{21}O_6S)_{72}Au_{125}$	11	10	13	51 937
GNP-3	1	1,66	140	$(C_{28}H_{56}N_2O_{10}S_2)_{24}(C_{11}H_{21}O_6S)_{72}Au_{140}$	24	25	25	63 255
GNP-4	1	1,61	140	$(C_{28}H_{56}N_2O_{10}S_2)_{39}(C_{11}H_{21}O_6S)_{46}Au_{140}$	39	50	46	65 596
GNP-5	1	1,44	116	$(C_{28}H_{56}O_{10}S_2)_{88}Au_{116}$	88	100	100	79 461
GNP-6	2	1,43	120	$(C_{28}H_{56}N_2O_{10}S_2)_{12}(C_{11}H_{21}O_6S)_{69}Au_{120}$	12	10	17	47 941
GNP-7	2	1,27	79	$(C_{28}H_{56}N_2O_{10}S_2)_{15}(C_{11}H_{21}O_6S)_{30}Au_{79}$	15	25	33	33 643
GNP-8	2	1,39	140	$(C_{28}H_{56}N_2O_{10}S_2)_{65}(C_{11}H_{21}O_6S)_{16}Au_{140}$	65	50	80	73 889
GNP-9	2	1,36	100	$(C_{28}H_{56}N_2O_{10}S_2)_{57}(C_{11}H_{21}O_6S)_7Au_{100}$	57	75	90	58 334
GNP-10	2	1,24	70	$(C_{28}H_{56}O_{10}S_2)_{67}Au_{70}$	67	100	100	56 890

Table 1 : Summary of GNPs synthesised.

Protein culture and purification: Con A was purchased from Sigma-Aldrich and used without further purification. BclA and PA-IL were cultured and purified following procedures previously reported by our laboratory.^{35, 41}

Interaction studies:

Haemagglutination Assay: Rabbit erythrocytes were bought from Biomerieux and used without further washing. The erythrocytes were diluted to a 2 % solution in NaCl (150 mM). Lectin solutions of 1 mg mL⁻¹ were prepared in Tris/HCl (0.1 M Tris/HCl, 3 μM CaCl₂, pH 7.5). The Haemagglutination unit (HU) was first obtained by the addition of 25 μL of the 2 % erythrocyte solution to 25 μL aliquots of sequential lectin dilutions. The mixture was incubated at 37 °C for 30 mins followed by incubation at RT for 30 mins. The HU was taken as the minimum lectin concentration required to prevent haemagglutination. For the following lectin-inhibition assays, lectin concentrations four times that of the haemagglutination unit were used. For Con A and PA-IL these concentrations were found to be 15.625 μg mL⁻¹ and 5 μg mL⁻¹ respectively. Subsequent assays were then carried out by the addition of 50 μL lectin solution (at the required concentration) to 50 μL of sequential dilutions of GNPs, monomer molecules and controls. These solutions were then incubated at 37 °C for 30 mins followed by 30 mins at RT. After which, 50 μL of 2 % erythrocyte solution was added followed by a further 30 mins incubation at 37 °C and 30 mins at RT. The minimum inhibitory concentration for each GNP molecule was recorded. Monosaccharide concentration was calculated using a modified Phenol-sulfuric acid method.⁴²

Surface plasmon resonance binding assays: All SPR experiments were carried out on a Biacore T100 instrument. CM5 sensor chips (Biacore/GE, Uppsala, Sweden) were equilibrated with HBS (HEPES-buffered saline: 10 mM HEPES and 150 mM NaCl, pH 7.4) containing 0.005 % (v/v) Tween 20 at 25 °C with a flow rate of 20 $\mu\text{L min}^{-1}$. Following equilibration, the chips were activated with two 7 minute pulses of a 1 : 1 mixture (v/v) of 0.1 M *N*-hydroxy-succinimide and 0.1 M *N*-ethyl-*N'*-(dimethylaminopropyl)carbodiimide, at 25 °C and flow rate of 5 $\mu\text{L min}^{-1}$. Ethanolamine hydrochloride was immobilised on channel one via an injection of 7 min (1.0 M, pH 8.5; ~80 RU) to measure the level of non-specific binding and to serve as a blank for mathematical data treatment. Con A was immobilised on channel 3 via a 60 s injection (100 $\mu\text{g mL}^{-1}$ in 10 mM Sodium Acetate buffer, pH 4.5; ~4100 RU). Con A was also immobilised on channel 4 via a 4 min injection (2 $\mu\text{g mL}^{-1}$; ~400 RU). Remaining *N*-hydroxy succinimide esters were blocked by a 7 min pulse of 1 M Ethanolamine hydrochloride, pH 8.5. A second chip was activated and Ethanolamine hydrochloride immobilised to channel one as described above. BclA was immobilised on channel 2 via a 7 min injection (10 $\mu\text{g mL}^{-1}$, Sodium Acetate buffer, pH 4.5; ~480 RU). Remaining *N*-hydroxy succinimide esters were blocked by a 7 min pulse of 1 M Ethanolamine hydrochloride, pH 8.5. PA-IL was immobilised to Channel 3 via a 41 mins injection (100 $\mu\text{g mL}^{-1}$, Sodium Acetate buffer, pH 4.5; ~300 RU). Remaining *N*-hydroxy succinimide esters were blocked by a 7 min pulse of 1 M Ethanolamine hydrochloride, pH 8.5.

GNP solutions (100 $\mu\text{g mL}^{-1}$, and dilutions thereof to 30 ng mL^{-1}) in HEPES buffer were flowed across the sensor chip surfaces for 3 mins at a flow rate of 20 $\mu\text{l min}^{-1}$, and were allowed to dissociate for 3 mins. To restore the response level to zero, injections of three 3 min pulses of 1 M Me- α -D-Mannose and 1 M Me- α -D-Galactose for assays involving the mannose specific lectins and PA-IL respectively.

Binding was measured as RU (resonance units) over time, and data were evaluated using the Biacore Evaluation Software, version 1.1, and were fitted using a kinetic model for 1 : 1 binding.

Isothermal Titration microCalorimetry: Titration calorimetry experiments were performed using a Microcal VP-ITC microcalorimeter. Titrations were carried out in 100 mM Tris/HCl

buffer (pH 7.5) containing 3 μM CaCl_2 , at 25 $^\circ\text{C}$. In the case of **GNP-8** and **GNP-10**, buffer solutions of 10 mM Tris/HCl were used due to solubility of the GNPs. Aliquots of 10 μL of lectin solutions, with concentrations of 0.21 mM to 1 mM for BclA and 0.23 mM to 1 mM for PA-IL, were added at 5 min intervals to the GNP solution present in the calorimeter cell. In the titrations, the GNP concentration varied from 0.5 mg mL^{-1} to 1.73 mg mL^{-1} for BclA and for 0.46 mg mL^{-1} to 1.12 mg mL^{-1} for PA-IL, giving a saccharide concentration of 0.03 mM to 0.1 mM and 0.031 mM to 0.076 mM respectively as calculated by a modified Phenol-sulfuric acid method.⁴² The corresponding monomer molecules (**1SH** for BclA and **2SAc** for PA-IL) were also injected into solutions of the corresponding lectin solutions. Monomer concentrations were 3 mM and 1.7 mM respectively and lectin concentrations of 0.31 mM (BclA) and 0.05 mM (PA-IL). The temperature of the cell was controlled to 25 ± 0.1 $^\circ\text{C}$. Control experiments performed by injection of buffer into the GNP solution yielded insignificant heats of dilution. Injections of lectin into control GNPs yielded insignificant heats of dilution and non-specific interactions. Repetitions of several experiments in phosphate buffered saline (PBS) demonstrated that Tris/HCl was the most suitable buffer system for the lectins studied. Integrated heat effects were analysed by non-linear regression using a two-site binding model and the classic one-site binding model (Origin 7.0) for BclA and PA-IL respectively.⁴³ Fitted data yielded association constants (K_a) and the enthalpy of binding (ΔH). Other thermodynamic parameters; changes in free energy, ΔG , and entropy, ΔS , were calculated from the equations:

$$\Delta G = \Delta H - T\Delta S = -RT \ln K_a$$

Where T is the absolute temperature and $R = 8.314$ $\text{J mol}^{-1}\text{K}^{-1}$. Three independent titrations were performed for each lectin - GNP combination.

Discussion

Haemagglutination Inhibition Assay: Haemagglutination assays were performed on Con A and PA-IL. It was found that BclA produced an inhibition unit of 2 mg mL^{-1} which was deemed too high and impractical to perform this test. Table 2 shows the relative activity of **GNP-1** to **GNP-10** for Con A and PA-IL.

	ConA			PA-IL	
	Av. No. of Sugars	Inhibition sugar conc. / μM	Rel. Act. / residue	Inhibition sugar conc. / μM	Rel. Act. / residue
1SH	1	6.05	1		
GNP-2	11 \pm 1	-	0		
GNP-3	24 \pm 1	-	0	-	0
GNP-4	39 \pm 1	5.45	1.17 \pm 0.03		
GNP-5	88 \pm 1	1.81	3.34 \pm 0.04		
2SAc	1			45.5	1
GNP-6	12 \pm 1			12.5	3.64 \pm 0.3
GNP-7	15 \pm 1			1.02	44.6 \pm 1
GNP-8	65 \pm 1	-	0	0.66	68.9 \pm 0.8
GNP-9	57 \pm 1			0.40	113.8 \pm 2
GNP-10	67 \pm 1			0.45	101.1 \pm 1.5
GNP-1	0	-	0	-	0

Table 2 : Results from haemagglutination inhibition assays. Left: Con A; PA-IL: right.

To allow for the comparison of the results for the GNPs, the corresponding monomers **1SH** and **2SAc** were assigned a relative activity value of 1 with the respective lectin even though the respective inhibiting concentrations of the monomers is different. From the photographs of the assay, a yellow discolouring of the solutions can be seen at high GNP concentrations due to haemolysis. We suspect there maybe cytotoxicity at such high concentrations possibly caused by the ethylene glycol units of the spacer molecule resulting in cell membrane damage. However, at lower concentrations, this is not seen. From the results of assays involving Con A, we can clearly see that low presentation densities do not inhibit haemagglutination and are thus less active than **1SH** in free solution. High presentation GNPs inhibit only marginally better, per mannose residue, than the monomer molecule. For PA-IL however, the results are more encouraging. With low density presentations a significant improvement in inhibition activity can be seen which increases with increasing presentation density to almost 70 times stronger per galactose for **GNP-8**.

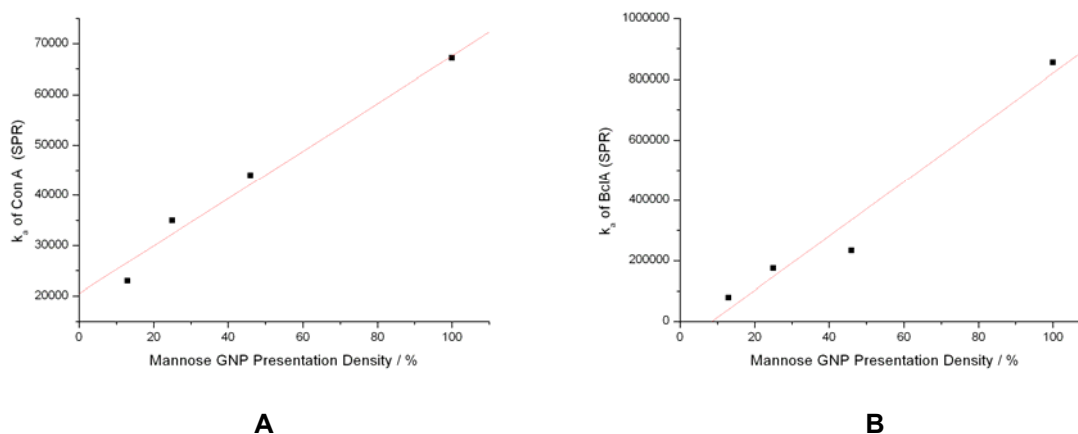
SPR Binding Assays: For Con A, results observed were similar to those found by Kamerling *et al.* whereby no signal was observed for the galactose functionalised GNPs. Strong signals were observed for the mannose functionalised GNPs, however, a second chip, with surface coverage of 4000 RUs of immobilised Con A was required for **GNP-1** and **GNP-2**. Also, interactions were observed for **GNP-1** due to competition with the dextran surface.²⁰

As expected, only the mannose functionalised GNPs showed a strong SPR binding signal for BclA (40, 175, 115 and 110 RU for **GNP-2** to **GNP-4** respectively). No response was

observed for **GNP-1** or **GNP-6 - GNP-10**. Likewise for PA-IL, only the galactose functionalised GNPs showed any SPR binding signal (120, 345, 355, 380 and 150 RUs for **GNP-6** to **GNP-10**). Sensorgrams for Con A, BclA and PA-IL can be found in the supporting information.

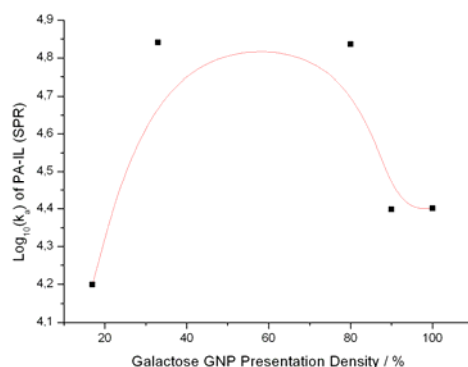
In all cases, a one site binding model was applied in the Biacore evaluation software (Uppsala, Sweden) as this gave the best fit, the lowest Chi² value and was the most reliable. Upon first inspection, all lectins provided strong positive SPR response signals showing that there is indeed an interaction between the immobilised lectins and their corresponding monosaccharide functionalised GNPs. It can also be observed that the affinity of the lectin increases with increasing presentation density as can be seen from the maximum response level, and is independent of GNP size. This is true for all lectins studied. For Con A, an affinity constant of $2.3 \times 10^4 \text{ M}^{-1}\text{s}^{-1}$ was observed for a presentation density of 13% mannose (**GNP-2**). Upon increasing this presentation density to 25, 46 and 100 %, k_a of 3.5×10^4 , 4.4×10^4 and $6.72 \times 10^4 \text{ M}^{-1}\text{s}^{-1}$ were observed. The k_a tripling upon increasing the coverage density from 13 to 100 % mannose (Graph 1,A).

For the BclA lectin, a similar pattern is observed yet the effect of presentation density is significantly more pronounced. **GNP-2** induced a k_a of $7.9 \times 10^4 \text{ M}^{-1}\text{s}^{-1}$ which increased to 17.5×10^4 , 23.3×10^4 and $85.5 \times 10^4 \text{ M}^{-1}\text{s}^{-1}$ for **GNP-3**, **GNP-4** and **GNP-5** respectively (graph 1,B), the lectin affinity increasing linearly with GNP presentation density.



Graph 1: Graph of lectin affinity against GNP presentation density for Con A (a), and BclA (b). Both lectins exhibit a linear dependence on presentation density.

For PA-IL a different situation was observed. The affinity of the lectin increases dramatically (> 4 fold) between **GNP-6** and **GNP-7**. As the presentation increases further, no significant change in lectin affinity is observed. However, upon reaching a presentation density of 90 % (**GNP-9**) and greater, lectin affinity decreases sharply down to comparable levels as for **GNP-6**. Graph 2 shows this more clearly.



Graph 2: Log(k_a) of PA-IL against Galactose presentation density. In contrast to graph 1, where the Log of the affinity of PA-IL is non-linear with presentation density.

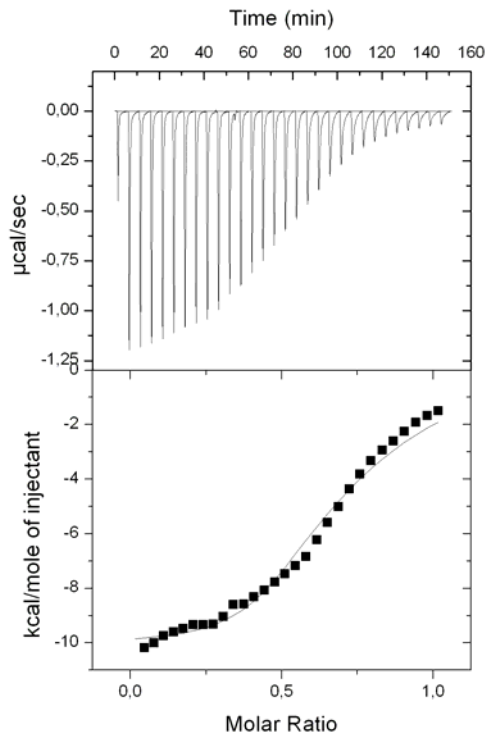
With Con A and BclA, the increase in lectin affinity appears to have a linear dependence on presentation density. This could be related to the local concentration of ligands at the GNP surface. As the concentration increases, the probability of a GNP-lectin interaction increases also, and hence increased association constants. With PA-IL, a more complex process can be observed. The affinity increases enormously with the presentation density until an optimum presentation is reached (33 %). Beyond this optimum presentation the ligand density becomes too high and perhaps the interaction of one galactose ligand is sterically impeded by the close proximity of other ligands on the same GNP. All SPR results can be seen in table 3.

GNP	k _a (SPR) M ⁻¹ s ⁻¹ / 10 ³		GNP	k _a (SPR) M ⁻¹ s ⁻¹ / 10 ³
	Con A	BclA		PA-IL
1	0.13	0	6	15.8
2	22.5	79	7	69.3
3	34.8	175	8	68.6
4	44.0	233	9	25.0
5	67.2	855	10	25.2

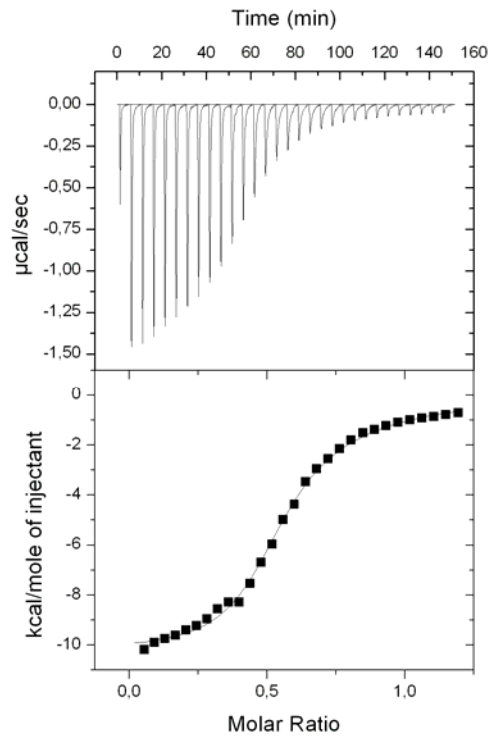
Table 3 : Lectin affinities for mannose and galactose GNPs as measured by SPR.

Calorimetry Studies: ITC has been used extensively for the investigation of carbohydrate-protein interactions as it permits the determination of all thermodynamic parameters in one experiment including the number of binding sites (*n*), binding enthalpy (ΔH), and the

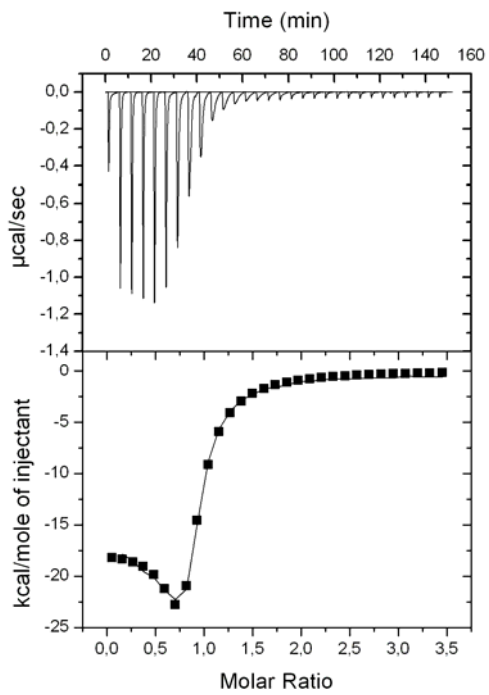
association constant (K_a) from which the free energy of binding (ΔG) and binding entropy (ΔS) can be calculated. Many examples can be found in the literature, including investigations into the lectins used here, for the binding of monosaccharide and small multivalent frameworks.^{30, 35, 44} However, few examples can be found in the literature for multivalent platforms such as dendrimers, micelles or nanoparticles etc.³¹ As previously mentioned, Con A is typically the lectin of choice for investigating multivalent platforms yet, when using ITC, the affinity of Con A for mannose and mannose derivatives is relatively weak. Thus, high concentrations of lectin and ligand (dendrimer or micelle) are required.³⁴ This in turn often leads to aggregation and precipitation which deem the experiment unusable, on a quantitative level at least, as complexes soluble for the duration of the experiment are required. Previous studies have discussed the use of ITC qualitatively or present the binding enthalpy only.^{31, 45, 46} We thus present here the first documented use of ITC for quantifying the thermodynamic parameters for the interaction of two multivalent lectins (BclA and PA-IL) with functionalised gold nanoparticles used as multivalent platforms. This was possible due to several characteristics of the lectins, the GNPs themselves and the experimental set-up used. Firstly, the lectins used for the ITC investigations exhibit exceptionally high affinities for their corresponding monosaccharide. This allows the use of low concentrated solutions which still produce significant ITC response signals. Also, the nanoparticles are very soluble in buffered solutions (although some more than others) thus reducing the occurrence of precipitation. Finally, a conventional experimental set-up was initially used (injections of GNPs into lectin solutions) however this frequently led to aggregation clearly visible in the ITC profile. Inverting the experimental set-up, where injections of lectin solutions into GNP solutions evaded this problem yet allowing the investigation of the same interaction. The ITC profiles of several GNP-lectin experiments can be seen in figure 2 and 3.



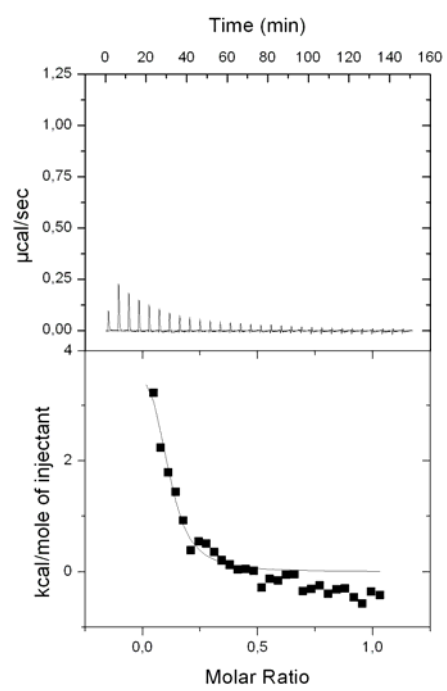
A



B



C



D

Figure 2 : ITC profiles of 30 BclA injections into solutions of GNP-2 (A), GNP-3(B), GNP-4(C) and GNP-8 at 25 °C.

It can be observed from the ITC profiles that injections of lectins to their corresponding GNP solutions produced exothermic interactions indicating positive interactions between the reacting partners. Secondly, injections of buffer solution into GNP solutions resulted in negligible heats of dilution. Injections of BclA into buffer solution revealed what could be significant enthalpies of dilution, however injections into solution of **GNP-1** and **GNP-8** showed non-specific interactions which countered the effect of lectin dilution (Figure 2, D). Likewise, injections of PA-IL into solutions of **GNP-1** and **GNP-2** showed negligible heats of dilution and thus served as a blank experiment for non-specific interactions (Figure 5, D). Injections of the monomers of molecules **1SH** and **2SAc** to BclA and PA-IL respectively were also plotted and can be seen in (supporting information).

In the case of BclA, as described in the literature,³⁵ a two-site binding model was used. The concentrations used were expressed as the concentration of whole lectin (i.e. dimer concentration) and the concentration of mannose residues (and not the concentration of GNPs) which was determined by a modified Phenol-sulfuric acid method.⁴² It can be seen that typical ITC profiles have been produced by **GNP-2** and **GNP-3**. These profiles greatly resemble that of the monomer molecule, **1SH**, suggesting that with these low density coverages, the mannose moieties presented on these nanoparticles behave as their monomer molecule counterparts in free solution. I.e. the GNP platform provides no advantageous presentation or macromolecular conformation which may improve the interaction of the lectin with the mannosides. This has recently been observed for other lectin and enzyme systems.²¹ However, for the injection of BclA into **GNP-4**, one can see that this ITC profile is significantly different, and resembles a highly cooperative interaction i.e. the binding of one mannoside residue induces a change in the second lectin binding site. The thermodynamic parameters for the interaction of BclA with **1SH** and **GNP-2** to **GNP-4** can be seen in table 4 and graph 3. In all cases, the first binding event is high in affinity (micromolar or nanomolar) which facilitates the second binding event. For the monomer, **1SH**, **GNP-2** and **GNP-3**, the association constants are relatively similar for the first binding event. This is reflected by the similar values for their Gibbs free energies. Enthalpically and entropically, these interactions are also very similar, with the enthalpic contribution being the most significant. This suggests that at low presentation densities, the mannoside residues behave independently of one another, as if in free solution, via the same reaction mechanism, which is enthalpically driven. The inter-residue distance induced by the presentation on the nanoparticle platform is too great in order to instigate a more favourable, multivalent interaction.

For **GNP-4** however, the binding affinity is significantly higher. **GNP-4** also exhibits an enthalpic contribution ~5 times larger than lower density GNPs or the monomer implying that this presentation density allows for an interaction which is enthalpically enhanced. The entropic contribution from **GNP-4** is also very different compared to other molecules tested as it is large and unfavourable, significantly countering the enthalpic contribution to the Gibbs free energy suggesting that more events are occurring other than the saccharide-lectin interaction, which contribute significantly to what is observed globally. It may be that at such a high presentation density, as the lectin approaches and binds with the first mannose residue, surrounding residues (both mannose and glucose) may be involved in secondary interactions either intra-molecularly or inter-molecularly thus contributing to the observed enthalpy. These molecules would also be very limited in terms of flexibility and conformation giving rise to large, unfavourable observed entropy. It could also be possible that there is in fact a clustering of mannose residues on the GNP surface. As shown below the inter-residue distance is less than half the inter-binding site distance of BclA. As it is highly unfavourable entropically that the residues will be equally distributed, it is possible that a random arrangement of mannose residues takes place at the Gold – Sulphur interface resulting in the clustering of mannoside residues on the GNP surface, also facilitated by the flexibility of the ethylene glycol units in the spacer molecule. If this is the case, it is possible that the lectin binds to one residue, but as it dissociates, a second mannose residue in the same cluster causes the lectin to re-bind to the GNP. Thus resulting in an interaction with a high global affinity to the mannoside cluster. Also, as several mannosides will be involved, the entropy of the system will be dramatically decreased thus resulting in the unfavourable entropy contribution.

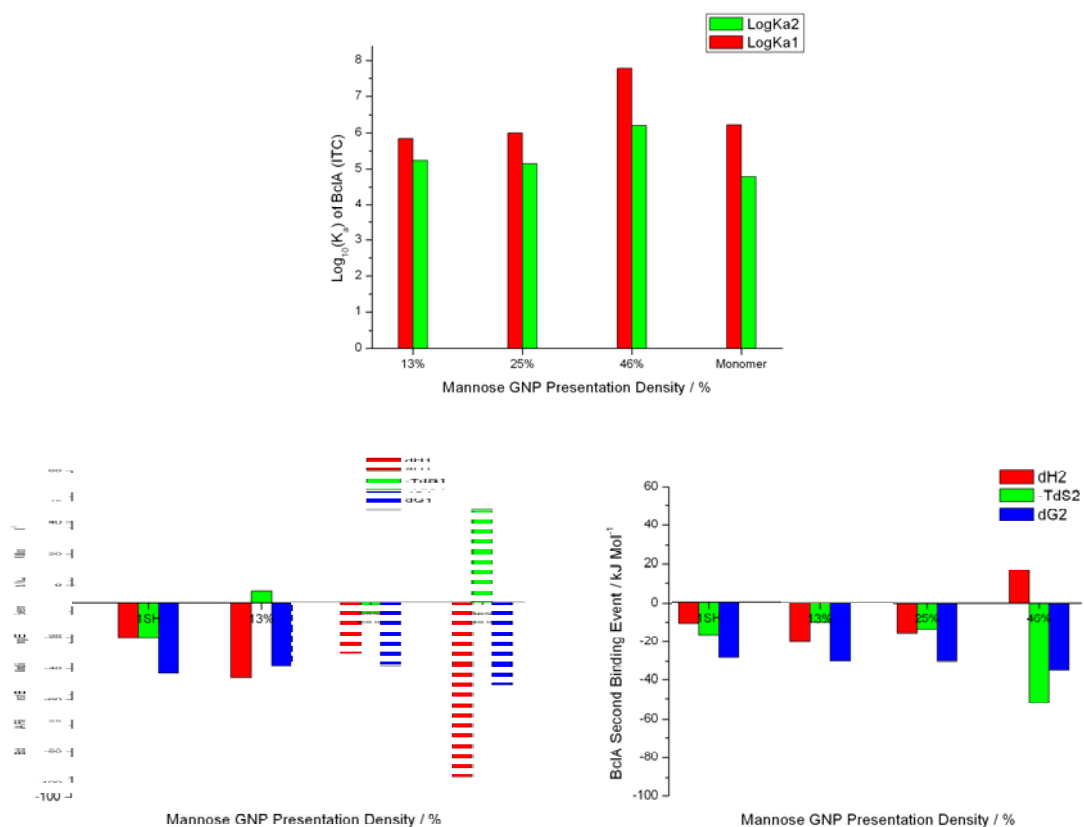
For the second binding event, the affinity is significantly lower than the first, by almost 40 times, whereas for **GNP-2** and **GNP-3** this difference is not so large. They also share similar Gibbs free energies of interaction. This is reflected by the similar values of enthalpy and entropy contributions suggesting that these interactions are equivalent for low presentation density, yet this second binding event is entropically driven. This could be due to the displacement of ordered water molecules from the binding site to the disordered bulk or to internal structural changes of the lectin.⁴⁷ For **GNP-4**, we again notice a significant decrease in binding affinity for the second binding event in comparison to the first however this remains one order of magnitude higher in comparison with the other systems tested. Enthalpically, this second interaction is unfavourable, which may be due to small geometric

changes required by the lectin and/or the GNP in order for the second binding event to take place, as one would expect the lectin to be conformationally restricted, an enthalpic penalty maybe induced.² Nevertheless, this second binding event is highly entropically favourable and indeed the most important contribution to this interaction. As described earlier, there maybe significant binding – re-binding occurring where the second binding site of the lectin is occupied and upon dissociation re-binds to the same, or another mannoside of close proximity, resulting in a globally high affinity interaction. Also, the binding of one binding site would be synergic with the binding / re-binding of the second. As the first interaction was an inter-molecular interaction between free lectin and free GNP, the second interaction will be an intra-molecular interaction by the already formed lectin-GNP complex. Thus effectively creating a “double bond” between the two species which would invoke considerable limitations on the rotational, stretching and bending flexibility of the complex yet would liberate ordered water molecules from the lectin binding site and also liberate the shell of ordered water molecules surrounding the GNP surface (Figure 4).⁴⁸ This is consistent with ITC studies by Rotello *et al.*³²

Therefore for BclA the “multivalence” seen maybe due to several factors; as the presentation density coverage increases the inter-mannoside distance decreases. This would in turn increase the probability of inter-mannoside cluster distances matching that of the inter-binding site distance of the lectin (40 Å, distance between the anomeric carbons of the two Me- α -D-Mannose molecules seen in the crystal structure) leading to favourable binding – re-binding events increasing the global affinity observed. An increase in the effective concentrations of the mannoside will also be experienced by the lectin, enhancing the observed affinity. For **GNP-4**, the displacement of large quantities of ordered water which surrounds the GNP surface may also contribute to the observed entropy (Fig. 4).

	1SH		GNP-2		GNP-3		GNP-4	
$K_{d1} / K_{d2} \cdot 10^6 \text{ M}^{-1}$	1.7	0.06	0.7	0.17	1	0.14	60	1.6
$K_{d1} / K_{d2} \cdot 10^{-8} \text{ M}$	58.8	1667	143	588	100	714	1.6	62.5
$\Delta G / \text{kJ Mol}^{-1}$	-36	-28	-32	-30	-34	-30	-44	-35
$\Delta H / \text{kJ Mol}^{-1}$	-18	-11	-38	-20	-27	-16	-92	17
$T\Delta S / \text{kJ Mol}^{-1}$	18	17	-6	10	7	14	-48	52

Table 4 : Results of the interactions between BclA and mannose functionalised GNPs, as found by ITC.



Graph 3 : Graphs of ITC Results for BclA Above: Association constants for the first (red) and second (green) binding events. Below: Thermodynamic parameters of the first (left) and second (right) binding events. ΔG , blue; ΔH , red and $T\Delta S$ green.

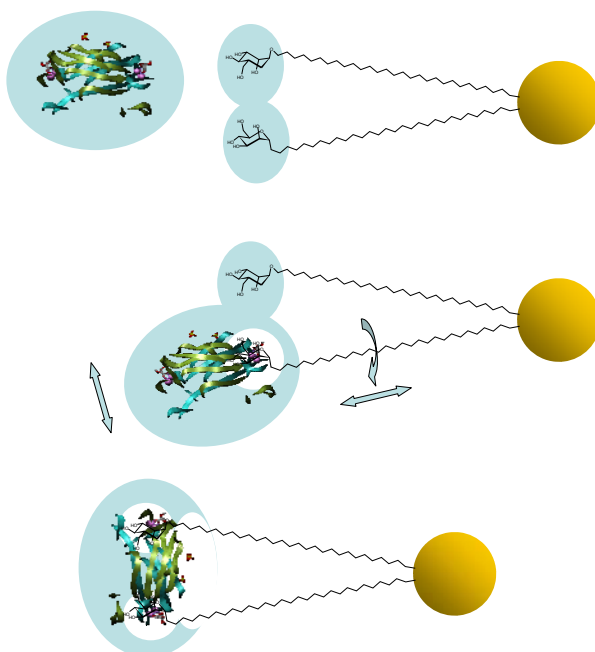
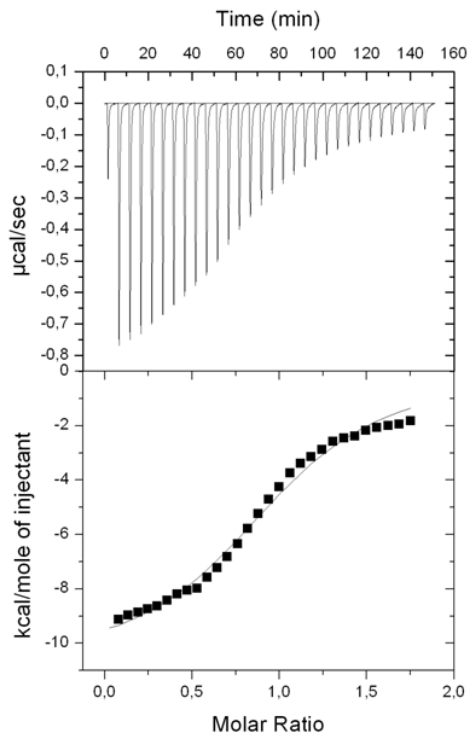
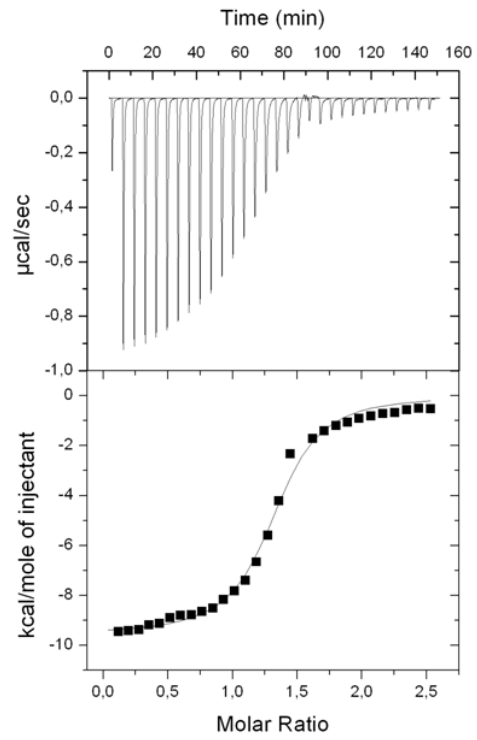


Fig 4 : Displacement of organised water molecules (shaded blue) surrounding both the lectin and GNP (upper) upon single (middle) and "double" (lower) binding events.

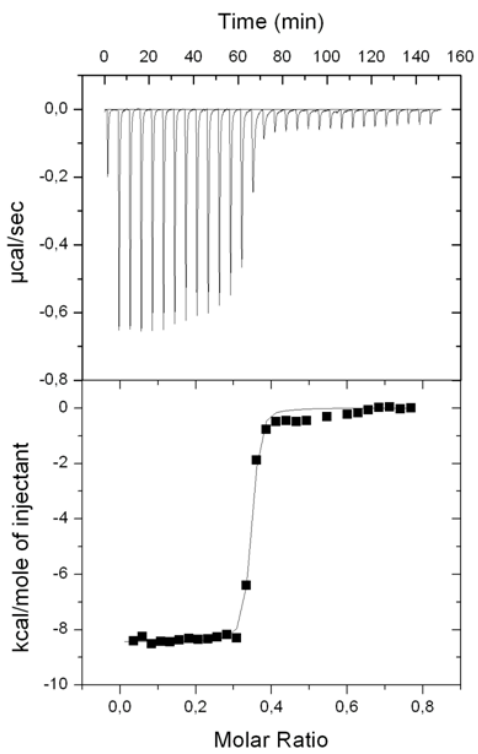
For calorimetry studies with PA-IL, the classic one site binding model was used to fit the integrated peak values. This meant that the concentrations used for the lectin are expressed as the concentration per lectin *monomer*. Therefore the values given for association constants and thermodynamic parameters are in fact an overall average of *all binding events* to the four possible binding sites. As for BclA, the concentration of the nanoparticles was expressed as concentration of galactose residues, confirmed by a modified Phenol-sulfuric acid method. In the case of PA-IL it was found that **GNP-8** and **GNP-9** which have a 80 and 90 % coverage of galactose residues respectively, were insoluble in buffer solutions hence no ITC data is given. From inspection of the ITC profiles one can see that standard curves were obtained for all nanoparticles tested (Fig. 5). Although one may note that the titration curves for **GNP-10** exhibits rapid saturation implying that the experimental conditions are nearing the maximum acceptable “c” value limits.⁴⁹ The results can be seen in table 5 and graph 4.



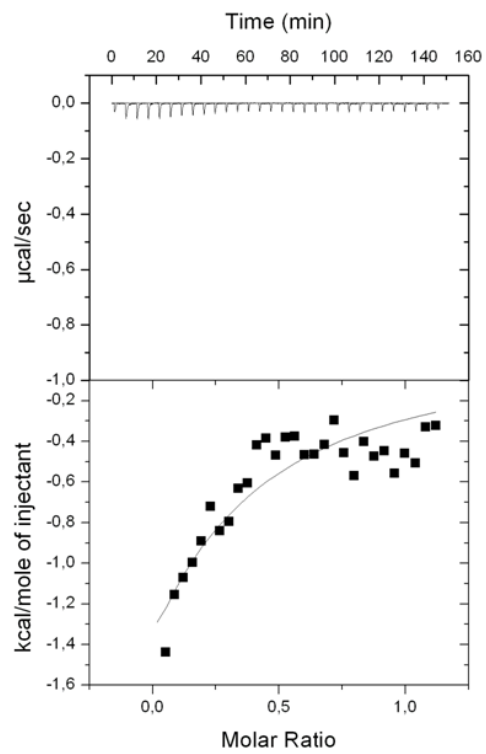
A



B



C

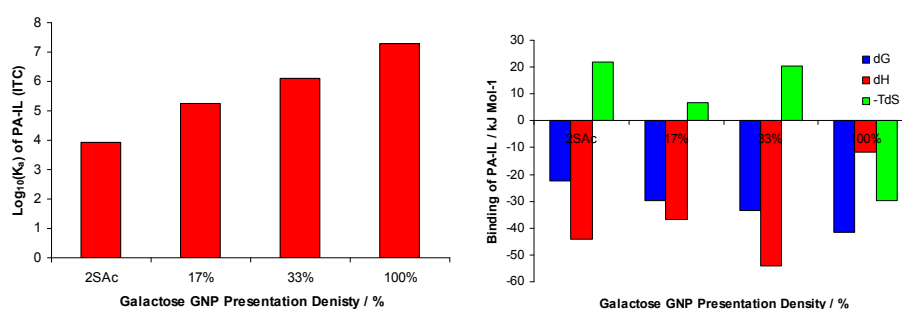


D

Figure 5 : ITC profiles of 30 PA-IL injections into solutions of GNP-6 (A), GNP-7(B), GNP-10(C) and GNP-3 at 25 °C.

	2SAc	GNP-6	GNP-7	GNP-10
K_D M ⁻¹	8.42E+03	1.72E+05	1.31E+06	2.00E+07
$K_D / 10^{-6}$ M	119	5.95	0.76	0.05
n (stoichiometry)	1.41	1.2	0.76	2.13
ΔG / kJ Mol ⁻¹	-22.47	-29.86	-33.62	-41.67
ΔH / kJ Mol ⁻¹	-44.25	-36.77	-53.94	-18.31
$-T\Delta S$ / kJ Mol ⁻¹	21.85	6.7	20.38	-23.39

Table 5 : Results of the interactions between PA-IL and galactose functionalised GNPs, as found by ITC.



Graph 4 : Graphs of ITC Results for PA-IL. Association constants shown on the left. Right: Thermodynamic parameters of the binding event. ΔG , blue; ΔH , red and $T\Delta S$ green.

From the ITC results one can clearly see an increase in affinity as the presentation density increases, approximately one order of magnitude between each GNP tested. This shows that even from a low presentation density, there is a degree of affinity enhancement per galactose residue. However, the concentration was expressed in terms of galactose residue, so for higher presentation densities not all galactose residues would be occupied by a lectin binding site, as seen by the value of n . As the presentation density increases, one would expect the affinity of each successive interaction to be greater than the “average” affinity for all four interactions. From the thermodynamic parameters, which are also calculated per galactose residue, one can see that there is an increase in the Gibbs free energy as the presentation density increases; however it seems that a small increase in the Gibbs free energy results in a large increase in lectin affinity. Enthalpically and entropically, for **GNP-6** and **GNP-7**, the energy released upon binding differs little in comparison to the monomer, **2SAc**, implying again that at low presentation densities, the galactose residues interact independently from one another and as if in free solution as previously seen for BclA. However, for **GNP-10**, this is not the case as the enthalpy of interaction is significantly smaller *per galactose* yet as it will be impossible for *all* galactose residues to interact with lectin binding sites, the total enthalpy released will be due to only several residues capable of interacting. What is interesting in the case of **GNP-10** is the large, favourable entropic contribution implying a large increase in disorder of the

system. This could again be attributed to the displacement of large quantities of ordered water from the binding site and surrounding the GNP surface, as for BclA. The large increases in affinity between the GNPs may be explained by the 3 inter-binding site distances seen in the PA-IL tetramer structure (29, 78 and 82 Å for the x, y and diagonal directions respectively as seen in (figure 6). This structural arrangement would allow synergic multivalent binding – re-binding events to occur at several presentation densities which would explain the range of binding affinities observed for the different GNPs.

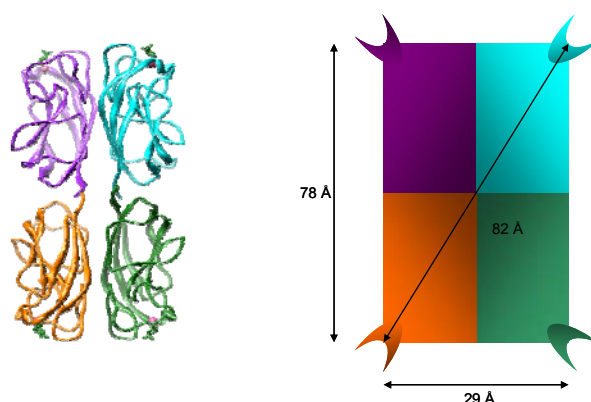


Figure 6 : Crystal structure of PA-IL complexed with Me-β-D-Gal (left) and its square planar architecture (right). ⁴¹

Relation of Biological Activity to GNP Structure: Although significant advances have recently been made with regards to the elucidation of the structure of gold clusters,^{50, 51} there is still a significant amount of information to be gained with respect to the conformation and behaviour of larger clusters and how ligands attach to their surface. Also, how these ligands are presented and their behaviour in solution is to be further enlightened. However, for our purposes, we have used a simple, purely mathematical method, of describing how ligands are displayed on a cluster as developed by Mirkin *et al.*⁵² and Keating *et al.*^{52, 53} As mentioned, this exercise was purely mathematical, and therefore is based on several assumptions:

- 1) The gold cluster is uniform and spherical in shape, corresponding to the *average* nanoparticle.
- 2) The number of active ligands corresponds to the average GNP
- 3) The ligands are rigid, adopt a linear form, are inert to themselves, and are distributed equally around the surface.

We have calculated that by increasing the presentation density of the active ligand on the GNP, the inter-ligand distance decreases.

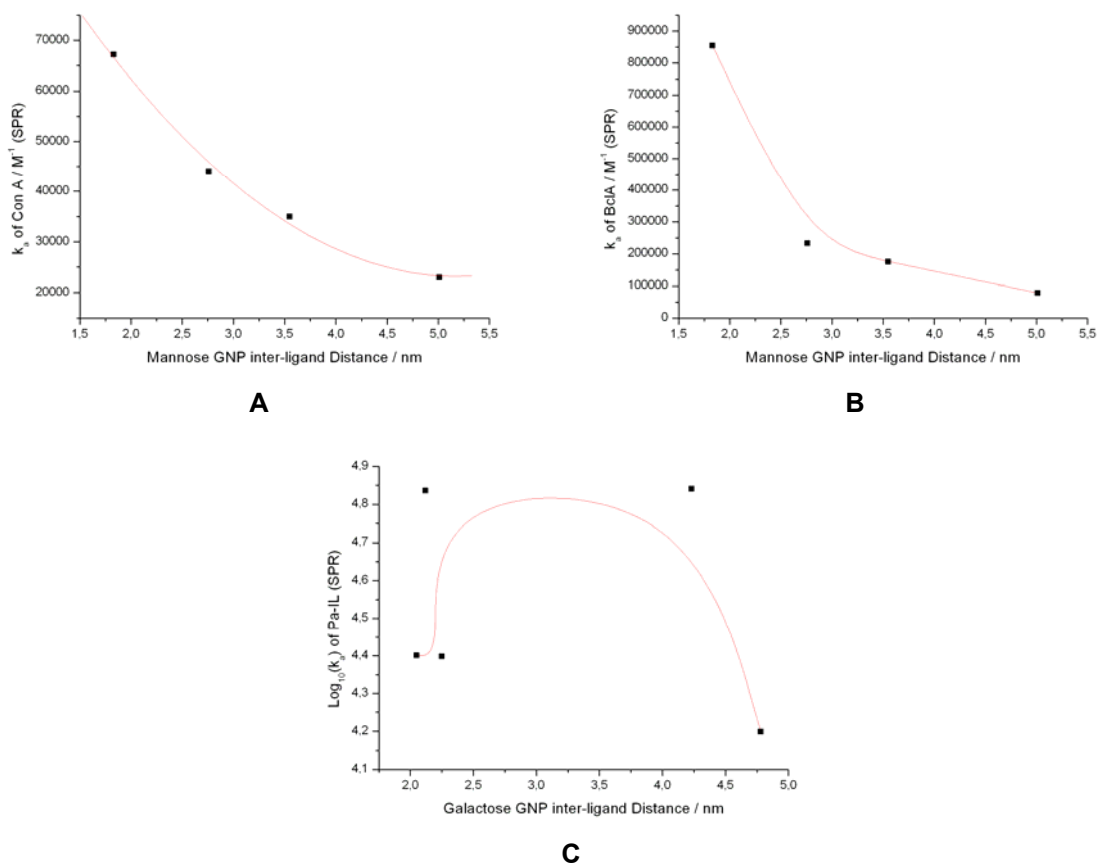
GNP	GNP Diameter / nm	Spere Surface Area / nm ²	No. Of Active Ligands	Deflection Angle / Rads	Interligand Distance / nm
GNP-2	1,49	238,07	11	1,23	5,01
GNP-3	1,66	247,46	24	0,82	3,55
GNP-4	1,61	244,68	39	0,64	2,76
GNP-5	1,44	235,34	88	0,43	1,83
GNP-6	1,43	234,80	12	1,17	4,78
GNP-7	1,27	226,19	15	1,04	4,23
GNP-8	1,39	232,63	65	0,50	2,12
GNP-9	1,36	231,01	57	0,53	2,25
GNP-10	1,24	224,59	67	0,49	2,05

Table 6 : Inter-ligand distance calculations for the GNPs tested.

SPR Results: For Con A and BclA it is clear that the augmentation of lectin affinity is linear with respect to presentation density. However, by analysing the results with respect to decreasing inter-ligand distance on the GNP surface, the lectin affinity increases linearly until an inter-ligand distance less than 2 nm is reached, where a higher order increase is observed. This can be rationalised by the fact that at higher inter-ligand distances, only one GNP-lectin interaction is allowed (intermolecular GNP-lectin interaction) as the second ligand on the GNP is unable to bind to the second lectin binding site (second intramolecular GNP-lectin interaction). Below an inter-ligand distance of 2 nm, the first interaction occurs as before, but now the “nearest neighbour” ligand on the GNP surface is able to bind with the second binding site in an intramolecular fashion. As BclA exhibits cooperativity, this second interaction would increase the binding strength and the overall affinity observed in the experiment. Con A does not exhibit inter-binding site cooperativity and may be for this reason that this effect is less exaggerated.

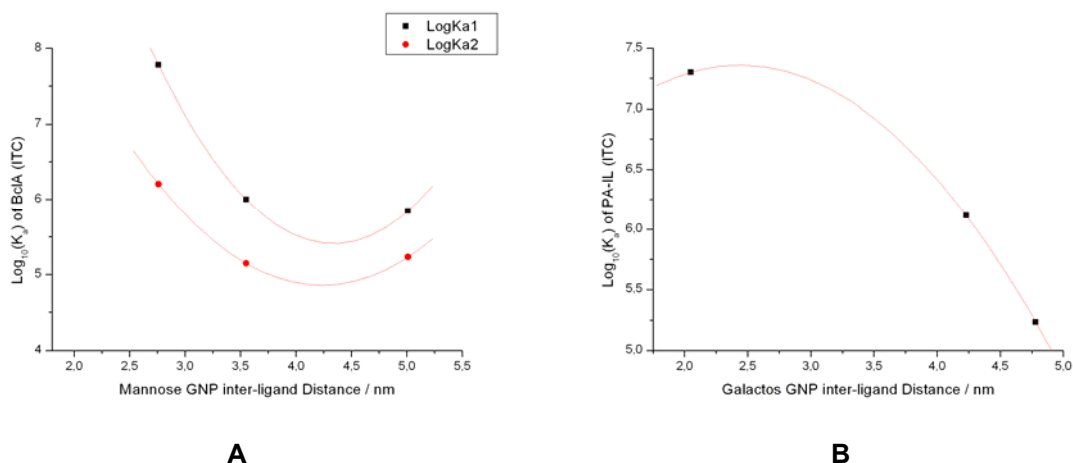
For PA-IL however, augmentation of affinity with respect to decreasing inter-ligand distance is not linear. This was explained earlier by the fact that Con A and BclA were immobilised as dimers on the SPR surface thus their inter-binding site distances are well defined whereas for PA-IL, the inter-binding site distances are much more varied. Also, PA-IL allows 4 interactions in total, which may also be synergic with one another, which would certainly increase the effective concentration of lectin binding sites. Therefore, as the inter-ligand distance decreases, a large increase in affinity is observed as the probability of intra-molecular GNP-lectin interactions increases, augmenting the observed affinity. As the inter-ligand distance decreases further, the ligands are packed too closely together and would impede each

other sterically from interacting with the first lectin binding site resulting in a decrease in observed affinity (Graph 5, C).



Graph 5 : Dependence of affinity on GNP interligand distance as found by SPR for Con A (A), BclA (B) and PA-IL (C).

ITC Results: Both BclA and PA-IL show non-linear augmentation of affinity with respect to inter-ligand distance (Graph 6). The affinity of BclA appears to increase dramatically with decreasing inter-ligand distance presumably until a maximum is reached where an enthalpy penalty from the architectural changes of the lectin structure counteracts the entropy released upon liberation of ordered water. This could be an effect relating to the cooperative nature of this lectin. PA-IL however indicates that decreasing inter-ligand distance will not greatly increase the affinity of the lectin lower than 1.15 nm, this may be due to a maximum presentation density (effective concentration) found at this value. However, more data will be required to confirm these hypotheses.



Graph 5 : Dependence of K_a on GNP interligand distance as found by ITC for BclA (A) and PA-IL (B).

In general, as the inter-ligand distance approaches the inter-carbohydrate binding site distance of the lectins, the affinity increases until a maximum is reached when:

$$\text{Inter-ligand Distance} \approx (\text{inter-binding site Distance}) / 2$$

As the inter-ligand distance decreases beyond this value, there is no significant increase in lectin affinity. This may give insights into the GNP structure and ligand formation at the GNP surface as well as the nature of the lectin interaction with multivalent ligands. As mentioned previously, it is highly unlikely that the GNPs organise the ligands on their surface in a perfectly ordered arrangement. Therefore there will be pockets, or clusters, of active ligands and likewise clusters of inactive ligands. As there is a difference between inter-binding site distance and inter-ligand distance of a factor of 2, one could say that the ligands graft themselves immediately to the surface as the dimer is reduced, which would be due to the self-oxidising nature of the thiol ligands **1**, **2** and **3**.

Conclusion

We have shown that gold nanoparticles can be used as multivalent platforms for presenting carbohydrate molecules. The augmentation in lectin affinity for nanoparticle based carbohydrate ligands has been observed both qualitatively by Haemagglutination inhibition assays, as well as quantitatively using surface plasmon resonance, and the first use of isothermal microcalorimetry for nanoparticle systems, for the Con A, BclA and PA-IL lectins. Essentially, upon increasing the presentation density of the active ligand, an optimal affinity

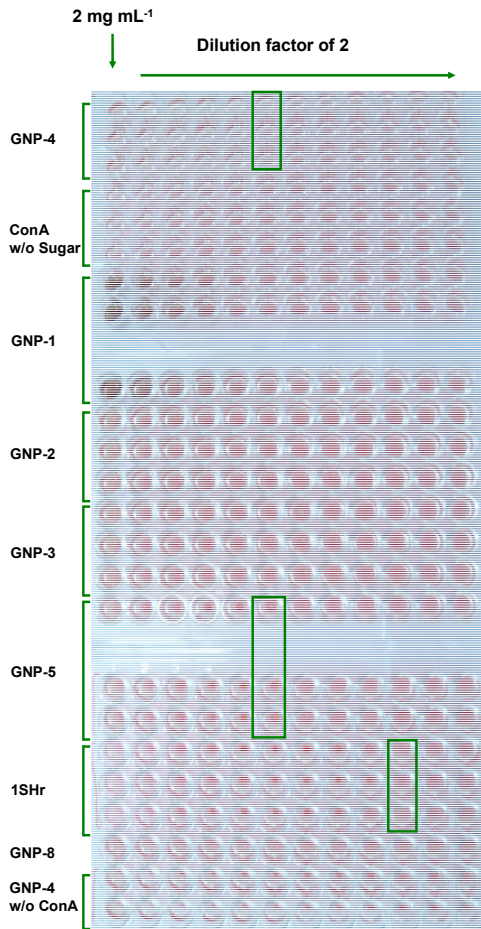
can be obtained, beyond which no significant increase was observed. We have also shown that when dealing with a multivalent target, one must consider several aspects when designing a multivalent ligand. The multivalent scaffold used should be carefully chosen and tailored so that all the desired qualities and functionalities may be incorporated, with reference to the multivalent target as well as any further applications or tools. Notably, the accessibility of the multiple binding sites, the inter-binding site distance and the arrangement of molecules presented at the nanoparticle surface should be well thought-out with respect to thermodynamic considerations and its implications in the multivalent effect. Also, one must consider binding – re-binding in order to augment even further the affinity of the multivalent target and application of effective concentrations. Finally, one must consider the effects of ordered solvent molecules on the enthalpy and entropy contributions to the interaction, which may differ on a multivalent level.

References

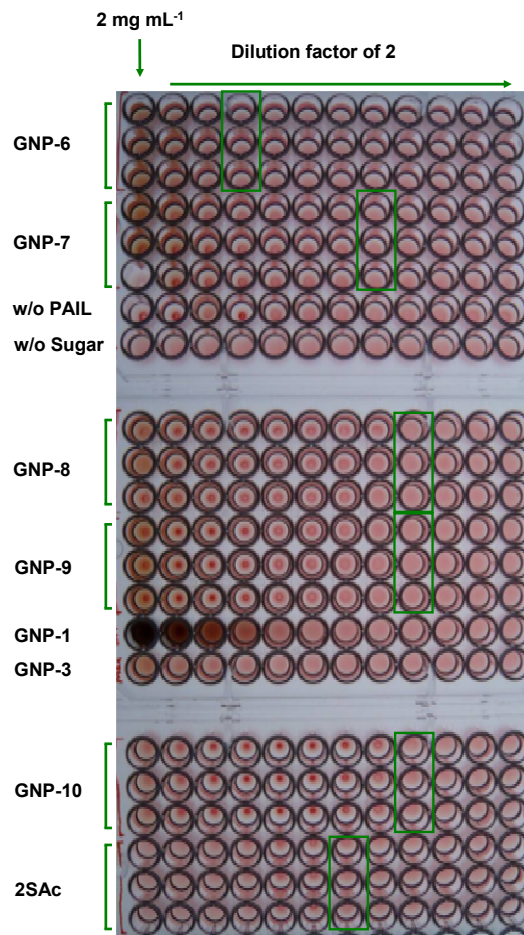
1. Lis, H.; Sharon, N., *Chem. Rev.*, **1998**, 98, (2), 637-674.
2. Mammen, M.; Choi, S. K.; Whitesides, G. M., *Angew.Chem. Int. Ed.*, **1998**, 37, (20), 2755-2794.
3. Kiessling, L. L.; Gestwicki, J. E.; Strong, L. E., *Curr. Opin. Chem. Biol.*, **2000**, 4, (6), 696-703.
4. Lundquist, J. J.; Toone, E. J., *Chem. Rev.*, **2002**, 102, (2), 555-78.
5. Kramer, R. H.; Karpen, J. W., *Nature*, **1998**, 395, (6703), 710-3.
6. Gargano, J. M.; Ngo, T.; Kim, J. Y.; Acheson, D. W.; Lees, W. J., *JACS*, **2001**, 123, (51), 12909-10.
7. Mulder, A.; Auletta, T.; Sartori, A.; Del Ciotto, S.; Casnati, A.; Ungaro, R.; Huskens, J.; Reinhoudt, D. N., *JACS*, **2004**, 126, (21), 6627-36.
8. Mulder, A.; Huskens, J.; Reinhoudt, D. N., *Org. Biomol. Chem.*, **2004**, 2, (23), 3409-24.
9. Baldini, L.; Casnati, A.; Sansone, F.; Ungaro, R., *Chem. Soc. Rev.*, **2007**, 36, (2), 254-66.
10. Benaissa-Trouw, B.; Lefeber, D. J.; Kamerling, J. P.; Vliegthart, J. F.; Kraaijeveld, K.; Snippe, H., *Infect. Immun.*, **2001**, 69, (7), 4698-701.
11. Cloninger, M. J., *Curr. Opin. Chem. Biol.*, **2002**, 6, (6), 742-8.
12. Roy, R.; Baek, M. G., *J. Biotechnol.*, **2002**, 90, (3-4), 291-309.
13. Turnbull, W. B.; Stoddart, J. F., *J. Biotechnol.*, **2002**, 90, (3-4), 231-55.
14. Heidecke, C. D.; Lindhorst, T. K., *Chemistry*, **2007**, 13, (32), 9056-67.
15. You, L. C.; Lu, F. Z.; Li, Z. C.; Zhang, W.; Li, F. M., *Macromolecules*, **2003**, 36, (1), 1-4.
16. Narain, R.; Armes, S. P., *Biomacromolecules*, **2003**, 4, (6), 1746-1758.
17. Bes, L.; Angot, S.; Limer, A.; Haddleton, D. M., *Macromolecules*, **2003**, 36, (7), 2493-2499.
18. Cade, D.; Ramus, E.; Rinaudo, M.; Auzely-Velty, R.; Delair, T.; Hamaide, T., *Biomacromolecules*, **2004**, 5, (3), 922-7.
19. Gestwicki, J. E.; Strong, L. E.; Borchardt, S. L.; Cairo, C. W.; Schnoes, A. M.; Kiessling, L. L., *Bioorg Med Chem*, **2001**, 9, (9), 2387-93.
20. Halkes, K. M.; de Souza, A. C.; Maljaars, C. E. P.; Gerwig, G. J.; Kamerling, J. P., *Eur. J. Org. Chem.*, **2005**, (17), 3650-3659.
21. Barrientos, A. G.; Fuente, J. M.; Jimenez, M.; Solis, D.; Canada, F. J.; Martin-Lomas, M.; Penades, S., *Carbohydr. Res.*, **2009**.
22. Chien, Y. Y.; Jan, M. D.; Adak, A. K.; Tzeng, H. C.; Lin, Y. P.; Chen, Y. J.; Wang, K. T.; Chen, C. T.; Chen, C. C.; Lin, C. C., *ChemBioChem*, **2008**, 9, (7), 1100-9.
23. de la Fuente, J. M.; Penades, S., *BBA*, **2006**, 1760, (4), 636-51.
24. Podsiadlo, P.; Sinani, V. A.; Bahng, J. H.; Kam, N. W.; Lee, J.; Kotov, N. A., *Langmuir*, **2008**, 24, (2), 568-74.
25. Nie, Z.; Liu, K. J.; Zhong, C. J.; Wang, L. F.; Yang, Y.; Tian, Q.; Liu, Y., *Free Radic. Biol. Med.*, **2007**, 43, (9), 1243-54.

26. Hosta, L.; Pla-Roca, M.; Arbiol, J.; Lopez-Iglesias, C.; Samitier, J.; Cruz, L. J.; Kogan, M. J.; Albericio, F., *Bioconjug. Chem.*, **2009**, 20, (1), 138-46.
27. Daniel, M. C.; Astruc, D., *Chem. Rev.*, **2004**, 104, (1), 293-346.
28. Crespo, P.; Litran, R.; Rojas, T. C.; Multigner, M.; de la Fuente, J. M.; Sanchez-Lopez, J. C.; Garcia, M. A.; Hernando, A.; Penades, S.; Fernandez, A., *Phys. Rev. Lett.*, **2004**, 93, (8), 087204.
29. Rich, R. L.; Myszk, D. G., *J. Mol. Recognit.*, **2003**, 16, (6), 351-82.
30. Dam, T. K.; Brewer, C. F., *Chem. Rev.*, **2002**, 102, (2), 387-429.
31. Rieger, J.; Stoffelbach, F.; Cui, D.; Imberty, A.; Lameignere, E.; Putaux, J. L.; Jerome, R.; Jerome, C.; Auzely-Velty, R., *Biomacromolecules*, **2007**, 8, (9), 2717-25.
32. De, M.; Miranda, O. R.; Rana, S.; Rotello, V. M., *Chem. Commun.*, **2009**, (16), 2157-9.
33. Dam, T. K.; Roy, R.; Das, S. K.; Oscarson, S.; Brewer, C. F., *J. Biol. Chem.*, **2000**, 275, (19), 14223-30.
34. Schlick, K. H.; Udelhoven, R. A.; Strohmeyer, G. C.; Cloninger, M. J., *Mol. Pharm.*, **2005**, 2, (4), 295-301.
35. Lameignere, E.; Malinowska, L.; Slavikova, M.; Duchaud, E.; Mitchell, E. P.; Varrot, A.; Sedo, O.; Imberty, A.; Wimmerova, M., *Biochem. J.*, **2008**, 411, (2), 307-18.
36. Glick, J.; Garber, N., *J. Gen. Microbiol.*, **1983**, 129, (10), 3085-90.
37. Barrientos, A. G.; de la Fuente, J. M.; Rojas, T. C.; Fernandez, A.; Penades, S., *Chem. Eur. J.*, **2003**, 9, (9), 1909-1921.
38. Martinez-Avila, O.; Hijazi, K.; Marradi, M.; Clavel, C.; Champion, C.; Kelly, C.; Penades, S., *Chemistry*, **2009**.
39. Ojeda, R.; de Paz, J. L.; Barrientos, A. G.; Martin-Lomas, M.; Penades, S., *Carbohydr. Res.*, **2007**, 342, (3-4), 448-59.
40. Hostetler, M. J.; Wingate, J. E.; Zhong, C.-J.; Harris, J. E.; Vachet, R. W.; Clark, M. R.; Londono, J. D.; Green, S. J.; Stokes, J. J.; Wignall, G. D.; Glish, G. L.; Porter, M. D.; Evans, N. D.; Murray, R. W., *Langmuir*, **1998**, 14, 17-30.
41. Cioci, G.; Mitchell, E. P.; Gautier, C.; Wimmerova, M.; Sudakevitz, D.; Perez, S.; Gilboa-Garber, N.; Imberty, A., *FEBS Lett.*, **2003**, 555, (2), 297-301.
42. Saha, S. K.; Brewer, C. F., *Carbohydr. Res.*, **1994**, 254, 157-67.
43. Origin (OriginLab, N., MA).
44. Blanchard, B.; Nurisso, A.; Hollville, E.; Tetaud, C.; Wiels, J.; Pokorna, M.; Wimmerova, M.; Varrot, A.; Imberty, A., *J. Mol. Biol.*, **2008**, 383, (4), 837-53.
45. Rieger, J.; Freichels, H.; Imberty, A.; Putaux, J. L.; Delair, T.; Jerome, C.; Auzely-Velty, R., *Biomacromolecules*, **2009**.
46. de la Fuente, J. M.; Eaton, P.; Barrientos, A. G.; Menendez, M.; Penades, S., *JACS*, **2005**, 127, (17), 6192-7.
47. Mitchell, E. P.; Sabin, C.; Snajdrova, L.; Pokorna, M.; Perret, S.; Gautier, C.; Hofr, C.; Gilboa-Garber, N.; Koca, J.; Wimmerova, M.; Imberty, A., *Proteins*, **2005**, 58, (3), 735-46.
48. Marradi, M.; Alcantara, D.; de la Fuente, J. M.; Garcia-Martin, M. L.; Cerdan, S.; Penades, S., *Chem. Commun.*, **2009**, (26), 3922-4.
49. Christensen, T.; Toone, E. J., *Methods Enzymol.*, **2003**, 362, 486-504.
50. Jadzinsky, P. D.; Calero, G.; Ackerson, C. J.; Bushnell, D. A.; Kornberg, R. D., *Science*, **2007**, 318, (5849), 430-3.
51. Huang, W.; Bulusu, S.; Pal, R.; Zeng, X. C.; Wang, L. S., *ACS Nano*, **2009**.
52. Hill, H. D.; Millstone, J. E.; Banholzer, M. J.; Mirkin, C. A., *ACS Nano*, **2009**, 3, (2), 418-24.
53. Cederquist, K. B.; Keating, C. D., *ACS Nano*, **2009**, 3, (2), 256-60.

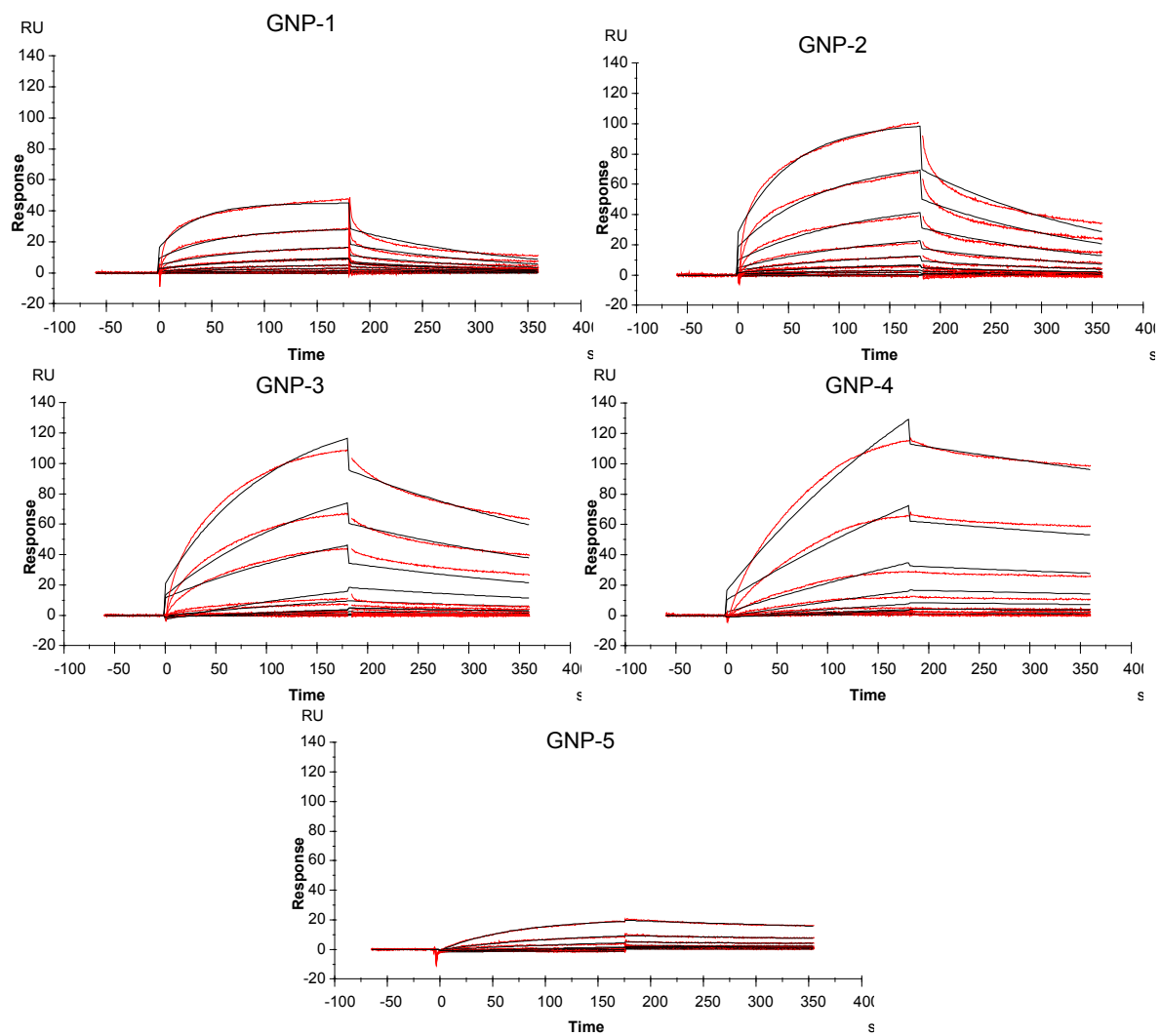
Supporting Information



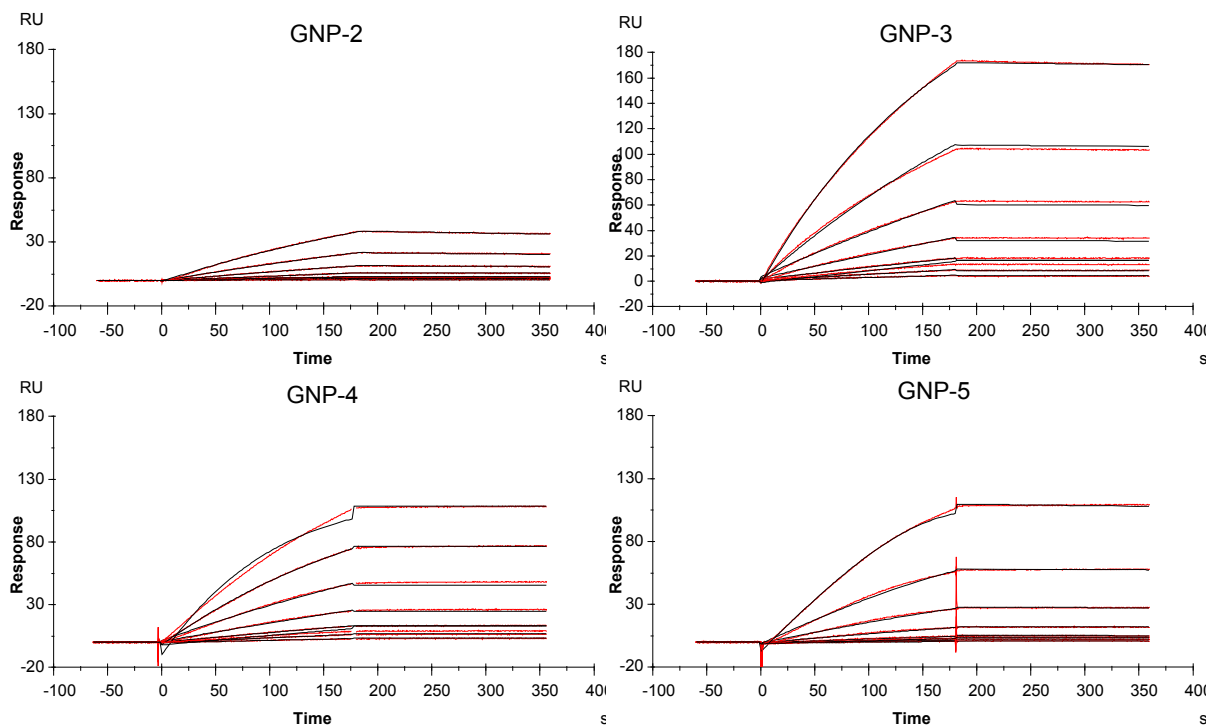
Supporting Figure 1 : Photograph of haemagglutination inhibition assay for Con A. Limits of inhibition highlighted by green boxes.



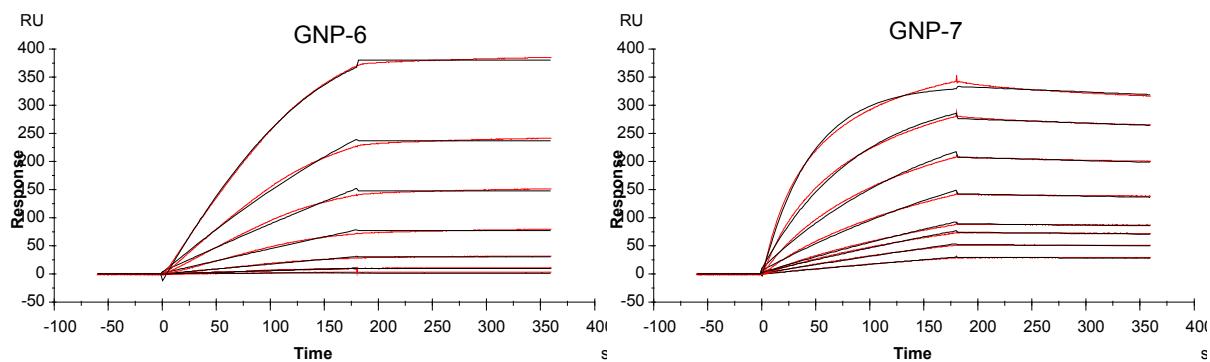
Supporting Figure 2 : Photograph of haemagglutination inhibition assay for PA-IL. Limits of inhibition highlighted by green boxes.

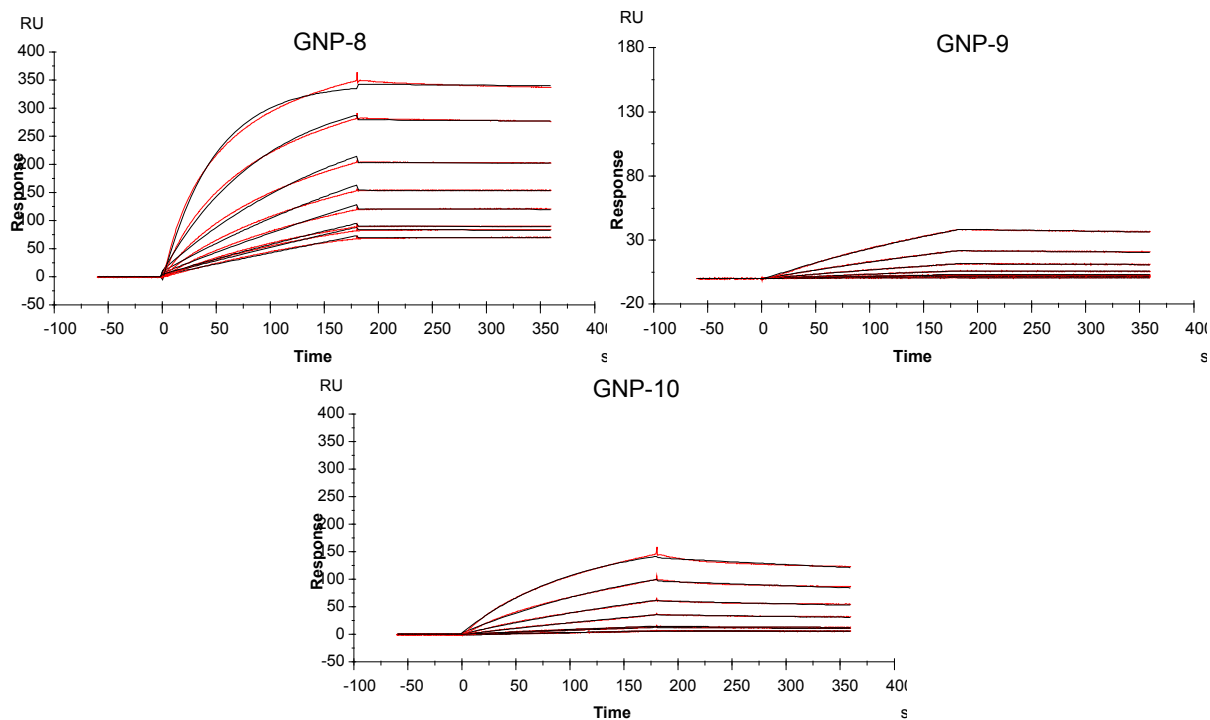


Supporting Figure 3 : SPR plots for raw data (red curves) and 1:1 interaction model (black curves) for the interactions of GNP-1 to GNP-5 passed over Con A functionalised chip surfaces. GNP serial dilutions of $2 \mu\text{g mL}^{-1}$ to 31.25 ng mL^{-1} were made.

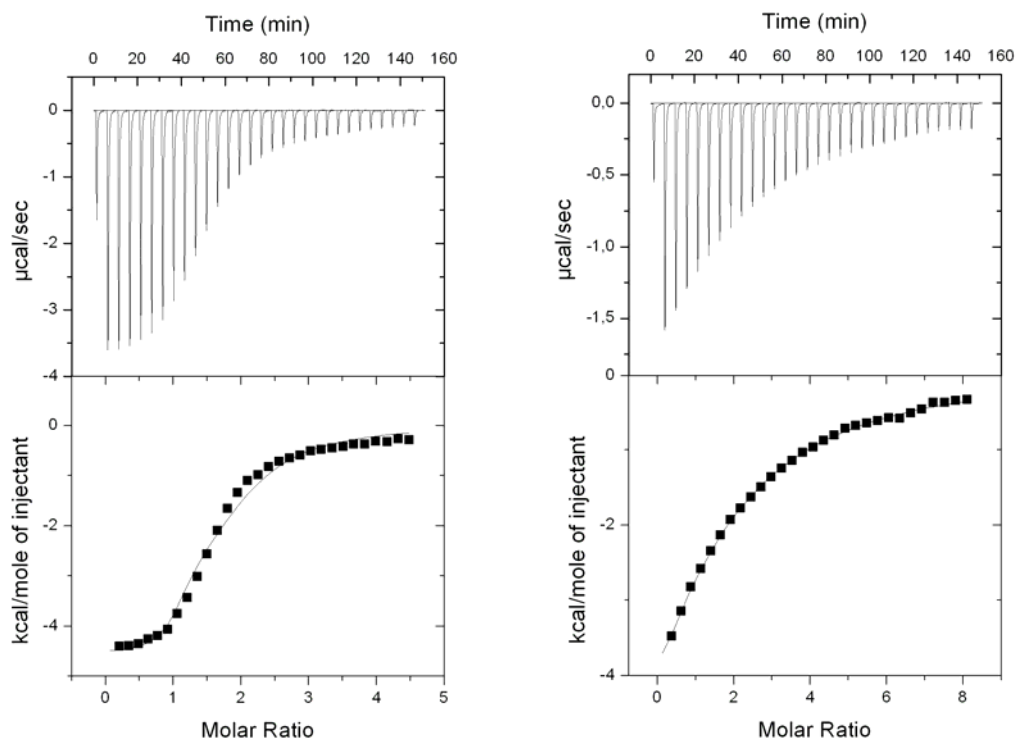


Supporting Figure 4 : SPR plots for raw data (red curves) and 1:1 interaction model (black curves) for the interactions of GNP-2 to GNP-5 passed over BclA functionalised chip surfaces. GNP serial dilutions of $2 \mu\text{g mL}^{-1}$ to 31.25 ng mL^{-1} were made.





Supporting Figure 5 : SPR plots for raw data (red curves) and 1:1 interaction model (black curves) for the interactions of GNP-6 to GNP-10 passed over PA-IL functionalised chip surfaces. GNP serial dilutions of $20 \mu\text{g mL}^{-1}$ to 312.5 ng mL^{-1} were made.



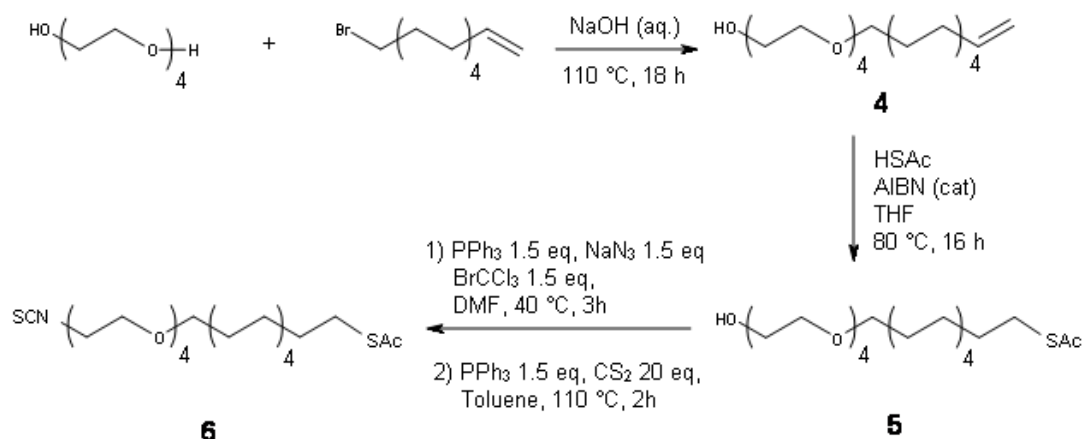
A

B

Supporting Figure 6 : Injections of 1SH into a solution of BclA (A) and injections of 3SAc into a solution of PA-IL (B).

5.2 Chemical Synthesis

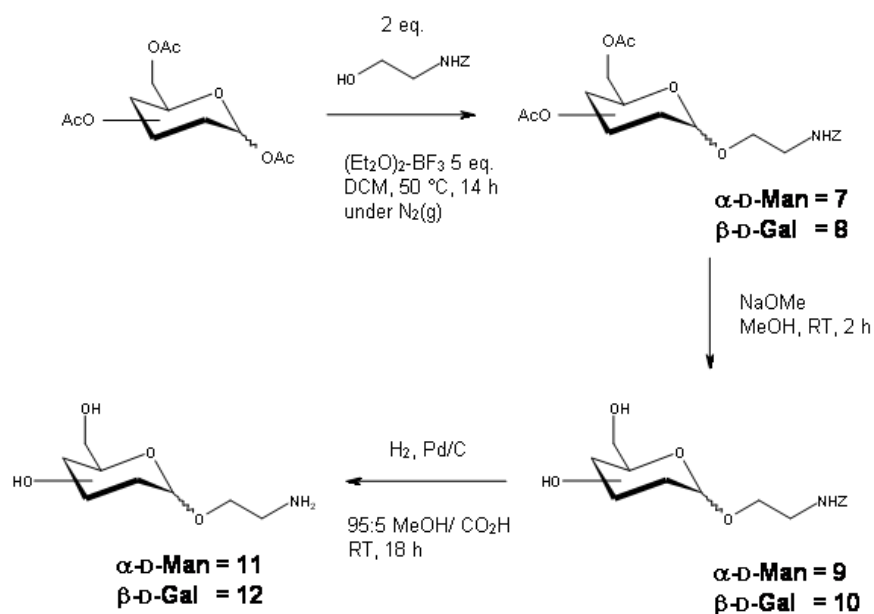
To functionalise gold GNPs, the use of thiolated ligands is a pre-requisite. As carbohydrate molecules do not come conveniently functionalised with thiol groups, one must incorporate a “linker” molecule at a suitable position in order to provide this functionality. If one chooses to use a linker molecule, one should consider the properties required from the linker which in turn would be adopted by the functionalised GNP. The use of different linkers for different pendant functionalities is also an option. For our needs, we required a linker which grafted easily and rapidly onto the GNP surface, which was also flexible and soluble in aqueous solutions. The potential of creating a library of thiolated ligands was also attractive; hence the ability to easily couple the linker to a library of pre-modified neoglycoconjugates was desirable. Thus for our uses, and following the work of Penades *et al.*^{197, 198} the following linker was synthesised. This linker includes a protected undecanthiol allowing favourable chemisorption to the GNP surface,^{182, 245} stabilising the GNP surface and providing rigidity. This is then conjugated to a tetra ethylene glycol unit in order to give both flexibility and solubility whilst also minimising non-specific interactions.^{188, 246} PEG groups could also be important to provide camouflage in order to prevent phagocytosis in any further biological applications.²⁴⁷(and references therein) Finally, an *iso*-thiocyanate was incorporated. This allowed fast, easy and high yielding coupling to amine-functionalised neoglycoconjugates, giving the thiourea bridged product. The thiourea bridge was preferred as it is thought to be more soluble and more flexible than the azide-alkyne Huisgen cycloaddition, or “click” coupling. The thiourea is also preferred over the peptidic coupling (or amide linkage) as this reaction requires an excess of the amine functionalised neoglycoconjugate and is a very slow reaction which also produces unwanted side products. The thiourea coupling however can be conducted in a wide range of solvents depending on the solubility of the two components. The reaction requires only mild conditions and takes very little time (~20 mins to 2 hours). There are no side products, only an excess of the *iso*-thiocyanate is required which can often be efficiently recovered (recovery of > 90 %) and the thiolated product is revealed after an efficient deprotection step. The coupling is also stable to the reactions which follow, including the reduction of the gold salt. This linker, with the thiourea - tetra ethylene glycol – undecanthiol functionalities, is designated the “mixed linker”. It has a calculated total length, from sulphur to terminal oxygen (which would become the centre of the glycosidic bond when functionalised with a saccharide), of 36.07 Å, or 3.61 nm, as calculated by SYBYL.²⁴⁸



Scheme 1: Synthesis of the *iso*-thiocyanate “mixed” linker, 47 % yield for 3 steps.

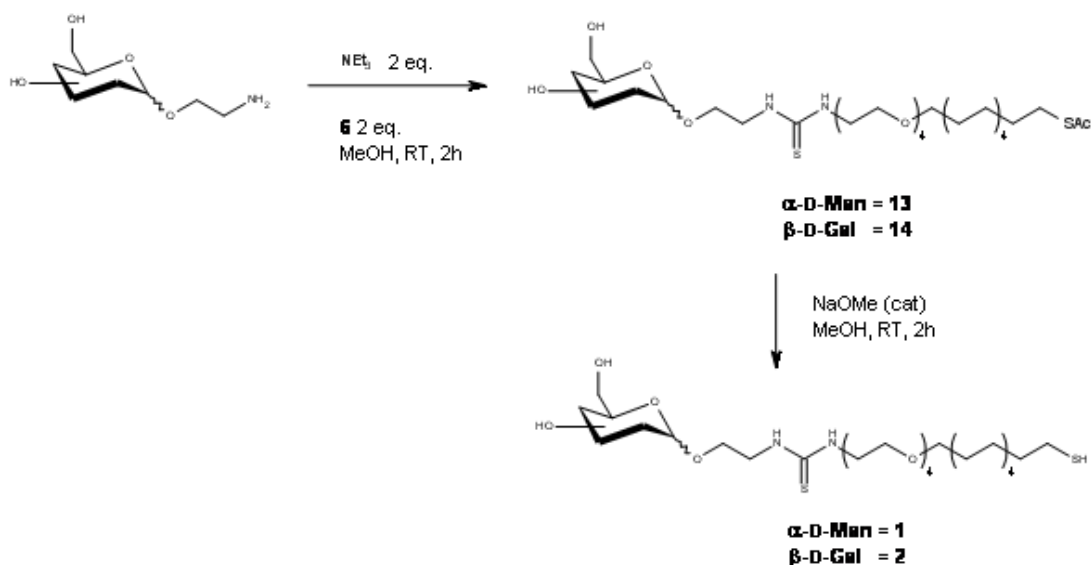
As mentioned previously, an amine functionalised neoglycoconjugate is used. As we were dealing with monosaccharide neoglycoconjugates only, only few synthetic steps were required, starting from conveniently protected monosaccharides. *Per*-acetylated mannose and galactose were glycosylated with a benzyloxycarbonyl protected ethanolamine. Following this, removal of the acetyl and benzyloxycarbonyl groups revealed the amine functionalised mannoside (**1**) and galactoside (**2**) with yields of 60 % and 27 % respectively over 3 steps (Scheme 2).

However, for larger and more complex neoglycoconjugates, the total synthesis of these *neo*-oligosaccharides with the amide functionality would be required.



Scheme 2: Synthesis of amine functionalised neoglycoconjugates. 60 % and 27 % yield over 3 steps for 2-aminoethyl $\alpha\text{-D-Mannoside}$ (10) and 2-aminoethyl $\beta\text{-D-Galactoside}$ (11) respectively.

Conjugation of **11** and **12** to the *iso*-thiocyanate spacer molecule (**6**) was facilitated under basic conditions using NEt_3 in methanolic solution. After purification and recovery of excess spacer molecule, the thiol functionality was revealed following deprotection of the thioacetate. This gives mannoside (**1**) and galactoside (**2**) with 84 % and 43 % respectively over 2 steps (scheme 3).



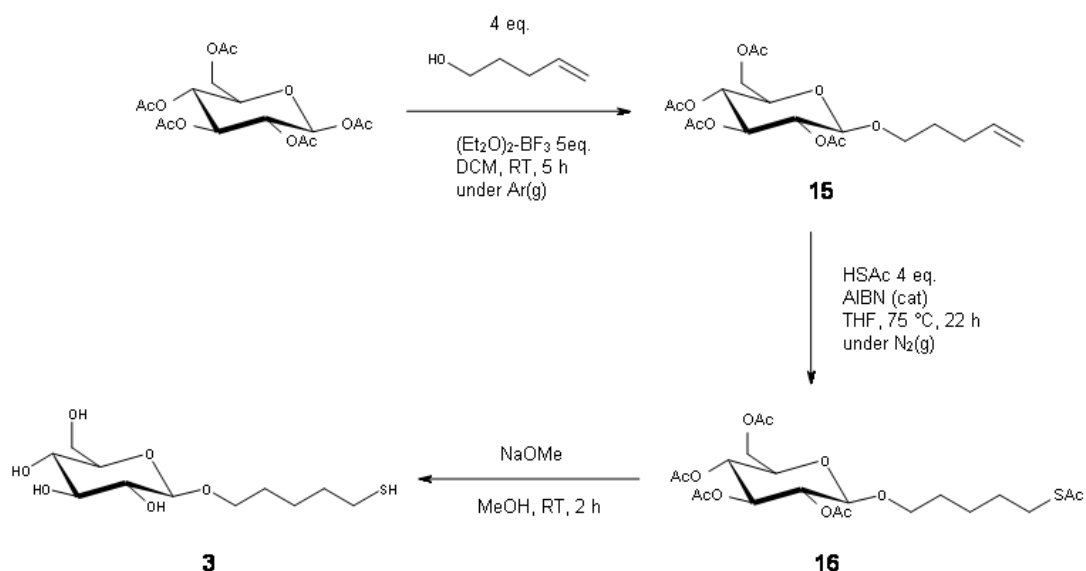
Scheme 3: Coupling of amine functionalised monosaccharides to *iso*-thiocyanate linker followed by thiol deprotection. Yields of 84 % and 43 % for 1 and 2 respectively over 2 steps.

In order to control the active ligand density on the GNP surface, using a combination of the active ligand with another inactive ligand is necessary. During GNP synthesis, a methanolic solution of the ligands is made, to which is added the gold salt in aqueous solution. By altering the stoichiometric ratios of active : inactive linkers in this methanolic solution, the density of active ligand on the GNP surface upon reduction of the gold salt can be controlled.

For the inactive, or inert component, a linker which would graft equally well to the GNP surface was required, but also, that the inert pendent group does not impede or influence the interactions of the active ligand, either sterically or by nonspecific interactions. However, the inactive linker may contribute to the physico-chemical properties of the GNP which do not relate to the biochemical interactions to be studied. For example, the inactive ligand used may contribute to GNP core size, solubility, or may indeed incorporate another functional group required for any further applications (fluorophores, charged groups etc). Several of these inert components can be used to give several functionalities and tunability to the system.

With the intention of investigating mannose and galactose specific lectins, using a saccharide molecule which exhibited no specific interactions was desirable. In fact, a non-active saccharide functionalised GNP was indeed necessary to be used as a “control” GNP for observing any significant contributions from the linker or the gold core. To this end, a glucose

ligand was synthesised as shown in scheme 4, with a yield of 23 % over 3 steps. A short thiol-functionalised alkyl chain was introduced, again, to allow favourable chemisorption to the GNP surface, yet the ligand would be short enough to remain hidden internally allowing correct presentation of the active ligands.



Scheme 4: Synthesis of the “inactive” glucose neoglycoconjugate, 3. 23 % yield over 3 steps.

5.3 Further Synthesis

As mentioned earlier in this chapter, the undecyl chain of the active ligand linker molecule is rigid in aqueous solution due to its hydrophobic character. Yet, the linker molecule for the inactive glucose ligand comprises only of a pentane alkyl chain. Therefore, if these two molecules were placed in close proximity to each other, as they would when attached to the GNP surface it is possible that the two molecules would repel one another due to the hydrophilic glucose pendant group interfering with the aliphatic chain of the neighbouring linker. This in turn could lead to the clustering of ligands at the GNP surface, with pockets of active ligands in high density, and likewise, pockets of inert ligands, resulting in an uneven distribution of ligands at the GNP surface as shown in figure 40.

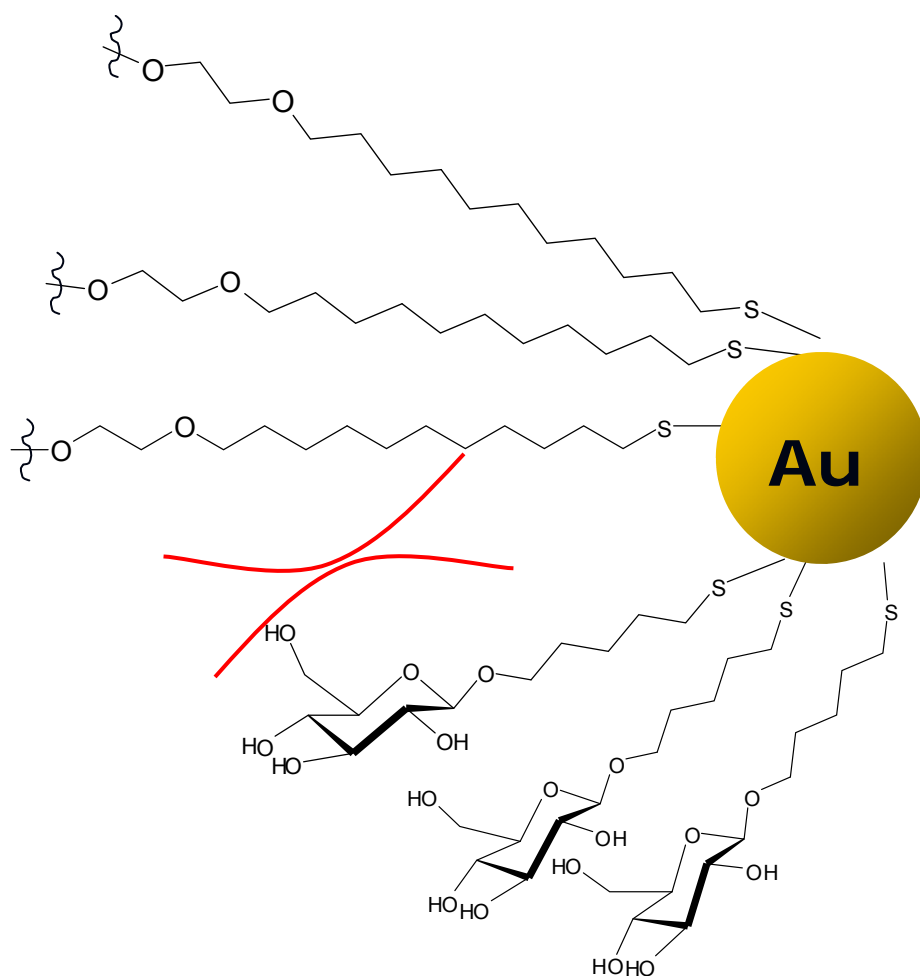


Figure 40 : Potential hydrophobic-hydrophilic interference leading to uneven ligand distribution at the GNP surface.

In order to investigate the influence of linker hydrophobic-hydrophilic interference on ligand presentation at the GNP surface, a second linker molecule was synthesised for the active ligands. Again, fusing a thiol-functionalised alkyl chain with a tetra ethylene glycol unit to incorporate good chemisorption to the GNP surface, and flexibility in aqueous solution. In this case, a 5-carbon pentyl unit was used as opposed to the undecyl chain used previously. This would allow the pendant glucose functionality to be in contact with the tetra ethylene glycol unit of the active linker molecule when immobilised on the GNP surface as shown in figure 41.

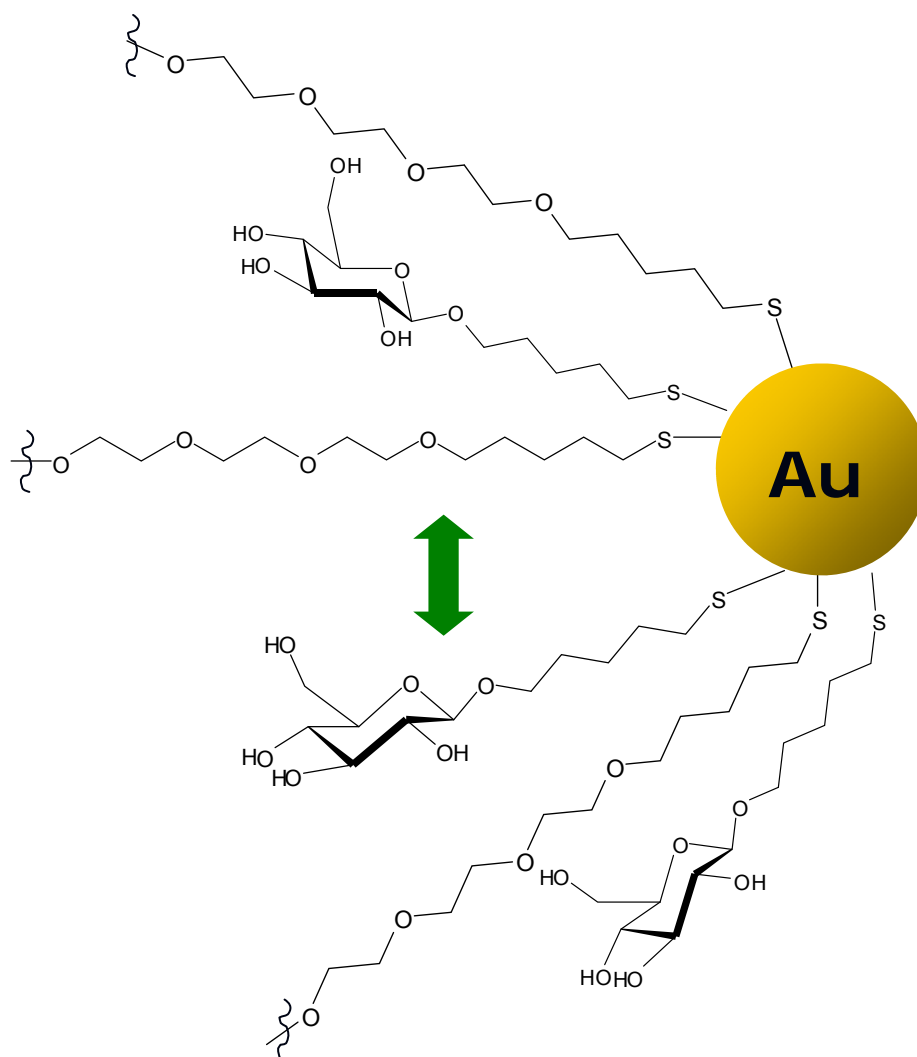
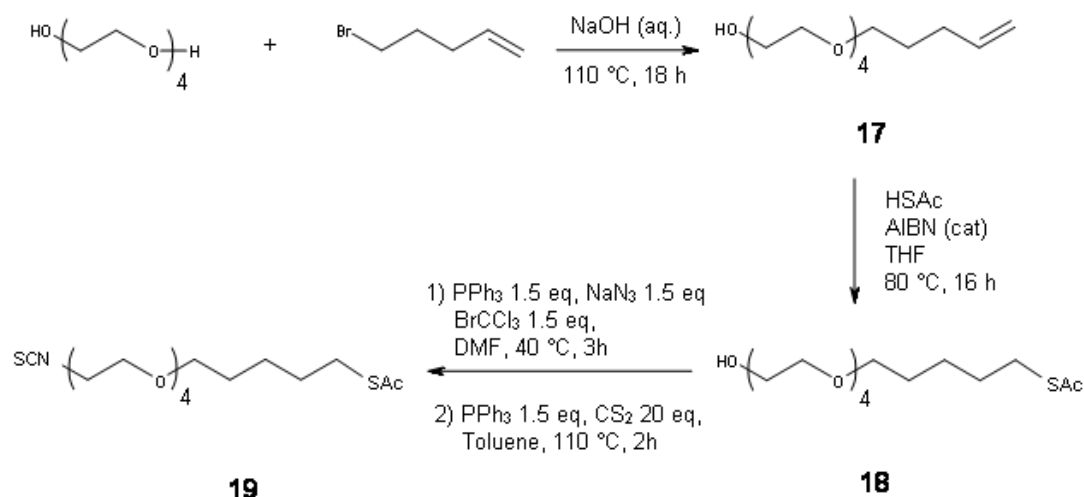


Figure 41 : Hydrophilic-hydrophilic harmonisation of ligands – allowing even distribution of ligands at the GNP surface?

The synthesis of this second linker, designated the “mixed-short” or “mixed(s)” linker, is analogous to the method used for the synthesis of the mixed linker (scheme 5). The calculated total length of this linker molecule, from sulphur to terminal oxygen, is 26.20 Å, or 2.62 nm, as calculated by SYBYL.²⁴⁸



Scheme 5 : Synthesis of the *iso*-thiocyanate “mixed(s)” linker, 19. 33 % yield for 3 steps.

Conjugation of this *iso*-thiocyanate to the amine-functionalised manno- and galactosides **11** and **12** gave the mannose-mixed(s)-SAc (**20**) and the galactose-mixed(s)-SAc (**21**) which were then deprotected to the mannose-mixed(s)-SH (**22**) and the galactose-mixed(s)-SH (**23**) ligands with yield of 32 % and 43 % respectively over 2 steps.

GNPs functionalised with Man-mixed(s) and Gal-mixed(s) ligands include **GNP-11** and **GNP-12** respectively. **GNP-11** has a 54 % presentation density, whereas **GNP-12** exhibits a 22 % presentation density. By using the shorter linker molecule, **GNP-11** exhibits smaller average core diameters (almost 0.2 nm reduction in size) which results in a lower active valency, but similar presentation densities. However, for **GNP-12**, the core diameter was found to be almost 0.2 nm bigger in size, yet exhibited better control over presentation density. **GNP-13** consisted of GNPs functionalised with 50% Man-mixed ligands as for **GNP-4**, however 5 equivalents of total ligands were used, as opposed to 3 equivalents used previously. It was thought that using a higher ligand : Au salt ratio would form smaller GNPs. However, these GNPs were observed to be significantly less soluble in aqueous and buffer solutions. Indeed, a ligand : Au salt ratio of 5 for galactose GNPs resulted in GNPs which were insoluble to the point that isolation and purification was not possible. Control GNPs, where the mixed ligands exhibited an alcohol functionality (both with and without the thiourea bridge), in place of the saccharide were also highly insoluble preventing isolation and purification. In spite of this, **GNP-13** was found to have an Au core diameter almost 0.2 nm smaller than that of **GNP-4**, however, more experimental evidence would be required to

formulate any solid relationship between ligand : Au ratio and core diameter. A summary of GNP-11 to GNP-13 can be seen in the table below.

Sample	GNP-11	GNP-12	GNP-13
No. Particles	443	536	511
Min Diameter / nm	0.65	0.65	0.74
Max Diameter / nm	2.59	3.10	2.45
Mean Diameter / nm	1.44	1.47	1.43
Standard Deviation / nm	0.35	0.39	0.26

Table 4 : Summary GNP-11 to GNP-13 from TEM results.

GNP	Active Neoglycoconjugate	Average Core Diameter (nm)	Average number of Au atoms	Average molecular formula	Number of active ligands	Desired Presentation density (%)	Actual Presentation Density	Average M_w
GNP-11	19	1.44	116	$(C_{22}H_{44}N_2O_{10}S_2)_{30}(C_{11}H_{21}O_6S)_{27}Au_{116}$	30	50	54	47 215
GNP-12	20	1.47	124	$(C_{22}H_{44}N_2O_{10}S_2)_{16}(C_{11}H_{21}O_6S)_{53}Au_{124}$	16	25	22	48 832
GNP-13	1	1.44	116	$(C_{28}H_{58}N_2O_{10}S_2)_{58}(C_{11}H_{21}O_6S)_{51}Au_{116}$	58	50	53	63 255

Table 5 : Summary of GNP-11 to GNP-13.

5.4 BIOPHYSICAL ANALYSIS

5.4.1 Haemagglutination inhibition assay

Biophysical evaluation of the binding events between the GNPs and lectin partners vary depending on the experiment used (HIA, SPR and ITC). From HIA, for Con A it can be seen that low presentation density GNPs exhibit no activity towards haemagglutination inhibition. Higher presentation densities do show increased activity with reference to the active ligand in free solution, although this augmentation in activity is only subtle. For PA-IL it can be clearly seen that as GNP presentation density increases, the activity of the galactose ligands increases. This augmentation in activity is much more noticeable than in Con A. At 90 % galactose presentation, each galactose ligand was almost 120 fold more active than if in free solution. However, at 100 % galactose presentation density, the active ligand activity reduces slightly. This supports the theory that ligand activity increases with presentation density due to decreasing inter-ligand distances or increased effective concentrations, until the presentation density becomes too great, where adjacent ligands may hinder interactions with the receptor due to steric crowding. Comparing to other multivalent scaffolds discussed earlier (table 1) the augmentation in affinity of Con A for the active ligands is significantly lower (2 to 3 orders of magnitude) with reference to dendrimers and cyclodextrin scaffolds used previously. However, Con A affinity augmentation by GNPs is comparable to other

scaffolds tested by HIA with other lectin systems (WGA, EcorL). The augmentation in PA-IL affinity for the active ligands on the GNP surface is comparable to those seen for the dendrimers and cyclodextrin structures tested with Con A.

5.4.2 Isothermal titration calorimetry

ITC of **GNP-2** to **GNP-10** yielded curves indicating reversible binding. Although this provided an ideal situation for the analysis of their interactions, it can be still considered surprising given that multivalent ligands are well known to precipitate multivalent lectins. Examination of the contents of the calorimeter cell initially showed no evidence of aggregation, however several hours later at ambient temperature aggregation was seen to occur. If this process were to occur rapidly, ligand binding during the ITC experiment would induce irreversible aggregation and remove lectin from the experiment by precipitation. This would then give the appearance of an infinite binding constant, resulting in a square ITC curve. If this aggregation/precipitation occurred more slowly, the value of c , which determines the shape of the curve, would change constantly resulting in a complex titration curve to which a theoretical binding model could not be fitted.¹¹⁹ Also, slow aggregation can be seen in the thermogram recorded by the apparatus. This process results in a secondary peak following the injection peak. This aggregation peak occurs long after the injection peak and is typically smaller in intensity and broader. Indeed, for **GNP-11** to **GNP-13**, aggregation was observed during the experiments. For **GNP-13**, this was most likely due to the insolubility of these GNPs, with the addition of lectin to the ITC cell inducing GNP aggregation. In the case of **GNP-11** and **GNP-12**, it was not possible to fit a theoretical binding model.

From the ITC results, it was observed that as the inter-ligand distance approached half of the inter-binding site distance of the lectins studied, the affinity increased (60 fold for BclA, 20 fold for PA-IL).

5.4.3 Inter-ligand distance calculations

The inter-ligand distance was calculated as follows: The distance between two ligands on the GNP surface can be treated as the distance between several uniformly spaced points on the surface of a sphere. This distance would depend on the number of points on the surface and the size (radius) of the sphere. The number of points on the surface refers to the number of

active ligands presented at the surface (GNP valency) and the radius of the sphere would correspond to the GNP core diameter and the linker molecular length (figure 42).

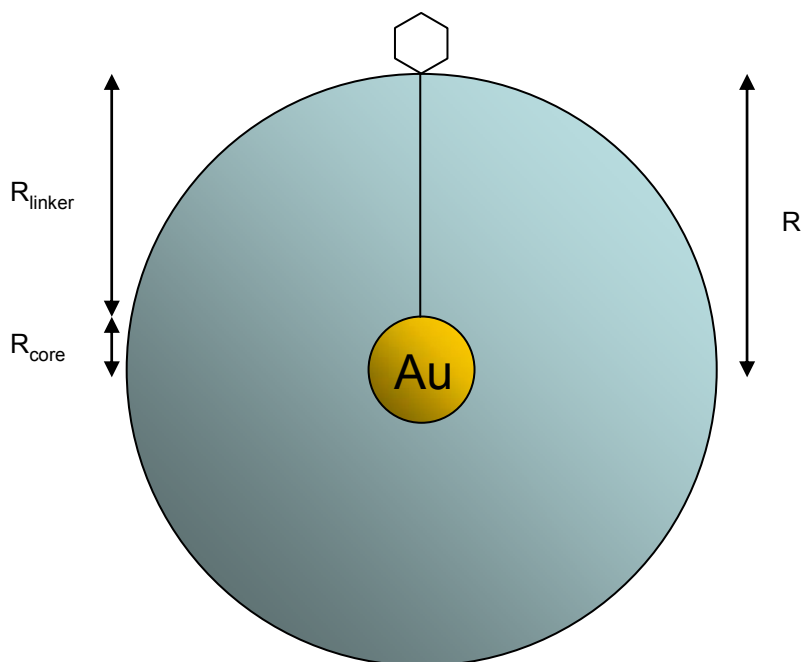


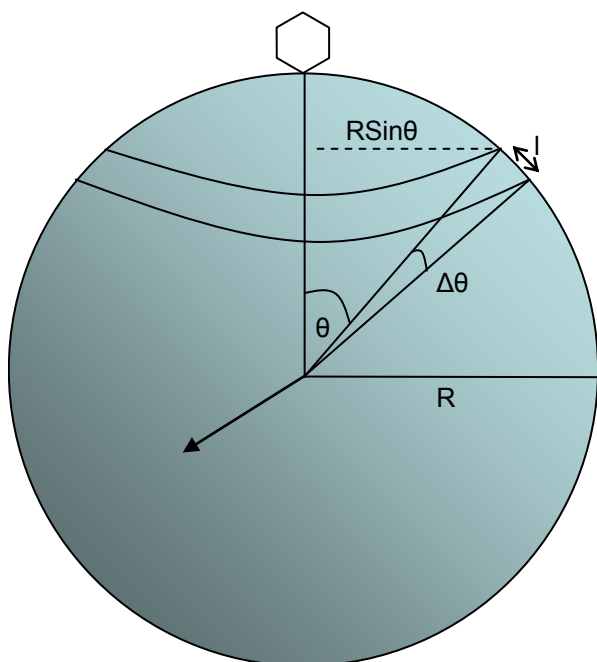
Figure 42 : Radius of theoretical sphere occupied by a ligand as a function of core size and linker molecule length.

Assuming that all the ligands of the GNP are distributed evenly, the surface area occupied by each ligand on the theoretical sphere would be equal to the total spherical surface area divided by the total number of ligands, n .

$$\textit{Theoretical sphere surface area} = 4\pi R^2 \quad \mathbf{E\ 33}$$

$$\textit{Partial surface area per ligand} = \frac{4\pi R^2}{n} \quad \mathbf{E\ 34}$$

The derivation of calculating the surface area of a sphere, and its partial surface area, can also be expressed using a polar coordinate system. This shows the variation of partial surface area on the angle between the polar axis and the extremity of the area to be calculated, θ :



$$\text{Length of } l = R \Delta \theta \quad \text{E 35}$$

$$\text{Length around sphere} = 2\pi \cdot R \sin \theta \quad \text{E 36}$$

$$\text{Partial sphere area} = \Delta SA = R \Delta \quad \text{E 37}$$

$$\Delta SA = 2\pi R^2 \sin \theta \cdot \Delta \theta \quad \text{E 38}$$

$$dSA = 2\pi R^2 \sin \theta d\theta \quad \text{E 39}$$

$$SA = 2\pi R^2 \int_0^\theta \sin \theta d\theta \quad \text{E 40}$$

$$SA = 2\pi R^2 [-\cos \theta]_0^\theta \quad \text{E 41}$$

$$SA = 2\pi R^2 (\cos 0 - \cos \theta) \quad \text{E 42}$$

$$SA = 2\pi R^2 (1 - \cos \theta) \quad \text{E 43}$$

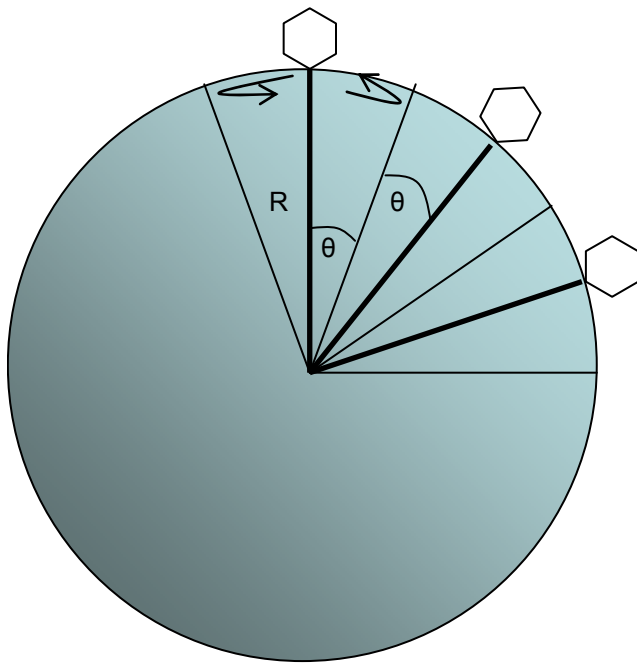
$$\cos \theta = 1 - \frac{SA}{2\pi R^2} \quad \text{E 44}$$

Figure 43 : Showing the dependence of (partial) sphere area on θ , the angle between the polar axis and the extremity of the area to be calculated.

Substituting total surface area for partial surface area:

$$\cos \theta = 1 - \frac{2}{n} \quad \text{E 45}$$

This angle, θ , represents the angle of the region occupied by the active ligand. However, this would only be half of the inter-ligand angle as shown in figure 44 below.



Inter-ligand angle = 2θ

Figure 44 : Inter-ligand angle on a GNP surface.

From this model, an isosceles triangle can be extracted, with the two ligands concerned making the base, and the sphere centre representing the point of the triangle (see below).

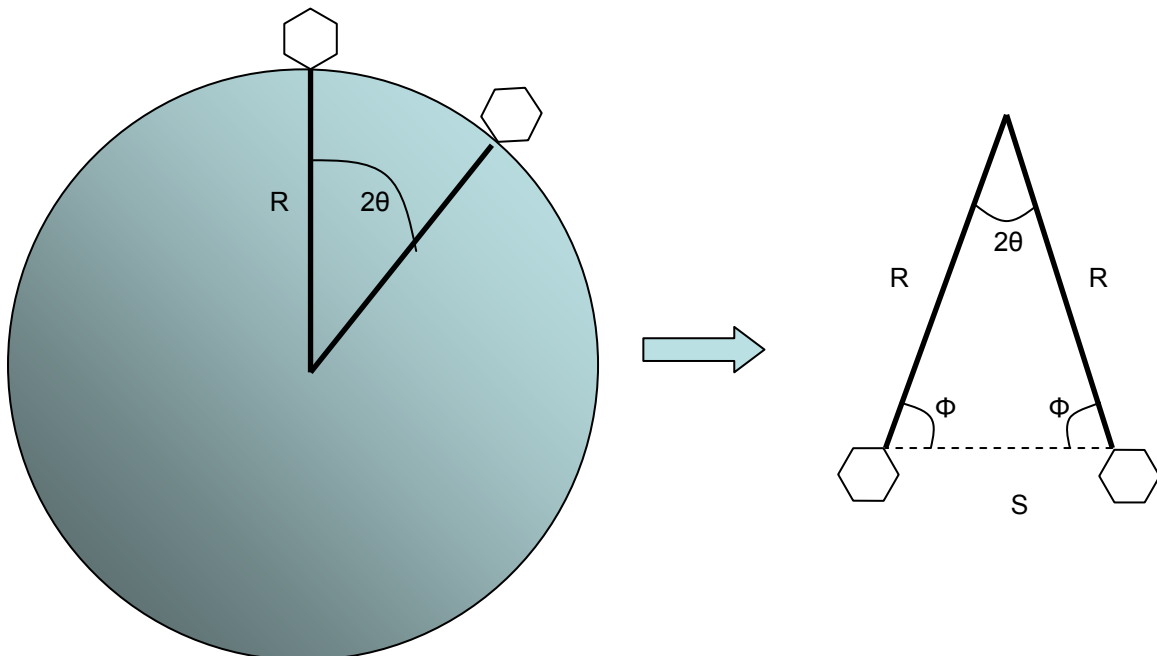


Figure 45 : Isosceles triangle showing the inter-ligand angle, 2θ , and the inter-ligand distance, S.

By using the sum of angles in a triangle, and the Sine rule, the values of Φ and S can be calculated as follows:

$$\phi = \frac{\pi - 2\theta}{2} \quad \text{E 47}$$

$$\frac{S}{\sin(2\theta)} = \frac{R}{\sin(\phi)} \quad \text{E 48}$$

$$S = \frac{R\sin(2\theta)}{\sin(\phi)} \quad \text{E 50}$$

This calculation depends on the assumptions relating to ligand behaviour at the GNP surface, as outlined previously:

- 1) The gold cluster is uniform and spherical in shape, corresponding to the *average* nanoparticle.
- 2) The number of active ligands corresponds to the average GNP
- 3) The ligands are rigid, adopt a linear form, are inert to themselves, and are distributed equally around the surface adopting a circular occupation of its designated partial surface area.

However, why results from ITC and SPR show increased lectin affinity at half of this value is unclear and could be due to several reasons related to the assumptions above.

First, the structure of the Au cluster at large sizes does exhibit a spherical structure. As the core size decreases the form of the Au core resembles a more icosahedral or truncated icosahedral structure with the emergence of vertex, edge and terrace Au surface atoms. This would lead to a non-spherical presentation of the ligands depending on the surface Au sites they occupy. Second, the ligands may not be completely rigid in aqueous solution. Indeed, the tetra(ethylene) glycol unit of the spacer molecules was incorporated in order to increase aqueous solubility and ligand flexibility (figure 46).

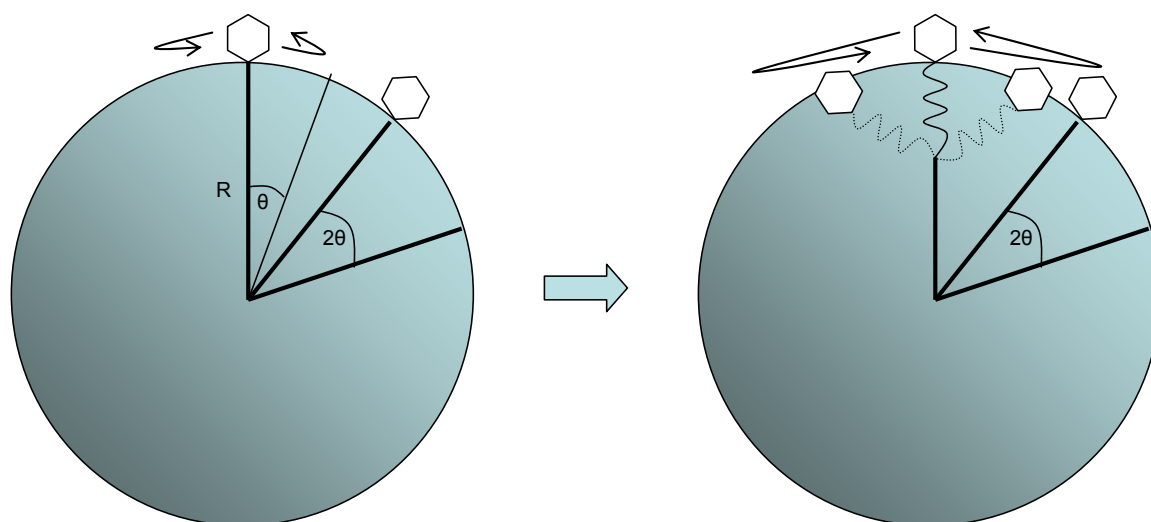


Figure 46 : Model showing a “rigid” ligand (left) and a semi-flexible ligand (right).

Also, the amphiphilic nature of the linker molecule may influence the structure of the Au-ligand polymer upon dissolution of the ligands and gold salts in the methanolic solution. Particularly in the case of the hybrid GNPs, with potential hydrophobic-hydrophilic repulsions between the active and inactive linker molecules as described above. This may in turn influence the presentation of the active ligands at the GNP surface upon borohydride reduction, leading to pockets of active and inactive ligands at the GNP surface. As well as amphiphilic interactions between the linker molecules, interactions between saccharide moieties may also influence the stacking of the ligands at the GNP surface both during GNP synthesis and when dissolved in aqueous solution. The presence of metal ions in solution may influence ligand presentation in a similar way, both during GNP synthesis and biophysical analysis. The metal ions (Ca^{2+} for example) may provide a template for chelation by several tetra ethylene glycol units. This in turn may direct the arrangement, or cause aggregation of active ligands at the GNP surface. Finally, the thiol species may influence this. If, for example, the active ligands formed this Au-ligand polymer from thiol-functionalised ligands, a random arrangement would be expected. However, if the ligands had oxidised to significant quantities of disulfides, this may encourage the formation of active ligands binding to the GNP surface as molecular pairs.

The inter-ligand distances were also calculated for **GNP-11** to **GNP-13**, as shown in table 6. It can be seen that upon comparing **GNP-11** with **GNP-4** (see earlier), the mixed(s)-linker molecule allows both smaller core diameters as well as linker lengths allowing for shorter inter-ligand distances (almost 0.4 nm). A slightly larger difference was calculated for **GNP-**

13, with a reduction of 0.5 nm. This difference is more exaggerated when comparing GNP-12 and GNP-7, where there is a reduction in the inter-ligand distance of over 1 nm.

GNP	GNP Diameter / nm	Sphere Surface Area / nm ²	No. Of Active Ligands	Deflection Angle / Rads	Interligand Distance / nm
GNP-11	1,44	140,19	30	0,73	2,40
GNP-12	1,47	141,45	16	1,01	3,25
GNP-13	1,44	235,34	58	0,53	2,25

Table 6 : Inter-ligand distances for GNP-11 to GNP-13.

5.5 Cluster Glycoside Effect at GNPs

Depending on the presentation density, or rather the inter-ligand distance, at the GNP surface there are several situations possible. The first, when the inter-ligand distance is too large with respect to the inter-binding site distance of the lectin receptor. Thermodynamically, this would mean that the ligands, or more specifically the linker molecules attached to the ligand, would have to pay a conformational enthalpy penalty upon adopting optimal multivalent binding conformations. The linker molecule would also have to compensate for the entropic penalty induced by restricted degrees of freedom. The resulting affinity constant would thus decrease, being enthalpically diminished and experiencing reduced entropic enhancement of the interaction. In terms of effective concentrations, at large inter-ligand distances the C_{eff} decreases rapidly. This may allow the bulk ligand concentration to be significantly competitive with the local effective concentration. In both cases, after the first binding event, a second intermolecular binding event would be favoured as opposed to the multivalent intramolecular interaction (Figure 47, A). As the inter-ligand distance decreases and approaches the inter-binding site distance of the lectin receptors, the enthalpy and entropy penalties would be reduced, increasing the observed affinity (Figure 47, B). This would be until an optimum inter-ligand distance is reached where further decreasing the inter-ligand would re-induce enthalpic and entropic penalties. Decreasing further the inter-ligand distance would lead to further reduction in the observed affinity. This would be due to steric hindrance of ligands presented on the same GNP inhibiting the receptor-ligand interaction. I.e. as the lectin interacts with one ligand, the surrounding ligands may impose on the lectin due to their close proximities. As the inter-ligand distance decreases further still, these steric repulsions increase, resulting in a further reduction in observed affinity. In terms of effective concentration, decreasing the inter-ligand distance would theoretically increase the observed affinity.

However, as the inter-ligand decreased further, the effective concentration should continue to increase, resulting in a continuous increase in the observed affinity (figure 47, C).

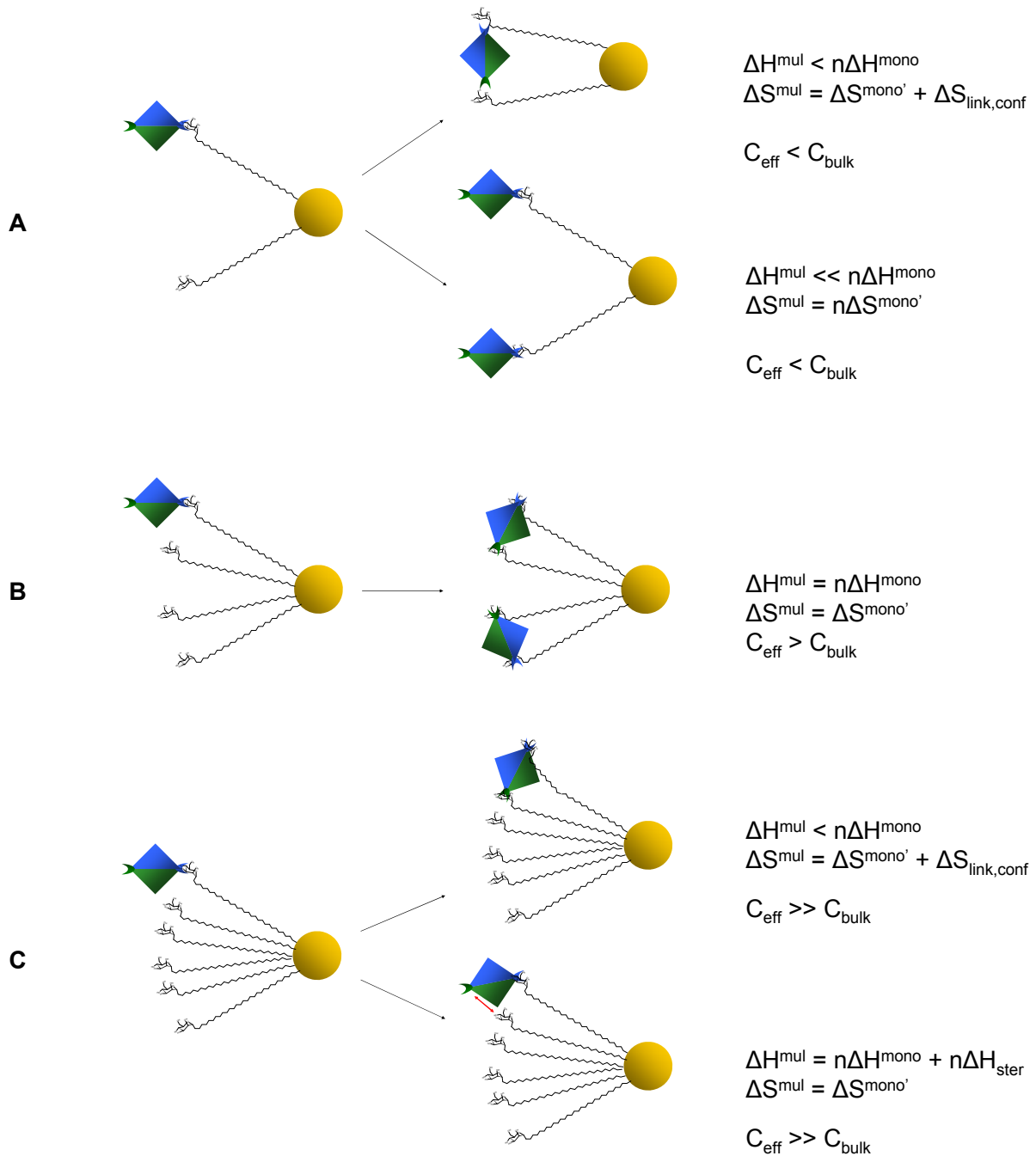
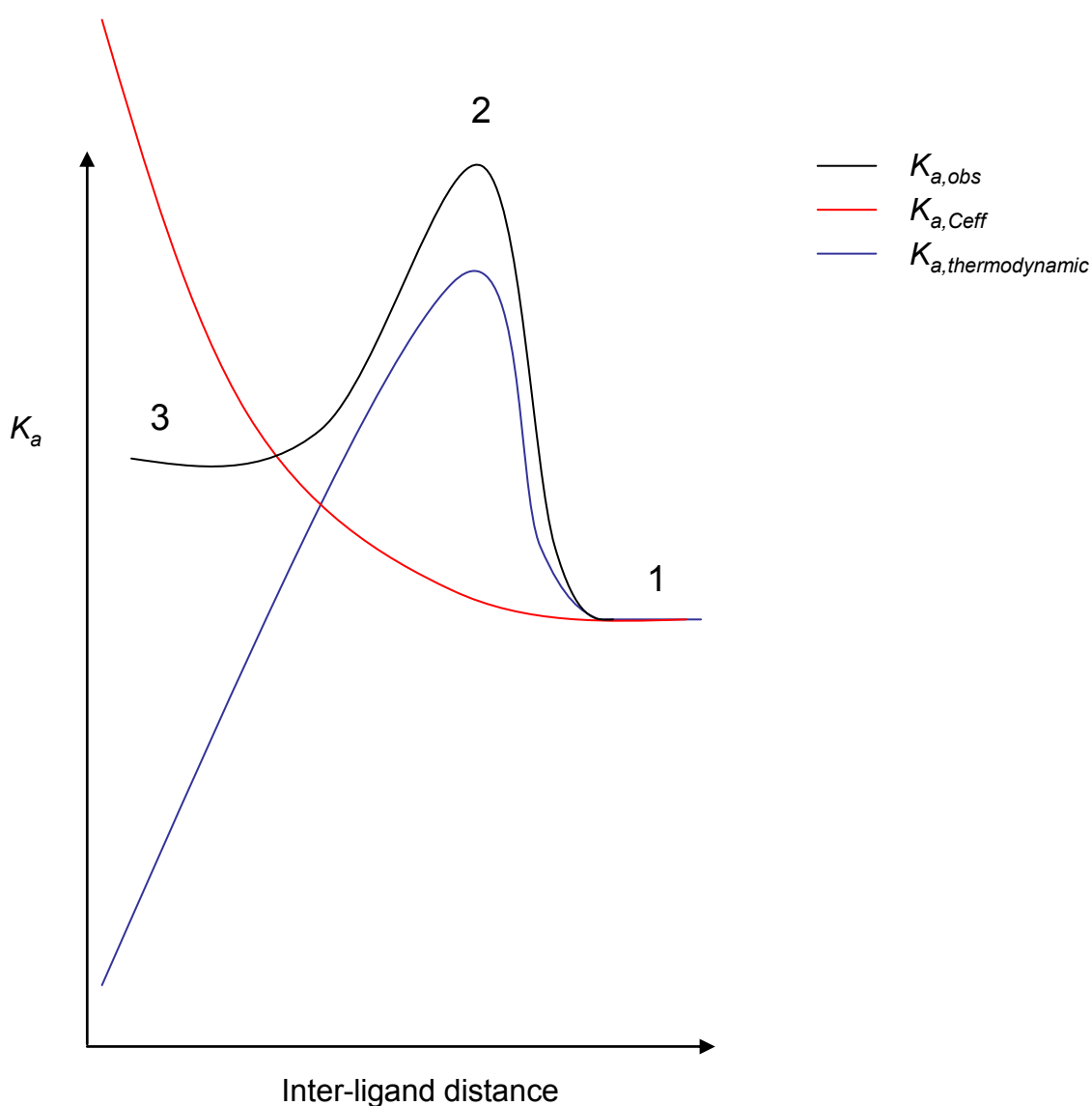


Figure 47 : Different situations involving lectin-GNP interactions. A: The inter-ligand distance on the GNP is too long leading to thermodynamically reduced observed affinities. B: complimentary inter-ligand and inter-binding site distances leading to thermodynamically enhanced affinities. C: inter-ligand distance too short leading to thermodynamically and sterically reduced observed affinities.

The thermodynamic and effective concentration dependence of the observed affinity may be expressed graphically for a typical multivalent interaction (graph 1). At position 1, the affinity

observed is equivalent to K_a^{mono} as the ligands are too far apart to allow multivalent binding. At position 2, the observed affinity increases due to the multivalent interaction being allowed and thermodynamically enhanced. The increase in local C_{eff} would also augment the observed affinity. At position 3, the interaction is thermodynamically disfavoured as steric hindrance becomes increasingly important with decreasing inter-ligand distance. At the same time, the local C_{eff} would continue to favour binding. Therefore the observed affinity would represent a compensation between steric and concentration effects.



Graph 1 : Dependence of the observed binding affinity with thermodynamic and concentration effects.

The width of the peak at position 2 in graph 1 would depend on both the flexibility of the linker molecule and the inter-binding site distances of the receptor. A rigid linker molecule

would give very sharp, discrete peaks, with the maximum centred on the inter-binding site distance of the receptor. Receptors which exhibit several binding site distances (PA-IL for example) may indeed exhibit multiple peaks in observed affinity, each maximum corresponding to each inter-binding site distance. Flexible linker molecules would increase the width of this peak, as more degrees of freedom are possible, increasing the number of correct ligand geometries for multivalent interactions effectively reducing the “resolution” of the multivalent scaffold separating the binding sites. Linker molecule flexibility would also however decrease the maximum affinity due to entropic penalties from losses of degrees of freedom upon binding.

If however, the ligands were presented on the GNP surface as molecular pairs or molecular clusters, this would increase the effective ligand concentration experienced by the lectin receptor. The contribution of effective concentration towards observed affinity constants would also increase. At reduced inter-ligand (cluster) distances however, greater contributions to steric hindrance would also occur.

GENERAL CONCLUSIONS

The synthesis and characterisation of thiol-functionalised mannoside and galactoside *neoglycoconjugates* **1** and **2** was successfully carried out. The thiol group was introduced following conjugation of amine functionalised *neoglycoconjugates* to *iso*-thiocyanate linker molecules, forming a thiourea bridge. This synthetic methodology developed by Penades *et al.* allows the rapid synthesis of a library of thiol functionalised *neoglycoconjugate* ligands for protecting AuNP surfaces. A third, glucose functionalised *neoglycoconjugate*, **3**, was also synthesised. Following this, several mannose and galactose functionalised GNPs were synthesised using an adapted Brust-Schiffrin method. The GNPs exhibited several presentation densities by tuning the mannose : glucose or galactose : glucose ligand ratios, ranging from 10 – 100 %. Good control of active ligand density (± 5 %) was observed in most cases. All GNPs were characterised by ^1H NMR, IR and UV/vis spectroscopy as well as high resolution TEM and elemental analysis. Characterisation confirmed their functionalisation with organic molecules. High resolution TEM was used to measure the size of the gold cores, with all GNPs exhibiting a monomodal population with a small size distribution. Statistical analysis of data allowed an estimate of the average core size for each GNP. These data, with the application of previous work, also allowed the calculation of the number of Au atoms in the average GNP. Combining this with elemental analysis, a theoretical GNP model was produced, with estimated molecular formulas, ligand presentation density and GNP valency. GNPs were also functionalised with a second “short” linker as well as changing the ligand : Au ratio in order to alter the inter-ligand distances on the GNPs.

Following GNP synthesis and characterisation, recombinant lectins (BclA and PA-IL) were expressed and purified following previously established methods. Interaction studies were carried out using these lectins, and the commercially available Con A, with the GNPs synthesised. Biophysical analysis techniques were used to study the lectin-GNP interactions. The interactions were measured both comparatively by Haemagglutination inhibition assays, as well as quantitatively using surface plasmon resonance, and the first use of isothermal titration (micro)calorimetry for nanoparticle systems. It was observed in all cases that an increasing presentation density of active ligands on the GNP surface lead to an increase in

ligand activity resulting in an increase in observed lectin affinity. Further analysis of the theoretical structure and presentation of the active ligands at the GNP surface from a purely mathematical basis allowed the analysis of ligand activity with respect to the inter-ligand distances at the GNP surface. It was found experimentally that large inter-ligand distances exhibit smaller activities comparable to that of monovalent ligands. Whereas decreasing the inter-ligand distance increased ligand activity and observed lectin affinity. For Con A and BclA the dependence of the association constant (K_a) on inter-ligand distance was found by SPR to be linear in nature at large inter-ligand distances, but higher order affinity enhancements at smaller inter-ligand distances. This relationship was found to be more complex in PA-IL. By ITC, it was found for BclA that large inter-ligand distances exhibit thermodynamic properties similar to that of monomeric ligands in free solution, whereas smaller inter-ligand distances (46% presentation density) exhibit larger thermodynamic contributions leading to a thermodynamically enhanced K_a . This suggested that for BclA, complementarity between ligand presentation and lectin architecture is important. However, for PA-IL, ITC studies showed that even large inter-ligand distances augment the kinetics of the interaction. Upon reducing the inter-ligand distance at the GNP surface, this augmentation is exaggerated further, suggesting a local concentration effect.

Taking in to consideration the two theories put forward for explaining the cluster glycoside effect; thermodynamic enhancement and effective concentrations, inter-ligand distances at the GNP surface corresponding to the inter-binding site appears to be important for inducing multivalent interactions. Large inter-ligand distances induce mono-ligand thermodynamics and concentration dependent kinetics, favouring the occurrence of multiple intermolecular associations which may lead to aggregation. Smaller inter-ligand distances favour multivalent intramolecular interactions both thermodynamically and kinetically (concentration dependent). At very small inter-ligand distances, the two models disagree. Thermodynamics would imply unfavourable steric interactions, reducing the occurrence of intramolecular interactions (but not necessarily increasing multiple intermolecular binding events) whereas concentration dependent kinetics would imply a continuing rise in intramolecular association. A combination of both models may be necessary to fully explain the glycoside cluster effect and its implications in experimental observations, particularly at very small inter-ligand distances.

When examining a multivalent target, one must consider several aspects when designing a multivalent ligand. The multivalent scaffold used should be carefully chosen and tailored so that all the desired qualities and functionalities may be incorporated, with reference to the multivalent target as well as any further applications. Notably, the accessibility of the multiple binding sites, the inter-binding site distance and the arrangement of molecules presented at the nanoparticle surface should be well thought-out. Also, one must consider binding – re-binding in order to augment the probability of a multivalent interaction taking place. Finally, the effects of ordered solvent molecules on the enthalpy and entropy contributions to the interaction should be considered, which may differ significantly on a multivalent level.

In order to further increase the affinity and specificity of the lectins for the GNPs (or indeed any multivalent scaffold) more complex ligands may be conjugated to the linker molecules. For example, the use of oligosaccharides in the place of monosaccharides [Man- α -(1-6)-Man for BclA] or monosaccharides functionalised with complimentary groups (*p*-Nitrophenyl α -D-mannoside for FimH).^{24, 56} However, the behaviour of both receptors and ligands may change significantly when the ligands are immobilised to multivalent scaffolds.

As well as this work, investigations into further GNP characterisation, using synchrotron radiation, have been initiated, as have investigations into the self-organisation of carbohydrate functionalised GNPs with a view to applications in nanochemistry and nanoelectronics. Applications towards TEM studies have also resulted from this work.

CONCLUSION GENERALE

Nous avons réalisées la synthèse et la caractérisation des *neoglycoconjugés* de mannose et galactose fonctionnalisés avec des thiols (**1** et **2**). La fonctionnalité thiol a été incorporée selon la conjugaison entre les *neoglycoconjugés*-aminés et les molécules bras-espaceurs *isothiocyanate* pour former des ponts thio-urés. Cette méthodologie, développée par Penadés *et al*, permet la synthèse rapide d'une bibliothèque de ligands pour la protection des nanoparticules d'or. Un troisième *neoglycoconjugé*, à base de glucose (**3**) a aussi été synthétisé. Par ailleurs, plusieurs glyco-nanoparticules (GNPs) ont été conçues en utilisant une méthode adaptée (Brust-Schiffrin). Les GNPs fonctionnalisés montrent plusieurs « densités de présentations » des ligands actifs en modifiant le rapport molaire mannose / glucose ou galactose / glucose. Une densité de présentation entre 10 et 100 % et une bonne reproductibilité (erreur ± 5 %) ont été observés dans la plupart des cas. Tous les GNPs ont été caractérisés par RMN ^1H , IR et spectroscopie UV/vis ainsi que par microscopie MET à haute résolution et par analyse élémentaire. Ces analyses ont confirmé que les GNPs sont bien fonctionnalisés par des molécules organiques. La microscopie MET à haute résolution nous a permis de mesurer les tailles des billes d'or ; tous les GNPs ont montrée une distribution de population monomodale et étroite. L'analyse statistique des données nous a permis d'estimer le diamètre moyen d'une bille d'or. Avec cette valeur, et en appliquant les travaux de Murray *et al*, la quantité d'atomes d'or dans un GNP de diamètre moyen a pu être calculé. En combinaison avec l'analyse élémentaire, un modèle théorique des GNPs a été créé, ceci permettant d'obtenir la formule moléculaire, la densité de présentation et la valence des GNPs. D'autres GNPs ont été conçues avec une deuxième molécule bras-espaceur, « bras-espaceur court », et en faisant varier le rapport molaire ligand / Au pour modifier les distances inter-ligands sur la surface des GNPs.

Une fois la synthèse et les caractérisations des GNPs réalisées, des lectines recombinantes ont été exprimées et purifiées via les méthodes déjà établies. Nous avons ensuite effectué l'étude des interactions entre ces lectines et les GNPs synthétisés, ainsi que celle des interactions entre des GNPs et la lectine commerciale, Con A. Des techniques d'analyses biophysiques ont

été utilisées pour étudier ces interactions. Celles-ci ont été mesurées comparativement en réalisant des essais d'inhibition d'haemagglutination (HIA) et quantitativement par une méthode de résonance plasmonique de surface (SPR) et par microcalorimétrie isotherme de titration (ITC). Il a été observé dans tous les cas qu'une densité de présentation croissante de ligands actifs chez les GNPs mène à une augmentation de l'activité des ligands, observée par une augmentation de l'affinité des lectines. L'analyse complémentaire de la structure théorique et de la présentation des ligands chez les GNPs, sur une base purement mathématique, a permis l'étude des activités des ligands par rapport aux distances inter-ligands à la surface des GNPs. Expérimentalement, il a été montré que des grandes distances inter-ligand exposent une faible activité comparable à celle de ligands monovalents, tandis que la diminution de la distance inter-ligand augmente leur activité. Pour la lectine commerciale, Con A, et la lectine BclA, il a été constaté que la constante d'association (K_a) est dépendante des distances inter-ligands ; cette dépendance est linéaire (montré par SPR). Mais, une dépendance d'ordre plus élevée a été observée pour les distances inter-ligand plus courtes. La dépendance du K_a sur les distances inter-ligands est plus complexe pour PA-IL dans le cas des expériences de SPR et de ITC.

Prenant en compte les deux théories présentées sur l'effet de multivalence dans le premier chapitre, c'est-à-dire les considérations thermodynamiques et les concentrations effectives, nous pouvons voir que les distances inter-ligands chez les GNPs sont assez importantes pour induire des interactions multivalentes. Des distances importantes induisent thermodynamiquement des interactions monovalentes avec des cinétiques dépendantes des concentrations et favorisant les associations *intermoléculaires*, qui peuvent aussi générer des agrégats. Des distances inter-ligands plus courtes favorisent, au contraire, des interactions multivalentes, tant thermodynamiquement qu'en raison des concentrations effectives. Par contre, quand les distances inter-ligands sont très courtes, les deux modèles ne sont pas en accord. Les effets thermodynamiques impliquent des interactions stériques défavorables, qui réduisent la probabilité des interactions multivalentes (mais qui n'augmentent pas nécessairement les interactions *intermoléculaires*). Par contre, en réduisant les distances inter-ligands, la concentration effective aurait toujours un effet d'augmentation des cinétiques des interactions ; et les interactions multivalentes seraient de conséquences encore plus favorisées. Il est alors probable qu'une combinaison des deux modèles puisse expliquer complètement l'effet de multivalence et ses implications dans les résultats observés, particulièrement dans le cas de distances inter-ligands très courtes.

Si on examine un récepteur multivalent, il faut considérer plusieurs aspects pour désigner le ligand multivalent. La plateforme multivalente utilisée doit être soigneusement choisie et modifiée par rapport au récepteur multivalent et aux applications, afin que toutes les qualités et fonctionnalités désirées puissent être incorporées ; notamment l'architecture du récepteur et la présentation des ligands. Il faut aussi considérer les effets des concentrations effectives qui peuvent encore augmenter la probabilité des interactions multivalentes. Les effets de solvatation sur les contributions d'enthalpie et d'entropie sur l'interaction globale doivent être également considérés, puisqu'ils peuvent aussi jouer un rôle important sur l'échelle de multivalence.

Pour augmenter l'affinité et la spécificité des lectines pour les GNPs (ou même pour toutes plateformes multivalentes), des ligands plus complexes peuvent être conjugués aux molécules bras-espaceurs, par exemple en utilisant des oligosaccharides à la place des monosaccharides [Man- α -(1-6)-Man pour BclA] ou des monosaccharides fonctionnalisés par des groupements complémentaires (*p*-Nitrophenyl α -D-mannoside pour FimH).^{24,56} Cependant, le comportement des récepteurs et des ligands peuvent changer de façon significative lorsque les ligands sont immobilisés sur des plateformes multivalentes.

Comme perspective de ce travail, des études plus approfondies sur la caractérisation des GNPs, via l'utilisation des rayons X synchrotrons (ESRF, Grenoble), ont été commencées. Des études sur l'auto-organisation des AuNPs fonctionnalisés avec des glucides et leurs applications dans les domaines de la nanochimie et des nanoélectroniques ont également démarrées. Enfin, des études par microscopie MET devraient aussi permettre d'obtenir des informations complémentaires sur ces travaux.

CHAPTER 6 :
Experimental – Biochemistry and
Interaction Studies

CHAPTER 6 :

Experimental – Biochemistry and Interaction Studies

6.1 Lectin Expression and Purification

The lectin BclA, from *Burkholderia cenocepacia*, was expressed and purified in recombinant form as documented from *Escherichia coli* as documented previously.^{23, 24} The PA-IL lectin, from *Pseudomonas aeruginosa*, was also expressed and purified in recombinant form from *Escherichia coli* as documented previously.¹⁶

The lectin Concanavalin A, from *Canavalia ensiformis* (Jack Bean), Type IV was bought from Sigma-Aldrich and used without further purification.

6.2 Haemagglutination Inhibition Assays

Rabbit erythrocytes were bought from Biomerieux and used without further washing. The erythrocytes were diluted to a 2 % solution in NaCl (150 mM). Lectin solutions of 1 mg / mL were prepared in Tris/HCl as for the calorimetry studies. The Haemagglutination unit (HU) was first obtained by the addition of 25 μ L of the 2 % erythrocyte solution to 25 μ L aliquots of sequential lectin dilutions. The mixture was incubated at 37 °C for 30 mins followed by incubation at RT for 30 mins. The HU was taken as the minimum lectin concentration required to prevent haemagglutination. For the following lectin-inhibition assays, lectin concentrations of four times that of the haemagglutination unit were used. For Con A, this concentration was found to be 15.625 μ g / mL. For BclA and PA-IL these were found to be 2 mg / mL and 5 μ g / mL respectively. Subsequent assays were then carried out by the addition of 50 μ L lectin solution (at the required concentration) to 50 μ L of sequential dilutions of GNPs, monomer molecules and controls. These solutions were then incubated at 37 °C for 30 mins followed by 30 mins at RT. After which, 50 μ L of 2 % erythrocyte solution was added

followed by a further 30 mins incubation at 37 °C and 30 mins at RT. The minimum inhibitory concentration for each GNP molecule was recorded.

6.3 Surface Plasmon Resonance (SPR) Binding Assays

All SPR experiments were carried out on a Biacore T100 instrument. CM5 sensor chips (Biacore/GE, Uppsala, Sweden) were equilibrated with HBS (HEPES-buffered saline: 10 mM HEPES and 150 mM NaCl, pH 7.4) containing 0.005 % (v/v) Tween 20 at 25 °C with a flow rate of 20 $\mu\text{L min}^{-1}$. Following equilibration, the chips were activated with two 7 minute pulses of a 1 : 1 mixture (v/v) of 0.1 M *N*-hydroxy-succinimide and 0.1 M *N*-ethyl-*N'*-(dimethylaminopropyl)carbodiimide, at 25 °C and flow rate of 5 $\mu\text{L min}^{-1}$. Ethanolamine hydrochloride was immobilised on channel one via an injection of 7 min (1.0 M, pH 8.5; ~80 RU) to measure the level of non-specific binding and to serve as a blank for mathematical data treatment. Con A was immobilised on channel 3 via an injection of 60 s (100 $\mu\text{g mL}^{-1}$ in 10 mM Sodium Acetate buffer, pH 4.5; ~4100 RU). Con A was also immobilised on channel 4 via an injection of 4 min (2 $\mu\text{g mL}^{-1}$; ~400 RU). Remaining *N*-hydroxy succinimide esters were blocked by a 7 min pulse of 1.0 Ethanolamine hydrochloride, pH 8.5. A second chip was activated and Ethanolamine hydrochloride immobilised to channel one as described above. BclA was immobilised to channel 2 via an injection of 7 min (10 $\mu\text{g mL}^{-1}$, Sodium Acetate buffer, pH 4.5; ~480 RU). Remaining *N*-hydroxy succinimide esters were blocked by a 7 min pulse of 1.0 Ethanolamine hydrochloride, pH 8.5. PA-IL was immobilised to Channel 3 via an injection of 41 mins (100 $\mu\text{g mL}^{-1}$, Sodium Acetate buffer, pH 4.5; ~300 RU). Remaining *N*-hydroxy succinimide esters were blocked by a 7 min pulse of 1.0 Ethanolamine hydrochloride, pH 8.5.

GNP solutions (100 $\mu\text{g mL}^{-1}$, and dilutions thereof to 30 ng mL^{-1}) in HEPES buffer were flowed across the sensor chip surfaces for 3 mins at a flow rate of 20 $\mu\text{L min}^{-1}$, and were allowed to dissociate for 3 mins. To restore the response level to zero, injections of three 3 min pulses of Me- α -D-Mannose and Me- α -D-Galactose for assays involving the mannose specific lectins and PA-IL respectively.

Binding was measured as RU (resonance units) over time, and data were evaluated using the Biacore Evaluation Software, version 1.1, and were fitted using a kinetic model for 1 : 1 binding.

6.4 Microcalorimetry

Titration calorimetry experiments were performed using a Microcal VP-ITC microcalorimeter. Titrations were carried out in 0.1 M Tris/HCl buffer (pH 7.5) containing 3 μM CaCl_2 , at 25 $^\circ\text{C}$. Aliquots of 10 μL of lectin solutions with concentrations of 0.21 mM to 1 mM for BclA and 0.23 mM to 1 mM for PA-IL, were added at 5 min intervals to the GNP solution present in the calorimeter cell. In the titrations, the GNP concentration varied from 0.5 mg mL^{-1} to 1.73 mg mL^{-1} for BclA and for 0.46 mg mL^{-1} to 1.12 mg mL^{-1} PA-IL, giving a saccharide concentration of 0.03 mM to 0.1 mM and respectively 0.031 mM to 0.076 mM. The corresponding monomer molecules (Man-mixed-SH for BclA and Gal-mixed-Sac for PA-IL) were also injected into solutions of the corresponding lectin solutions. Monomer concentrations were 3 mM and 1.7 mM respectively and lectin concentrations of 0.31 mM (BclA) and 0.05 mM (PA-IL). The temperature of the cell was controlled to 25 ± 0.1 $^\circ\text{C}$. Control experiments performed by injection of buffer into the GNP solution yielded insignificant heats of dilution. Injections of lectin into buffer however, yielded heats of dilution, thought to be significant, and were hence subtracted from experimental data during the data processing phase. Integrated heat effects were analysed by non-linear regression using a two-site binding model (Origin 7.0). Fitted data yielded association constants (K_a) and the enthalpy of binding (ΔH). Other thermodynamic parameters, i.e.; changes in free energy, ΔG , and entropy, ΔS , were calculated from the equation:

$$\Delta G = \Delta H - T\Delta S = -RT\ln K_a$$

Where T is the absolute temperature and $R = 8.314$ $\text{J mol}^{-1}\text{K}^{-1}$. Three independent titrations were performed for each lectin - GNP combination.

6.5 Transmission Electron Microscopy

GNPs were characterised by high resolution electron microscopy (HREM). 20 μL of a 100 $\mu\text{g mL}^{-1}$ aq. solution of GNPs were spotted onto 200 square mesh copper grids, covered in carbon. After 3 mins, excess water was removed by filter paper followed by air drying. Examinations were performed with a JEOL 3010, at 300 kV to a magnification of 500 000. The photographs were taken on Kodak SO163 films which were then digitalised using a Kodak Mega Plus camera. The diameter of the particles was measured using the Scandium 5.0 software (Soft Imaging Systems). To determine the organisation and the mean inter-particle distance was carried out using the DigitalMicrograph software (Gatan).

TEM experiments involving the incubation of lectins with GNPs were carried out as follows: GNP solutions (100 $\mu\text{g mL}^{-1}$ in water) were prepared and centrifuged at 13 000 rpm for 5 mins. 10 μL of this solution was diluted to 50 μL to which was added 10 μL of lectin solution (50 $\mu\text{g mL}^{-1}$ in water) and the solution incubated at room temperature for 1 h. After which, the solutions were centrifuged at 13 000 rpm for 5 mins and 5 μL spotted on to 200 mesh copper grids and analysed as above.

6.6 Monosaccharide Analysis

Monosaccharide analysis was carried out using a variation of the Phenol-sulfuric acid method documented by Brewer *et. al.*²⁴⁹ Calibration curves were made using solutions of varying concentrations (31.3 ng mL^{-1} to 1 mg mL^{-1}) of Me- β -D-Glucopyranoside, Me- α -D-Mannopyranoside and Me- β -D-Galactopyranoside.

To 50 μL of GNP solution, 50 μL of 5 % (v/v) Phenol (aq.) solution was added and mixed. 250 μL of H_2SO_4 was added, the mixture was vortexed, and allowed to stand for 30 mins at room temperature. Readings were taken at 490 nm against a blank prepared substituting distilled water or buffer solution for the GNP solution. A Varian Cary 50 Bio spectrophotometer was used for the absorbance measurements at 490 nm.

CHAPTER 7 :
Experimental – Chemical Synthesis

CHAPTER 7 :

Experimental – Chemical Synthesis

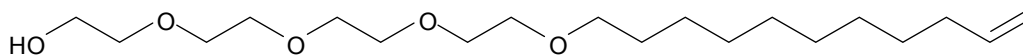
All starting materials were purchased from Sigma-Aldrich and used without further purification with the exception of Chloroauric acid monohydrate which was purchased from Strem Chemicals and used without further purification.

TLC was performed on Silica Gel 60 F254 pre-coated on aluminium plates (E. Merck) and the compounds were detected by UV (254 nm) and staining with *para*-anisaldehyde solution [anisaldehyde (25 mL), H₂SO₄ (25 mL), EtOH (450 mL) and CH₃COOH (1 mL)], molybdic solution [phosphomolybdic acid (1.3 g), cerium (IV) sulfate monohydrate (1 g), concentrated sulfuric acid (6 mL) water (made up to 100 mL)] or Potassium permanganate solution [KMnO₄ (2.5 g), K₂CO₃ (20 g), NaOH (10%), H₂O (200 mL)] as stated in the protocol followed by heating at over 200 °C.

Column chromatography was carried out on Silica Gel 60 (0.063-0.2 mm; E. Merck). All dialyses were carried out using snakeskin pleated sheet dialysis membranes (3500 mwco).

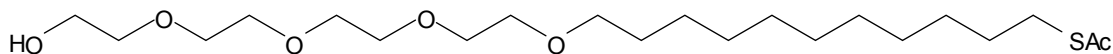
¹H and ¹³C NMR spectra were acquired on Bruker AVANCE 500 MHz, Bruker AVANCE 400 MHz and Bruker AC 300 MHz spectrometers, chemical shifts are given in parts per million (δ) relative to tetramethylsilane as an internal reference. ¹H and ¹³C assignments were made systematically using ¹H, ¹³C, COSY and HMQC experiments. Infrared spectra were recorded on a Perkin Elmer using KBr discs and suitable blanks. Mass spectra were recorded on a ZQ Waters Electrospray LC/MS.

Undec-1-en-11-yltetra(ethylene glycol), 4



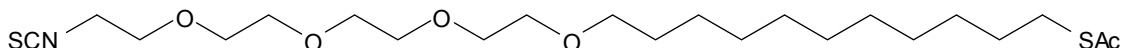
NaOH, as a 50% aq. Solution (0.18 mL, 0.09 g, 11.5 mmol, 1eq) was added dropwise to tetraethylene glycol (1.99 mL, 2.23 g, 11.5 mmol, 5 eq) at room temperature. Reaction mixture was tested as pH = 12 and heated to 110 °C (reflux). After 18 h the reaction mixture was allowed to cool to room temperature, after which 11-bromoundec-1-ene (0.5 mL, 0.537 g, 2.3 mMol, 1 eq.) was added. The reaction mixture was then heated to 110 °C (reflux) for a further 18 h. After which, the mixture was allowed to cool to room temperature and diluted with DCM (30 mL) and washed with brine (3 x 100 mL). Aq. phase washed with DCM (3 x 50 mL). Organic layers combined, dried (Na₂SO₄), filtered (cotton wool) and concentrated *in vacuo*. Purification by column chromatography (diameter of 4 cm, 12 cm of EtOAc silica media gel, eluted with 9 : 1 EtOAc / MeOH) to give pure **4** (0.52 g, 65 %) as a clear yellow viscous oil. TLCs were ran in EtOAc visualised by UV (254 nm) and KMnO₄, R_f = 0.33. ¹H NMR (CDCl₃, 300 MHz): δ 5.70-5.90 (complicated splitting pattern, 1H, CH=CH₂), 4.85-5.05 (m, 2H, CHCH₂), 3.50-3.75 (m, 16H, OCH₂CH₂O), 3.38-3.45 (t, *J*= 6.8 Hz, 2H, OCH₂C₁₀H₁₉), 1.95-2.07 (m, 2H, OCH₂CH₂C₉H₁₇), 1.92 (bs, OH), 1.50-1.60 (m, 2H, CH₂CH=CH₂), 1.20-1.40 (m, 12H, C₂H₄C₆H₁₂C₃H₅) ppm. Spectra corresponded to previous work.²⁴⁵

23-thioacetyl-3,6,9,12-tetraoxatricosan-1-ol, **5**



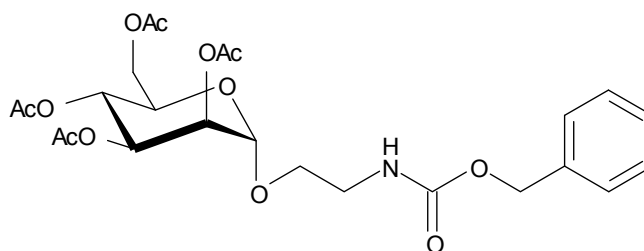
Undec-1-en-11-yltetra(ethylene glycol), **4**, (0.5 g, 1.44 mmol, 1 eq.) was dissolved in dry THF (12 mL) to which was added thioacetic acid (0.82 mL, 0.86 g, 11.4 mmol, 8 eq) dropwise at room temperature followed by AIBN (cat, 1 spatula). The mixture was then heated to reflux (80 °C). After 2 h, more AIBN was added (cat, 1 spatula) and the mixture was reheated to reflux for a further 14 h. After cooling to room temperature, the mixture was diluted with EtOAc (30 mL) to which was added sat. aq. NaHCO₃ solution until pH 7. Mixture was separated and the organic phase dried (Na₂SO₄), filtered (cotton), and concentrated *in vacuo*. Purification by column chromatography (diameter of 4 cm, 16 cm of EtOAc silica media gel, eluted with EtOAc) to give pure **5** (0.49 g, 81 %) as a clear yellow viscous oil. TLCs were ran in EtOAc visualised by UV (254 nm) and mitico, R_f = 0.47. ¹H NMR (CDCl₃, 300 MHz): δ 3.50-3.75 (m, 16H, OCH₂CH₂O), 3.38-3.45 (t, *J* = 6.8 Hz, 2H, OCH₂C₁₀H₁₉), 2.79-2.88 (t, *J* = 7.3 Hz, 2H, CH₂SAC), 2.29 (s, 3H, SAC), 1.95 (bs, OH), 1.24-1.60 (m, 4H, OCH₂CH₂C₇H₁₄CH₂CH₂SAC), 1.18-1.35 (m, 14H, OC₂H₄C₇H₁₄C₂H₄SAC) ppm. IR (KBr): λ_{max} = 3406 (broad), 2924, 1691 cm⁻¹. ESI-LRMS (MeOH) for C₂₂H₄₁NO₅S₂ [M+Na]⁺ Calc. 486.23, found 486.2; [M+K]⁺ Calc 502.21, found 502.1.

1-Isothiocyanate-3,6,9,12-tetraoxa-23-thioacetyltricosane, 6



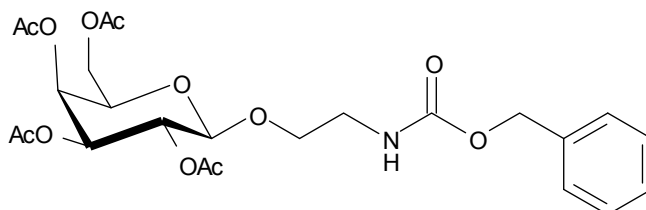
To a solution of 23-thioacetyl-3,6,9,12-tetraoxatricosan-1-ol, **5**, (3 g, 7.10 mmol, 1 eq.) in DMF (10.5 mL) was added PPh₃ (2.8 g, 10.6 mmol, 1.5 eq.) followed by NaN₃ (0.92 g, 14.2 mmol, 2 eq.). The mixture was then stirred at room temperature for 5 mins under an N₂ atmosphere. After which BrCCl₃ (2.11 g, 1.05 mL, 10.65 mmol, 1.5 eq.) was added dropwise and the cloudy yellow mixture was stirred at 40 °C for 3 h. The reaction mixture was then diluted with Et₂O (150 mL) and washed with H₂O (150 mL). The organic layers were combined, dried (Na₂SO₄), filtered (cotton) and concentrated *in vacuo*. The orange oil was then dissolved in toluene (30 mL) to which was added PPh₃ (2.8 g, 10.6 mmol, 1.5 eq.) and CS₂ (10.8 g, 8.54 mL, 142 mmol, 20 eq.) dropwise. The mixture was heated to 110 °C with a condenser attached. After 2 h the reaction mixture was allowed to cool to room temperature, concentrated *in vacuo* and purified by flash column chromatography (4 cm diameter, 30 cm of 5 : 1 Pet. Ether / EtOAc silica media gel, eluted with 5 : 1 Pet. Ether / EtOAc with a gradient to 1 : 1 Pet. Ether / EtOAc) to give **6** as a clear yellow oil (3 g, 90 %) TLC ran in 1 : 1 Pet. Ether / EtOAc, visualised by UV (254 nm) and KMnO₄, R_f = 0.38. ¹H NMR (CDCl₃, 500 MHz): δ 3.62-3.8 (m, 14H, 7 x CH₂ of tetra ethylene glycol), 3.56-3.59 (m, 2H, TEG-O-CH₂-alkyl), 3.44 (t, *J*=6.8 Hz, 2H, NCS-CH₂), 2.85 (t, *J*= 7.3 Hz, CH₂-SAC), 2.32 (s, 3H, SAC), 1.51-1.60 (m, 4H, TEG-CH₂-CH₂-C₇H₁₄-CH₂-CH₂-SAC), 1.23-1.37 (m, 14H, TEG-CH₂-CH₂-C₇H₁₄-CH₂-CH₂-SAC) ppm. IR (KBr): λ_{max} = 2113.5 (NCS-), 1691 (C=O), 1131 cm⁻¹. ESI-LRMS (MeOH) for C₂₂H₄₁NO₅S₂ [M+Na]⁺ Calc. 486.23, found 486.2; [M+K]⁺ Calc 502.21 found 502.1. Spectra corresponded to previous work.¹⁹⁸

2-*N*-benzyloxycarbonylaminoethyl tetra-*O*-acetyl- α -D-mannopyranoside, **7**



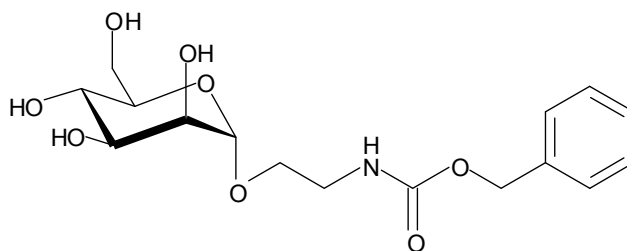
To a solution of α -D-Mannopyranose pentaacetate, (10.203 g, 26.1 mmol, 1 eq.) in anhydrous DCM (45 mL) under an N_2 atmosphere was added 2-(*N*- benzyloxycarbonyl)aminoethanol (10.249 g, 52.5 mmol, 2 eq.) at room temperature. To this mixture was added boron trifluoride diethyl etherate (19.04 g, 19.04 mL, 134 mmol, 5.1 eq.) dropwise and the yellow solution was heated to reflux (50 °C) for 12 h. After which, the red solution was diluted with EtOAc (100 mL) and washed with sat. aq. $NaHCO_3$ solution (2 x 100 mL). The aq. layers were combined and washed with EtOAc (100 mL). The organic portions were combined, dried (Na_2SO_4), filtered (cotton wool) and concentrated *in vacuo*. The compound was purified by flash column chromatography (Diameter of 8 cm, 20 cm of 4 : 1 Hexanes / EtOAc silica media gel eluted with 4 : 1 Hexanes / EtOAc then a gradient was made to 1 : 1 Hexanes / EtOAc) to give **7** as a cloudy white viscous oil (9.071 g, 66 %). TLC ran in 1 : 1 Hexanes / EtOAc, visualised by UV (254 nm) and *para*-anisaldehyde, $R_f = 0.25$. 1H NMR ($CDCl_3$, 500 MHz): δ 7.30-7.40 (m, 5H, Ar-H), 5.24-5.35 (m, 4H, H-2, H-3, H-4, NH), 5.14 (s, 2H, CH_2Ph), 4.84 (d, 1H, $J = 1.0$ Hz, H-1), 4.27 (dd, 1H, $J_1 = 5.7$ Hz $J_2 = 8.5$ Hz, H-6a), 4.07-4.16 (m, 1H, H-6b), 3.95-4.01 (m, 1H, H-5), 3.38-3.83 (3m, 4H, $-OCH_2CH_2NH-$), 2.17, 2.10, 2.05 and 2.01 (4s, 4 x 3H, 4 $-OC(O)CH_3$) ppm. Spectra corresponded to previous work.¹⁹⁸

2-*N*-benzyloxycarbonylaminoethyl 2,3,4,6-tetra-*O*-acetyl- β -D-galactopyranoside, **8**



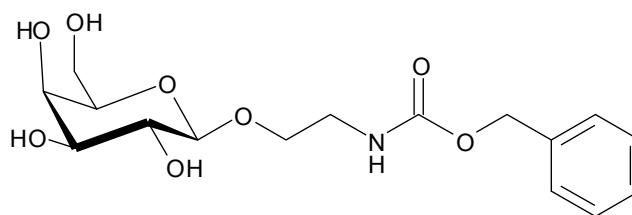
To a solution of β -D-Galactopyranose pentaacetate, (10.24 g, 26 mmol, 1 eq.) in anhydrous DCM (50 mL) under an N_2 atmosphere was added 2-*N*- benzyloxycarbonylaminoethanol (10.24 g, 52 mmol, 2 eq.) at room temperature. To this mixture was added boron trifluoride diethyl etherate (18.62 g, 16.5 mL, 131 mmol, 5 eq.) dropwise and the yellow solution was heated to reflux (50 °C) for 14 h. After which, the red solution was diluted with EtOAc (100 mL) and washed with sat. aq. $NaHCO_3$ solution (2 x 100 mL). The aq. layers were combined and washed with EtOAc (100 mL). The organic portions were combined, dried (Na_2SO_4), filtered (cotton wool) and concentrated *in vacuo*. The compound was purified by flash column chromatography (Diameter of 7 cm, 17 cm of 3 : 1 Pet. Ether / EtOAc silica media gel eluted with 3 : 1 Pet. Ether / EtOAc then a gradient was made to 1 : 1 Pet. Ether / EtOAc) to give **8** as a cloudy white viscous oil (7.51 g, 55 %). TLC ran in 1 : 1 Pet. Ether / EtOAc, visualised by UV (254 nm) and *para*-anisaldehyde, $R_f = 0.6$. 1H NMR ($CDCl_3$, 400 MHz): δ 7.30-7.40 (m, 5H, Ar-H), 5.40-5.47 (d, $J = 3.12$ Hz, 1H, H-4), 5.16-5.23 (m, 2H, H-2, H-5), 5.13 (bs, 2H, 2 x H-6), 5.00-5.06 (dd, 1H, $J_1 = 3.48$ Hz $J_2 = 10.51$ Hz, H-3), 4.46-4.48 (d, $J = 7.95$ Hz, 1H, H-1), 4.12-4.18 (m, 2H, OCH_2CH_2NH) 3.88-3.94 (m, 2H, OCH_2CH_2NH) 3.68-3.75 (m, 1H, NH) 3.35-3.52 (m, 2H, CH_2Ph) 2.18, 2.07, 2.03 and 2.01 (4s, 4 x 3H, 4 $-OC(O)CH_3$) ppm. ^{13}C NMR ($CDCl_3$, 400 MHz): δ 128.5 (Aromatic), 128.2 (Aromatic), 101.5 (C-1), 70.7 (C-3), 69.4 (OCH_2CH_2NH), 68.8 (C-2), 66.9 (C-4), 66.7(C-5 and C-6) 61.3 (OCH_2CH_2NH) 40.8 (CH_2Ph), 20.5-20.6 ($OCOCH_3$) ppm. IR (KBr): $\lambda_{max} = 3405$ (broad), 1752, 1528, 1371, 1223 (broad), 1059 (broad) cm^{-1} .

2-*N*-benzyloxycarbonylaminoethyl α -D-mannopyranoside, **9**



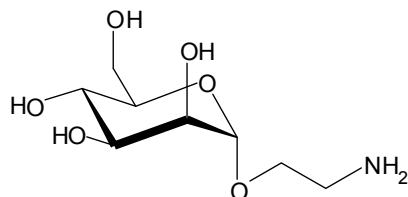
To a solution of 2-*N*-benzyloxycarbonylaminoethyl 2,3,4,6-tetra-*O*-acetyl- α -D-mannopyranoside, **7**, (7.531 g, 14.3 mmol, 1 eq.) in MeOH (200 mL) was added NaOMe (0.775 g, 14.3 mmol, 1 eq.) at room temperature and stirred for 2 h. After which the mixture was neutralised using Amberlite IRC-120 ion-exchange resin, filtered (cotton wool) and concentrated *in vacuo* to yield a clear oil as the crude product (5.285 g, 103 %). The compound was purified by flash column chromatography (Diameter of 4 cm, 10 cm of 9 : 1 DCM / MeOH silica media gel eluted with 9 : 1 DCM / MeOH) to give **9** as a white foam (4.637 g, 92 %). TLC ran in 9 : 1 DCM / MeOH, visualised by UV (254 nm) and *para*-anisaldehyde, $R_f = 0.47$. ^1H NMR (CDCl_3 , 500 MHz): δ 7.20-7.40 (m, 5H, Ar-H), 6.15 and 5.8. (2 x s, 1H, NH), 4.9-5.3 (m, 2H, CH_2Ph), 4.85 (s, 1H, H-1), 3.1-4.0 (m, 10H, H-2, H-3, H-4, H-5, 2 x H-6, $-\text{OCH}_2\text{CH}_2\text{NH}$) ppm. ^{13}C NMR (CDCl_3 , 500 MHz): δ 128.5 (Ar), 128.2 (Ar) 128.1 (Ar), 100.0 (C-1), 72.5 (C-5), 71.3 (C-3), 70.6 (C-2), 66.3-66.8 ($-\text{OCH}_2\text{CH}_2\text{NH}$, CH_2Ph , C-4), 61.0 (C-6), 40.6 ($\text{CH}_2\text{NHC(O)}$) ppm. CO not seen.

2-*N*-benzyloxycarbonylaminoethyl β-D-galactopyranoside, **10**



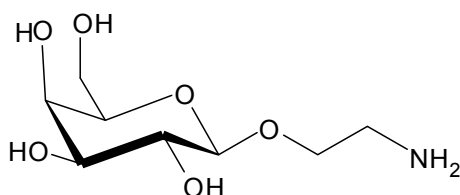
To a solution of 2-*N*-benzyloxycarbonylaminoethyl 2,3,4,6-tetra-*O*-acetyl-β-D-galactopyranoside, **8**, (1.5 g, 2.85 mmol, 1 eq.) in MeOH (50 mL) was added NaOMe (0.154 g, 2.85 mmol, 1 eq.) at room temperature and stirred for 2 h. After which the mixture was neutralised using Amberlite IRC-120 ion-exchange resin, filtered (cotton wool) and concentrated *in vacuo* to yield a clear oil. The compound was purified by flash column chromatography (Diameter of 4 cm, 15 cm of 9 : 1 DCM / MeOH silica media gel eluted with 9 : 1 DCM / MeOH) to give **10** as a white foam (0.52 g, 51 %). TLC ran in 9 : 1 DCM / MeOH, visualised by UV (254 nm) and KMnO₄, R_f = 0.7. ¹H NMR (MeOD, 400 MHz): δ 7.18-7.33 (m, 5H, Ar-H), 4.15 (d, *J* = 7.46, 1H, H-1), 3.82-3.90 (m, 1H, H-5), 3.74-3.77 (dd, *J*₁ = 3.1 Hz *J*₂ = 0.9 Hz, 1H, H-3), 3.56-3.72 (m, 2H, OCH₂), 3.28-3.52 (m, 6H, H-2, H-4, 2 x H-6 and CH₂NH) ppm. ¹³C NMR (MeOD, 400 MHz): δ 129.5 (Aromatic), 129.0 (Aromatic), 128.8 (Aromatic), 105.1 (C-1), 76.7, 74.8, 72.6, 70.3 (C-5), 69.9, 67.5 (CH₂Ph), 62.5 (C-4), 42.1 (CH₂NH) ppm. IR (KBr): λ_{max} = 3313 (broad), 2896, 1688, 1556, 1274, 1063 (broad) cm⁻¹.

2-aminoethyl α -D-mannopyranoside, **11**



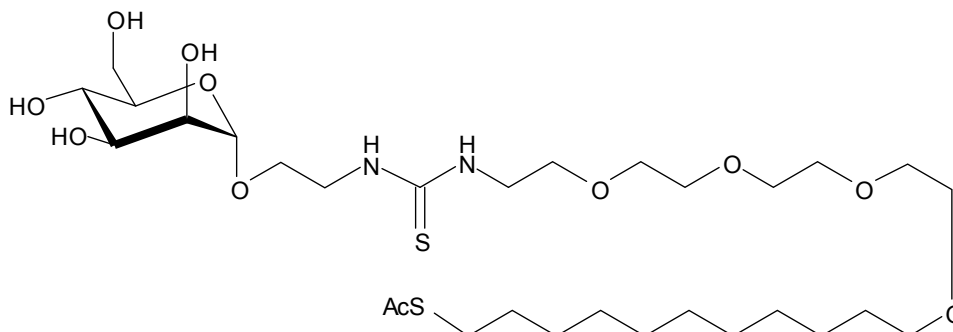
To a solution of 2-*N*-benzyloxycarbonylaminoethyl- α -D-mannopyranoside, **9**, (0.217 g, 0.601 mmol, 1 eq.) in MeOH / HCO₂H 95 : 5 (v/v) (2 mL) was purged with N₂ gas. 10 % Pd/C (0.110 g) was then added at room temperature, the reaction flask purged with N₂, followed by H₂, and stirred for 14 h under an atmosphere of H₂. After which the mixture was neutralised with NEt₃, filtered (celite), and concentrated *in vacuo* to yield **11** as a white foam (0.133 g, 98 %). TLC ran in 9 : 1 DCM /MeOH, visualised by UV (254 nm) and *para*-anisaldehyde, R_f = 0. ¹H NMR (D₂O, 500 MHz): δ 4.88 (s, 1H, H-1), 3.95-3.99 (m, 1H, H-2) 3.90 (d, *J*= 12.1 Hz, 1H, H-6), 3.81-3.86 (m, 1H, H-3), 3.73-3.80 (m, 2H, OCH₂) 3.63-3.67 (m, 2H, H-4, H-5) 3.52-3.58 (m, 1H, H-6), 2.79-2.90 (m, 2H, CH₂ND₂) ppm. ¹³C NMR (D₂O, 500 MHz): δ 99.8 (C1), 72.7 (C4/5), 70.5 (C3), 70.0 (C2), 68.8 (CH₂), 66.8 (C4/5), 60.9 (C6), 39.9 (CH₂ND₂) ppm. ESI-LRMS (MeOH) for C₈H₁₇NO₆ [M+H]⁺ Cal. 224.23, Found 224.22; [M+Na]⁺ Cal. 246.22, found 246.19. Spectra corresponded to previous work.^{198, 250}

2-aminoethyl β -D-galactopyranoside, **12**



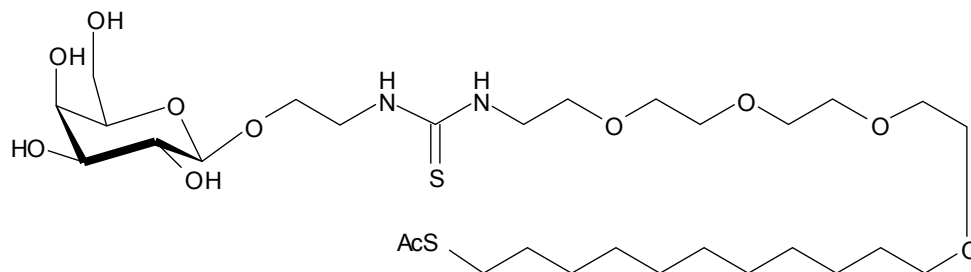
To a solution of 2-*N*-benzyloxycarbonylaminoethyl- β -D-galactopyranoside, **10**, (0.52 g, 1.45 mmol, 1 eq.) in MeOH / HCO₂H 95 : 5 (v/v) (10 mL) was purged with N₂ gas. 10 % Pd/C (0.26 g) was then added at room temperature, the reaction flask purged with N₂, followed by H₂, and stirred for 14 h under an atmosphere of H₂. After which the mixture was neutralised with NEt₃, filtered (celite), and concentrated *in vacuo* to yield **12** as a white foam (0.28 g, 97 %). TLC ran in 9 : 1 DCM /MeOH, visualised by UV (254 nm) and *para*-anisaldehyde, R_f = 0. ¹H NMR (D₂O, 400 MHz): δ 4.46(d, *J*= 7.83, 1H, H-1), 4.01-4.18 (m, 1H, 1 x OCH₂CH₂ND₂), 3.94-4.02 (m, 2H, 1 x OCH₂CH₂ND₂, H-4), 3.65-3.85 (m, 4H, 2 xH-6, H-5, H-3), 3.55-3.61 (dd, *J*₁= 7.83 Hz, *J*₂= 10.9 Hz, 1H, H-2), 3.26-3.31 (t, *J*= 5.00 Hz, 2H, OCH₂CH₂ND₂) ppm. ¹³C NMR (D₂O, 400 MHz): δ 103.4 (C-1), 75.9 (C-5), 73.2 (C-3), 71.4 (C-2), 69.2 (C-4), 66.4 (OCH₂CH₂ND₂), 61.7 (C-6), 40.2 (OCH₂CH₂ND₂) ppm. IR (KBr): λ_{\max} = 3272 (broad), 2677, 1588, 1048 (broad) cm⁻¹. ESI-LRMS (MeOH) for C₈H₁₇NO₆ [M+H]⁺ Cal. 224.23, Found 224.22; [M+Na]⁺ Cal. 246.22, found 246.19.

***N*-(ethyl α -D-mannopyranosyl), *N'*-(3,6,9,12-tetraoxa-23-thioacetyl-
tricosanyl) thiourea, **13****



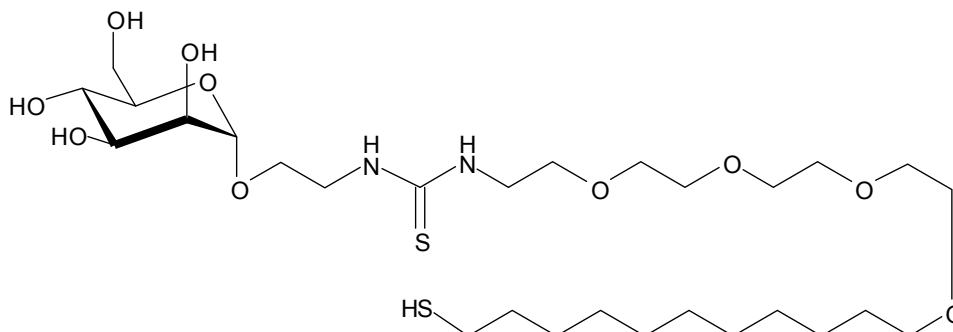
To a solution of 2-aminoethyl- α -D-mannopyranoside, **11**, (43 mg, 0.193 mmol, 1 eq.) in MeOH (0.45 mL) was added a solution of 1-*Is*othiocyanate-3,6,9,12-tetraoxa-23-thioacetyltricosane, **6**, (171 mg, 0.385 mmol, 2 eq.) in MeOH (1 mL) and the mixture was stirred at room temperature for 3 h. After which NEt_3 (0.039 g, 53 μL , 0.386 mmol, 2 eq.) was added dropwise and the mixture was stirred at room temperature for a further 2 h. After this time the reaction mixture was concentrated *in vacuo* and purified by flash column chromatography (2 cm diameter, 6 cm of 100 % DCM silica media gel, eluted with 49 : 1 DCM / MeOH with a gradient up to 8 : 2 DCM / MeOH) to give **13** as a clear oil (122 mg, 92 %). TLC ran in 9 : 1 DCM / MeOH, visualised by UV (254 nm) and *para*-anisaldehyde, $R_f = 0.58$. ^1H NMR (MeOD, 500 MHz): δ 4.78 (d, $J = 1.6$, 1H, H-1), 3.48-3.86 (m, 26H, 8 x CH_2 of tetra ethylene glycol, Man- $\text{OCH}_2\text{CH}_2\text{N}$, H-2, H-3, H-4, H-5, 2 x H-6), 3.47 (t, $J = 6.6$ Hz, 2H, TEG-O- CH_2 -alkyl), 2.86 (t, $J = 7.3$ Hz, CH_2 -SAc), 2.30 (s, 3H, SAc), 1.52-1.60 (m, 4H, TEG- CH_2 - CH_2 - C_7H_{14} - CH_2 - CH_2 -SAc), 1.28-1.40 (m, 14H, TEG- CH_2 - CH_2 - C_7H_{14} - CH_2 - CH_2 -SAc) ppm. IR (KBr): $\lambda_{\text{max}} = 2113.5, 2186.2 \text{ cm}^{-1}$. ESI-LRMS (MeOH) for $\text{C}_{30}\text{H}_{58}\text{N}_2\text{O}_{11}\text{S}_2$ $[\text{M}+\text{Na}]^+$ calc. 709.34, found 709.3; $[\text{M}+\text{K}]^+$ calc 683.3, found 683.2. Spectra correspond to previous work.¹⁹⁸

***N*-(ethyl β-D-galactopyranosyl), *N'*-(3,6,9,12-tetraoxa-23-thioacetyl-
tricosanyl) thiourea, **14****



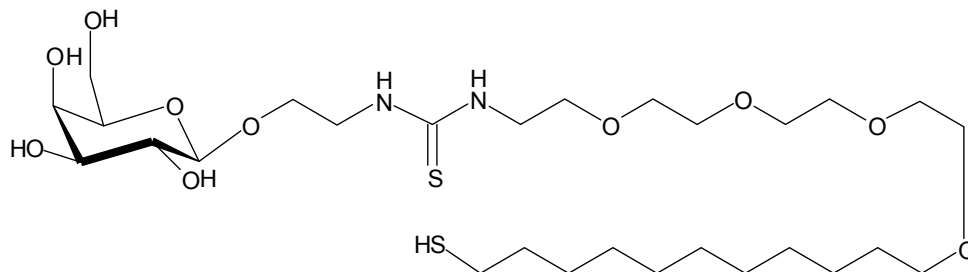
To a solution of 2-aminoethyl-β-D-galactopyranoside, **12**, (60 mg, 0.26 mmol, 1 eq.) in MeOH (3.5 mL) was added NEt₃ (0.072 mL, 51.9 mg, 0.52 mmol) and stirred for 5 mins. A solution of 1-*Iso*thiocyanate-3,6,9,12-tetraoxa-23-thioacetyltricosane, **6**, (238 mg, 0.52 mmol, 2 eq.) in MeOH (3.5 mL) was added and the mixture was stirred at room temperature for 2 h. The reaction mixture was then concentrated *in vacuo* and purified by flash column chromatography (2 cm diameter, 6 cm of 30 : 1 DCM / MeOH silica media gel, eluted with 30 : 1 DCM / MeOH with a gradient up to 10 : 1 DCM / MeOH) to give **14** as a clear oil (120 mg, 68 %). TLC ran in 9 : 1 DCM / MeOH, visualised by UV (254 nm) and mitico, R_f = 0.75. ¹H NMR (MeOD, 300 MHz): δ 4.20-4.26 (m, 1H, H-1), 3.40-3.95 (m, 28H, 8 x CH₂ of tetra ethylene glycol, Gal-OC₂H₄N, H-2, H-3, H-4, H-5, 2 x H-6, TEG-CH₂-alkyl), 2.86 (m, 2H, CH₂-SAc), 2.28 (s, 3H, SAc), 1.45-1.60 (m, 4H, TEG-CH₂-CH₂-C₇H₁₄-CH₂-CH₂-SAc), 1.20-1.40 (m, 14H, TEG-C₂H₄-C₇H₁₄-C₂H₄-SAc) ppm. ¹³C NMR (MeOD 400 MHz): δ 168.8 (C=O), 163.9 (C=S), 105.4 (C-1), 76.9, 74.9, 70.3-72.6 (m, CH₂ from tetra ethylene glycols, OCH₂CH₂N and Gal-C), 62.7, 47.8, 29.7-30.8 (m, CH₂-alkyl and CH₂S), 27.2, 9.2 (CH₂CH₂S) ppm.

***N*-(ethyl α -D-mannopyranosyl), *N'*-(3,6,9,12-tetraoxa-23-mercapto-
tricosanyl) thiourea, **1****



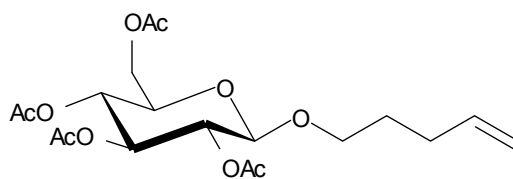
To a solution of *N*-(ethyl α -D-mannopyranosyl), *N'*-(3,6,9,12-tetraoxa-23-thioacetyl-
tricosanyl) thiourea, **13**, (40 mg, 0.058 mmol, 1 eq.) in MeOH (2 mL) was added NaOMe (4
mg, 0.077 mmol, 1.3 eq.) and the mixture was stirred at room temperature for 2 h. After
which the mixture was neutralised with Amberlite IRC-120 ion-exchange resin, filtered
(celite) and concentrated in vacuo to give a crude yield of 34 mg (91 %). The compound was
purified by a Sephadex column (2 cm diameter, 28 cm of 9 : 1 DCM / MeOH LH-20
Sephadex gel, eluted with 9 : 1 DCM / MeOH) to give **1** as a clear oil (32 mg, 91 %). ^1H NMR
(D_2O , 500 MHz): δ 4.89 (s, 1H, H-1), 3.40-4.00 (m, 28H, H-2, H-3, H-4, H-5, 2 x H-6,
 $\text{OCH}_2\text{CH}_2\text{NH}$ -, TEGCH_2 -alkyl, 8 x CH_2 of tetra ethylene glycol,), 2.72 (bs) and 2.54 (t, J =
7.29 Hz) (2H, combination of CH_2 -SH and $\text{CH}_2\text{S-S}$), 1.58-1.76 (m, 4H, $\text{TEG-CH}_2\text{-CH}_2$ -
 $\text{C}_7\text{H}_{14}\text{-CH}_2\text{-CH}_2\text{-SAC}$), 1.26-1.48 (m, 14H, $\text{TEG-C}_2\text{H}_4\text{-C}_7\text{H}_{14}\text{-C}_2\text{H}_4\text{-SH}$) ppm. IR (KBr): λ_{max}
= 3340 (broad), 2925, 2855, 1633, 1095 (broad). ESI-LRMS (MeOH) for $\text{C}_{28}\text{H}_{56}\text{N}_2\text{O}_{10}\text{S}_2$
 $[\text{M}+\text{Na}]^+$ Cal. 667.33, found 667.2; $[\text{M}+\text{K}]^+$ Cal. 683.3, found 683.2. Spectra correspond to
previous work.¹⁹⁸

***N*-(ethyl β-D-galactopyranosyl), *N'*-(3,6,9,12-tetraoxa-23-mercapto-
tricosanyl) thiourea, **2****



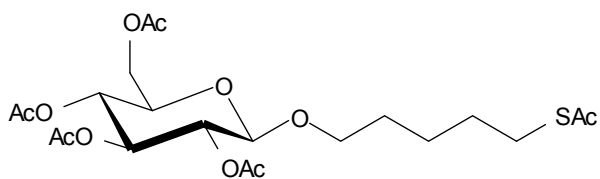
To a solution of *N*-(ethyl β-D-galactopyranosyl), *N'*-(3,6,9,12-tetraoxa-23-thioacetyl-tricosanyl) thiourea, **14**, (120 mg, 0.175 mmol, 1 eq.) in MeOH (5 mL) was added NaOMe (10 mg, 0.175 mmol, 1 eq.) and the mixture was stirred at room temperature for 20 mins. After which the mixture was neutralised with Amberlite IRC-120 ion-exchange resin, filtered (celite) and concentrated *in vacuo*. The compound was purified by flash column chromatography (2 cm diameter, 9 cm of 19 : 1 DCM / MeOH silica media gel, eluted with 9 : 1 DCM / MeOH) to give **2** as a clear oil (71 mg, 63 %). ¹H NMR (MeOD, 300 MHz): δ 4.37 (d, *J*= 6.8 Hz, 1H, H-1), 3.55-4.10 (m, 28H, H-2, H-3, H-4, H-5, 2 x H-6, OCH₂CH₂NH-, 8 x CH₂ of tetra ethylene glycol, TEG-O-CH₂-alkyl), 2.80 and 2.60 (t, *J*= 6.9 Hz, 2H, combination of CH₂-SH and CH₂S-S-), 1.60-1.85 (m, 4H, TEG-CH₂-CH₂-C₇H₁₄-CH₂-CH₂-SH), 1.35-1.55 (m, 14H, TEG-C₂H₄-C₇H₁₄-C₂H₄-SH) ppm. ¹³C NMR (MeOD, 400 MHz): δ 105.4 (C-1), 76.9, 74.5, 70.3-72.6 (m, CH₂ from tetra ethylene glycols, OCH₂CH₂N and Gal-C), 62.7, 39.9 (CH₂S), 35.2, 30-31 (m, CH₂-alkyl), 29.4, 27.2, 25.0 ppm. C=S not seen. ESI-LRMS (MeOH) for C₂₈H₅₆N₂O₁₀S₂ [M+Na]⁺ Cal. 667.33, found 667.31.

4-pentenyl tetra-*O*-acetyl- β -D-glucopyranoside, **15**



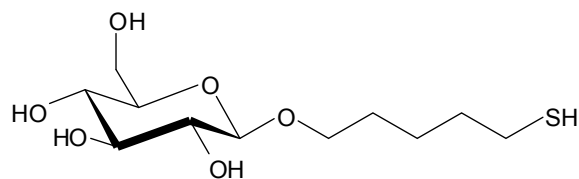
To a dry round-bottomed flask was added β -D-Glucopyranose pentaacetate (8 g, 20.5 mmol, 1 eq.) which was then dissolved in anhydrous DCM (40 mL) under an Ar atmosphere. To this solution was added 4-penten-1-ol (7.061 g, 8.466 mL, 81.980 mmol, 4 eq.) followed by dropwise addition of boron trifluoride diethyl etherate (14.544 g, 12.814 mL, 102.474 mmol, 5 eq.) and the brown mixture was stirred at room temperature under an Ar atmosphere for 5 h. After which, the orange / brown mixture was neutralised with a sat. aq. solution of NaHCO_3 . The solution was then diluted with DCM up to the same volume of the aq. solution. The reaction mixture was then washed with sat. aq. NaHCO_3 (2 250 x mL) followed by brine (250 mL). The organic layers were then combined, filtered (sintered glass) and concentrated *in vacuo* to give the crude product as an orange oil which was purified by column chromatography (7 cm diameter, 16 cm 4 : 1 Hexanes / EtOAc with a gradient to 3 : 1 Hexanes / EtOAc) gave pure **15** as white crystals (2.848 g, 34 %). TLCs ran in 2 : 1 Hexanes / EtOAc visualised by UV (254 nm) and *para*-anisaldehyde, $R_f = 0.5$. ^1H NMR (MeOD, 500 MHz): δ 5.82 (m, 1H, $\text{CH}_2\text{-CH}=\text{CH}_2$), 5.25 (t, 1H, $J = 9.52$ Hz, H3), 4.86-5.04 (3m, 4H, H4, H2, $\text{CH}=\text{CH}_2$), 4.64 (d, 1H, $J = 8.00$ Hz, H1), 4.27 (dd, 1H, $J = 12.32$, $J = 4.64$ Hz, H6), 4.12 (dd, 1H, $J = 12.28$, $J = 2.44$ Hz, H6), 3.82-3.88 (m, 2H, $\text{CH}_2\text{CH}=\text{CH}_2$), 3.51-3.58 (m, 1H, H5), 2.07-2.13 (m, 2H, $\text{OCH}_2\text{-C}_4\text{H}_7$), 2.05, 2.02, 2.00, 1.96 (4s, 4 x 3H, 4 -OCOCH_3), 1.61-1.69 (m, 2H, $\text{-OCH}_2\text{CH}_2\text{CH}_2\text{CHCH}_2$) ppm.

5-thioacetylpentyl tetra-*O*-acetyl- β -D-glucopyranoside, **16**



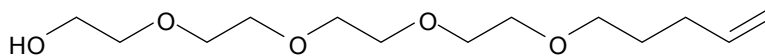
4-pentenyl tetra-*O*-acetyl- β -D-Glucopyranoside, **15**, (2.818 g, 6.767 mmol, 1 eq.) was dissolved in anhydrous THF (60 mL) and flushed with N₂ gas. To this solution was added thioacetic acid (1.93 mL, 2.060 g, 27.069 mmol, 4 eq.) followed by AIBN (1 spatula). The mixture was then heated to reflux at 75 °C under N₂ gas for 22 h. After which, the mixture was allowed to cool to room temperature and diluted with EtOAc (75 mL). Sat. aq. NaHCO₃ solution was added until a pH of 7 was achieved (125 mL). The organic layer was extracted and washed with sat. aq. NaHCO₃ (125 mL) followed by brine (125 mL). The organic layers were combined, dried (Na₂SO₄), filtered (celite, sintered glass) and concentrated *in vacuo*. The crude product (4.023 g, 120 %, pale yellow oil) was purified by column chromatography (diameter of 7 cm, 14 cm of 2 : 1 Hexanes / EtOAc of silica media gel, eluted with 2 : 1 Hexanes / EtOAc) to give **16** as a pale yellow oil (2.945 g, 88 %). TLCs were ran in 3 : 2 Hexanes / EtOAc visualised by UV (254 nm) and *para*-anisaldehyde, R_f = 0.52. ¹H NMR (CDCl₃, 500 MHz): δ 5.20 (t, *J* = 9.5 Hz, 1H, H-3), 5.08 (t, *J* = 9.5 Hz, 1H, H-4), 4.96 (t, *J* = 8.0 Hz, 1H, H-2), 4.47 (d, *J* = 8.0 Hz, 1H, H-1), 4.25 (dd, *J* = 12.28 Hz, 4.73 Hz, 1H, H-6), 4.12 (dd, *J* = 12.26 Hz, 2.60 Hz, 1H, H-6), 3.83-3.90 (dt, *J* = 9.63 Hz, 6.20 Hz, 1H, 1 x OCH₂), 3.66-3.71 (m, 1H, H-5), 3.44-3.50 (dt, *J* = 9.63 Hz, 6.60 Hz, 1H, 1 x OCH₂), 2.85 (t, *J* = 7.30 Hz, 2H, CH₂SAc), 2.33 (s, 3H, SC(O)CH₃), 2.08, 2.05, 2.02, 2.01 (4s, 12H, 4 x -OC(O)CH₃), 1.53-1.65 (m, 4H, OCH₂CH₂CH₂CH₂CH₂SAc), 1.32-1.45 (m, 2H, OC₂H₄CH₂C₂H₄SAc) ppm.

5-thiopentyl β -D-glucopyranoside, **3**



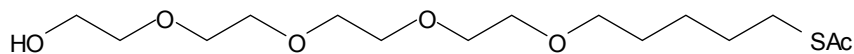
5-thioacetylpentyl tetra-*O*-acetyl- β -D-glucopyranose, **16**, (2.885 g, 5.857 mmol, 1 eq.) was dissolved in MeOH (90 mL) to which was added NaOMe (0.333 g, 6.166 mmol, 1.05 eq.) and the mixture stirred at room temperature. Immediately upon addition of NaOMe the solution was observed to have changed from a clear pale yellow to a clear pale green then back to a clear pale yellow colour. The pH was observed to be 8. After 2 h, the reaction mixture was neutralised with Amberlite IR-120 ion-exchange resin, filtered, and concentrated *in vacuo* to give the crude product (1.645 g, 99 %). Purification by column chromatography (diameter of 4 cm, 10 cm of 19 : 1 DCM / MeOH silica media gel, eluted with 19 : 1 DCM / MeOH) to give pure **3** (1.258, 76 %) as a clear viscous oil. TLCs were ran in 1 : 1 EtOAc / Hexanes visualised by UV (254 nm) and *para*-anisaldehyde, $R_f = 0.3$. ^1H NMR (D_2O , 500 MHz): δ 4.47 (d, $J = 8.02$ Hz, 1H, H-1), 3.90-3.97 (m, 2H, 2x H-6), 3.66-3.76 (m, 2H, OCH_2), 3.44-3.52 (m, 2H, H-3 and H-5), 3.36-3.41 (m, 1H, H-4), 3.24-3.29 (m, 1H, H-2), 2.57 (t, $J = 7.20$, 2H, CH_2SH) 1.61-1.69 (m, 4H, OCH_2CH_2 and $\text{CH}_2\text{CH}_2\text{SH}$), 1.43-1.51 (m, 2H, $\text{OC}_2\text{H}_4\text{CH}_2\text{C}_2\text{H}_4\text{SH}$) ppm. ^{13}C NMR (D_2O , 500 MHz): δ 102.6 (C-1), 76.3 (C-4), 76.2 (C-2), 73.6 (OCH_2), 70.8 (C-3), 61.2 (C-6), 61.1 (C-5), 33.1 (OCH_2CH_2), 28.6 ($\text{CH}_2\text{CH}_2\text{S}$), 24.3 (CH_2S), 24.0 ($\text{OC}_2\text{H}_4\text{CH}_2\text{C}_2\text{H}_4\text{S}$) ppm. IR (KBr): $\lambda_{\text{max}} = 3391$ (broad), 2932, 1429, 1379, 1078, 1035 cm^{-1} . ESI-LRMS (MeOH) for $\text{C}_{11}\text{H}_{22}\text{O}_6\text{S}$ $[\text{M}+\text{Na}]^+$ Cal. 305.35, found 305.18.

pent-1-en-5-yltetra(ethylene glycol), **17**



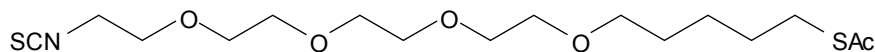
NaOH, as a 50% aq. Solution (2.03 mL, 1.01 g, 25.3 mmol, 1eq) was added dropwise to tetraethylene glycol (21.9 mL, 24.6 g, 126 mmol, 5 eq) at room temperature. Reaction mixture was heated to 110 °C (reflux) for 30 mins, after which, the reaction mixture was allowed to cool to room temperature and 5-bromo-1-pentene (3.77 g, 3 mL, 25.3 mmol, 1 eq) was added dropwise. Reaction mixture was heated to 110 °C for 14 h. After cooling to room temperature, the reaction mixture was diluted with DCM (25 mL) and washed with brine (2 x 100 mL). Aq. phase washed with DCM (100 mL). Organic layers combined, dried (Na₂SO₄), filtered (cotton) and concentrated *in vacuo*. Purification by column chromatography (diameter of 4 cm, 20 cm of EtOAc silica media gel, eluted with EtOAc) to give pure **17** (4.27 g, 64 %) as a clear yellow viscous oil. TLCs were ran in 20 : 1 EtOAc / MeOH visualised by UV (254 nm) and KMnO₄, R_f = 0.53. ¹H NMR (CDCl₃, 300 MHz): δ 5.70-5.90 (complicated splitting pattern, 1H, CH=CH₂), 4.90-5.10 (m, 2H, CH=CH₂), 3.50-3.75 (m, 16H, OCH₂CH₂O), 3.40-3.50 (t, *J*= 6.8 Hz, 2H, OCH₂C₄H₇), 2.70 (bs, OH), 2.05-2.15 (m, 2H, OCH₂CH₂C₃H₅), 1.60-1.73 (m, 2H, C₂H₄CH₂C₂H₃) ppm.

17-thioacetyl-3,6,9,12-tetraoxaheptadecan-1-ol, **18**



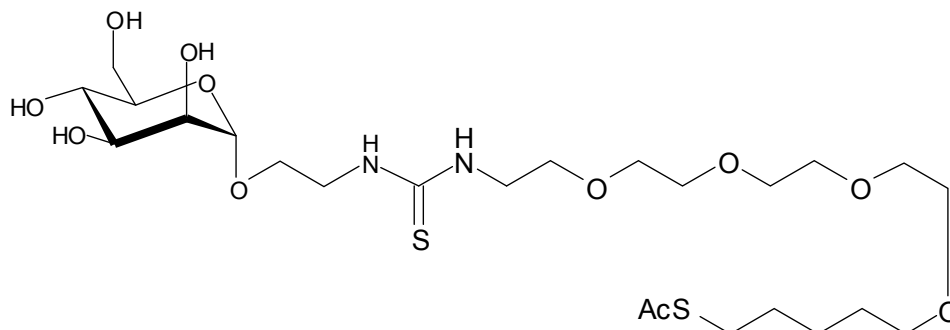
Pent-1-en-5-yltetra(ethylene glycol), **17**, (4.27 g, 16.3 mmol, 1 eq.) was dissolved in dry THF (60 mL) to which was added thioacetic acid (4.65 mL, 4.96 g, 65 mmol, 4 eq) dropwise at room temperature followed by AIBN (cat, 1 spatula). The mixture was then heated to reflux (80 °C). More AIBN was added (cat, 1 spatula) after 6, 24 and 28 hours. After 32 h the reaction mixture was allowed to cool to room temperature, was diluted with EtOAc (100 mL) to which was added sat. aq. NaHCO₃ solution until pH 7. Mixture was separated and the organic phase dried (Na₂SO₄), filtered (cotton), and concentrated *in vacuo*. Purification by column chromatography (diameter of 4 cm, 24 cm of EtOAc silica media gel, eluted with EtOAc) to give pure **18** (3.90 g, 71 %) as a clear yellow viscous oil. TLCs were ran in 20 : 1 EtOAc visualised by UV (254 nm) and mitico, R_f = 0.44. ¹H NMR (CDCl₃, 300 MHz): δ 3.55-3.80 (m, 16H, OCH₂CH₂O), 3.47 (t, *J*= 6.6 Hz, 2H, OCH₂C₄H₈), 2.89 (t, *J*= 7.3 Hz, 2H, CH₂SAc), 2.35 (s, 3H, SAc), 1.55-1.70 (m, 4H, OCH₂CH₂CH₂CH₂CH₂SAc), 1.40-1.50 (m, 2H, OC₂H₄CH₂C₂H₄SAc) ppm. IR (KBr): λ_{max} = 3436 (broad), 2933, 2869, 1691, 1125 cm⁻¹.

1-Isothiocyanate-3,6,9,12-tetraoxa-17-thioacetylheptadecane, **19**



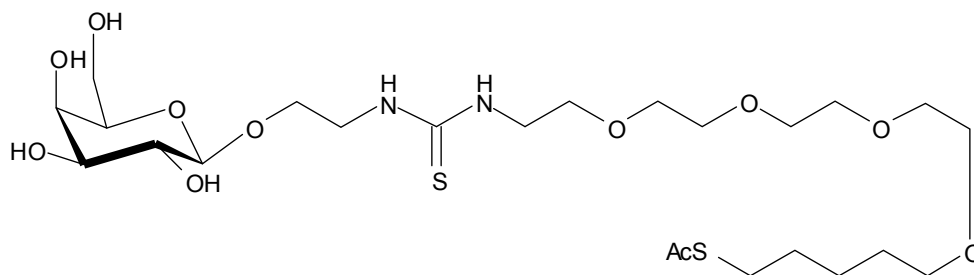
To a solution of 17-thioacetyl-3,6,9,12-tetraoxaheptadecan-1-ol, **18**, (2.73 g, 8.56 mmol, 1 eq.) in DMF (10.2 mL) was added PPh₃ (3.3 g, 12.6 mmol, 1.5 eq.) followed by NaN₃ (1.3 g, 20 mmol, 2.5 eq.). The mixture was then stirred at room temperature for 5 mins under an N₂ atmosphere. After which BrCCl₃ (2.54 g, 1.25 mL, 12.9 mmol, 1.6 eq.) was added dropwise and the cloudy yellow mixture was stirred at 47 °C for 14 h. The reaction mixture was then heated to 100 °C for 6 h following the addition of a further addition of PPh₃ NaN₃ (1 spatula each) followed by CBrCl₃ (1 mL). The reaction mixture was then diluted with Et₂O (250 mL) and washed with H₂O (2 x 100 mL). The organic layers were combined, dried (Na₂SO₄), filtered (cotton) and concentrated *in vacuo*. The orange oil was then dissolved in toluene (35 mL) to which was added PPh₃ (3.3 g, 12.8 mmol, 1.5 eq.) and CS₂ (13 g, 10.3 mL, 171 mmol, 20 eq.) dropwise. The mixture was heated to 110 °C with a condenser attached. After 14 h the reaction mixture was allowed to cool to room temperature, concentrated *in vacuo* and purified by flash column chromatography (7 cm diameter, 20 cm of 1 : 1 Pet. Ether / EtOAc silica media gel, eluted with 1 : 1 Pet. Ether / EtOAc with a gradient to 9 : 1 EtOAc / MeOH) to give **19** as a clear yellow oil (2.35 g, 72 %) TLC ran in EtOAc, visualised by UV (254 nm) and KMnO₄, R_f = 0.38. ¹H NMR (CDCl₃, 300 MHz): δ 3.60-3.75 (m, 14H, 7 x OCH₂CH₂O), 3.54-3.60 (m, 2H, TEG-O-CH₂-alkyl), 3.44 (t, *J*=6.8 Hz, 2H, NCS-CH₂), 2.87 (t, *J*= 7.1 Hz, 2H, CH₂-SAc), 2.31 (s, 3H, SAc), 1.52-1.65 (m, 4H, TEG-CH₂-CH₂-CH₂-CH₂-SAC), 1.23-1.37 (m, 2H, TEG-C₂H₄-CH₂-C₂H₄-SAC) ppm. IR (KBr): λ_{max} = 2113.5, 2186.2 cm⁻¹.

N*-(ethyl α -D-mannopyranosyl), *N'*-(3,6,9,12-tetraoxa-17-thioacetylheptadecane) thiourea, **20*



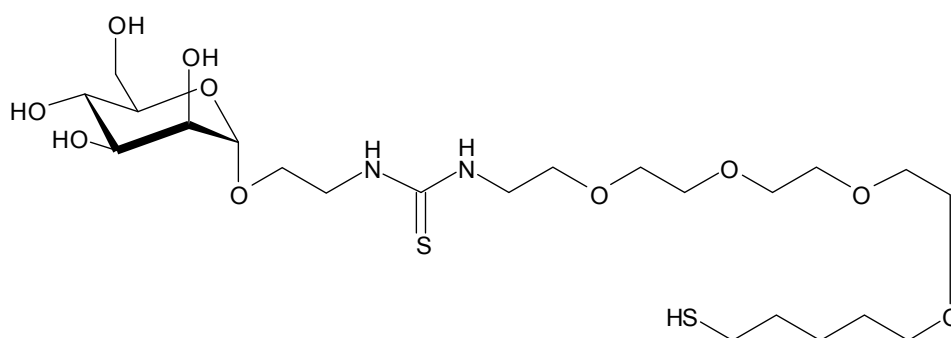
To a solution of 2-aminoethyl α -D-mannopyranoside, **11**, (120 mg, 0.536 mmol, 1 eq.) in MeOH (7 mL) was added NEt₃ (108 mg, 0.15 mL, 1.075 mmol, 2 eq) and stirred for 5 mins. After which, a solution of 1-Isothiocyanate-3,6,9,12-tetraoxa-17-thioacetylheptadecane, **19**, (408 mg, 1.075 mmol, 2 eq.) in MeOH (7 mL) and the mixture was stirred at room temperature for 24 h. The reaction mixture was concentrated *in vacuo* and purified by flash column chromatography (4 cm diameter, 14 cm of DCM silica media gel, eluted with 25 : 1 DCM / MeOH with a gradient up to 8 : 2 DCM / MeOH) to give **20** as a clear oil (260 mg, 80 %). TLC ran in 9 : 1 DCM / MeOH, visualised by UV (254 nm) and *para*-anisaldehyde, R_f = 0.58. ¹H NMR (CDCl₃, 300 MHz): δ 4.86 (s, 1H, H-1), 3.46-4.00 (m, 26H, 8 x CH₂ of tetra ethylene glycol, Man-OCH₂CH₂N, H-2, H-3, H-4, H-5, 2 x H-6), 3.35-3.45 (m, 2H, TEG-CH₂-alkyl), 2.86 (t, *J* = 7.1 Hz, 2H, CH₂-SAc), 2.28 (s, 3H, SAc), 1.47-1.65 (m, 4H, TEG-CH₂-CH₂-CH₂-CH₂-CH₂-SAc), 1.20-1.40 (m, 2H, TEG-C₂H₄-CH₂-C₂H₄-SAc) ppm. ¹³C NMR (MeOD 400 MHz): δ 100.8 (C-1), 73.8, 70.1-71.6 (m, CH₂ from tetra ethylene glycols, OCH₂CH₂N and Man-C), 69.7, 68.4, 67.6, 66.4, 61.9, 38.7 (CH₂S), 34.6, 28.7-29.7 (m, CH₂-alkyl), 25.1-25.6 (m) ppm. C=S and C=O not seen.

***N*-(ethyl β-D-galactopyranosyl), *N'*-(3,6,9,12-tetraoxa-17-thioacetyl-
heptadecane) thiourea, **21****



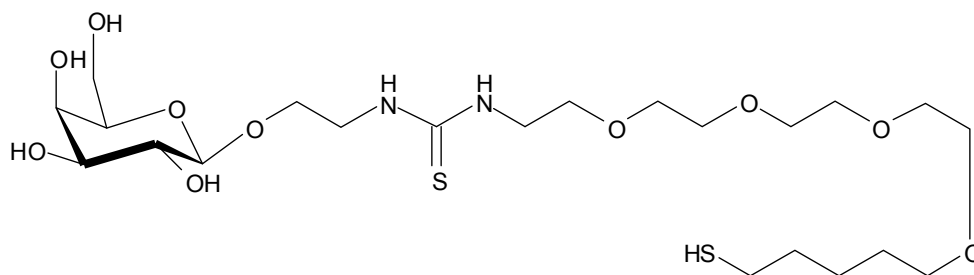
To a solution of 2-aminoethyl β-D-galactopyranoside, **12**, (69 mg, 0.309 mmol, 1 eq.) in MeOH (4 mL) was added NEt_3 (63 mg, 0.09 mL, 0.618 mmol, 2 eq) and stirred for 5 mins. After which, a solution of 1-*Iso*thiocyanate-3,6,9,12-tetraoxa-17-thioacetylheptadecane, **19**, (257 mg, 0.664 mmol, 2.1 eq.) in MeOH (4 mL) and the mixture was stirred at room temperature for 24 h. The reaction mixture was concentrated *in vacuo* and purified by flash column chromatography (4 cm diameter, 6 cm of 30 : 1 DCM / MeOH silica media gel, eluted with 25 : 1 DCM / MeOH with a gradient up to 8 : 2 DCM / MeOH) to give **21** as a clear oil (150 mg, 71 %). TLC ran in 9 : 1 DCM / MeOH, visualised by UV (254 nm) and *para*-anisaldehyde, $R_f = 0.58$. $^1\text{H NMR}$ (CDCl_3 , 300 MHz): δ 4.27 (d, $J = 7.3$ Hz, 1H, H-1), 3.40-4.10 (m, 28H, 8 x CH_2 from tetra ethylene glycol, Gal- $\text{OCH}_2\text{CH}_2\text{N}$, H-2, H-3, H-4, H-5, 2 x H-6, TEG- CH_2 -alkyl), 2.86 (t, $J = 7.3$ Hz, 2H, CH_2SAc), 2.32 (s, 3H, SAc), 1.50-1.63 (m, 4H, $\text{OCH}_2\text{CH}_2\text{CH}_2\text{CH}_2\text{CH}_2\text{S}$), 1.35-1.50 (m, 2H, $\text{OC}_2\text{H}_4\text{CH}_2\text{C}_2\text{H}_4\text{S}$) ppm.

N*-(ethyl α -D-mannopyranosyl), *N'*-(3,6,9,12-tetraoxa-17-mercaptoheptadecane), **22*



To a solution of *N*-(ethyl α -D-mannopyranosyl), *N'*-(3,6,9,12-tetraoxa-17-thioacetylheptadecane) thiourea, **20**, (95.5 mg, 0.158 mmol, 1 eq.) in MeOH (2.4 mL) was added NaOMe (1 spatula) and the mixture was stirred at room temperature for 2 h. After which the mixture was neutralised with Amberlite IRC-120 ion-exchange resin, filtered (celite) and concentrated *in vacuo*. The compound was purified by flash column chromatography (4 cm diameter, 6 cm of 9 : 1 DCM / MeOH silica media gel, eluted with 9 : 1 DCM / MeOH) to give **22** as a clear viscous oil (34 mg, 39 %). TLC ran in 9 : 1 DCM / MeOH, visualised by UV (254 nm) and *para*-anisaldehyde, $R_f = 0.58$. $^1\text{H NMR}$ (CD_3OD , 300 MHz): δ 5.55 (s, 1H, H-1), 3.50-3.98 (m, 28H, 8 x CH_2 of tetra ethylene glycol, Man- $\text{OCH}_2\text{CH}_2\text{N}$, H-2, H-3, H-4, H-5, 2 x H-6, TEG- CH_2 -alkyl), 2.77 and 2.57(m, 2H, combination of $\text{CH}_2\text{-S-SCH}_2$ and $\text{CH}_2\text{-SH}$), 1.43-1.72 (m, 4H, TEG- $\text{CH}_2\text{-CH}_2\text{-CH}_2\text{-CH}_2\text{-CH}_2\text{-S}$), 1.30-1.42 (m, 2H, TEG- $\text{C}_2\text{H}_4\text{-CH}_2\text{-C}_2\text{H}_4\text{-S}$) ppm.

N*-(ethyl β-D-galactopyranosyl), *N'*-(3,6,9,12-tetraoxa-17-mercaptoheptadecane) thiourea, **23*



To a solution of *N*-(ethyl β-D-galactopyranosyl), *N'*-(3,6,9,12-tetraoxa-17-thioacetylheptadecane) thiourea, **21**, (72 mg, 0.119 mmol, 1 eq.) in MeOH (1.8 mL) was added NaOMe (1 spatula) and the mixture was stirred at room temperature for 2 h. After which the mixture was neutralised with Amberlite IRC-120 ion-exchange resin, filtered (celite) and concentrated *in vacuo*. The compound was purified by flash column chromatography (4 cm diameter, 6 cm of 9 : 1 DCM / MeOH silica media gel, eluted with 9 : 1 DCM / MeOH) to give **23** as a clear viscous oil (40 mg, 60 %). TLC ran in 9 : 1 DCM / MeOH, visualised by UV (254 nm) and *para*-anisaldehyde, $R_f = 0.58$. $^1\text{H NMR}$ (MeOD, 400 MHz): δ 4.17 (d, $J = 7.3$ Hz, 1H, H-1), 3.38-3.90 (m, 28H, H-2, H-3, H-4, H-5, 2 x H-6, $\text{OCH}_2\text{CH}_2\text{NH}$ -, TEGCH_2 -alkyl, 8 x CH_2 of tetra ethylene glycol.), 2.63 (t, $J = 7.3$ Hz) and 2.44 (t, $J = 7.5$ Hz) (2H, combination of $\text{CH}_2\text{-SH}$ and $\text{CH}_2\text{S-S}$ -), 1.58-1.67 (m, 2H, $\text{TEG-OCH}_2\text{CH}_2\text{C}_3\text{H}_6$), 1.48-1.58 (m, 2H, $\text{CH}_2\text{CH}_2\text{SH}$), 1.35-1.45 (m, 2H, $\text{TEG-C}_2\text{H}_4\text{-CH}_2\text{-C}_2\text{H}_4\text{-SH}$) ppm.

7.1 General Protocol for Nanoparticle Synthesis

Experimental Procedure for nanoparticle synthesis

HAuCl₄·4H₂O in water (25 mM, 1eq.) was added to ligand solution in MeOH (12 mM, 3 eq. total). The mixture was shaken for 5 mins at 200 rpm, 25 °C. Following this, a methanolic NaBH₄ solution was added (1 M, 27 eq.) in four equal portions, with rapid shaking. The reaction mixture turned an instant dark brown colour and was shaken for a further 2 h at 200 rpm, 25 °C. After this period, the supernatant was extracted for further analysis (see below). The aggregates were resuspended in water and dialysed exhaustively against water. After this, the aqueous solution was centrifuged at 13 000 rpm, the supernatant extracted and lyophilised to yield the GNPs as a brown amorphous powder. The GNPs were characterised by 400 MHz ¹H NMR in D₂O, IR (KBr), elemental analysis and TEM.

The reaction mixture supernatant was concentrated *in vacuo* and redissolved in 1 : 1 DCM / MeOH. The mixture was then filtered (cotton wool) and purified using a Sephadex column (2 cm diameter, 28 cm of 9 : 1 DCM / MeOH LH-20 Sephadex gel, eluted with 9 : 1 DCM / MeOH).

GNP-1: Reaction of **3** (49.2 mg, 0.17 mmol) with HAuCl₄ (19.7 mg, 0.06 mmol) gave **GNP-1** (18.4 mg, 5 × 10⁻⁴ mmol) as a dark brown powder. Average diameter and no. of Au atoms: 1.34 nm, 100; ¹H NMR (400 MHz, D₂O): δ = 4.35-4.55 (s, br), 3.25-4.10 (m, br), 1.40-2.10 (m, br); UV/Vis (H₂O): λ = 494 nm (SPR band); IR (KBr): ν = 3360 (br), 2924, 1384, 1078, 1034 cm⁻¹; elemental analysis calculated (%) for (C₁₁H₂₁O₆S)₄₁Au₁₀₀ (31 222 g/mol): C 17.33, H 2.78; found C 17.39, H 2.94

GNP-5: Reaction of **1** (46.3 mg, 0.07 mmol) with HAuCl₄ (8.1 mg, 0.02 mmol) gave **GNP-5** (13.4 mg, 1.7 × 10⁻⁴ mmol) as a dark brown powder. Average diameter and no. of Au atoms: 1.36 nm, 116; UV/Vis (H₂O): λ = 493 nm (w, br, SPR band); IR (KBr): ν = 3373 (broad), 2915, 2851, 1634, 1558, 1465, 1349, 1296, 1096 (broad) cm⁻¹; elemental analysis calculated (%) for (C₂₈H₅₆N₂O₁₀S₂)₈₈Au₁₁₆ (79 461 g/mol): C, 37.21 H, 6.14 N, 3.10; found C 37.23, H 6.13, N 2.94

GNP-10: Reaction of **2** (36 mg, 0.06 mmol) with HAuCl_4 (6.3 mg, 0.018 mmol) gave **GNP-10** (11.3 mg, 1.98×10^{-4} mmol) as a light brown powder. Average diameter and no. of Au atoms: 1.24 nm, 70; ^1H NMR (400 MHz, D_2O): $\delta = 4.30\text{-}4.40$ (s, br), $3.20\text{-}4.10$ (m, br), $1.00\text{-}1.80$ (m, br) ppm; UV/Vis (H_2O): $\lambda = 491$ nm (w, br, SPR band); IR (KBr): $\nu = 3432$ (broad), 2921, 2852, 2360, 1690, 1642, 1098 cm^{-1} ; elemental analysis calculated (%) for $(\text{C}_{28}\text{H}_{56}\text{N}_2\text{O}_{10}\text{S}_2)_{67}\text{Au}_{70}$ (56 890 g/mol): C, 39.57 H, 6.53 N, 3.30; found C, 39.58 H, 6.55 N, 3.31

Preparation of GNP-2 to GNP-4 and GNP-11: Mother solutions of the Man-mixed-SH (**1**) or Man-mixed(s)-SH (**22**) ligands in MeOD and Glc-C5-SH (**3**) in MeOD were made. Reaction solutions of the required ratios were made and confirmed by ^1H NMR (integrations of the anomeric protons) at 400 MHz, 323 K. The MeOD solutions were then concentrated *in vacuo* then redissolved in MeOH to give the required concentrations. Procedure is then as described above.

GNP-2: Reaction of **1** (26 mg, 0.04 mmol) and **3** (102 mg, 0.36 mmol) with HAuCl_4 (45.7 mg, 0.134 mmol) gave **GNP-2** (32.4 mg, 0.006 mmol) as a dark brown powder. Average diameter and no. of Au atoms: 1.49 nm, 125; ^1H NMR (400 MHz, D_2O): $\delta = 4.35\text{-}4.50$ (s, br), $3.20\text{-}4.05$ (m, br), $1.30\text{-}2.10$ (m, br) ppm; UV/Vis (H_2O): $\lambda = 489$ nm (w, br, SPR band); IR (KBr): $\nu = 3401$ (broad), 2923, 1638, 1078 (broad) cm^{-1} ; elemental analysis calculated (%) for $(\text{C}_{28}\text{H}_{56}\text{N}_2\text{O}_{10}\text{S}_2)_{11}(\text{C}_{11}\text{H}_{21}\text{O}_6\text{S})_{72}\text{Au}_{125}$ (51 937 g/mol): C 24.41, H 4.13, N 0.55; found C 25.41, H 4.71, N 0.55; Presentation density of **1**: 13 %

GNP-3: Reaction of **1** (44 mg, 0.07 mmol) and **3** (57 mg, 0.20 mmol) with HAuCl_4 (30.7 mg, 0.09 mmol) gave **GNP-3** (26.25 mg, 4×10^{-4} mmol) as a dark brown powder. Average diameter and no. of Au atoms: 1.66 nm, 140; ^1H NMR (400 MHz, D_2O): $\delta = 4.35\text{-}4.50$ (s, br), $3.25\text{-}4.05$ (m, br), $1.25\text{-}1.90$ (m, br) ppm; UV/Vis (H_2O): $\lambda = 488$ nm (w, br, SPR band); IR (KBr): $\nu = 3372$ (broad), 2922, 1585, 1384, 1082 (broad) cm^{-1} ; elemental analysis calculated (%) for $(\text{C}_{28}\text{H}_{56}\text{N}_2\text{O}_{10}\text{S}_2)_{24}(\text{C}_{11}\text{H}_{21}\text{O}_6\text{S})_{72}\text{Au}_{140}$ (63 255 g/mol): C 27.77 H 4.51, N 1.06; found C 27.81, H 4.64, N 0.92; Presentation density of **1**: 25 %

GNP-4: Reaction of **1** (32.6 mg, 0.05 mmol) and **3** (14 mg, 0.05 mmol) with HAuCl_4 (11.5 mg, 0.03 mmol) gave **GNP-4** (12.31 mg, 1.9×10^{-4} mmol) as a dark brown powder. Average diameter and no. of Au atoms: 1.61 nm, 140; ^1H NMR (400 MHz, D_2O): $\delta = 4.75\text{-}4.85$ (s, br),

3.20-4.00 (m, br), 1.15-1.75 (m, br) ppm; UV/Vis (H₂O): SPR band not seen; IR (KBr): $\nu = 3387$ (broad), 2922, 2852, 1634, 1580, 1506, 1456, 1350, 1298, 1096 (broad) cm⁻¹; elemental analysis calculated (%) for (C₂₈H₅₆N₂O₁₀S₂)₃₉(C₁₁H₂₁O₆S)₄₆Au₁₄₀ (65 596 g/mol): C 29.23 H 4.78, N 1.67; found C 29.12, H 5.03, N 1.66; Presentation density of **1**: 46 %

GNP-11: Reaction of **22** (15.5 mg, 0.03 mmol) and **3** (7.8 mg, 0.03 mmol) with H₂AuCl₄ (6.3 mg, 0.018 mmol) gave **GNP-11** (1.96 mg, 4.2 x 10⁻⁵ mmol) as a dark brown powder. Average diameter and no. of Au atoms: 1.44 nm, 116; ¹H NMR (400 MHz, D₂O): $\delta = 3.05$ -3.90 (m, br), 1.10-1.70 (m, br) ppm; UV/Vis (H₂O): $\lambda = 491$ nm (w, br, SPR band); elemental analysis calculated (%) for (C₂₂H₄₄N₂O₁₀S₂)₃₀(C₁₁H₂₁O₆S)₂₇Au₁₁₆ (47215 g/mol): C, 24.32; H 3.96; N, 1.78; found C 24.31, H 3.74, N 1.76 Presentation density of **22**: 54 %

Preparation of GNP-6 to GNP-9 and GNP-12: Mother solutions of the Gal-mixed-SH (**3**) and Gal-mixed(s)-SH (**23**) ligands in MeOD and Glc-C5-SH (**3**) in MeOD were made. Reaction solutions of the required ratios were made and confirmed by quantitative ¹³C NMR (integration of the anomeric carbons) at 400 MHz, 398 K. The MeOD solutions were then concentrated *in vacuo* then redissolved in MeOH to give the required concentrations. Procedure is then as described above.

GNP-6: Reaction of **2** (7.2 mg, 0.01 mmol) and **3** (28 mg, 0.1 mmol) with H₂AuCl₄ (12.6 mg, 0.04 mmol) gave **GNP-4** (12.97 mg, 2.7 x 10⁻⁴ mmol) as a dark brown powder. Average diameter and no. of Au atoms: 1.43 nm, 120; ¹H NMR (400 MHz, D₂O): $\delta = 4.35$ -4.55 (s, br), 3.25-4.05 (m, br), 1.25-2.10 (m, br) ppm; UV/Vis (H₂O): SPR band not seen; IR (KBr): $\nu = 3431$ (broad), 2923, 1642, 1078 cm⁻¹; elemental analysis calculated (%) for (C₂₈H₅₆N₂O₁₀S₂)₁₂(C₁₁H₂₁O₆S)₅₉Au₁₂₀ (47 941 g/mol): C 24.65 H 4.02, N 0.70; found C 24.57, H 4.21, N 0.69; Presentation density of **2**: 17 %

GNP-7: Reaction of **2** (21.8 mg, 0.03 mmol) and **3** (28.7 mg, 0.1 mmol) with H₂AuCl₄ (15.3 mg, 0.04 mmol) gave **GNP-7** (14.79 mg, 4.4 x 10⁻⁴ mmol) as a dark brown powder. Average diameter and no. of Au atoms: 1.27 nm, 79; ¹H NMR (400 MHz, D₂O): $\delta = 4.35$ -4.50 (s, br), 3.20-4.15 (m, br), 1.20-1.90 (m, br) ppm; UV/Vis (H₂O): $\lambda = 490$ nm (w, br, SPR band); IR (KBr): $\nu = 3387$ (broad), 2922, 2856, 1635, 1587, 1380, 1300, 1079 cm⁻¹; elemental analysis calculated (%) for (C₂₈H₅₆N₂O₁₀S₂)₁₅(C₁₁H₂₁O₆S)₃₀Au₇₉ (33 643 g/mol): C 26.74 H 4.40, N 1.25; found C 26.67, H 4.77, N 1.23 Presentation density of **2**: 33 %

GNP-8: Reaction of **2** (16.8 mg, 0.03 mmol) and **3** (7.4 mg, 0.3 mmol) with H₂AuCl₄ (5.9 mg, 0.017 mmol) gave **GNP-8** (6.92 mg, 9×10^{-5} mmol) as a dark brown powder. Average diameter and no. of Au atoms: 1.39 nm, 140; ¹H NMR (400 MHz, D₂O): $\delta = 3.80\text{-}3.90$ (s, br), 3.10-3.80 (m, br), 1.15-1.80 (m, br) ppm; UV/Vis (H₂O): SPR band not seen; IR (KBr): $\nu = 3434$ (broad), 2922, 1636, 1421, 1347, 1115 (broad) cm⁻¹; elemental analysis calculated (%) for (C₂₈H₅₆N₂O₁₀S₂)₆₅(C₁₁H₂₁O₆S)₁₆Au₁₄₀ (73 889 g/mol): C 32.39 H 5.42, N 2.46; found C 33.29, H 5.52, N 2.46; Presentation density of **2**: 80 %

GNP-9: Reaction of **2** (20 mg, 0.03 mmol) and **3** (2.9 mg, 0.01 mmol) with H₂AuCl₄ (7 mg, 0.02 mmol) gave **GNP-9** (6.72 mg, 1.15×10^{-4} mmol) as a dark brown powder. Average diameter and no. of Au atoms: 1.39 nm, 140; ¹H NMR (400 MHz, D₂O): $\delta = 4.30\text{-}4.40$ (s, br), 3.00-4.10 (m, br), 1.10-1.80 (m, br) ppm; UV/Vis (H₂O): $\lambda = 492$ nm (w, br, SPR band); IR (KBr): $\nu = 3431$ (broad), 2922, 2361, 1636, 1094 cm⁻¹; elemental analysis calculated (%) for (C₂₈H₅₆N₂O₁₀S₂)₅₇(C₁₁H₂₁O₆S)₇Au₁₀₀ (58 334 g/mol): C, 34.42 H, 5.67 N, 2.74; found C, 34.39 H, 5.63 N, 2.84; Presentation density of **2**: 90 %

GNP-12: Reaction of **22** (10 mg, 0.018 mmol) and **3** (15 mg, 0.05 mmol) with H₂AuCl₄ (8 mg, 0.024 mmol) gave **GNP-12** (12.8 mg, 2.6×10^{-4} mmol) as a dark brown powder. Average diameter and no. of Au atoms: 1.47 nm, 124; ¹H NMR (400 MHz, D₂O): $\delta = 4.20\text{-}4.30$ (s, br), 3.10-3.95 (m, br), 1.10-1.80 (m, br) ppm; UV/Vis (H₂O): SPR band not seen; IR (KBr): $\nu = 3420, 2931, 1633, 1077$ cm⁻¹; elemental analysis calculated (%) for (C₂₂H₄₄N₂O₁₀S₂)₁₆(C₁₁H₂₁O₆S)₅₃Au₁₂₄ (48832 g/mol): C, 23.24; H, 3.79; N, 0.93; found C, 23.28 H, 3.68 N, 0.89; Presentation density of **22**: 22 %

Preparation of GNP-13: Preparations as for **GNP-4** with the exception that 5 equivalents of total ligands were used. Reaction of **1** (40 mg, 0.06 mmol) and **3** (17 mg, 0.06 mmol) with H₂AuCl₄ (8.4 mg, 0.025 mmol) gave **GNP-13** (6.74 mg, 9.1×10^{-5} mmol) as a dark brown powder. Average diameter and no. of Au atoms: 1.44 nm, 116; ¹H NMR (400 MHz, D₂O): $\delta = 4.25\text{-}4.30$ (d, $J = 7.6$ Hz, Glc-H-1), 3.10-4.00 (m, br), 2.55-2.65 (t, $J = 7.6$ Hz, CH₂S), 1.10-1.55 (m, br) ppm; IR (KBr): $\nu = 3390, 2920, 1230, 1110$ cm⁻¹; elemental analysis calculated (%) for (C₂₈H₅₆N₂O₁₀S₂)₅₈(C₁₁H₂₁O₆S)₅₁Au₁₁₆ (74216 g/mol): C, 35.20; H, 5.76; N, 2.18; S, 7.17; found C, 35.19 H, 5.77 N, 2.18 S, 4.69; Presentation density of **1**: 53

BIBLIOGRAPHY

BIBLIOGRAPHY

1. Cremer, D.; Pople, J. A., *JACS*, **1975**, 97, (6), 1358-1367.
2. McNaught, A. D., *Carbohydr. Res.*, **1997**, 297, (1), 1-92.
3. Ogawa, S., *Trends Glycosci. Glyc.*, **2004**, 16, (87), 33-53.
4. Lindhorst, T. K., *Essentials of Carbohydrate Chemistry and Biochemistry*. Third ed.; Wiley-VCH: Weinheim, 2007.
5. Dwek, R. A., *Chem. Rev.*, **1996**, 96, (2), 683-720.
6. Sato, S.; St-Pierre, C.; Bhaumik, P.; Nieminen, J., *Immunol. Rev.*, **2009**, 230, (1), 172-87.
7. Gamblin, D. P.; Scanlan, E. M.; Davis, B. G., *Chem. Rev.*, **2009**, 109, (1), 131-63.
8. Levitt, M.; Perutz, M. F., *J. Mol. Biol.*, **1988**, 201, (4), 751-4.
9. Lemieux, R. U., *Acc. Chem. Res.*, **1996**, 29, (8), 373-380.
10. Engelsen, S. B.; Perez, S., *Carbohydr. Res.*, **1996**, 292, 21-38.
11. Engelsen, S. B.; Perez, S., *J. Phys. Chem. B*, **2000**, 104, (39), 9301-9311.
12. Reynolds, M.; Fuchs, A.; Lindhorst, T. K.; Perez, S., *Mol. Simul.*, **2008**, 34, (4), 447-460.
13. Perez, S.; Mouhous-Riou, N.; Nifant'ev, N. E.; Tsvetkov, Y. E.; Bachet, B.; Imberty, A., *Glycobiology*, **1996**, 6, (5), 537-42.
14. Sharon, N.; Lis, H., *Lectins*. Second ed.; Kluwer Academic Publishers: Dordrecht, 2003.
15. Aragao, K. S.; Satre, M.; Imberty, A.; Varrot, A., *Proteins*, **2008**, 73, (1), 43-52.
16. Cioci, G.; Mitchell, E. P.; Gautier, C.; Wimmerova, M.; Sudakevitz, D.; Perez, S.; Gilboa-Garber, N.; Imberty, A., *FEBS Lett.*, **2003**, 555, (2), 297-301.
17. Wu, Y. P.; Liu, Z. H.; Wei, R.; Pan, S. D.; Mao, N. Y.; Chen, B.; Han, J. J.; Zhang, F. S.; Holmskov, U.; Xia, Z. L.; de Groot, P. G.; Reid, K. B.; Xu, W. B.; Sorensen, G. L., *Scand. J. Immunol.*, **2009**, 69, (6), 508-15.
18. van Asbeck, E. C.; Hoepelman, A. I.; Scharringa, J.; Herpers, B. L.; Verhoef, J., *BMC Microbiol.*, **2008**, 8, 229.
19. Geijtenbeek, T. B.; Kwon, D. S.; Torensma, R.; van Vliet, S. J.; van Duijnhoven, G. C.; Middel, J.; Cornelissen, I. L.; Nottet, H. S.; KewalRamani, V. N.; Littman, D. R.; Figdor, C. G.; van Kooyk, Y., *Cell*, **2000**, 100, (5), 587-97.
20. Turnbull, W. B.; Precious, B. L.; Homans, S. W., *JACS*, **2004**, 126, (4), 1047-54.
21. Fukuta, S.; Magnani, J. L.; Twiddy, E. M.; Holmes, R. K.; Ginsburg, V., *Infect. Immun.*, **1988**, 56, (7), 1748-53.
22. Chemani, C.; Imberty, A.; de Bentzmann, S.; Pierre, M.; Wimmerova, M.; Guery, B. P.; Faure, K., *Infect. Immun.*, **2009**, 77, (5), 2065-75.
23. Lameignere, E.; Malinowska, L.; Slavikova, M.; Duchaud, E.; Mitchell, E. P.; Varrot, A.; Sedo, O.; Imberty, A.; Wimmerova, M., *Biochem. J.*, **2008**, 411, (2), 307-18.
24. Lameignere, E. Etudes structurales et fonctionelle de lectines solubles de *Burkholderia cenocepacia*. Université de Grenoble I - Joseph Fourier, Grenoble, 2009.
25. Benaissa-Trouw, B.; Lefeber, D. J.; Kamerling, J. P.; Vliegthart, J. F.; Kraaijeveld, K.; Snippe, H., *Infect. Immun.*, **2001**, 69, (7), 4698-701.
26. Doores, K. J.; Gamblin, D. P.; Davis, B. G., *Chemistry*, **2006**, 12, (3), 656-65.
27. Organisation, W. H., Pandemic (H1N1) 2009 - update 69. In 2009.
28. Imberty, A.; Varrot, A., *Curr. Opin. Struct. Biol.*, **2008**, 18, (5), 567-76.
29. Kuchipudi, S. V.; Nelli, R.; White, G. A.; Bain, M.; Chang, K. C.; Dunham, S., *J. Mol. Genet. Med.*, **2009**, 3, (1), 143-51.
30. Rademacher, T. W.; Parekh, R. B.; Dwek, R. A., *Annu. Rev. Biochem.*, **1988**, 57, 785-838.
31. Current outbreak of swine influenza, *Expert Rev. Anti Infect. Ther.*, **2009**, 7, (5), 503-505.
32. Demydenko, D.; Berest, I., *Exp Oncol.*, **2009**, 31, (2), 74-9.
33. Imberty, A.; Perez, S., *Chem. Rev.*, **2000**, 100, (12), 4567-88.
34. Naismith, J. H.; Emmerich, C.; Habash, J.; Harrop, S. J.; Helliwell, J. R.; Hunter, W. N.; Raftery, J.; Kalb, A. J.; Yariv, J., *Acta Crystallogr., Sect. D: Biol. Crystallogr.*, **1994**, 50, (Pt 6), 847-58.
35. Drickamer, K., *J. Biol. Chem.*, **1988**, 263, (20), 9557-60.
36. Sanders, J. N.; Chenoweth, S. A.; Schwarz, F. P., *J. Inorg. Biochem.*, **1998**, 70, (2), 71-82.
37. Bradbrook, G. M.; Gleichmann, T.; Harrop, S. J.; Habash, J.; Raftery, J.; Kalb, J.; Yariv, J.; Hillier, I. H.; Helliwell, J. R., *J. Chem. Soc., Faraday Trans.*, **1998**, 94, (11), 1603.

38. Gupta, D.; Dam, T. K.; Oscarson, S.; Brewer, C. F., *J. Biol. Chem.*, **1997**, 272, (10), 6388-92.
39. Dam, T. K.; Roy, R.; Das, S. K.; Oscarson, S.; Brewer, C. F., *J. Biol. Chem.*, **2000**, 275, (19), 14223-30.
40. Mandal, D. K.; Kishore, N.; Brewer, C. F., *Biochemistry*, **1994**, 33, (5), 1149-56.
41. Rieger, J.; Stoffelbach, F.; Cui, D.; Imberty, A.; Lameignere, E.; Putaux, J. L.; Jerome, R.; Jerome, C.; Auzely-Velty, R., *Biomacromolecules*, **2007**, 8, (9), 2717-25.
42. Rieger, J.; Freichels, H.; Imberty, A.; Putaux, J. L.; Delair, T.; Jerome, C.; Auzely-Velty, R., *Biomacromolecules*, **2009**.
43. Blanchard, B.; Nurisso, A.; Hollville, E.; Tetaud, C.; Wiels, J.; Pokorna, M.; Wimmerova, M.; Varrot, A.; Imberty, A., *J. Mol. Biol.*, **2008**, 383, (4), 837-53.
44. Imberty, A.; wimmerova, M.; Mitchell, E. P.; Gilboa-Garber, N., *Microbes Infect.*, **2004**, 6, (2), 221-8.
45. Stoitsova, S. R.; Boteva, R. N.; Doyle, R. J., *BBA*, **2003**, 1619, (2), 213-9.
46. Garber, N.; Guempel, U.; Belz, A.; Gilboa-Garber, N.; Doyle, R. J., *BBA*, **1992**, 1116, (3), 331-3.
47. Zinger-Yosovich, K. D.; Gilboa-Garber, N., *J. Agric. Food. Chem.*, **2009**.
48. Denguise, I.; Lagnoux, D.; Roy, R., *New J. Chem.*, **2007**, 31, (7), 1321.
49. Vanden Broeck, D.; Horvath, C.; De Wolf, M. J., *Int. J. Biochem. Cell Biol.*, **2007**, 39, (10), 1771-5.
50. Bavington, C.; Page, C., *Respiration*, **2005**, 72, (4), 335-44.
51. Gabius, H. J., *Eur. J. Biochem.*, **1997**, 243, (3), 543-76.
52. Lee, R. T.; Lee, Y. C., *Glycoconj. J.*, **2000**, 17, (7-9), 543-51.
53. Lundquist, J. J.; Toone, E. J., *Chem. Rev.*, **2002**, 102, (2), 555-78.
54. Lee, Y. C.; Lee, R. T., *Acc. Chem. Res.*, **1995**, 28, (8), 321-327.
55. Perez, S. unpublished work
56. Sperling, O.; Fuchs, A.; Lindhorst, T. K., *Org. Biomol. Chem.*, **2006**, 4, (21), 3913-22.
57. Mammen, M.; Choi, S. K.; Whitesides, G. M., *Angew.Chem. Int. Ed.*, **1998**, 37, (20), 2755-2794.
58. Badjic, J. D.; Nelson, A.; Cantrill, S. J.; Turnbull, W. B.; Stoddart, J. F., *Acc. Chem. Res.*, **2005**, 38, (9), 723-32.
59. Kramer, R. H.; Karpen, J. W., *Nature*, **1998**, 395, (6703), 710-3.
60. Gargano, J. M.; Ngo, T.; Kim, J. Y.; Acheson, D. W.; Lees, W. J., *JACS*, **2001**, 123, (51), 12909-10.
61. Mulder, A.; Auletta, T.; Sartori, A.; Del Ciotto, S.; Casnati, A.; Ungaro, R.; Huskens, J.; Reinhoudt, D. N., *JACS*, **2004**, 126, (21), 6627-36.
62. Mulder, A.; Huskens, J.; Reinhoudt, D. N., *Org. Biomol. Chem.*, **2004**, 2, (23), 3409-24.
63. Baldini, L.; Casnati, A.; Sansone, F.; Ungaro, R., *Chem. Soc. Rev.*, **2007**, 36, (2), 254-66.
64. Kiessling, L. L.; Gestwicki, J. E.; Strong, L. E., *Curr. Opin. Chem. Biol.*, **2000**, 4, (6), 696-703.
65. Dam, T. K.; Oscarson, S.; Roy, R.; Das, S. K.; Page, D.; Macaluso, F.; Brewer, C. F., *J. Biol. Chem.*, **2005**, 280, (10), 8640-6.
66. Cloninger, M. J., *Curr. Opin. Chem. Biol.*, **2002**, 6, (6), 742-8.
67. Sisu, C.; Baron, A. J.; Branderhorst, H. M.; Connell, S. D.; Weijers, C. A.; de Vries, R.; Hayes, E. D.; Pukin, A. V.; Gilbert, M.; Pieters, R. J.; Zuilhof, H.; Visser, G. M.; Turnbull, W. B., *ChemBioChem*, **2009**, 10, (2), 329-37.
68. Lindhorst, T. K.
69. Marotte, K.; Preville, C.; Sabin, C.; Moume-Pymbock, M.; Imberty, A.; Roy, R., *Org. Biomol. Chem.*, **2007**, 5, (18), 2953-61.
70. Fortier, S.; Touaibia, M.; Lord-Dufour, S.; Galipeau, J.; Roy, R.; Annabi, B., *Glycobiology*, **2008**, 18, (2), 195-204.
71. Touaibia, M.; Shiao, T. C.; Papadopoulos, A.; Vaucher, J.; Wang, Q.; Benhamioud, K.; Roy, R., *Chem. Commun.*, **2007**, (4), 380-2.
72. Dubber, M.; Lindhorst, T. K., *Org. Lett.*, **2001**, 3, (25), 4019-22.
73. Dubber, M.; Sperling, O.; Lindhorst, T. K., *Org. Biomol. Chem.*, **2006**, 4, (21), 3901-12.
74. Sperling, O.; Dubber, M.; Lindhorst, T. K., *Carbohydr. Res.*, **2007**, 342, (5), 696-703.
75. Dubber, M.; Lindhorst, T. K., *J. Org. Chem.*, **2000**, 65, (17), 5275-81.
76. Nepogodiev, S. A.; Stoddart, J. F., *Chem. Rev.*, **1998**, 98, (5), 1959-1976.
77. Huskens, J.; Mulder, A.; Auletta, T.; Nijhuis, C. A.; Ludden, M. J.; Reinhoudt, D. N., *JACS*, **2004**, 126, (21), 6784-97.
78. Fulton, D. A.; Stoddart, J. F., *Org. Lett.*, **2000**, 2, (8), 1113-6.
79. Sallas, F.; Niikura, K.; Nishimura, S., *Chem. Commun.*, **2004**, (5), 596-7.
80. Furuike, T.; Aiba, S.; Nishimura, S.-I., *Tetrahedron*, **2000**, 56, (51), 9909-9915.
81. Chwalek, M.; Auzely, R.; Fort, S., *Org. Biomol. Chem.*, **2009**, 7, (8), 1680-8.
82. Meunier, S. J.; Roy, R., *Tetrahedron Lett.*, **1996**, 37, (31), 5469-5472.
83. Roy, R.; Kim, J. M., *Angew.Chem. Int. Ed.*, **1999**, 38, (3), 369-372.
84. Fujimoto, T.; Shimizu, C.; Hayashida, O.; Aoyama, Y., *JACS*, **1998**, 120, (3), 601-602.

85. Andre, S.; Sansone, F.; Kaltner, H.; Casnati, A.; Kopitz, J.; Gabius, H. J.; Ungaro, R., *ChemBioChem*, **2008**, 9, (10), 1649-61.
86. Arosio, D.; Fontanella, M.; Baldini, L.; Mauri, L.; Bernardi, A.; Casnati, A.; Sansone, F.; Ungaro, R., *JACS*, **2005**, 127, (11), 3660-1.
87. Moni, L.; Pourceau, G.; Zhang, J.; Meyer, A.; Vidal, S.; Souteyrand, E.; Dondoni, A.; Morvan, F.; Chevolut, Y.; Vasseur, J. J.; Marra, A., *ChemBioChem*, **2009**, 10, (8), 1369-78.
88. You, L. C.; Lu, F. Z.; Li, Z. C.; Zhang, W.; Li, F. M., *Macromolecules*, **2003**, 36, (1), 1-4.
89. Wilczewski, M.; Van der Heyden, A.; Renaudet, O.; Dumy, P.; Coche-Guerente, L.; Labbe, P., *Org. Biomol. Chem.*, **2008**, 6, (6), 1114-22.
90. Schlick, K. H.; Udelhoven, R. A.; Strohmeyer, G. C.; Cloninger, M. J., *Mol. Pharm.*, **2005**, 2, (4), 295-301.
91. Appelhans, D.; Komber, H.; Quadir, M. A.; Richter, S.; Schwarz, S.; van der Vlist, J.; Aigner, A.; Muller, M.; Loos, K.; Seidel, J.; Arndt, K. F.; Haag, R.; Voit, B., *Biomacromolecules*, **2009**.
92. Mangold, S. L.; Cloninger, M. J., *Org. Biomol. Chem.*, **2006**, 4, (12), 2458-65.
93. Mangold, S. L.; Morgan, J. R.; Strohmeyer, G. C.; Gronenborn, A. M.; Cloninger, M. J., *Org. Biomol. Chem.*, **2005**, 3, (12), 2354-8.
94. Wolfenden, M. L.; Cloninger, M. J., *JACS*, **2005**, 127, (35), 12168-9.
95. Imberty, A.; Chabre, Y. M.; Roy, R., *Chemistry*, **2008**, 14, (25), 7490-9.
96. Morvan, F.; Meyer, A.; Jochum, A.; Sabin, C.; Chevolut, Y.; Imberty, A.; Praly, J. P.; Vasseur, J. J.; Souteyrand, E.; Vidal, S., *Bioconjug. Chem.*, **2007**, 18, (5), 1637-43.
97. Touaibia, M.; Wellens, A.; Shiao, T. C.; Wang, Q.; Sirois, S.; Bouckaert, J.; Roy, R., *ChemMedChem*, **2007**, 2, (8), 1190-201.
98. Roy, R.; Baek, M. G., *J. Biotechnol.*, **2002**, 90, (3-4), 291-309.
99. Roy, R.; Baek, M. G., *Methods Enzymol.*, **2003**, 362, 240-9.
100. Heidecke, C. D.; Lindhorst, T. K., *Chemistry*, **2007**, 13, (32), 9056-67.
101. Lindhorst, T. K.; Kieburg, C.; Krallmann-Wenzel, U., *Glycoconj. J.*, **1998**, 15, (6), 605-13.
102. Shon, Y. S.; Choi, D.; Dare, J.; Dinh, T., *Langmuir*, **2008**, 24, (13), 6924-31.
103. Otsuka, I.; Hongo, T.; Nakade, H.; Narumi, A.; Sakai, R.; Satoh, T.; Kaga, H.; Kakuchi, T., *Macromolecules*, **2007**, 40, (25), 8930-8937.
104. Gestwicki, J. E.; Strong, L. E.; Borchardt, S. L.; Cairo, C. W.; Schnoes, A. M.; Kiessling, L. L., *Bioorg. Med. Chem.*, **2001**, 9, (9), 2387-93.
105. Ogata, M.; Hidari, K. I.; Kozaki, W.; Murata, T.; Hiratake, J.; Park, E. Y.; Suzuki, T.; Usui, T., *Biomacromolecules*, **2009**.
106. Davis, N. E.; Karfeld-Sulzer, L. S.; Ding, S.; Barron, A. E., *Biomacromolecules*, **2009**.
107. Dam, T. K.; Gerken, T. A.; Brewer, C. F., *Biochemistry*, **2009**.
108. Szarpak, A.; Pignot-Paintrand, I.; Nicolas, C.; Picart, C.; Auzely-Velty, R., *Langmuir*, **2008**, 24, (17), 9767-74.
109. Bes, L.; Angot, S.; Limer, A.; Haddleton, D. M., *Macromolecules*, **2003**, 36, (7), 2493-2499.
110. Iwasaki, Y.; Maie, H.; Akiyoshi, K., *Biomacromolecules*, **2007**, 8, (10), 3162-8.
111. Murthy, B. N.; Voelcker, N. H.; Jayaraman, N., *Glycobiology*, **2006**, 16, (9), 822-32.
112. Thomas, G. B.; Rader, L. H.; Park, J.; Abezgauz, L.; Danino, D.; Deshong, P.; English, D. S., *JACS*, **2009**.
113. van Kasteren, S. I.; Kramer, H. B.; Gamblin, D. P.; Davis, B. G., *Nat. Protoc.*, **2007**, 2, (12), 3185-94.
114. Rendle, P. M.; Seger, A.; Rodrigues, J.; Oldham, N. J.; Bott, R. R.; Jones, J. B.; Cowan, M. M.; Davis, B. G., *JACS*, **2004**, 126, (15), 4750-1.
115. Revell, D. J.; Knight, J. R.; Blyth, D. J.; Haines, A. H.; Russell, D. A., *Langmuir*, **1998**, 14, (16), 4517-4524.
116. Kleinert, M.; Winkler, T.; Terfort, A.; Lindhorst, T. K., *Org. Biomol. Chem.*, **2008**, 6, (12), 2118-32.
117. Lienemann, M.; Paananen, A.; Boer, H.; de la Fuente, J. M.; Garcia, I.; Penades, S.; Koivula, A., *Glycobiology*, **2009**, 19, (6), 633-43.
118. Blixt, O.; Head, S.; Mondala, T.; Scanlan, C.; Huflejt, M. E.; Alvarez, R.; Bryan, M. C.; Fazio, F.; Calarese, D.; Stevens, J.; Razi, N.; Stevens, D. J.; Skehel, J. J.; van Die, I.; Burton, D. R.; Wilson, I. A.; Cummings, R.; Bovin, N.; Wong, C. H.; Paulson, J. C., *Proc. Nat. Acad. Sci. U.S.A.*, **2004**, 101, (49), 17033-8.
119. Dimick, S. M.; Powell, S. C.; McMahon, S. A.; Moothoo, D. N.; Naismith, J. H.; Toone, E. J., *JACS*, **1999**, 121, (44), 10286-10296.
120. Daniel, M. C.; Astruc, D., *Chem. Rev.*, **2004**, 104, (1), 293-346.
121. Cotton, F.; Wilkinson, G., *Advanced Inorganic Chemistry*. Fifth edition ed.; Wiley-Interscience: New York, 1988.
122. Thomas, J. M., *Pure Appl. Chem.*, **1988**, 60, (10), 1517-1528.

123. Brust, M.; Walker, M.; Bethell, D.; Schiffrin, D. J.; Whyman, R., *J. Chem. Soc., Chem. Comm.*, **1994**, (7), 801-802.
124. Cliffler, D. E.; Zamborini, F. P.; Gross, S. M.; Murray, R. W., *Langmuir*, **2000**, 16, 9699-9702.
125. Kanaras, A. G.; Kamounah, F. S.; Schaumburg, K.; Kiely, C. J.; Brust, M., *Chem. Commun.*, **2002**, (20), 2294-5.
126. Templeton, A. C.; Wuelfing, W. P.; Murray, R. W., *Acc. Chem. Res.*, **2000**, 33, (1), 27-36.
127. Brust, M.; Kiely, C. J., *Colloids Surf., A*, **2002**, 202, (2-3), 175-186.
128. Smetana, A. B.; Wang, J. S.; Boeckl, J.; Brown, G. J.; Wai, C. M., *Langmuir*, **2007**, 23, (21), 10429-32.
129. Sardar, R.; Functon, A. M.; Mulvaney, P.; Murray, R. W., *Langmuir*, **2009**, currently ASAP article.
130. Fuss, M.; Luna, M.; Alcantara, D.; Fuente, J. M.; Penades, S.; Briones, F., *Langmuir*, **2008**, 24, (9), 5124-8.
131. Ai, K.; Liu, Y.; Lu, L., *JACS*, **2009**.
132. Newman, J. D.; Maccreehan, W. A., *Langmuir*, **2009**.
133. Pacchioni, G.; Sicolo, S.; Valentin, C. D.; Chiesa, M.; Giamello, E., *JACS*, **2008**, 130, (27), 8690-5.
134. Suzuki, K.; Hosokawa, K.; Maeda, M., *JACS*, **2009**, 131, (22), 7518-9.
135. Williams, D. P.; Satherley, J., *Langmuir*, **2009**.
136. Sihelnikova, L.; Tvaroska, I., *Chem. Papers.*, **2007**, 61, (4), 237-255.
137. Jadzinsky, P. D.; Calero, G.; Ackerson, C. J.; Bushnell, D. A.; Kornberg, R. D., *Science*, **2007**, 318, (5849), 430-3.
138. Zhu, M.; Aikens, C. M.; Hollander, F. J.; Schatz, G. C.; Jin, R., *JACS*, **2008**, 130, (18), 5883-5.
139. Tambasco, M.; Kumar, S. K.; Szleifer, I., *Langmuir*, **2008**, 24, (16), 8448-51.
140. Huang, W.; Bulusu, S.; Pal, R.; Zeng, X. C.; Wang, L. S., *ACS Nano*, **2009**.
141. Wu, Z.; Gayathri, C.; Gil, R. R.; Jin, R., *JACS*, **2009**, 131, (18), 6535-42.
142. Hasan, M.; Bethell, D.; Brust, M., *JACS*, **2002**, 124, (7), 1132-3.
143. Porta, F.; Krpetic, Z.; Prati, L.; Gaiassi, A.; Scari, G., *Langmuir*, **2008**, 24, (14), 7061-4.
144. Cheng, P. P.; Silvester, D.; Wang, G.; Kalyuzhny, G.; Douglas, A.; Murray, R. W., *J. Phys. Chem. B*, **2006**, 110, (10), 4637-44.
145. Luo, W.; Pennycook, S. J.; Pantelides, S. T., *Nano Lett.*, **2007**, 7, (10), 3134-7.
146. Zhu, M.; Aikens, C. M.; Hendrich, M. P.; Gupta, R.; Qian, H.; Schatz, G. C.; Jin, R., *JACS*, **2009**, 131, (7), 2490-2.
147. Crespo, P.; Litran, R.; Rojas, T. C.; Multigner, M.; de la Fuente, J. M.; Sanchez-Lopez, J. C.; Garcia, M. A.; Hernando, A.; Penades, S.; Fernandez, A., *Phys. Rev. Lett.*, **2004**, 93, (8), 087204.
148. Crespo, P.; Garcia, M. A.; Fernandez Pinel, E.; Multigner, M.; Alcantara, D.; de la Fuente, J. M.; Penades, S.; Hernando, A., *Phys. Rev. Lett.*, **2006**, 97, (17), 177203.
149. Saldin, D. K.; Spence, J. H. C., *Ultramicroscopy*, **1994**, 55, 397-406.
150. Ichikawa, S.; Akita, T.; Okumura, M.; Kohayama, M.; Tanaka, K., *JEOL News*, **2003**, 38, 6-9.
151. Hill, H. D.; Millstone, J. E.; Banholzer, M. J.; Mirkin, C. A., *ACS Nano*, **2009**, 3, (2), 418-24.
152. Cederquist, K. B.; Keating, C. D., *ACS Nano*, **2009**, 3, (2), 256-60.
153. Virel, A.; Saa, L.; Pavlov, V., *Anal. Chem.*, **2009**, 81, (1), 268-72.
154. Rance, G. A.; Marsh, D. H.; Khlobystov, A. N., *Chem. Phys. Lett.*, **2008**, 460, (1-3), 230-236.
155. Guzman, J.; Gates, B. C., *JACS*, **2004**, 126, (9), 2672-3.
156. Turner, M.; Golovko, V. B.; Vaughan, O. P.; Abdulkin, P.; Berenguer-Murcia, A.; Tikhov, M. S.; Johnson, B. F.; Lambert, R. M., *Nature*, **2008**, 454, (7207), 981-3.
157. Corma, A.; Gonzalez-Arellano, C.; Iglesias, M.; Sanchez, F., *Angew. Chem. Int. Ed.*, **2007**, 46, (41), 7820-2.
158. Corma, A.; Serna, P., *Science*, **2006**, 313, (5785), 332-4.
159. Lemire, C.; Meyer, R.; Shaikhutdinov, S.; Freund, H. J., *Angew. Chem. Int. Ed.*, **2004**, 43, (1), 118-21.
160. Abad, A.; Concepcion, P.; Corma, A.; Garcia, H., *Angew. Chem. Int. Ed.*, **2005**, 44, (26), 4066-9.
161. Chomposor, A.; Han, G.; Rotello, V. M., *Bioconjug. Chem.*, **2008**, 19, (7), 1342-5.
162. Hong, R.; Han, G.; Fernandez, J. M.; Kim, B. J.; Forbes, N. S.; Rotello, V. M., *JACS*, **2006**, 128, (4), 1078-9.
163. Hosta, L.; Pla-Roca, M.; Arbiol, J.; Lopez-Iglesias, C.; Samitier, J.; Cruz, L. J.; Kogan, M. J.; Albericio, F., *Bioconjug. Chem.*, **2009**, 20, (1), 138-46.
164. Podsiadlo, P.; Sinani, V. A.; Bahng, J. H.; Kam, N. W.; Lee, J.; Kotov, N. A., *Langmuir*, **2008**, 24, (2), 568-74.
165. Gibson, J. D.; Khanal, B. P.; Zubarev, E. R., *JACS*, **2007**, 129, (37), 11653-61.
166. Ghosh, P.; Han, G.; De, M.; Kim, C. K.; Rotello, V. M., *Adv. Drug Deliv. Rev.*, **2008**, 60, (11), 1307-15.
167. Ghosh, P. S.; Kim, C. K.; Han, G.; Forbes, N. S.; Rotello, V. M., *ACS Nano*, **2008**, 2, (11), 2213-8.
168. Bergen, J. M.; von Recum, H. A.; Goodman, T. T.; Massey, A. P.; Pun, S. H., *Macromol. Biosci.*, **2006**, 6, (7), 506-16.

169. Nie, Z.; Liu, K. J.; Zhong, C. J.; Wang, L. F.; Yang, Y.; Tian, Q.; Liu, Y., *Free Radic. Biol. Med.*, **2007**, 43, (9), 1243-54.
170. Huang, T.; Nallathamby, P. D.; Gillet, D.; Xu, X. H., *Anal. Chem.*, **2007**, 79, (20), 7708-18.
171. Javier, D. J.; Nitin, N.; Levy, M.; Ellington, A.; Richards-Kortum, R., *Bioconjug. Chem.*, **2008**, 19, (6), 1309-12.
172. Lin, C. A.; Yang, T. Y.; Lee, C. H.; Huang, S. H.; Sperling, R. A.; Zanella, M.; Li, J. K.; Shen, J. L.; Wang, H. H.; Yeh, H. I.; Parak, W. J.; Chang, W. H., *ACS Nano*, **2009**, 3, (2), 395-401.
173. van Kasteren, S. I.; Campbell, S. J.; Serres, S.; Anthony, D. C.; Sibson, N. R.; Davis, B. G., *Proc. Nat. Acad. Sci. U.S.A.*, **2009**, 106, (1), 18-23.
174. von Maltzahn, G.; Ren, Y.; Park, J. H.; Min, D. H.; Kotamraju, V. R.; Jayakumar, J.; Fogal, V.; Sailor, M. J.; Ruoslahti, E.; Bhatia, S. N., *Bioconjug. Chem.*, **2008**, 19, (8), 1570-8.
175. Paasonen, L.; Laaksonen, T.; Johans, C.; Yliperttula, M.; Kontturi, K.; Urtti, A., *J. Controlled Release*, **2007**, 122, (1), 86-93.
176. Wu, G.; Mikhailovsky, A.; Khant, H. A.; Fu, C.; Chiu, W.; Zasadzinski, J. A., *JACS*, **2008**, 130, (26), 8175-7.
177. Hirsch, L. R.; Stafford, R. J.; Bankson, J. A.; Sershen, S. R.; Rivera, B.; Price, R. E.; Hazle, J. D.; Halas, N. J.; West, J. L., *Proc. Nat. Acad. Sci. U.S.A.*, **2003**, 100, (23), 13549-54.
178. Tong, L.; Zhao, Y.; Huff, T. B.; Hansen, M. N.; Wei, A.; Cheng, J. X., *Adv. Mater. Deerfield*, **2007**, 19, 3136-3141.
179. de la Fuente, J. M.; Penades, S., *Glycoconjugate J.*, **2004**, 21, (3-4), 149-63.
180. de la Fuente, J. M.; Penades, S., *BBA*, **2006**, 1760, (4), 636-51.
181. de La Fuente, J. M.; Barrientos, A. G.; Rojas, T. C.; Rojo, J.; Canada, J.; Fernandez, A.; Penades, S., *Angew.Chem. Int. Ed.*, **2001**, 40, (12), 2257-2261.
182. Barrientos, A. G.; de la Fuente, J. M.; Rojas, T. C.; Fernandez, A.; Penades, S., *Chem. Eur. J.*, **2003**, 9, (9), 1909-1921.
183. Otsuka, H.; Akiyama, Y.; Nagasaki, Y.; Kataoka, K., *JACS*, **2001**, 123, (34), 8226-30.
184. Lin, C. C.; Yeh, Y. C.; Yang, C. Y.; Chen, C. L.; Chen, G. F.; Chen, C. C.; Wu, Y. C., *JACS*, **2002**, 124, (14), 3508-9.
185. Lin, C. C.; Yeh, Y. C.; Yang, C. Y.; Chen, G. F.; Chen, Y. C.; Wu, Y. C.; Chen, C. C., *Chem. Commun.*, **2003**, (23), 2920-1.
186. Halkes, K. M.; de Souza, A. C.; Maljaars, C. E. P.; Gerwig, G. J.; Kamerling, J. P., *Eur. J. Org. Chem.*, **2005**, (17), 3650-3659.
187. Chien, Y. Y.; Jan, M. D.; Adak, A. K.; Tzeng, H. C.; Lin, Y. P.; Chen, Y. J.; Wang, K. T.; Chen, C. T.; Chen, C. C.; Lin, C. C., *ChemBioChem*, **2008**, 9, (7), 1100-9.
188. Barrientos, A. G.; Fuente, J. M.; Jimenez, M.; Solis, D.; Canada, F. J.; Martin-Lomas, M.; Penades, S., *Carbohydr. Res.*, **2009**.
189. Schofield, C. L.; Field, R. A.; Russell, D. A., *Anal. Chem.*, **2007**, 79, (4), 1356-61.
190. Spain, S. G.; Albertin, L.; Cameron, N. R., *Chem. Commun.*, **2006**, (40), 4198-200.
191. de la Fuente, J. M.; Penades, S., *Tetrahedron: Asymmetry*, **2002**, 13, (17), 1879-1888.
192. Hernaiz, M. J.; De la Fuente, J. M.; Barrientos, A. G.; Penades, S., *Angew.Chem. Int. Ed.*, **2002**, 41, 1554-1557.
193. de la Fuente, J. M.; Eaton, P.; Barrientos, A. G.; Menendez, M.; Penades, S., *JACS*, **2005**, 127, (17), 6192-7.
194. Carvalho de Souza, A.; Halkes, K. M.; Meeldijk, J. D.; Verkleij, A. J.; Vliegthart, J. F. G.; Kamerling, J. P., *Eur. J. Org. Chem.*, **2004**, (21), 4323-4339.
195. Carvalho de Souza, A.; Halkes, K. M.; Meeldijk, J. D.; Verkleij, A. J.; Vliegthart, J. F.; Kamerling, J. P., *ChemBioChem*, **2005**, 6, (5), 828-31.
196. Reynolds, A. J.; Haines, A. H.; Russell, D. A., *Langmuir*, **2006**, 22, (3), 1156-1163.
197. Martinez-Avila, O.; Bedoya, L. M.; Marradi, M.; Clavel, C.; Alcami, J.; Penades, S., *ChemBioChem*, **2009**, 10, (11), 1806-1809.
198. Martinez-Avila, O.; Hijazi, K.; Marradi, M.; Clavel, C.; Campion, C.; Kelly, C.; Penades, S., *Chemistry*, **2009**.
199. Chen, Y. J.; Chen, S. H.; Chien, Y. Y.; Chang, Y. W.; Liao, H. K.; Chang, C. Y.; Jan, M. D.; Wang, K. T.; Lin, C. C., *ChemBioChem*, **2005**, 6, (7), 1169-73.
200. Nakamura-Tsuruta, S.; Kishimoto, Y.; Nishimura, T.; Suda, Y., *J. Biochem.*, **2008**, 143, (6), 833-9.
201. Astruc, D.; Daniel, M. C.; Ruiz, J., *Chem. Commun.*, **2004**, (23), 2637-49.
202. Mastroianni, A. J.; Claridge, S. A.; Alivisatos, A. P., *JACS*, **2009**.
203. Joshi, H.; Shirude, P. S.; Bansal, V.; Ganesh, K. N.; Sastry, M., *J. Phys. Chem. B*, **2004**, 108, (31), 11535-11540.
204. Aili, D.; Enander, K.; Baltzer, L.; Liedberg, B., *Nano Lett.*, **2008**, 8, (8), 2473-8.

205. Templeton, A. C.; Chen, S. W.; Gross, S. M.; Murray, R. W., *Langmuir*, **1999**, 15, (1), 66-76.
206. Swift, J.; Butts, C. A.; Cheung-Lau, J.; Yerubandi, V.; Dmochowski, I. J., *Langmuir*, **2009**.
207. Qi, L.; Gao, X., *ACS Nano*, **2008**, 2, (7), 1403-10.
208. Yong, K. T.; Ding, H.; Roy, I.; Law, W. C.; Bergey, E. J.; Maitra, A.; Prasad, P. N., *ACS Nano*, **2009**, 3, (3), 502-10.
209. Kekkonen, V.; Lafreniere, N.; Ebara, M.; Saito, A.; Sawa, Y.; Narain, R., *J. Magn. Magn. Mater.*, **2009**, 321, 1393-1396.
210. de la Fuente, J. M.; Alcantara, D.; Eaton, P.; Crespo, P.; Rojas, T. C.; Fernandez, A.; Hernando, A.; Penades, S., *J. Phys. Chem. B*, **2006**, 110, (26), 13021-8.
211. de la Fuente, J. M.; Alcantara, D.; Penades, S., *IEEE Trans. Nanobiosci.*, **2007**, 6, (4), 275-81.
212. Marradi, M.; Alcantara, D.; de la Fuente, J. M.; Garcia-Martin, M. L.; Cerdan, S.; Penades, S., *Chem. Commun.*, **2009**, (26), 3922-4.
213. Ojeda, R.; de Paz, J. L.; Barrientos, A. G.; Martin-Lomas, M.; Penades, S., *Carbohydr. Res.*, **2007**, 342, (3-4), 448-59.
214. Scandium (Olympus Soft Imaging Solutions, L., CO).
215. Pyrz, W. D.; Buttrey, D. J., *Langmuir*, **2008**, 24, (20), 11350-60.
216. Hostetler, M. J.; Wingate, J. E.; Zhong, C.-J.; Harris, J. E.; Vachet, R. W.; Clark, M. R.; Londono, J. D.; Green, S. J.; Stokes, J. J.; Wignall, G. D.; Glish, G. L.; Porter, M. D.; Evans, N. D.; Murray, R. W., *Langmuir*, **1998**, 14, 17-30.
217. Saha, S. K.; Brewer, C. F., *Carbohydr. Res.*, **1994**, 254, 157-67.
218. Wu, Z.; Jin, R., *ACS Nano*, **2009**.
219. Beulen, M. W. J.; Huisman, B.-H.; van der Heijden, P. A.; van Veggel, F. C. J. M.; Simons, M. G.; Biemond, E. M. E. F.; de Lange, P. J.; Reinhoudt, D. N., *Langmuir*, **1996**, 12, (26), 6170-6172.
220. Beulen, M. W. J.; Bügler, J.; Lammerink, B.; Geurts, F. A. J.; Biemond, E. M. E. F.; van Leerdam, K. G. C.; van Veggel, F. C. J. M.; Engbersen, J. F. J.; Reinhoudt, D. N., *Langmuir*, **1998**, 14, (22), 6337-6340.
221. Zhang, F.; Skoda, M. W.; Jacobs, R. M.; Zorn, S.; Martin, R. A.; Martin, C. M.; Clark, G. F.; Goerigk, G.; Schreiber, F., *J. Phys. Chem. A*, **2007**, 111, (49), 12229-37.
222. Dam, T. K.; Roy, R.; Page, D.; Brewer, C. F., *Biochemistry*, **2002**, 41, (4), 1359-63.
223. Rich, R. L.; Myszkka, D. G., *J. Mol. Recognit.*, **2008**, 21, (6), 355-400.
224. Mann, D. A.; Kanai, M.; Maly, D. J.; Kiessling, L. L., *JACS*, **1998**, 120, (41), 10575-10582.
225. Gutierrez Gallego, R.; Haseley, S. R.; van Miegem, V. F.; Vliegthart, J. F.; Kamerling, J. P., *Glycobiology*, **2004**, 14, (5), 373-86.
226. Hernaiz, M. J.; de la Fuente, J. M.; Barrientos, A. G.; Penades, S., *Angew Chem Int Ed Engl*, **2002**, 41, (9), 1554-7.
227. Bjelic, S.; Jelesarov, I., *J. Mol. Recognit.*, **2008**, 21, (5), 289-312.
228. Wiseman, T.; Williston, S.; Brandts, J. F.; Lin, L. N., *Anal. Biochem.*, **1989**, 179, (1), 131-7.
229. Christensen, T.; Toone, E. J., *Methods Enzymol.*, **2003**, 362, 486-504.
230. Turnbull, W. B.; Daranas, A. H., *JACS*, **2003**, 125, (48), 14859-66.
231. Okhrimenko, O.; Jelesarov, I., *J. Mol. Recognit.*, **2008**, 21, (1), 1-19.
232. Bouchemal, K., *Drug Discov. Today*, **2008**, 13, (21-22), 960-72.
233. Dam, T. K.; Roy, R.; Page, D.; Brewer, C. F., *Biochemistry*, **2002**, 41, (4), 1351-8.
234. Williams, B. A.; Chervenak, M. C.; Toone, E. J., *J. Biol. Chem.*, **1992**, 267, (32), 22907-11.
235. Leipzig, N. Analytical Ultracentrifugation. (06/07/2009),
236. Schuck, P., *Biophys. J.*, **2000**, 78, (3), 1606-19.
237. Schuck, P., *Analytical Ultracentrifugation Techniques and Methods*. Royal Society of Chemistry: 2005.
238. Machtle, W.; Borger, L., *Analytical Ultracentrifugation of Polymers and Nanoparticles*. Springer Berlin: Heidelberg, 2006.
239. McPherson, A., *Eur. J. Biochem.*, **1990**, 189, (1), 1-23.
240. Cioci, G.; Rivet, A.; Koca, J.; Perez, S., *Carbohydr. Res.*, **2004**, 339, (5), 949-59.
241. Case, D. A.; Darden, T. A.; Cheatham, T. E.; Simmerling, C. L.; Wang, J.; Duke, R. E.; Luo, R.; Merz, K. M.; Wang, B.; Pearlman, D. A.; Crowley, M.; Brozell, S.; Tsui, V.; Gohlke, H.; Mongan, J.; Hornak, V.; Cui, G.; Beroza, P.; Schafmeister, C.; Caldwell, J. W.; Ross, W. S.; Kollman, P. A.
242. Perez, S.; Imberty, A.; S.B., E.; Gruzaa, J.; Mazeau, K.; Jimenez-Barbero, J.; Poveda, A.; Espinosa, J.-F.; van Eyck, B. P.; Johnson, G.; French, A. D.; Kouwijzer, M. L. C. E.; Grootenuis, P. D. J.; Bernardi, A.; Raimondi, L.; Senderowitz, H.; Durier, V.; Vergoten, G.; Rasmussen, K., *Carbohydr. Res.*, **1998**, 314, 141-155.
243. Neumann, D.; Lehr, C. M.; Lenhof, H. P.; Kohlbacher, O., *Adv. Drug. Deliv. Rev.*, **2004**, 56, (4), 437-57.

244. Takae, S.; Akiyama, Y.; Otsuka, H.; Nakamura, T.; Nagasaki, Y.; Kataoka, K., *Biomacromolecules*, **2005**, 6, (2), 818-824.
245. Pale-Grosdemange, C.; Simon, E. S.; Prime, K. L.; Whitesides, G. M., *JACS*, **1991**, 113, (1), 12-20.
246. Dalsin, J. L.; Lin, L.; Tosatti, S.; Voros, J.; Textor, M.; Messersmith, P. B., *Langmuir*, **2005**, 21, (2), 640-6.
247. Dobrovolskaia, M. A.; McNeil, S. E., *Nat. Nanotechnol.*, **2007**, 2, (8), 469-78.
248. SYBYL, T. A., 1699 S. Hanley Road, Suite 303, St Louis, MO 63144 USA.
249. Saha, S. K.; Brewer, C. F., *Carbohydr Res*, **1994**, 254, 157-67.
250. Lindhorst, T. K.; Kotter, S.; Krallmann-Wenzel, U.; Ehlers, S., *J. Chem. Soc., Perkin Trans. 1*, **2001**, 823-831.

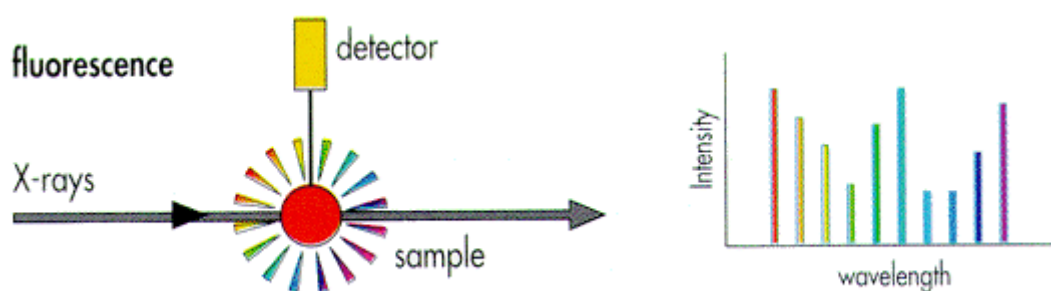
ANNEXES

ANNEX I :

Further GNP Characterisation

Introduction: As discussed in chapter 2, AuNPs exhibit a range of interesting physical properties: surface plasmon resonance, fluorescence, magnetism and very high mean inner potentials. These effects are clearly related to the unique electronic structure of the AuNP cluster which is itself dependent on core size and the nature of the surface bound ligands. These properties are also known to influence AuNP catalytic activity and are related to various potential physico-chemical applications. Nanoparticle core composition would also influence the electronic structure at the AuNP core. In particular, impurities found in the core material in significant quantities may dramatically influence the overall electronic activity and hence their physical properties and applications.

Materials and method: In order to supplement the characterisation of these carbohydrate functionalised gold clusters, several samples were analysed by elemental imaging at the hard x-ray nanoprobe ID22NI, ESRF, Grenoble. Samples were subject to x-ray fluorescence using a 100 nm beam with photon energies of up to 17.5 keV in order to detect and reveal the composition of nanoparticle core materials (Scheme 1).



Scheme 1 : Schematic diagram of XRF experiment. ¹

Results and discussion: Subsequent analysis revealed that several metallic species were present in what was believed to be a “pure gold” cluster sample. The results shown in Fig. 1

revealed the presence of Au as the primary constituent (98 %) however Ca, Fe and Ni were also co-localised in significant quantities (1.7, 0.1, and 0.2 % respectively).

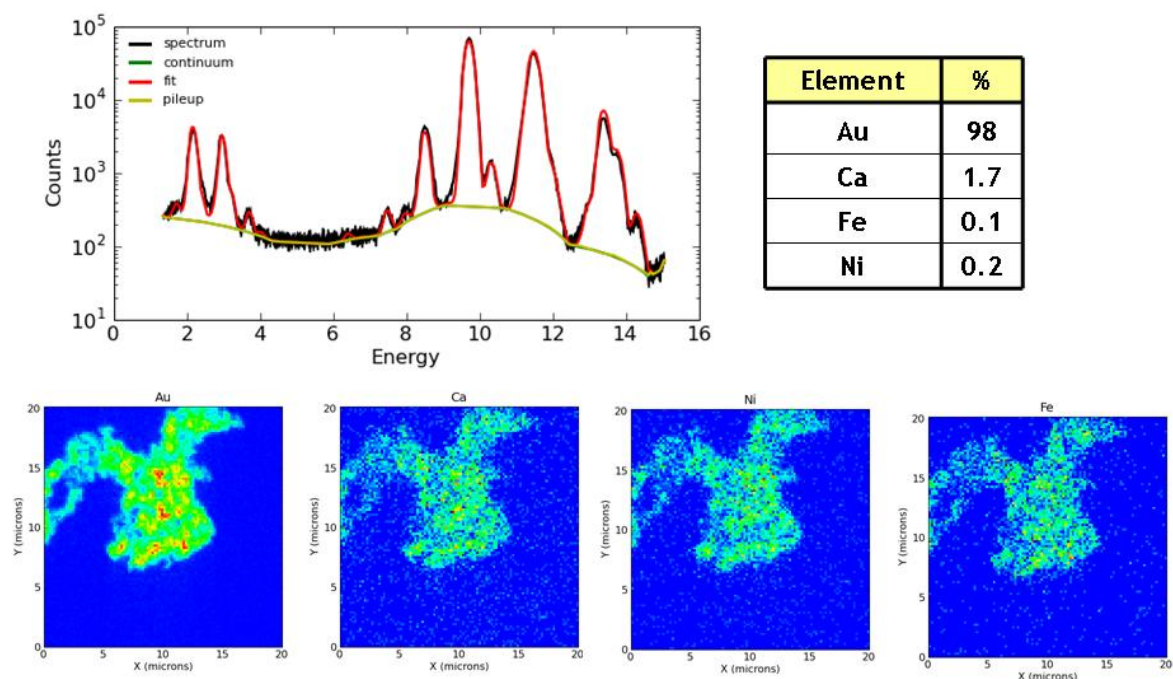


Figure 1: Cumulated x-ray fluorescence spectrum taken at 17.5 keV over a scanned area of 20x20 μm^2 of gold nanoparticles deposited on a kapton membrane (above). XRF images obtained by measuring the $K\alpha$ line intensity of Au, Ca, Ni and Fe (below). The pixel size is 50x50 nm^2 . Red indicates high fluorescence intensity, blue low intensity. A rough estimate of the average elemental content over the whole scanned area is also reported.

The origin of these impurities has not yet been identified. The $\text{HAuCl}_4 \cdot \text{H}_2\text{O}$ (Au salt starting material) analysis certificate from Strem chemicals does not indicate any significant trace element concentration (several ppm only) for the corresponding lot number. Therefore, contamination at some later stage in AuNP synthesis and handling, or properties adopted by the ligands (coordination to Ca etc) may be responsible. Further x-ray fluorescence (XRF) experiments with other AuNP samples and the $\text{HAuCl}_4 \cdot \text{H}_2\text{O}$ starting material are required to confirm this. Simultaneous x-ray diffraction experiments will also be performed to investigate the influence of the metallic elements in the nanostructures. Also, how the presence of these metallic species change the electronic structure of these clusters, what effect this would have on experimentally measured physical properties such as magnetism, fluorescence and surface plasmon resonance, and their contribution to the catalytic activity and electrochemistry will be investigated.

This work was carried out, and will be continued, in collaboration with Dr Gema Martinez-Criado, Micro-Fluorescence, Imaging and Diffraction group, ESRF.

ANNEX II :

Further GNP Applications I

1. Self-Organisation of GNPs

Introduction: The controlled and organised deposition of nanoparticles and molecules has attracted a great deal of interest in recent years for applications towards nano-electronics and nanochemistry.² The *bottom up* approach, taking inspiration from biological systems by exploiting order-inducing elements, offers several advantages over the current *top down* fabrication of nanostructures. In particular, the potential for size reduction to several nm or even to the molecular level, as well as organisation from superlattice up to 3D structures and the potential for commercial mass production.³ Therefore, a fundamental understanding of how nano-sized objects self-organise as well as influencing and controlling this organisation is an attractive research topic. Ideally, the nano-substrates should be well characterised with a uniform size and shape and chemically versatile to withstand a number of chemical reactions in order to display a particular structural or functional role in the material. Therefore, NPs (metal-NPs, quantum dots etc) which have all benefitted from advances in synthetic methodologies to improve these prerequisites, as well as their inherent physical properties (magnetism, catalytic activity etc) prove interesting candidates for order-inducing substrates for materials science.⁴

Several methods currently exist for the deposition of various nanoparticle systems including adsorption on a patterned substrate, micro-contact printing, droplet evaporation, layer by layer absorption and self-assembly in solution or at phase boundaries.^{2, 3, 5-9}(and references therein) There are also uses of biologically important molecules as scaffolds and templates for organising metal nanoparticles. Examples of proteins and DNA can be found.^{10, 11}

Self-association of carbohydrate molecules is controversial due to their highly soluble nature and difficulty in characterising these associations using biophysical methods. However, Penades *et al.* have proved both on a molecular level and by using functionalised nanoparticle clusters, the 3D self-association of amphiphilic biologically important carbohydrate molecules.^{12, 13} They had shown that complementarity between Van der Waals surfaces of the

amphiphilic carbohydrate molecules were fundamental in the self-association process as measured by AFM. However, the self-association of carbohydrate molecules had previously been shown in the crystal structure of Le^x trisaccharide, which formed dimers upon forming the crystal lattice, supported by inter-molecular hydrogen bond contacts and the presence of structural water molecules.¹⁴

Results and discussion: Here, we present the apparent self-organisation properties of carbohydrate functionalised AuNPs. As seen by high resolution TEM, GNP droplets deposited on carbon grids exhibited varying organisational properties depending on the carbohydrate presented at the GNP surface, as well as ligand presentation density. Figure 2 shows the TEM images from **GNP-2** and **GNP-6**, which have a 10% presentation density for mannose and galactose, respectively.

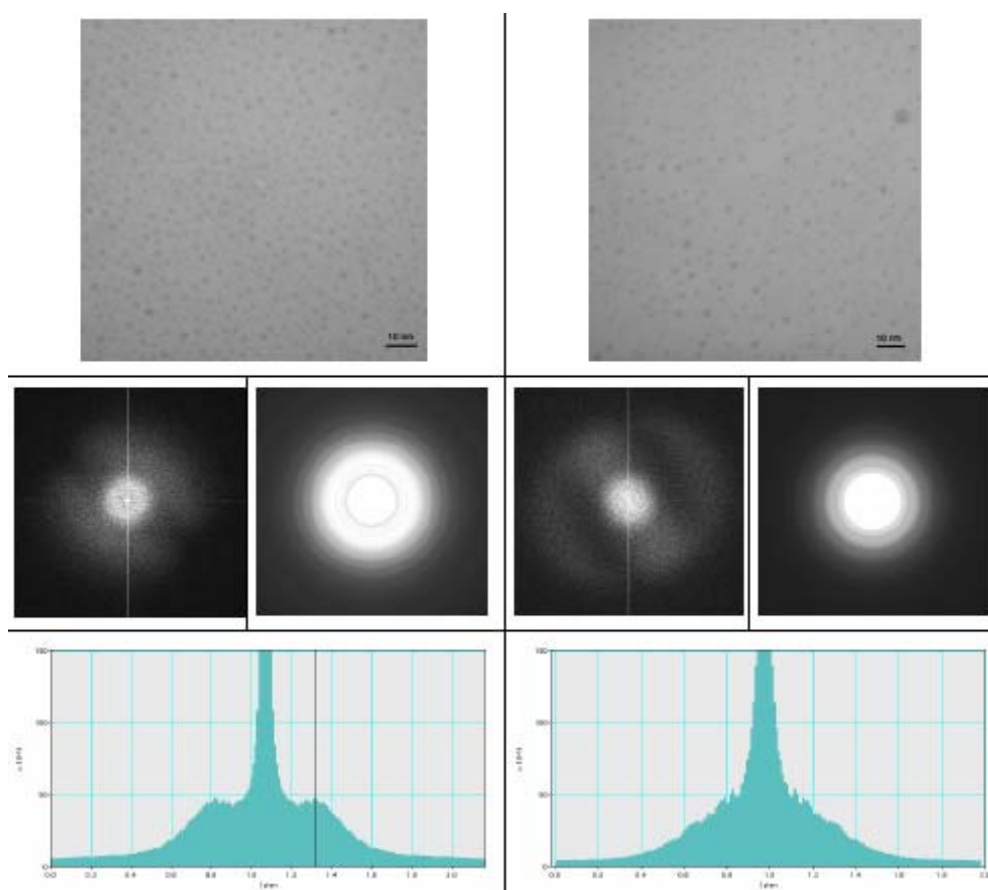


Figure 2 : Examples of GNP self-organisation observed with GNP-2 (left) and no observed organisation observed with GNP-6. Top: TEM photographs, middle: Fourier transform of measured inter-GNP distances, bottom: cross section of FT surface.

The TEM images were processed using DigitalMicrograph software (Gatan) from which a Fourier transform surface in reciprocal space was produced. From this, organisation can be

observed. For **GNP-6**, the cross-section of the FT-reciprocal space exhibits a relatively regular exponential decay, suggesting random organisation of the GNPs i.e. the presence of one GNP does not statistically significantly affect or influence a neighbouring GNP (at this concentration). For **GNP-2** however, a non-regular exponential decay is observed, with maximums observed at 0.25 nm^{-1} from the theoretical GNP centre of mass. This corresponds to an inter-GNP distance of 4.1 nm, meaning that there is a statistically significant reason why GNP nearest neighbours in this sample prefer to space themselves 4.1 nm from each other (at this concentration). For **GNP-2**, the average GNP diameter is 0.75 nm, with a linker molecule length of 3.61 nm, giving a total GNP radius of 4.36 nm. Therefore, the last 0.26 nm of the linker and the carbohydrate molecules are overlapping with that of a neighbouring GNP. Assuming linear linker conformations, this suggests that the α -mannosides are interacting with the thiourea bridges of the neighbouring GNPs in a fashion that the β -galactosides are not. It is possible that the α -conformation encourages hydrogen bonds to form between equatorial hydroxyl groups of the carbohydrates and the thiourea bridges (Figure 3), whereas a β -conformation would not. However, with β -galactosides, the hydroxyl group at C4 would still, in theory, be capable of forming some hydrogen bond connections. At higher presentation densities, this overlapping interaction is not observed, suggesting that steric hindrance may become increasingly important in dehydrated environments.

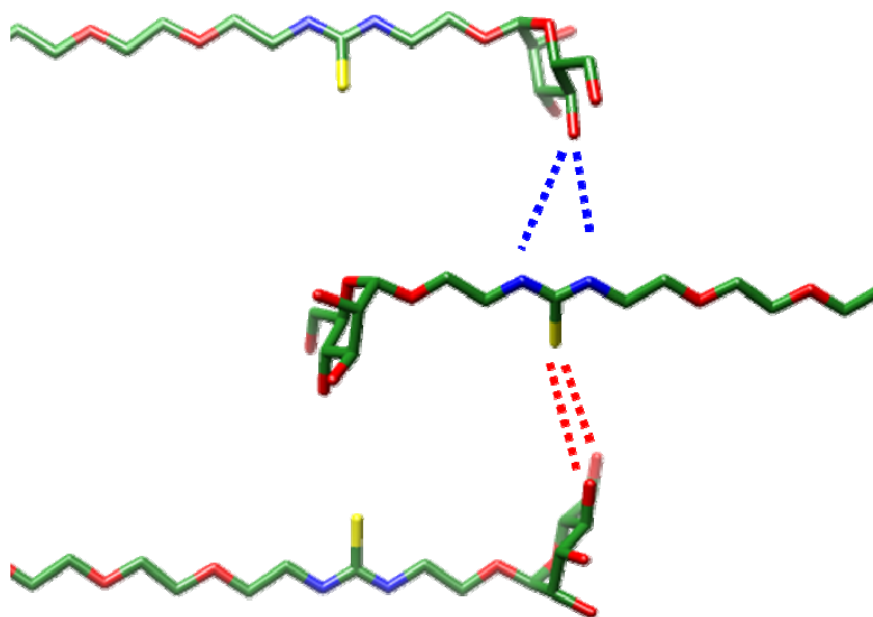


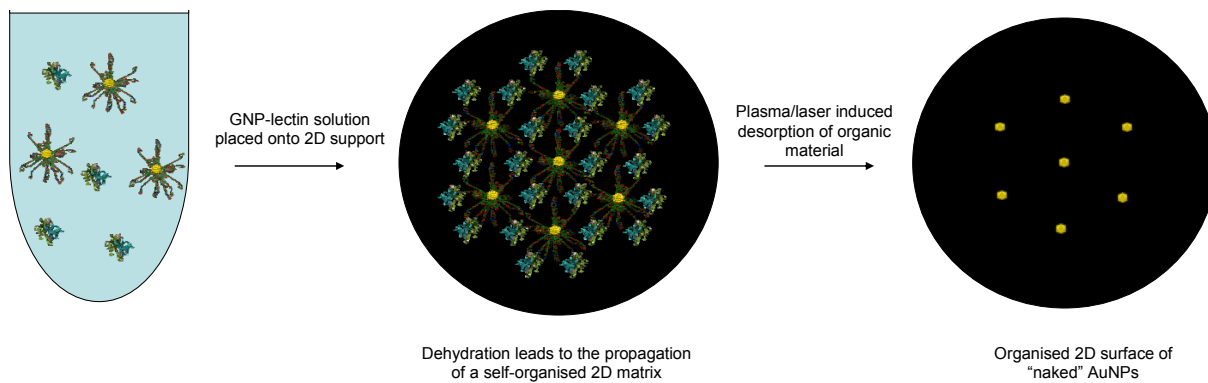
Figure 3 : Possible ligand overlapping interactions. Between the mannoside and the amide groups (above), and the thiocarbonyl (below). Carbon atoms coloured green, Oxygen coloured red, Nitrogen coloured blue and Sulphur coloured yellow. Hydrogen atoms not shown.

2. Self-Organisation of Lectin–Carbohydrate Complexes

As well as carbohydrates, multivalent lectins have also been shown to co-organise with multivalent ligands. Tetrameric Con A was shown by AFM to organise around symmetric mannoside dimer and trimer ligand templates.¹⁵ BclA, a dimeric lectin, was also shown by AFM and crystallography to generate uniform linear structures with a trimeric mannoside ligand.¹⁶ The ligand exhibited a valency of 2, forming (BclA-ligand)-polymers. In the cases of both Con A and BclA, random aggregation of lectins was observed in the absence of ligand.

3. Self-Organisation of Lectin–GNP Complexes

From both of these studies, it is clear that lectin architecture (tetrahedral for Con A, linear for BclA) greatly influences organisation properties when condensed on to a 2D surface. The architecture of the carbohydrate ligand has also been shown to influence organisation properties of the lectin-carbohydrate complex when condensed to a 2D surface. Therefore, we propose that, by a combination of modifying lectin architecture (Con A, BclA, PA-IL – carbohydrate planar), as well as controlling the valency of the GNP (ligand architecture), organisation and dispersion of AuNPs on a 2D surface can be controlled and modified. In short, different combinations of lectin and GNP architectures would give different organisation patterns and surface concentrations (different inter-GNP distances at the 2D surface). This could lead to organised AuNP functionalised surfaces for catalytic or nano-electronic applications. However, it would be important to remove organic material from the AuNPs once the ordered surface has been formed, exposing the AuNP surface atoms (scheme 2). Plasma or laser induced desorption could be investigated, however, mass spectrometry experiments have shown that the sulfide ligands may also remove a surface Au atom upon desorption.^{17, 18}



Scheme 2 : Potential use of GNPs and lectins as sacrificial templates for forming 2D organised AuNP matrices.

ANNEX III :

Further GNP Applications II

Mean Inner Potential

As discussed earlier, the mean inner potential (MIP) is the volume-averaged electrostatic contribution to the crystal potential. Previously, theoretical models were used to describe the MIP however this was difficult due to the lack of analytical expressions of various parameters such as atomic potentials. These theoretical models can be solved with the use of approximations (spherical symmetry, no perturbation when expanding from atomic to material scales) and crystallographic data.

Electrons in a transmission electron microscope experience a phase shift upon interaction with the sample under study. This phase shift is dependent on the sample thickness and surface potential, which can be approximated to the MIP. Off-axis electron holography can be used to measure the phase difference of an electron passing through the sample and an electron passing through a vacuum (reference). As the MIP is dependent on atomic arrangement and electron distribution in the crystal lattice, variation with nanoparticle structures (in particular nanoparticle size) can be measured. High resolution electron microscopy is also used as a powerful tool for nanoparticle characterisation. However, few instruments provide the necessary features to both characterise the nanomaterial and study the MIP. The following article describes a convenient method whereby high resolution TEM can be used for material characterisation and a focal series of images are taken to derive quantitative phase maps, which are then applied to a theoretical model and approximations allowing the calculation of the MIP.

This work was carried out in collaboration with Isabelle Paintrand (CERMAV) and Dr. Patricia Donnadiou, SIMAP, INP Grenoble-CNRS-UJF, Grenoble, France.

Article 2

**Seeing structures and measuring properties with transmission electron
microscopy images: A simple combination to study size effects in
nanoparticles systems**

Patricia Donnadieu, Sorin Lazar, Gianluigi A. Botton, Isabelle Pignot-Paintrand,
Michael Reynolds, and Serge Perez

Appl. Phys. Lett. (2009) **94**, 263116 (published online) doi: 10.1063/1.3168525

ANNEX IV :

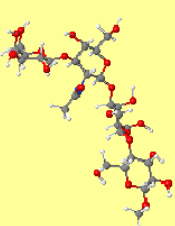
Molecular Modelling of Carbohydrates

1. 3D Biologically Active Oligosaccharide (3D BAO) Database

The structural determination of oligosaccharides is vitally important for investigating their biological activity at the molecular level. Although much is already known with regards to carbohydrate interactions and their role in many biological processes, very little is known about the specific details of these processes. One reason for this is the diversity observed in biological systems, again a testament to the versatile nature of oligo- and polysaccharides, their many different forms of storing the glycode and their conjugation to other biologically important molecules. To counter this, many tools have been developed to aid the comprehension of carbohydrate interactions as well as an electronic library storing information on carbohydrate structure and related experimental data (NMR, mass spectroscopy, HPLC profiles etc).^{19, 20} A new database has been developed in CERMAV for storing and organising three-dimensional structures of carbohydrates. Structures of bio-active oligosaccharides ranging from monosaccharides, disaccharides, neutral and sialylated oligosaccharides from human milk and urine, cell adhesion, blood groups, head groups of common glycosphingolipids, lectin binding oligosaccharides and glycosaminoglycans have been collected and optimised using computational methods. Further processing and application of computation methods has allowed the generation of structural “families” of the lowest energy conformers for each molecule. More specifically, a genetic algorithm is used to minimise the structures, followed by clustering algorithms which organise the molecular hyperspace into conformational families. The lowest energy conformer for each cluster family becomes the representative of that particular cluster. The cluster algorithms incorporate factors such as glycosidic torsion angles and atom root-mean-squared deviation (RMSD) to separate the different clusters. The data are presented in a database, the 3D biologically active oligosaccharide (3D-BAO) database which will be available via the internet. The oligosaccharides can be selected by a particular monosaccharide which they contain, a particular sequence motif, biological origin or a combination of several of these. All structures are available to download in a variety of formats which can be further modified by

the user or directly used as input files for further computational studies (Figure 4). Currently there are over 300 structures in the database, each with their 10 lowest energy conformations.

Lacto-N-tetraose

Primary Structure	<chem>b-D-Galp-(1-3)-b-D-GlcpNAc-(1-3)-b-D-Galp-(1-4)-b-D-Glcp</chem>	Text File
3D Interactive Structure	 Jmol	PDB File
Molecular Weight (g/mol)	707.636	
Origin	Human Milk	
Glycan Family	N-linked	
Lowest Energy Conformers	<input type="button" value="Lacto-N-tetraose"/>	

[back to top page](#)

Figure 4 : Screen shot of the results page from the 3D BAO.

2. NanoGoldBuilder

The NanoGoldBuilder is an online tool developed for constructing Gold nanoparticles functionalised with a variety of molecules. The builder allows the user to choose from a range of available AuNP cores (from 1 to 3 Au shells corresponding to 13, 33 and 55 Au atoms). Following AuNP core selection, the spacer molecules are chosen. Several spacer molecule structures are available in to builder database itself; however, the user can also upload new spacer molecule structures in several formats (PDB, MOL, MOL2). The thiol functionality is automatically connected to the Au core by the builder, and the furthest heteroatom from the thiol will be automatically designated the atom to be substituted by the functionality in later steps. Several spacer molecules can be selected for the same nanoparticle, allowing the building of hybrid NPs. Spacer selection can be made by selecting a particular molecule or by “backbone” length. In the final step, the functionalities are selected. Different functionalities can be assigned to the different spacer molecules. For carbohydrates, the structures and conformations available in the 3D BAO will be made available as well as other biologically important molecules (fluorophores etc). The reducing anomeric centre is automatically

assigned as the spacer conjugation position. Once all functionalities have been assigned to the different spacer molecules, the NP presentation density of the functionalities is assigned (numerically or as a percentage). Other molecules can be uploaded by the user for conjugating to the spacer molecule. Following functionality and presentation density assignment, the NP is constructed and available for downloading, again, as several file formats as for the 3D BAO. As of yet, the ligand molecules are built to the AuNP core in a random fashion, and the builder does not yet include parameters for NP structure. However, the future perspectives include implementing AuNP construction and interaction parameters from computation and crystallographic studies, as well as including other core materials and core-ligand couplings.

3. Hydration Studies of Carbohydrates

As well as refining carbohydrate structures and their lowest energy conformers *in vacuo*, it is vitally important to study their structural and conformational behaviour in physiological environments. As well as studying the behaviour of the carbohydrate solute, it is important to investigate the behaviour of the solvent molecules in the local environment. In particular, the residence times of water molecules which are bound to the solute via hydrogen bonds. Long residence times may indicate structural solvent molecules, which serve as a “molecular mortar” for restricting solute movement. “Bridging” water molecules may be found where one water molecule binds to several residues of the solute, forming a temporary, reversible, bimolecular structure. This may hold the solute in a particular conformation, especially if the bridging event occurs between several different monomers of the solute. These bridging solvent molecules may be conserved or replaced by other heteroatoms upon association of the solute with a lectin binding site.

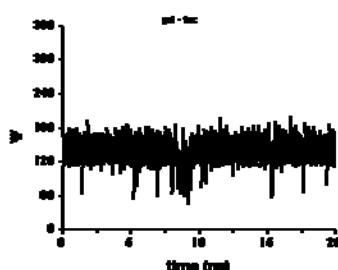


Figure 3f: Variation of ΨLe^y glycosidic linkage torsion angle around Galp(3)-Fucp(4) not included in the following article.

Article 3

The hydration features of carbohydrate determinants of Lewis antigens

Michael Reynolds, Andreas Fuchs, Thisbe K. Lindhorst and Serge Perez

Molecular Simulation (2008) **34**, 447 (published online) doi:

10.1080/08927020701713878

ANNEX BIBLIOGRAPHY

1. <http://www.esrf.eu/UsersAndScience/Experiments/Imaging/ID22/Applications>
2. Ben Ali, M.; Ondarcuhu, T.; Brust, M.; Joachim, C., *Langmuir*, **2002**, 18, (3), 872-876.
3. Brust, M.; Kiely, C. J., *Colloids Surf., A*, **2002**, 202, (2-3), 175-186.
4. Claridge, S. A.; Castleman, A. W., Jr.; Khanna, S. N.; Murray, C. B.; Sen, A.; Weiss, P. S., *ACS Nano*, **2009**, 3, (2), 244-55.
5. Werts, M. H. V.; Lambert, M.; Bourgoïn, J. P.; Brust, M., *Nano Letters*, **2002**, 2, (1), 43-47.
6. Khatri, O. P.; Adachi, K.; Murase, K.; Okazaki, K.; Torimoto, T.; Tanaka, N.; Kuwabata, S.; Sugimura, H., *Langmuir*, **2008**, 24, (15), 7785-92.
7. Li, J. R.; Lusker, K. L.; Yu, J. J.; Garno, J. C., *ACS Nano*, **2009**.
8. Hassenkam, T.; Norgaard, K.; Iversen, L.; Kiely, C. J.; Brust, M.; Bjornholm, T., *Adv. Mat.*, **2002**, 14, (16), 1126-1130.
9. Ling, X. Y.; Phang, I. Y.; Reinhoudt, D. N.; Vancso, G. J.; Huskens, J., *Int. J. Mol. Sci.*, **2008**, 9, (4), 486-97.
10. Swift, J.; Butts, C. A.; Cheung-Lau, J.; Yerubandi, V.; Dmochowski, I. J., *Langmuir*, **2009**.
11. Mastroianni, A. J.; Claridge, S. A.; Alivisatos, A. P., *JACS*, **2009**.
12. Fuss, M.; Luna, M.; Alcantara, D.; de la Fuente, J. M.; Enriquez-Navas, P. M.; Angulo, J.; Penades, S.; Briones, F., *J. Phys. Chem. B*, **2008**, 112, (37), 11595-600.
13. Fuss, M.; Luna, M.; Alcantara, D.; Fuente, J. M.; Penades, S.; Briones, F., *Langmuir*, **2008**, 24, (9), 5124-8.
14. Perez, S.; Mouhous-Riou, N.; Nifant'ev, N. E.; Tsvetkov, Y. E.; Bachet, B.; Imberty, A., *Glycobiology*, **1996**, 6, (5), 537-42.
15. Gour, N.; Verma, S., *Tetrahedron*, **2008**, 64, (30-31), 7331-7337.
16. Lameignere, E. Etudes structurales et fonctionelle de lectines solubles de *Burkholderia cenocepacia*. Université de Grenoble I - Joseph Fourier, Grenoble, 2009.
17. Beulen, M. W. J.; Huisman, B.-H.; van der Heijden, P. A.; van Veggel, F. C. J. M.; Simons, M. G.; Biemond, E. M. E. F.; de Lange, P. J.; Reinhoudt, D. N., *Langmuir*, **1996**, 12, (26), 6170-6172.
18. Beulen, M. W. J.; Bügler, J.; Lammerink, B.; Geurts, F. A. J.; Biemond, E. M. E. F.; van Leerdam, K. G. C.; van Veggel, F. C. J. M.; Engbersen, J. F. J.; Reinhoudt, D. N., *Langmuir*, **1998**, 14, (22), 6337-6340.
19. GLYCO3D? [HTTP://www.cermav.cnrs.fr/glyco3D/index.php](http://www.cermav.cnrs.fr/glyco3D/index.php)
20. EuroCarbDB, <http://www.eurocarb.org/>

ABSTRACT

The implication of carbohydrate interactions in many normal and pathological biological processes (cell communication, adhesion, bacterial and viral invasion, cancer metastasis etc.) has encouraged the development of interdisciplinary research in the fields of glycochemistry and glycobiology. These interactions are typically highly specific, yet low in affinity. Nature overcomes this by presenting multiple copies of both carbohydrate ligands and protein (lectin) receptors. However, the overall interaction observed is significantly enhanced with respect to the sum of the individual interactions. This phenomenon is known as the “cluster glycoside effect”, or “multivalent effect”.

Carbohydrate functionalised Gold nanoparticles (glycol-nanoparticles, GNPs) represent a new group of glycoclusters for studying this phenomenon. As well as their relatively simple synthesis, they also offer many physicochemical properties such as tuneable presentation densities, tuneable gold core sizes and size related electronic, magnetic and optical properties.

Here we present the synthesis and characterisation of mannose and galactose functionalised GNPs and investigate their interactions with the multivalent proteins (lectins) Con A, BclA and PA-IL, using biophysical techniques, namely surface plasmon resonance (SPR) and isothermal titration microcalorimetry (ITC). It was found that lectin affinities for the GNPs varied significantly with carbohydrate presentation density. As well as being used for interaction studies, GNPs offer interesting potential as novel diagnostic and therapeutic applications in glycobiology, biotechnology and materials science applications.

Key words: Gold nanoparticles, protein-carbohydrate interactions, glycochemistry, multivalence

RESUME

Les interactions des glucides sont impliquées dans plusieurs processus biologiques normaux ou bien pathologiques (la communication cellulaire, l'adhésion et l'entrée de pathogènes dans la cellule ou encore de carcinomes métastatiques). Souvent, ces interactions ont une forte spécificité mais une affinité faible. *In vivo*, cette faible affinité est résolue par la présentation de copies multiples des ligands glucidiques à des multimères de récepteurs protéiques (lectines). Globalement, l'interaction observée est alors largement supérieure à la somme des interactions individuelles. Ce phénomène est connu comme « l'effet cluster glycosidique ». Ces interactions ont encouragées le développement des recherches interdisciplinaires dans les domaines de la glycochimie et de la glycobiologie.

Les nanoparticules d'or, fonctionnalisées avec des glucides (glyco-nanoparticules, GNPs) constituent un nouvel outil pour étudier ce phénomène. Leur synthèse est assez simple, et ils montrent plusieurs propriétés physicochimiques comme la modification de la densité de présentation, le control de la taille de la particule, et ils ont aussi des propriétés électroniques, magnétiques et optiques, liées aux effets quantums.

Nous présentons la synthèse et la caractérisation des GNPs fonctionnalisées avec du mannose et du galactose dans le but d'étudier les interactions avec des protéines multivalentes (les lectines Con A, BclA et PA-IL), en utilisant des techniques biophysiques comme la résonance plasmonique de surface, et le microcalorimétrie isotherme de titration. Ces techniques ont montrées que l'affinité des lectines varie avec la densité de présentation des ligands chez les GNPs. Les GNPs sont un outil novateur pour développer des nouvelles méthodes de diagnostics ou thérapeutiques dans les domaines de la glycobiologie, des biotechnologies et de la science des matériaux.

Mots clés : Nanoparticules d'or, interactions protéines-glucides, glycochimie, multivalence